The optimisation of an iPSC-derived cortical neuronal platform for the study of excitatory synaptic transmission and plasticity in neurological disorders

Emma Whiteley

Thesis submitted for the degree of Doctor of Philosophy

Brasenose College
University of Oxford
Trinity Term 2018

Abstract

Many neurological disorders affecting the central nervous system exhibit alterations in glutamatergic synapse function. One such disorder is Alzheimer's disease (AD), which affects 5 % of the world's population. With an aging population and a lack of disease-modifying therapeutics, the prevalence of this disease is only expected to increase. Therefore, it is essential that we gain a greater understanding of AD pathogenesis in order to develop successful therapeutics. In AD, synapse loss is the best correlate of cognitive decline, and evidence from rodent studies suggests that this is preceded by synaptic dysfunction, primarily manifesting as alterations in glutamatergic synaptic plasticity. The advent of induced pluripotent stem cell (iPSC) technology has made it possible to investigate disease pathophysiology in patient-derived cells. Biochemical alterations in line with AD pathology have been described in AD-patient iPSC-derived neurons, but changes in synaptic transmission are yet to be investigated. The functional properties described for iPSC-derived neurons are often immature, and it is unclear whether they exhibit the pre- and post-synaptic properties required for the induction and expression of glutamatergic synaptic plasticity. A limited number of reports have described synaptic plasticity-like phenomena in iPSC-derived neurons. However, these studies use non-physiological methods, often show poor reproducibility and lack direct evidence for an activity-dependent change in synaptic efficacy.

The objective of this thesis was to determine methods to enhance neuronal maturity, and to generate a well-characterized platform for the study of physiological forms of synaptic plasticity. To this end, I first used whole-cell patch clamp electrophysiology to extensively characterize the functional properties of healthy control and familial AD patient iPSC-derived cortical neurons and found them to be immature. From several strategies tested, only the co-culture of iPSC-derived cortical neurons with rat astrocytes was found to robustly enhance intrinsic neuronal maturity and produce modest increases in excitatory synaptic transmission. Taking an alternative approach, I refined a transcription factor-based neuronal differentiation protocol and found that the exogenous expression of neurogenin-2 in iPSC-derived neural progenitor cells generated highly active excitatory synaptic networks.

Physiological synaptic plasticity assays require the isolation and manipulation of monosynaptic connections. Dual-patch recordings in the neurogenin-2 iPSC-derived cortical cultures revealed a low probability (10 %) of detecting an excitatory monosynaptic response. However, the expression of the optogenetic tool, channelrhodopsin-2 (ChR2), in a subset of neurons enabled the generation of light-evoked monosynaptic responses, which were three-fold more frequent. Excitatory monosynaptic responses exhibited similar properties to connections in rodent cortex, and demonstrated robust expression of functional synaptic AMPA and NMDA receptors. Monosynaptic connections failed to exhibit spike-timing dependent plasticity or classical long-term potentiation (LTP) using a pairing-protocol, and similarly, no changes were exhibited in spontaneous excitatory synaptic transmission following a chemical LTP protocol. However, prolonged optogenetic activation of pre-synaptic ChR2-expressing neurons for 2-4 days during cell culturing induced an activity-dependent potentiation of spontaneous excitatory current amplitude. This was primarily expressed by a subset post-synaptic neurons with mature intrinsic properties and thereby suggests that the degree of neuronal maturity is likely to be critical factor when exploring synaptic plasticity. This work provides a foundation for future investigations into synaptic plasticity and extends the range of experimental assays that can be applied to human iPSC-derived cortical neurons for the study of excitatory synaptic transmission.

Acknowledgements

First and foremost, I offer my sincerest gratitude to my supervisors Prof. Colin Akerman and Prof. Richard Wade-Martins. I feel incredibly honoured to have been a part of their research groups.

I am indebted to Prof. Colin Akerman who has supported me throughout my DPhil and has shown exceptional generosity with his time, kindness and patience. I greatly appreciate his enthusiastic attitude and constructive suggestions offered during my DPhil. He is an inspirational role model and I am in awe of his seemingly endless concentration span, wealth of ideas and pure passion for science.

I am forever grateful to Prof. Richard Wade-Martins for opening the door into the world of stem-cell research, for providing guidance throughout my DPhil and for always being incredibly positive.

I would like to thank Dr. Sarah Newey- my "third supervisor" and mentor, for her compassion, honesty and invaluable support. Without her understanding, advice and encouragement this DPhil would have been a very different experience. I greatly admire both her personal and scientific qualities, and I feel incredibly privileged to have her friendship.

I am grateful to the past and present members of the Akerman lab who have created a friendly and supportive environment in the basement, and the Wade-Martins group for always being welcoming and helpful, despite my relatively brief visits. I would especially like to thank Anne Hedegaard, for sharing in the joys and sorrows of iPSC-based neuroscience research, Louise Kay, Sophie Nixon, Sophie Avery and Brent Ryan, who have been incredibly supportive and encouraging over the past few years.

I would like to thank the Alzheimer's Society for providing funding for this research project.

I am immensely grateful to my family and friends, especially my parents and "The Pobbles" for their love, support and belief in me. They have provided never ending encouragement and optimism and I hope I will continue to make them proud.

And last, but by no means least, I owe a huge debt of gratitude to Tom. Without his unwavering support this DPhil would not have been completed. I thank him for believing in me and for being my light at the end of the tunnel. It is his love and friendship that have seen me through the highs and lows of my DPhil, and for that I am eternally grateful.

Collaborations

I would like to thank Paul Brodersen for writing a program to assist with the analysis of monosynaptic EPSCs, and Joram van Rheede for creating a Matlab script to extract the membrane test values used to assess recording quality and stability.

I am grateful to Sarah Newey for providing the RT-PCR in Figure 3.1b and the synaptic stainings in Figure 3.4b-d.

I would also like to thank Sunniva Bostrand for performing the GAD quantification and electrophysiology shown in Figure 3.2l, and Figure 5.4.

I would like to offer my sincere thanks to Anne Hedegaard for the recording and analysis of the EPSCs presented in Figure 3.1i-k and Figure 4.1d-f, and for contributing to the dataset presented in Figure 4.2.

Table of Contents

List of Figures

List of Tables

Abbreviations

AD: Alzheimer's disease

ALS: Amyotrophic lateral sclerosis

AMPA: α-amino-3-hydroxy-5-methyl-4-isoxazolepropionic acid

ANOVA: Analysis of variance

AP: Action potential

ApoE: Apolipoprotein-E

APP: Amyloid precursor protein

AraC: Cytosine arabinoside

Aβ: Amyloid-β

bAP: Backpropagating action potential

BDNF: Brain-derived neurotrophic factor

bHLH: Basic helix-loop-helix

CaMKIIα: Calcium/calmodulin-dependent protein kinase type II alpha chain

cAMP: 3',5'-cyclic adenosine monophosphate

cDNA: Complementary deoxyribonucleic acid

ChR2: Channelrhodopsin-2

cLTP: Chemical long-term potentiation

CNQX: 6-Cyano-7-nitroquinoxaline-2,3-dione

COV: Coefficient of variation

D: Day

DAP: Depolarizing after potential

DIV: Days *in vitro*

DL-AP5: DL-2-Amino-5-phosphonopentanoic acid

EGF: Epidermal growth factor

eGFP: Enhanced green fluorescent protein

EOAD: Early-onset Alzheimer's disease

EPSC: Excitatory post-synaptic current

EPSCaT: Excitatory post-synaptic calcium transient

EPSP: Excitatory post-synaptic potential

ESC: Embryonic stem cell

fAD: Familial Alzheimer's disease

FGF2: Fibroblast growth factor 2

GABA: γ-aminobutyric acid

GAD: Glutamic acid decarboxylase

GDNF: Glial cell-derived neurotrophic factor

GFAP: Glial fibrillary acidic protein

GWAS: Genome wide association studies

hAPP: Human APP

IPC: Intermediate progenitor cell

iPSC: Induced pluripotent stem cell

IPSC: Inhibitory post-synaptic current

IQR: Interquartile range

K-S: Kolmogorov–Smirnov

LED: Light-emitting diode

LOAD: Late-onset Alzheimer's disease

LTD: Long-term depression

LTP: Long-term potentiation

mEPSC: Miniature excitatory post-synaptic current

MGE: Medial ganglionic eminence

mGluR: Metabotropic glutamate receptor

mNgn2: Mouse Neurogenin-2

mRNA: Messenger ribonucleic acid

M-W: Mann-Whitney

NIM: Neural induction medium

NMDA: N-Methyl-D-aspartic acid

NMM: Neuronal maintenance medium

NPC: Neural progenitor cell

ns: Not significant

NSC: Neural stem cell

PBS: Phosphate buffered saline

PCW: Post-conceptional week

PPD: Paired-pulse depression

PPF: Paired-pulse facilitation

PTX: Picrotoxin

RMP: Resting membrane potential

RT: Room temperature

RT-PCR: Reverse transcriptase polymerase chain reaction

sAD: Sporadic Alzheimer's disease

SFEB: Serum-free embryoid body

STDP: Spike-timing dependent plasticity

STP: Short-term plasticity

tLTD: Spike-timing dependent LTD

tLTP: Spike-timing dependent LTP

Tuj: βIII-tubulin

VGCCs: Voltage-gated calcium channels

VZ: Ventricular zone

I: Introduction

The dysfunction of synaptic transmission is an important factor in many neurological disorders. This dysfunction can manifest at any stage of life, for example during development in disorders such as autism, or during aging as in neurodegenerative conditions like Alzheimer's disease (AD) [1]. If we are to advance our understanding of such neurological disorders, it is imperative that we develop experimental methods and models that give us access to the key cellular processes underlying disease progression. AD is the most common cause of dementia, which is characterized by memory impairment and cognitive dysfunction, and in many cases is accompanied by other psychiatric changes such as anxiety, depression and delusional episodes [2, 3]. AD affects approximately 5 % of the world's population and also represents one of the leading causes of death amongst adults over the age of 65 [4]. Furthermore, the global impact of this disease is only set to rise due to an increase in both the total number and the proportion of the population that are aged over 60 years as a result of increased life expectancy and declining birth rates [2]. AD has been extensively modelled in animals, which have provided the foundation for the majority of drug development strategies [5]. However, 99 % of AD therapeutics entering clinical trials fail, and no current AD treatments are able to modify disease progression, which suggests that pre-clinical research in a more human-relevant system could provide valuable insights into AD pathogenesis and enable the identification of potential targets for use in drug discovery [6, 7]. The worldwide prevalence of AD and lack of successful pharmacological and therapeutic interventions highlight the necessity to develop new methods to investigate human-specific processes involved in AD pathophysiology, which will be the focus of this thesis.

1.1. Alzheimer's disease

AD was first described by Alois Alzheimer in 1906, and is a neurodegenerative disease leading to progressive cognitive decline over decades. AD is characterized by the specific pathological hallmarks of extracellular amyloid plaques, which are insoluble deposits comprised mainly of

amyloid-beta (Aβ) 42 peptide, and intracellular neurofibrillary tangles, which are aggregates of hyperphosphorylated tau protein. The main hypothesis proposes that accumulation of Aβ is the disease trigger leading to downstream alterations in tau protein, synapse dysfunction and ultimately death of predominantly cholinergic and glutamatergic neurons [8]. The exact mechanisms linking Aβ to pathogenic alterations in tau are yet to be established, however there is considerable evidence that tau is essential for Aβ-mediated synaptic dysfunction and neuronal toxicity [9-11]. Aβ induces pathological hyperphosphorylation of tau that subsequently causes tau aggregation, mislocalization to somatodendritic regions and the formation of neurofibrillary tangles [12, 13]. Pathogenic tau hyperphosphorylation impairs the binding and stabilization of microtubules by tau, which can cause disruption of axonal transport and subsequent neuronal dysfunction [12]. Aβ has been shown to affect synapse function by altering NMDA receptor regulation and this can result in the activation of signalling pathways leading to excitotoxicity, which is one mechanism thought to be involved in neuronal death in AD [14-17].

The development of neurofibrillary tau tangle pathology follows a predictable pattern, first being observed in the transentorhinal area, spreading through the limbic cortex and hippocampus, then into the neocortex [18, 19]. However, the deposition of amyloid is often diffuse and does not follow that of neurofibrillary tangles [18, 19]. The extent of tau tangle pathology has been shown to correlate more closely with disease severity than amyloid plaque burden [20]. Aged, non-demented control individuals can show similar levels of amyloid pathology as AD patients suggesting that plaques alone are not sufficient to cause cognitive dysfunction [21]. This may seem contradictory to the leading hypothesis, however studies suggest that it is soluble Aβ oligomers that are the toxic species, rather than the insoluble aggregates [22]. In support of this, a study in human post-mortem tissue demonstrated that the ratio of soluble Aβ oligomers relative to plaque density was more highly correlated in AD patients than in non-demented controls with amyloid pathology, and was sufficient to separate the disease and control groups [23].

The greatest risk factor for AD is age, with less than 4 % of patients being under the age of 65, compared to 81 % that are over 75 years of age [24]. In the majority of cases there is no known cause of the disease, but in a small proportion (around 1% of cases) there is a known genetic mutation [25]. These mutations cause early-onset AD (EOAD; before the age of 65) and are largely autosomal dominant and highly penetrant. They have been identified in the genes encoding presenilin 1 (*PSEN1*), presenilin 2 (*PSEN2*) and amyloid precursor protein (*APP*) (see http://www.molgen.vib-ua.be/ADMutations [26]), which are involved in the generation of Aβ peptides. APP is a widely expressed transmembrane protein involved in signalling, although its specific function remains unclear. APP can be processed through the constitutive non-amyloidogenic pathway or the non-amyloidogenic pathway, depending on whether it is first cleaved by α- or β-secretase, respectively (***Figure 1.1a***). This initial cleavage event produces C-terminal fragments that are subsequently cleaved by γ-secretase, αCTF to p83, or βCTF fragments to Aβ [27]. The γ-secretase mediated cleavage can generate Aβ fragments of varying lengths depending upon cleavage site [28]. The shorter Aβ40 is the predominant species produced, however, it is Aβ42 which is the more hydrophobic and aggregation prone form [29]. The mutations in APP are clustered around the cleavage sites where they are thought to affect catalytic processing, and therefore Aβ production [30] (***Figure 1.1bi***). Individuals with trisomy 21 (Down Syndrome) are highly likely to develop Alzheimer's disease, and often by the age of 40, which may largely be due to overexpression of APP that is located on chromosome 21 [31]. Meanwhile, presenilin is part of the γ-secretase complex and, in comparison to APP, mutations in presenilin are distributed across the protein and may result in impaired protein function [30, 32] (***Figure 1.1bii***). These AD-associated mutations largely result in either increased production of Aβ42, or alterations in the ratio of Aβ42:40 [30, 33]. Despite a key role for tau in AD, no mutations have yet been associated with this disease. Instead, tau mutations have only been identified in relation to frontotemporal dementia [34].

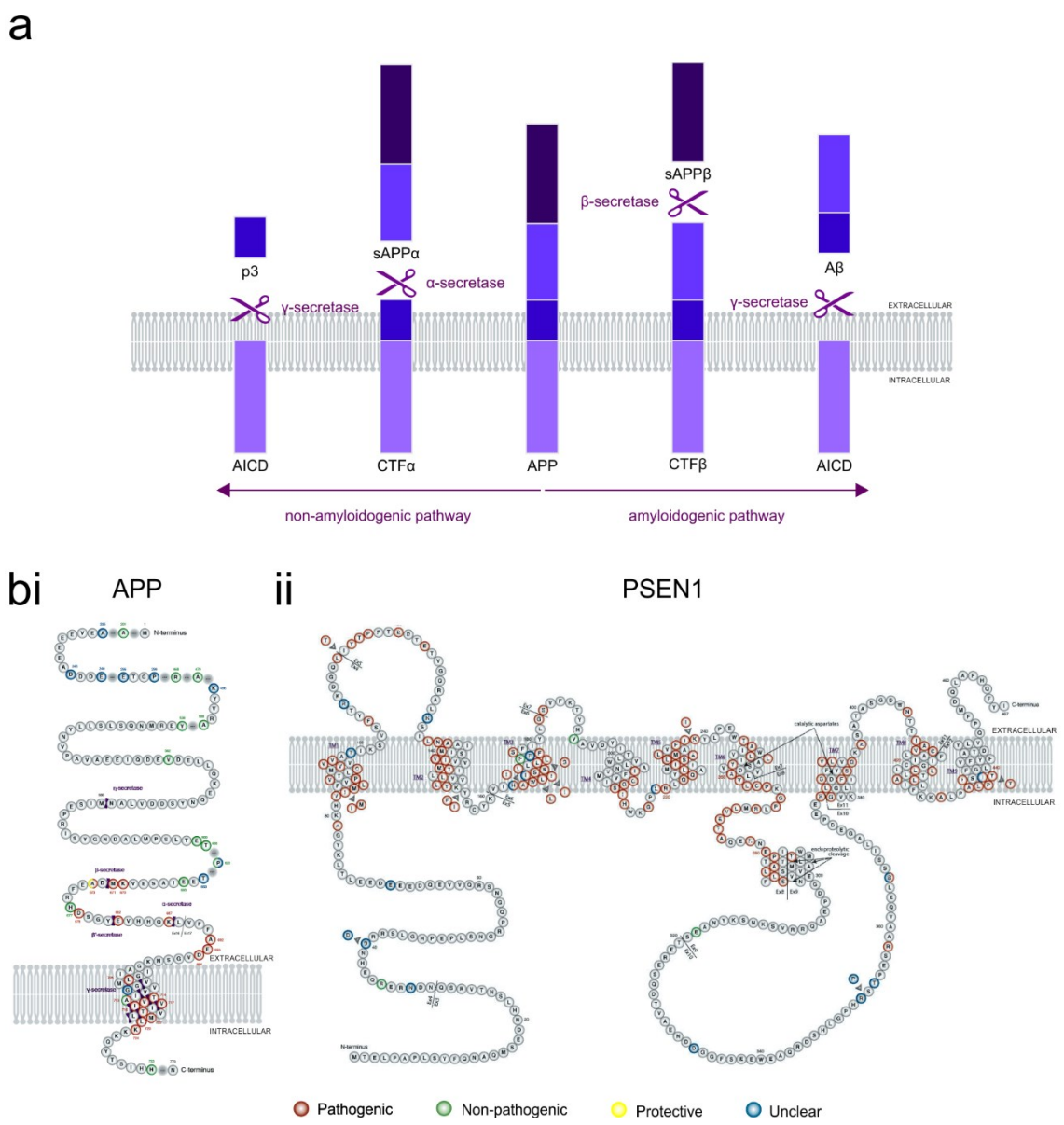

Figure 1.1. APP and PSEN1. (a) Schematic of the processing of APP. The non-amyloidogenic pathway involves the sequential cleavage of APP with α-secretase, to generate the soluble APPα (sAPPα) fragment and C-terminal fragment-α (CTFα), and then γ-secretase to generate the p3 peptide and the APP intracellular domain (AICD). In the amyloidogenic pathway, APP is first cleaved by β-secretase, to generate sAPPβ and CTFβ, and subsequently by γ-secretase to generate Aβ and the AICD. **(b)** Diagram showing the amino acid sequence for **(i)** APP and **(ii)** PSEN1. The fAD-associated mutations (red), non-pathogenic mutations (green), protective mutations (yellow) and mutations with unclear effects (blue) are highlighted on the sequence. The primary cleavage sites on APP are depicted in purple. Figure adapted from [35].

Late-onset AD (LOAD), diagnosed after the age of 65, is sporadic in nature and accounts for the vast majority of cases. However, the clinical presentation is highly similar to EOAD and evidence suggests that they are likely to converge upon the same pathological mechanisms [36]. Through genome-wide association studies (GWAS), the greatest genetic risk factor for LOAD has been identified as the ApoE4 allele [37]. There are three different isoforms of Apolipoprotein E (ApoE), E2, E3 and E4, which differ by only two single nucleotide polymorphisms, which are unique to humans. The majority of individuals are ApoE3/E3, however those that carry the ApoE4 allele have twice the risk of developing AD. This increases to five-times for E4 homozygotes, and ApoE4 carriers are likely to develop the disease at earlier ages [25, 38]. Conversely, ApoE2 is considered to be protective by lowering the risk of AD relative to the other alleles [39]. ApoE is a protein involved in the transport of cholesterol and other lipids for processes such as neuronal growth and repair. ApoE has also been shown to bind Aβ, and studies have found that the ApoE isoforms differentially affect the production, clearance efficiency and degradation of Aβ peptides [40-42]. A number of other AD genetic susceptibility factors have also been identified through GWAS studies [37, 43]. They have been associated with a range of functional roles which include the endosomal pathway, the immune system, lipid metabolism, axonal transport and cytoskeletal architecture, which are processes that can affect Aβ generation, trafficking and clearance [43].

There are currently only a small number of approved treatments for AD, which can provide some alleviation of symptoms but are unable to modify disease progression [6]. These drugs inhibit acetylcholinesterase to increase the levels of synaptic acetylcholine, or antagonise the NMDA receptor to protect against excitotoxicity. Meanwhile, there are a number of different strategies being used in the development of disease-modifying therapeutics. These approaches are largely based upon the amyloid hypothesis and therefore have focussed upon the generation of pharmacological compounds and immunotherapies that are designed to affect the production, deposition or aggregation of Aβ or tau protein [6].

1.2. Animal models of Alzheimer's disease

Animal models expressing familial AD (fAD) mutations have provided important insights into disease pathogenesis. However, animal models have struggled to recapitulate all aspects of disease pathology observed in humans. Mice expressing human APP (hAPP) containing fAD mutations can generate considerable amyloid-pathology and functional deficits, but lack neurofibrillary tangles and major neuronal loss [44]. The introduction of human APP with multiple fAD-associated mutations can accelerate pathology in transgenic mice, which demonstrate increased production of Aβ peptides, amyloid plaques and age-dependent memory impairment [45]. Furthermore, the age of amyloid pathology development correlates with the degree of APP overexpression [45]. Unlike humans, transgenic mice expressing fAD mutations in presenilin do not develop marked neuropathology, although have shown elevations of Aβ42 peptide and neuronal loss that increase with age [46, 47]. However, the introduction of presenilin mutations to transgenic mice expressing mutant APP has enabled the generation of age-dependent memory impairment and acceleration of amyloid pathology [46, 48, 49]. However, transgenic mice expressing mutations in PSEN1 and/or APP do not exhibit tau pathology. In order to produce pathological changes in tau in mice, researchers have had to introduce tau mutations, which are associated with frontotemporal dementia (FTD), not AD. When expressed alone, tau mutations result in neurofibrillary tangle formation and significant cognitive deficits, but in the absence of amyloid pathology, consistent with a FTD [50]. To generate tau pathology in addition to amyloid plaques, researchers have had to introduce tau mutations on top of fAD mutations in APP and PSEN1/2 [51]. The triple transgenic AD mouse model overexpresses P301L mutant human tau, hAPP with the Swedish mutation, and M146V mutant presenilin, and has been the most successful model to recapitulate AD pathology [51]. These mice generate age-dependent tau-tangle pathology in a distribution pattern akin to human AD patients, which develops after the deposition of amyloid plaques. The functional deficits in these mice occur before major pathology, but are associated with increased soluble Aβ levels

and intracellular Aβ immunoreactivity [51]. However, the pathology is not as extensive as that observed in humans and only minimal neurodegeneration occurs [52].

It is evident that researchers have been forced to take a combinatorial approach by multiple mutant transgenes in order to create more robust phenotypes and capture a more complete AD pathology in mice. However, these genetic alterations do not occur in human AD patients and the mutant transgenes are often expressed at non-physiological levels, therefore transgenic mouse models are not truly representative of fAD and cannot provide a model of sAD. Key genomic differences between rodents and humans are likely to contribute to their ability to capture human AD pathology. For example, mice and rats have a different Aβ sequence to humans and lack comparable post-translational modifications, which results in a peptide of higher solubility than human Aβ [53]. In adult humans six tau isoforms are expressed: 0N3R, 1N3R, 2N3R, 0N4R, 1N4R, 2N4R, with 3R and 4R expressed with approximately equal abundance [54]. In contrast, mouse and human tau share only 88 % sequence homology, and adult mice express only 4R isoforms and exhibit differences in subcellular tau distribution [52, 55]. The impact of these differences in tau is evident in humanized tau mice, which generate age-dependent tangle pathology only when human tau is expressed in the absence of mouse tau [56]. In contrast to mice, rats express 6 different tau isoforms that are highly similar to those found in humans. Although 4R tau is nine-fold more abundant than 3R tau in rats, compared to the 1:1 ratio observed in humans [57]. Interestingly, a transgenic rat that overexpressed the APP Swedish and presenilin ΔE9 mutations was able to generate significant age-dependent cognitive deficits associated with amyloid deposits, neurofibrillary tangles and neuronal loss without the expression of mutant tau [58]. A further confounding factor in rodent models of AD is the short lifespan of rats and mice. However, there has been evidence that another member of the rodent family, the degu, could exhibit spontaneous AD-like pathology when raised in captivity, which increases the mean lifespan from <1 year to 5-8 years [59, 60]. This phenotype may also result from a greater similarity in the amino acid sequence

of Aβ, which differs by only 1 residue, in contrast to mice and rats which differ by 3 residues, compared to human Aβ [59]. Whilst degus could present a promising rodent model of sAD, the development of AD pathology appears to be limited by laboratory breeding and extensive neuronal loss has not been observed [59-61].

The role of ApoE has also been explored in combination with other AD rodent models. ApoE mice expressing transgenes of different human isoforms can exhibit functional alterations alone, but crossing them with AD-mouse models has provided the opportunity to investigate the interactions between ApoE and Aβ [62] ApoE knockout mice expressing mutant V717F APP showed significantly fewer amyloid deposits, whilst soluble Aβ in younger animals was unchanged [63]. Lentiviral delivery of the different ApoE isoforms to the hippocampus of this mutant APP mouse differentially altered the levels of Aβ and amyloid deposits, with ApoE4 producing the greatest level of pathology, whilst the delivery of ApoE2 resulted in reduced amyloid burden [64].

It is evident that rodent models of AD can provide valuable insights into AD pathogenesis. However, such models have failed to recreate a complete Alzheimer's disease like phenotype using human AD-relevant approaches, which is a likely result of species-specific differences. Therefore, researchers have also explored the ability of other species to exhibit AD- like pathology. Rabbits share the same Aβ sequence and AD-like pathology can be induced by a high-cholesterol diet [65]. Dogs are more cognitively advanced than rodents and aged animals can spontaneously generate amyloid plaques, but do not exhibit tau tangles. Non-human primates are our most closely related species and do spontaneously develop neurodegeneration and cognitive deficits that are associated with amyloid plaques, and in some cases tau pathology [66]. Nevertheless, there are no animal models that have been able to generate qualitatively comparable AD-pathology to humans, which are able to capture the variations in the distribution of pathology across the brain and at a cellular level, and the biochemical properties of amyloid and tau aggregates [5, 66]

1.3. Alzheimer's disease and synapses

The extent of synapse loss has been identified as the best correlate of disease severity [67]. Cortical biopsies from patients with EOAD have shown a 25-35 % decrease in the total density of synapses and a 15-35 % decrease in the number of synapses per neuron [68]. Studies have also demonstrated a 25 % decrease in the immunoreactivity of the pre-synaptic protein synaptophysin in patients with early AD [69]. The extent of the synaptic loss associated with cognitive impairment has been found to correlate with total Aβ in post-mortem AD patient cortical tissue [70]. In transgenic animal models, similar synaptic deficits have also been observed that present before plaque generation, but correlate with the levels of soluble Aβ [71]. This has provided further support for Aβ as a causative factor in synapse loss. There is also mounting evidence, primarily from studies using rodent tissue, that Aβ can induce synaptic dysfunction before synapse loss occurs [72-74]. Most notably, many rodent models of AD have demonstrated alterations in synaptic plasticity [51, 75, 76]. This includes long-term potentiation (LTP), which causes a persistent increase in synapse efficacy and is considered to be the cellular basis of memory [77] (see section 1.7 for a review of synaptic plasticity).

Transgenic mice that express mutant human APP demonstrate a range of age-dependent synaptic deficits, although there are some discrepancies between studies that are yet to be understood. The synaptic deficits identified include impaired basal excitatory transmission, and deficits in the degree and maintenance of LTP, which have been primarily assessed in the hippocampus [72, 75, 78, 79] but also in the cortex [80, 81]. These deficits were often associated with poorer performance in memory-related behavioural tasks [72, 75, 78, 79]. In contrast, mice expressing presenilin mutations have demonstrated facilitated LTP whereby the magnitude or persistence of the potentiation is enhanced [51, 82-84]. This has also been associated with pre-synaptic changes in neurotransmitter release probability [51]. In addition, mutant presenilin has been shown to confer increased vulnerability to glutamate-mediated excitotoxicity [83]. It is thought that these effects

may be attributed to a role of presenilin in intracellular calcium regulation via modulation of endoplasmic reticulum calcium stores [83, 85]. However, when the presenilin mutation (M146V) is combined with mutations in tau and APP, in a model that more closely recapitulates human AD pathology, there are age-dependent impairments in basal excitatory synaptic transmission and hippocampal LTP [51].

It is clear from studies of knock-out mice lacking APP or presenilin that these proteins have important roles in synaptic transmission, plasticity and neuronal viability. In the hippocampus of mice lacking APP, neurons show a decreased dendritic length and deficits in LTP [86]. Knockout of presenilin 1/2 is embryonic lethal, likely due to its role in Notch signalling during development [87]. However, mice with a conditional postnatal double knockout of presenilin 1/2 in the forebrain exhibited mild memory impairments and a significantly reduced magnitude of LTP [88]. Later studies determined that it was pre-synaptic presenilin expression that was critical for LTP induction [89]. Normal basal transmission was not altered in these mice, although there were alterations in the relative levels of post-synaptic glutamate receptors. Furthermore, older mice also developed hyper-phosphorylated tau and exhibited considerable neurodegeneration [88].

Meanwhile, the application of exogenous Aβ, either *in vitro* or *in vivo,* consistently results in impaired LTP in rodents [9, 74, 90, 91]. Focal injections of synthetic Aβ into the dorsal dentate gyrus of the rat has led to the deposition of amyloid and neuronal atrophy around the injection site. When assessed functionally 4 weeks following injection, this resulted in a significant reduction of both baseline synaptic transmission and the magnitude of LTP [90]. Similarly, the acute application of synthetic human Aβ *in vitro* onto rodent hippocampal slices impairs LTP, although does not affect basal synaptic transmission [9, 73, 92]. These effects of Aβ1-42 could also be reproduced by the shorter, non-fibril forming, but toxic Aβ25-35 fragment [73, 92]. The aggregation state of synthetic Aβ peptides can be difficult to define and may not accurately mimic physiologically occurring Aβ species [93, 94]. Therefore, researchers have explored the use of naturally occurring Aβ species.

Human Aβ oligomers can be secreted by cell lines expressing human APP and exhibit similar properties to the soluble species found in AD patient tissue [95]. In rats, the injection of cell medium derived from mutant hAPP expressing cells has been shown to inhibit LTP *in vivo* [96]. The enzymatic degradation of Aβ monomers did not relieve the effect, thereby implicating oligomeric forms as the toxic species [96].

Rodent models have also provided insights into the mechanisms by which Aβ causes synaptic toxicity and have implicated tau as the key mediator. The exposure to Aβ fibrils for 1- 4 days causes degeneration of cultured rodent neurons, which can be abolished by the knock-out of tau protein [10]. Furthermore, in rodent hippocampal slices the Aβ-mediated impairment of LTP is blocked by the absence of tau [9]. Pharmacological inhibition of GSK3β, a kinase that can mediate Aβ-induced tau hyperphosphorylation, was sufficient to rescue the LTP impairment in wild type tau-expressing mouse tissue [9]. Similarly, hAPP mutant mice showed reduced learning deficits, despite comparable amyloid pathology, and protection against excitotoxic insults following the *in vivo* knockout of tau [11]. A study comparing the protein components of the human and mouse cortical post-synaptic compartment has shown differences in both the composition and relative abundance of proteins in the post-synaptic density between the two species [97]. Whilst ≈ 1500 post-synaptic proteins were identified in each species, 30 % of proteins were non-overlapping and only present in either humans or mice. Furthermore, many well-characterized post-synaptic proteins were expressed at several-fold greater abundance in mouse, than in humans [97]. As a result, the processes that occur at human cortical synapses following exposure to pathological levels of Aβ may differ from those observed in rodents.

The study of cortical tissue from Alzheimer's disease patients has been limited to post-mortem samples, which not only largely represents the end-stage of the disease, but prohibits functional assessment. Meanwhile, live resected neuronal tissue can occasionally be obtained from patients during surgery for neurological conditions such as epilepsy or brain tumours. However, to my

knowledge, the assessment of neuronal function in resected tissue from AD patients, or the evaluation of Aβ-induced functional effects in resected tissue from individuals without dementia, has not been performed. As a result, researchers have used non-invasive methods to explore LTP-like phenomena (see section 1.7) in healthy control subjects and AD patients. Such methods cannot directly assess changes in synaptic function however, the electrical readout in response to electrical stimulation protocols suggest that underlying changes in synaptic efficacy do occur. In line with rodent models of AD, these studies have demonstrated a specific impairment of LTP in the cortex [80, 98-100]. Comparatively, long-term depression (LTD), which causes a persistent reduction in synaptic efficacy, appears to be unaffected [98-100].

1.4. Induced pluripotent stem cell (iPSC) technology

The development of human induced pluripotent stem cell (iPSC) technology has marked a new chapter in research. This is particularly evident for the field of neuroscience [101] and is likely to be due to the scarcity of neurological tissue, which is also primarily acquired post-mortem and thus offers a limited insight into early stages of disease pathogenesis. Preceding the development of iPSC technology, embryonic stem cells (ESCs) were the only mammalian pluripotent cell type identified. Human ESCs have been used for disease modelling of a relatively small number of monogenetic disorders that can be identified through pre-implantation genetic screening or that have been generated using gene editing techniques [102-105]. Comparatively, the generation of human iPSCs has enabled the exploration of disease pathogenesis in human cells that have been derived from patients with a detailed clinical history, which could be used to associate iPSC-derived cellular phenotypes with the characteristics of disease presentation or progression. Furthermore, patient-derived iPSCs can provide the opportunity model a wide range of disorders, from monogenic diseases to sporadic or polygenic disorders.

ESCs and iPSCs are pluripotent stem cells, which are able to undergo unlimited proliferation and possess the ability to differentiate into any cell type in the body. ESCs are derived from the inner cell mass of the blastocyst, which forms early in mammalian development [106]. In the developing embryo, ESCs differentiate into the three germ layers (endoderm, mesoderm and ectoderm), which ultimately generate all the tissues in the body [106]. In 1981, the first established embryonic stem cell lines were isolated from mouse blastocysts and successfully maintained in culture [107]. Nearly twenty years later, the isolation of the first human ESC lines was reported and two of these lines, H1 and H9, are often considered to be the "gold standard" human stem cell lines for differentiation studies [108]. However, the ethical issues surrounding the generation of these cell lines limits the routine and widespread use of human ESCs.

It is now more than 10 years since Yamanka and colleagues discovered that differentiated, somatic cells could be converted back into an embryonic-like state by the delivery of just four key transcription factors: Oct3/4, Sox2, c-Myc, and Klf4 [109]. They initially started with 24 candidate genes that were involved in pluripotency or associated with tumorigenesis and when delivered in combination to mouse fibroblasts could generate stem-cell like colonies. Through the assessment of colony-formation after the withdrawal of individual genes, these were narrowed down to just 4 genes that were sufficient and necessary to generate and maintain ESC-like characteristics in culture. The pluripotent nature of these cells was assayed by teratoma formation in which they were able to generate cells from all three germ-layers [109]. The iPSCs clustered with ESCs in their global gene expression, and also separated from their parental fibroblasts [109]. Having performed their initial experiments using mouse fibroblasts, they later demonstrated that iPSCs could also be generated from human fibroblasts (***Figure 1.2***) [110]. Since these seminal papers, iPSCs have also been derived from a number of other somatic cell types, which are largely acquired by invasive methods, such as blood cells [111] and dental pulp stem cells [112]. The initial generation of iPSCs relied on transgene delivery and integration via retrovirus [109], but this approach carries the risk

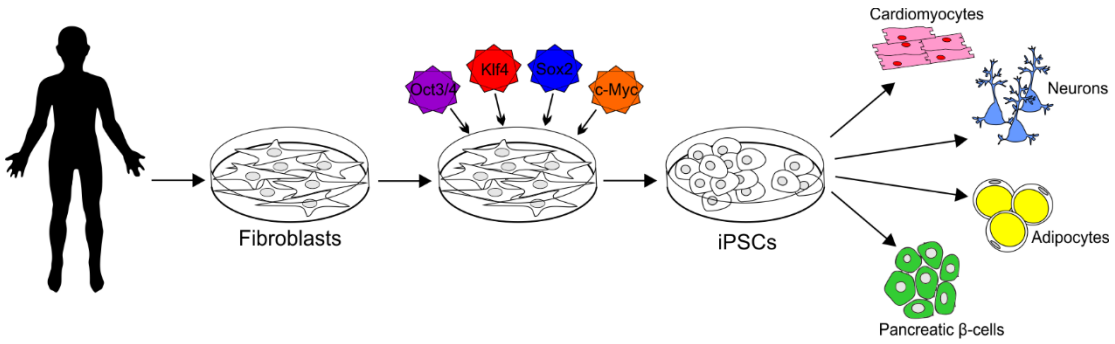

Figure 1.2. Overview of iPSC technology. Fibroblasts can be cultured from skin biopsies acquired from patients or healthy control individuals. For reprogramming, the four Yamanaka factors (Oct3/4, Klf4, Sox2 and c-Myc) are delivered by virus to the cultured fibroblasts. This results in the generation of colonies of iPSCs, which can be isolated and expanded. The iPSCs are pluripotent stem cells and can be differentiated into any cell type in the body, for example, cardiomyocytes, neurons, adipocytes, or pancreatic β-cells.

of transgene reactivation and tumorigenesis in the case of transplanted cells [113]. More recently, non-integrating methods of transgene delivery have been developed. The most successful and efficient is the use of the RNA-based Sendai virus, which enables the expression of exogenous genes at high-levels, and has since been commercialised into reprogramming kits that can be applied to many different cell types [114].

Human iPSCs and ESCs are often assumed to possess comparable properties, but differences in transcriptomic profiles, epigenetic signatures and differentiation capacity have shown that these cell types are not equivalent [109, 115-120]. iPSC lines have shown varying degrees of incomplete reprogramming, evident from differentially methylated regions, and do not exhibit epigenetic modifications comparable to ESCs [115]. Furthermore, iPSCs have also been shown to retain epigenetic signatures present in the somatic donor cells from which they were derived [121]. This so-called “epigenetic memory” has been implicated in the variable differentiation potential of iPSC lines, such that iPSCs derived from the same donor cell type cluster together at a transcriptomic level, and more readily differentiate into the same cell type from which they were derived [116, 117]. A study has reported that background genetic variability between individuals generates the greatest difference in transcriptional profiles between cell lines [122]. To overcome this obstacle,

studies investigating monogenetic diseases are now taking advantage of gene editing technologies to generate isogenic cell lines, which differ only by the presence or absence of a mutation relative to the parent cell line [123]. This approach should enable a more precise investigation of the contribution a specific mutation has in disease pathogenesis, and control for individual-specific genetic variation.

Regardless of the issues iPSCs can present, these cells offer a unique opportunity to investigate disease pathogenesis in familial and sporadic disorders in a human system, and also provide a human-specific platform for drug discovery and assessment of toxicity. The “3 pillars of survival” describe three key elements that are fundamental for the success of a candidate drug in clinical trials. The first pillar; exposure to the target site of action, requires a whole-organism approach to determine the pharmacokinetics of the drug and in the case of neurological disorders, blood-brain barrier penetration [124]. However, the other two pillars; target binding and functional efficacy could be assessed in an *in vitro* human system [124, 125]. One possibility is the use of resected non-pathological human brain tissue, however, this is a limited resource, has a finite lifespan and is obtained from patients with neurological conditions with unknown consequences on neuronal physiology. Comparatively, human iPSC-derived neuronal models have the potential to overcome these limitations and following further development and optimisation could be a valuable resource for drug discovery [125]. An example of the promise that iPSCs may offer comes from a study of amyotrophic lateral sclerosis (ALS). Motor neurons were generated from ALS patient-derived iPSCs and demonstrated a hyperexcitable phenotype associated with alterations in the activity of a subtype of potassium channels. The authors were able to correct the phenotype with an already approved antiepileptic drug, which subsequently resulted in phase II clinical trials to assess its efficacy in ALS [126, 127]. Whilst completed in February 2018, the results are yet to be reported (ClinicalTrials.gov Identifier: NCT02450552). Although primarily using human ESC-derived cells, researchers are also exploring the potential for cell transplantation therapy. To date, a small

number of cell transplantation therapies have entered the early stages of clinical trials, which primarily assess safety and side effects of the treatment [128]. Specifically, transplantation of autologous or allogeneic iPSC-derived cell types may be able to circumvent the problem of transplant rejection, which is associated with a lack of histocompatibility [129]. Indeed, the first iPSC based transplantation therapy was performed in Japan in 2014 to one patient with wet acute macular degeneration [130]. Two years after the surgery no adverse effects were reported and there was no indication of graft rejection, despite the absence of immunosuppressive treatment, and the patient's corrected visual acuity had neither been improved nor worsened. This study shows that cellular transplantation therapies may be feasible, although future assessments will determine whether this treatment provided any clinical benefit [130].

1.5. The differentiation of human iPSCs into cortical neurons

The dysfunction of cortical excitatory synaptic transmission is thought to be involved in many neurological disorders, such as autism and schizophrenia. Specifically in AD, the cortex exhibits extensive degeneration, and the density of synapses in this region inversely correlate with disease severity [68, 131]. There are now a multitude of published protocols generating cortical neurons from stem cells. These have adopted two main strategies: 1) to mimic the developmental cues that occur during *in vivo* generation of the cortex, or 2) to force the expression of transcription factors that are switched on during cortical differentiation.

Development of the cortex

In the developing embryo, the ectoderm goes through a process of infolding, known as neurulation, in order to generate the neural tube structure that subsequently differentiates to form the entire central nervous system [132]. The notochord, a temporary structure derived from mesoderm, secretes the factors noggin, chordin and follistatin. These factors act to inhibit the formation of epidermis from ectoderm by antagonizing bone morphogenic protein (BMP) signalling and allowing

the cells to differentiate down the “default” pathway to neuroectoderm and then proliferative neuroepithelium [132, 133]. Before each end of the neural tube closes, the rostral end undergoes rapid expansion and division to form the forebrain, midbrain, hindbrain and ventricles. The telencephalon, the most anterior part, goes on to form the cortex [134]. The neuroepithelial cells of the telencephalon first divide symmetrically to form the ventricular zone (VZ), and then asymmetrically to generate neurons. During neurogenesis the neuroepithelial cells undergo changes in morphology to become radial glia. These cells express the transcription factors Pax6, Foxg1 and Emx1/2, and extend a long apical process to the pial surface, along which newborn neurons migrate [135, 136]. In addition to neurons, radial glia generate two populations of progenitor cells that reside above the VZ in the sub-ventricular zone (SVZ). These are known as intermediate progenitor cells (IPCs) that express Tbr2, but not Pax6, and outer radial glia (oRG) [135, 136]. The cortex is a laminar structure that is formed in an inside out fashion. Initial pioneer neurons, predominantly Cajal-Retzius cells, migrate and occupy the space between the VZ and the pial surface to generate layer I, also known as the preplate. Subsequently, newly born neurons generate layers VI-II between the VZ and the preplate, starting with the deep layers first and the upper layers later [135, 136]. These neurons that populate the cortical plate are solely excitatory and glutamatergic in nature. The bulk of evidence suggests that cortical GABAergic interneurons are generated more ventrally in the ganglionic eminences and migrate tangentially into the cortex [137]. However, there are reports that a population of interneurons may also be generated in the human cortex [138]. After a period of neurogenesis, the progenitor cells switch to gliogenesis to produce the astrocytes that reside in the cortex [136].

Directed differentiation of iPSCs into cortical neurons using patterning factors

Early studies that attempted to initiate neural differentiation from human stem cells started with the formation of embryoid bodies (EBs). The formation of EBs, which are 3D aggregates of pluripotent stem cells, causes the initiation of spontaneous differentiation. Zhang et al., (2001)

described the generation of proliferative nestin-positive neural stem cells, organized into rosettes, when EBs derived from human ESCs were cultured in suspension in the presence of FGF2 [139]. Dissociation into an adherent culture and withdrawal of FGF2 stimulated the differentiation into mainly glutamatergic MAP2/Tuj-positive neurons and GFAP-positive astrocytes when cultured for longer periods [139]. A similar approach was also developed in a mouse ESC system, termed the serum-free embryoid body (SFEB) protocol [140]. This study utilised Wnt and Nodal antagonism during the early stages to drive a more efficient neural differentiation. The use of the patterning factors Wnt3a and Shh to drive dorsalization for Pax6-positive cells or ventralization for Nkx2.1/Islet1/2 respectively, was also described [140]. The protocol was further optimized by accelerating the more uniform formation of EBs using quick-aggregation methods, which improved forebrain differentiation efficiency, and was later adapted for use with human ESCs by the addition of the anti-apoptotic ROCK inhibitor Y-27632 [141, 142]. The SFEB protocol generated a 3D polarized structure with an inner proliferative zone and an outer neuronal shell, which was maintained for up to 121 days [142, 143]. These structures exhibited some degree of regional separation, reminiscent of *in vivo* cortex formation. The inner Pax6-positive progenitor zone had Tbr2-positive IPCs, which were largely distributed as an upper layer. Above this SVZ-like region formed a layer of post-mitotic neurons that were predominantly positive for the deep-layer markers Tbr1 and Ctip2, but there also included a small population of upper-layer Satb2 positive neurons. The 3D structure also demonstrated dorsal-ventral polarity marked by the presence of separate domains expressing Pax6 or Nkx2.1 [142, 143]. This protocol was later applied by Mariani et al., (2012) to two different human iPSC cell lines that also produced 3D structures containing predominantly deep-layer neurons. The global gene expression of the aggregates after 50 days *in vitro* was largely correlated with cortical tissue samples of 8-10 postconceptional weeks (PCW) [144].

Using a similar approach, Lancaster et al., (2013) described the formation of large 3D brain organoids comprised of distinct regions that resembled brain structures, such as the cortex, choroid plexus and retina, based upon histology and gross morphology [145]. Instead of static suspension culture, the authors found that a spinning bioreactor generated a more continuous neuroepithelium instead of multiple rosette-like structures. In cortical regions a degree of spatial separation of layer-specific neurons was also observed. Whilst the organoids could survive for extensive culture periods, their maximal size was limited by an inability of oxygen and nutrient penetration to the dense tissue, which resulted in the formation of a necrotic core [145]. This study also generated organoids from iPSCs derived from a patient with a severe genetic microcephaly, which demonstrated a phenotype of premature neural differentiation reflected by an increase in the ratio of neurons to radial glia [145].

Despite the ability of aggregate-based protocols to recapitulate many aspects of *in vivo* human cortical development, the structures can be highly heterogeneous in nature and present limitations to imaging and functional analysis [145]. To counteract this, researchers have looked to develop simple and defined neural differentiation protocols that could be applied to adherent stem cell monolayers to increase homogeneity. These strategies sought to mimic the developmental cues that drive neurulation *in vivo*. However, the inhibition of BMP signalling alone, by mammalian recombinant noggin, was not sufficient to drive efficient neural induction from stem cells. Signalling by Activin and Nodal are involved in maintaining the self-renewal and pluripotency of stem cells, and also in the generation of mesoendoderm [146, 147]. Chambers et al., (2009) identified that the inhibition of BMP, Activin and Nodal and subsequent downstream SMAD signalling via the application of Noggin and SB431542 was highly efficient at inducing the neural fate of adherent, monolayer human ESCs [148]. This approach, termed dual-SMAD inhibition, has since been used as the basis for many hiPSC-derived neuronal differentiation protocols.

In 2012 Shi et al., described the generation of cortical neurons over a period of 90 days from iPSCs using a simple, dual-SMAD inhibition based protocol [149, 150]. Like EB-based methods, this protocol also captured many of the cell types and temporal order seen in *in vivo* human cortical development. Cells expressing the markers and morphology of radial glia, IPCs and oRG were all observed [150]. Following neural induction the progenitor cells formed polarized rosettes that shared many characteristics of neural tube derived neuroepithelium, such as interkinetic nuclear migration during ventricular mitoses. The neurons generated were reported to be purely excitatory and contained subpopulations expressing a number of different transcription factors that are representative of each of the cortical layers. BrdU birthdating also revealed that the neurons matched the temporal sequence of layer generation, with most deep-layer Tbr1-positive neurons generated by day 50 whilst upper-layer Satb2-positive neurons appeared after day 65, however no spatial organisation was evident. After several months in culture, qualitative evidence was presented to show that the cells could demonstrate the functional properties that are the hallmark of neurons, including action potential firing and glutamatergic synaptic activity [150].

Pasca and colleagues adapted the monolayer-derived dual SMAD inhibition approach to generate 3D aggregates consisting of only forebrain cortical-like tissue, comparable in size to brain organoids [151]. Freely-formed iPSC-aggregates were subjected to dual-SMAD inhibition to induce neural differentiation, which was followed by growth in EGF and FGF2 containing media to promote progenitor cell proliferation. The removal of growth factors and addition of neurotrophic factors caused neuronal differentiation. As with others, this model conserved the temporal order of layer-specific cortical neurons but also showed a degree of cortical lamination reflected by the more superficial localization of upper-layer neurons, relative to neurons expressing deep-layer markers. At 10 weeks these cultures contained equal representation of upper and deep-layer neurons and had a transcriptional profile similar to human tissue of 19-24 PCWs [151].

Generation of human cortical neurons by forced expression of transcription factors

An alternative approach to differentiate neurons is to force the expression of transcription factors that are expressed during neural fate commitment and neuronal differentiation. This was initially developed using somatic cells, which avoids the time-consuming and inefficient step of reprogramming to iPSCs, and also ablates the risk of tumorigenicity as cells do not have an intermediate proliferative stage. The starting material was primarily cultures of fibroblasts, but these cells can exhibit slow proliferation and limited self-renewal that consequently affect total cell yield and scalability [152-154]. The nature of this method means that the range of neural subtypes, their temporal sequence of production and spatial organization seen in development are poorly recreated.

In 2010 Vierbuchen et al., tested a pool of 19 genes for their ability to elicit neuronal conversion in mouse embryonic and postnatal fibroblasts [152]. Through a number of experiments they were able to reduce this pool to a combination of 3 key genes, Brn2, Ascl1 and Myt1l, subsequently known as the BAM factors, which were able to convert fibroblasts to functional neurons. The majority of cells differentiated into excitatory neurons expressing the deep-layer marker Tbr1, whereas less than 1 % were GAD-positive interneurons. However, only approximately 20 % of the initial cells plated were Tuj-positive neurons indicating that the conversion process was relatively inefficient [152]. This method also successfully converted human ESCs but required the addition of NeuroD1. However, the conversion rate was far lower in the human system, with less than 5 % cells converted to neurons, of which a considerable proportion expressed a marker of peripheral neurons [154]. The efficiency of neuronal conversion was shown to be enhanced by the addition of two microRNAs, miR-9/9* and miR-124 [155].

To boost cell yield others have explored the direct conversion of fibroblasts to a proliferative neural stem cell (NSC) intermediate stage before differentiation [156, 157]. A further advantage of this

method is that the NSCs can generate cells of multiple neural lineages. Therefore, this multipotency can enable the production of numerous neuronal subtypes, astrocytes and oligodendrocytes. However, the initial conversion event is a highly inefficient process [156, 157].

The lack of efficiency and fibroblast associated limitations has limited the appeal of many of these direct neural conversion protocols. Zhang et al., (2013) more recently demonstrated that expression of a single pro-neural transcription factor, neurogenin-2, could drive an efficient and rapid conversion of human ESCs and iPSCs to cortical neurons. They also reported that comparable effects could be achieved by the expression of NeuroD1 [158]. This method yielded a largely pure population of excitatory neurons expressing Brn2 and Foxg1 transcripts, consistent with a layer 2/3 cortical phenotype [158]. The neurons demonstrated action potential firing and the formation of active, excitatory synaptic networks, but lacked the expression of subtypes of glutamate receptors that are critical for synaptic plasticity [158].

In general, transcription-factor based conversion protocols can enable neuronal differentiation in a considerably shorter time period, but can lack representation of the full diversity of cortical layer markers, in contrast to directed differentiation protocols [150, 158]. Typically, the functional characteristics of neurons generated by all of these protocols display immature properties, and often only qualitative descriptions are reported [118, 150, 159-163]. Therefore, the field requires the thorough assessment of iPSC-derived cortical neuronal function and the development of methods to promote maturation.

1.6. The modelling of AD using neurons generated from human iPSCs

There have been numerous publications that have utilised human stem cell-derived neurons, primarily grown in 2D cultures, to model Alzheimer's disease. These studies commonly use iPSC lines that have been generated from patients with familial mutations [160, 164-173]. However, cell lines derived from sporadic patients have also been used [160, 164, 170, 173, 174]. In other cases,

researchers have used genetic engineering to introduce fAD mutations into healthy control iPSC lines [175, 176], or have assessed the responses of healthy control iPSC-derived neurons to cell stressors, such as Aβ [177, 178]. Human stem cell lines with AD-associated mutations are commonly reported to have equal differentiation capacity to controls [160, 164, 166, 167, 169] Although, one study has described premature neuronal differentiation in two patient lines with mutations in PSEN1 [179].

The levels and composition of secreted Aβ peptides is the most widely assessed property in iPSC-derived neuronal models of AD. An increase in the Aβ42:40 ratio has been consistently and robustly demonstrated in nearly all fAD patient neuronal cultures, which includes numerous mutations in PSEN1 (A246E, M146I/L, Y115C, S169Δ, Intron 4Δ), PSEN2 (N141I), APP (V717I/L, E693Δ), trisomy 21, and APP duplications [164-171, 173, 179]. In some cases, differences have also been identified in the total production of Aβ peptides, which primarily manifests as an elevation of total Aβ42 levels [160, 164-167, 170, 171, 173, 179, 180]. Meanwhile, the demonstration of changes in secreted Aβ peptides in sporadic AD (sAD)-patient derived neurons has been much more variable, whereby only subsets of sAD cell lines have exhibited significant differences relative to healthy control neurons [160, 164, 170, 173]. This is perhaps unsurprising given that the pathogenesis of sAD is thought to involve the interaction of numerous genetic and environmental factors, and thereby indicates that modelling the sporadic form may require a greater level of complexity. The generation of Aβ peptides in iPSC-derived neurons has been shown to significantly increase with the age of the culture [166, 167]. As the greatest risk factor for sAD is age [24], limits on culture duration may contribute to the absence of Aβ phenotypes in some sAD cell lines. There have also been a small number of reports describing the presence of oligomeric Aβ species and the formation of Aβ aggregates that occur at both intracellular and extracellular locations [164, 167, 180, 181]. Indeed, it appears that 3D cultures, such as organoids [180] or cultures that use artificial matrices [181],

may limit the diffusion and clearance of secreted peptides, which is likely to be beneficial for studies trying to recapitulate insoluble or aggregated pathogenic proteins.

The occurrence of tau phenotypes has been less frequently described in AD patient iPSC-derived neurons. These include increases in phosphorylated or total tau, and aberrant tau localisation [160, 165-167, 172, 179, 180]. However, the appearance of these phenotypes has typically required a more prolonged culture period than was necessary for the alterations in Aβ peptides [166, 180]. A number of other biochemical phenotypes that are consistent with AD pathology have also been reported in iPSC-derived models of AD. Post-mortem tissue has shown an accumulation of large endosomes in some AD-patient brains, and evidence suggests that the majority of amyloidogenic processing of APP occurs in the endosomal compartment [182, 183]. In line with these observations, several iPSC-derived models of AD have demonstrated increases in the numbers of large endosomes and increased co-localisation of APP with endosomal markers in neuronal cultures generated from fAD patient cell lines with mutations in APP [160, 166, 180]. In addition, there have also been reports of increased reactive oxygen species production, ER stress and decreased cell viability in AD patient iPSC-derived neurons [164, 167].

Perhaps the most successful human cell culture model of AD-associated Aβ and tau phenotypes was by Choi et al., (2014), which demonstrated insoluble aggregates most akin to the AD pathology observed in post-mortem tissue [181]. Instead of using iPSCs, Choi et al., (2014), utilised an immortalized human neural progenitor cell (NPC) line. The NPCs were transduced with lentiviral constructs encoding APP with multiple mutations (K670N/M671L and V717I) and mutant PSEN1 Δ Ex9 in order to overexpress these mutant fAD proteins. Subsequently the cultures were enriched for transgene-expressing NPCs via FACS, embedded into a 3D matrigel matrix and differentiated into neurons. 3D cultures of mutant cells exhibited aggregated insoluble Aβ and elevated phosphorylated Tau, which could be associated with dystrophic neurites in cells with a high tau

burden. Cultures enriched for high mutant transgene expression also produced a fraction of insoluble, detergent-resistant, filamentous tau [181].

It is thought that fAD mutations cause alterations in APP processing that lead to changes in Aβ peptide production and composition [30]. Therefore, many iPSC-derived AD studies have explored whether the pharmacological manipulation of the β and γ-secretases involved in amyloidogenic processing affect Aβ peptides and other phenotypes. The ability for γ-secretase inhibitors and modulators to reduce Aβ peptide production or alter the ratio of Aβ-peptide species has been consistently demonstrated [160, 166, 167, 169]. Meanwhile, in some cases, γ-secretase inhibitor treatment has also abolished the phenotypes observed in tau, whilst in other studies the inhibition of β-secretase inhibitors was required, either alone or in addition to γ-secretase inhibition [160, 180, 181]. To further interrogate the interactions between Aβ and tau, Moore et al., (2015) differentiated several iPSC lines with mutations in APP and PSEN1 and observed that the presence of a tau phenotype did not correlate with the Aβ42:40 ratio [165]. They went on to demonstrate that the modulation of APP metabolism via pharmacological alteration of γ-secretase or β-secretase activity could affect tau expression, irrespective of genotype. Overall, the relationship between Aβ species and tau phenotypes in human iPSC-derived neurons requires further investigation, and studies have suggested that APP cleavage molecules other than Aβ may be involved.

A number of studies have used stem cell-derived neurons generated from healthy individuals to investigate cell subtype specific vulnerability in AD [178, 184]. One study showed that iPSC-derived glutamatergic neurons were more susceptible to toxicity induced by exogenous Aβ peptides than GABAergic neuronal populations [178]. The glutamatergic neurons appeared to have a greater affinity to bind Aβ oligomers, which was further enhanced by age [178]. Meanwhile, another study used the transplantation of human ESC-derived neurons into the brain of an AD mouse model to demonstrate that human neurons show greater vulnerability and more exaggerated pathology than mouse neurons [184]. In this case, the human neurons appeared to integrate into the host tissue

and the grafted cells were assessed up to 8 months after transplantation. Over this period, the human neurons exhibited greater decreases in dendritic projections around Aβ plaques and increased presentation of dystrophic neurites. The degeneration of human neurons, but not mouse neurons, was associated with the development of Aβ plaques, and up to one-third of human neurons had evidence of necrosis, which was not observed in host neurons or human neurons that had been grafted into wild-type mice [184].

As described above, the majority of phenotypes demonstrated in iPSC-models of AD are simple, biochemical changes that are consistent with disease pathology. However, some researchers have begun to investigate whether these models exhibit synaptic alterations. Molecular assessment of synaptic puncta in fAD patient-derived neurons has not revealed any differences in synapse density [160, 167]. Meanwhile, the functional assessment in these studies has been largely limited to the qualitative demonstration of action-potential firing and voltage-gated currents [160, 164, 167, 168, 173]. To date, there have been no reports evaluating the synaptic function of AD patient iPSC-derived neurons. However, ESC-derived neurons overexpressing mutant PSEN1 have exhibited decreased spontaneous excitatory synaptic activity, whilst inhibitory activity was unaffected [176]. Meanwhile, a decrease in miniature EPSC (mEPSC) amplitude, which was associated with a reduction in the density of post-synaptic AMPA receptor clusters, was detected in healthy control iPSC-derived neurons following an 8 day incubation with Aβ peptides after an extensive culture period [177].

1.7. Synaptic plasticity

Experimental evidence and molecular mechanisms of glutamatergic synaptic plasticity

Synaptic plasticity is the ability of a synapse to undergo activity-dependent changes in strength and is typically assessed by measuring the size of an evoked synaptic response. The first-described form of synaptic plasticity, and the most well studied, is LTP [77]. The concept of LTP was first postulated

in 1949 by Hebb whom proposed that “When an axon of cell A is near enough to excite a cell B and repeatedly or persistently takes part in firing it, some growth process or metabolic change takes place in one or both cells such that A's efficiency, as one of the cells firing B, is increased” [185]. However, LTP was not reported experimentally until almost 25 years later, which described a persistent synaptic potentiation in response to high-frequency stimulation in the rabbit hippocampus *in vivo* [186, 187]. Subsequently, further investigation into the expression and mechanisms of LTP became more accessible following the demonstration of robust LTP in hippocampal slice preparations [188], which are now a widely used model. LTP has been described in many brain regions and is commonly induced by repetitive extracellular high-frequency electrical stimuli that result in an enhancement of synaptic efficacy, reflected by an increased amplitude of the post-synaptic potential [188-191] (***Figure 1.3a***). These studies take advantage of the known functional circuitry that is retained in slice preparations, which can enable the spatial separation of afferent pathway stimulation and the recording of a post-synaptic response, often from a neuronal population. The optogenetic tool, Channelrhodopsin-2 (ChR2), has provided an alternative and non-invasive approach to stimulate afferent pathways. ChR2 is a light-activated ion channel that, when expressed by neurons, causes depolarization and reliable action potential firing in response to light stimulation [192]. In this manner, the targeted light activation of a pre-synaptic ChR2-expressing neuronal population has been used evoke a post-synaptic response for the study of synaptic plasticity [193, 194].

The induction of LTP requires concurrent synaptic activation and post-synaptic depolarization in order to relieve the NMDA-receptor voltage-dependent Mg^{2+} block and thereby enable the influx of calcium into the post-synaptic terminal. It is the role of the NMDA-receptor as a molecular coincidence detector that confers the characteristics of associativity, cooperativity and input-specificity upon LTP [197]. The cooperativity enables the potentiation of weak inputs when simultaneously activated, but not when activated alone, thereby setting a threshold for LTP

induction. Meanwhile, the associativity can enable a weak input to become potentiated if concurrently activated with a strong input that can drive coincidental post-synaptic depolarization. LTP is input-specific and therefore only simultaneously activated inputs become potentiated, whilst inactive synapses on the same cell remain unchanged [77, 197]. High-frequency stimulation is often used to induce LTP, which causes the summation of post-synaptic potentials that results in sufficient depolarization to enable robust NMDA-receptor activation [198]. However, LTP can also be induced by low-frequency stimulation when the post-synaptic cell is artificially depolarized via somatic current injection, commonly referred to as a pairing-protocol [190, 199]. Studies have also shown that a pairing-protocol can induce LTP when pre-synaptic neurons are stimulated by light-activation

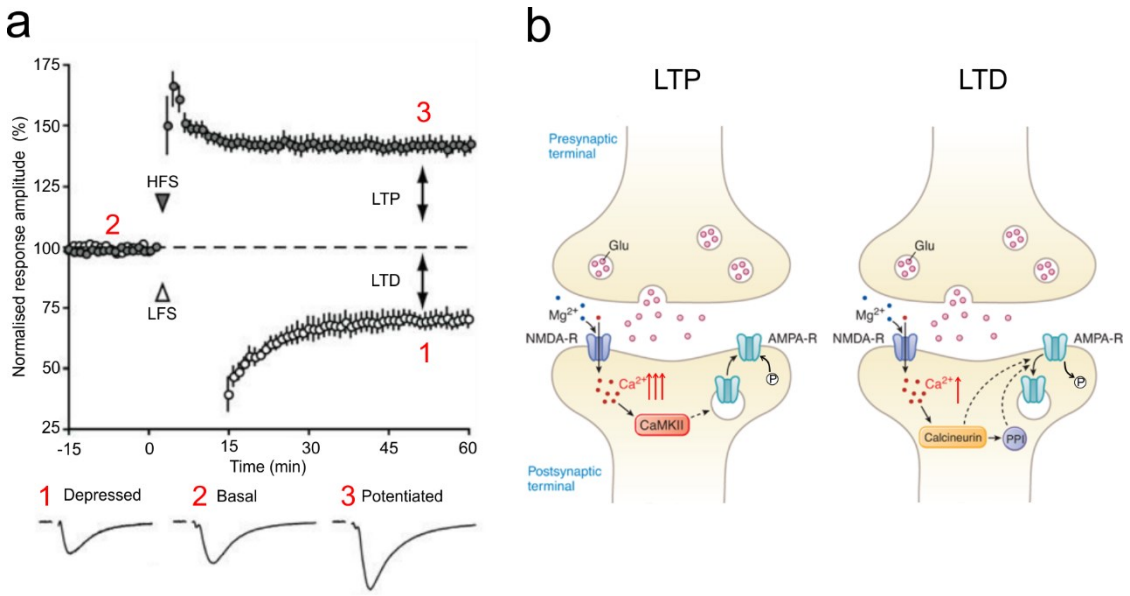

Figure 1.3. Synaptic plasticity: Long-term potentiation (LTP) and long-term depression (LTD). (a) In classical synaptic plasticity experiments the synaptic efficacy is commonly assessed by measuring the amplitude of the post-synaptic response, which is elicited by low-frequency test stimuli. Classical synaptic plasticity protocols typically involve the application of high-frequency stimulation (HFS) to induce LTP, or low-frequency stimulation (LFS) to induce LTD. Subsequently, the response amplitude is assessed, often up to 60 minutes post-induction, and compared to the basal value derived from the baseline to determine the change in synapse strength. Figure adapted from [195]. **(b)** A simplified model of the molecular mechanism of NMDA-receptor dependent LTP (*left*) and LTD (*right*). In LTP, strong stimulation of AMPA and NMDA-receptors leads to a large influx in Ca^{2+}, which activates CaMKII and signalling cascades involved in LTP. This results in the phosphorylation and upregulation of AMPA-receptors in the post-synaptic membrane. Comparatively, in LTD, weak synaptic stimulation causes a modest increase in post-synaptic Ca^{2+}, which leads to the activation of calcineurin and PP1. This results in the dephosphorylation and endocytosis of AMPA-receptors in the post-synaptic membrane. Figure adapted from [196].

of ChR2, instead of electrical stimulation, or when post-synaptic depolarization is mediated by ChR2 activation [200, 201]. The NMDA-receptor mediated calcium influx results in the activation and translocation of CaMKII [202]. Activated CaMKII mediates the phosphorylation of the GluR1 subunit, thereby increasing the AMPA receptor conductance [203], and drives the incorporation of AMPA-receptors into the synaptic membrane. In the initial phases of LTP the additional AMPA-receptors are thought to arise from the lateral movement of extra-synaptic receptors into the synapse, whilst later phases may involve the *de novo* synthesis and exocytosis of AMPA-receptors (***Figure 1.3b***) [202, 204].

It is well established within the field that induction of NMDA-receptor dependent LTP occurs post-synaptically, but the subsequent locus of LTP expression is widely debated [205, 206]. There is consistent evidence for post-synaptic changes across LTP studies. However, in some cases, the expression of LTP has been associated with a decrease in the failure rate and the coefficient of variation (COV) [207-209], which has led researchers to suggest that LTP may also induce pre-synaptic changes in neurotransmitter release probability [206]. Imaging methods have predominantly been used to investigate pre-synaptic alterations following LTP induction. For example, FM-dye studies have indicated an increased frequency of synaptic vesicle fusion [210-212], and synaptopHluorins have suggested the occurrence of greater synaptic vesicle recycling [213]. Spines are dendritic protrusions that harbour the excitatory post-synaptic density. The imaging of Ca^{2+} transients in single spines, known as excitatory post-synaptic calcium transients (EPSCaTs), are considered to be indicative of the binding of glutamate to NMDA-receptors and therefore reflective of neurotransmitter release at a single synapse [214]. Following LTP induction, EPSCaT generation at a single synapse was more frequent and therefore was suggestive of an enhancement in neurotransmitter release probability [215]. Meanwhile, the discovery of “silent” synapses, which contain only NMDA-receptors and can be “unsilenced” via the LTP-mediated insertion of AMPA-receptors, has generated a post-synaptic explanation for many of these

observations [216, 217]. Likewise, the generation of LTP at single spines via the uncaging of glutamate paired with post-synaptic depolarization negates the requirement for pre-synaptic changes [218]. LTP is primarily expressed by AMPA-mediated responses, whilst the NMDA-receptor mediated component typically undergoes minimal or no potentiation, which is consistent with a post-synaptic locus of expression [190, 219-222]. There is substantial evidence for pre-synaptic changes associated with NMDA-receptor independent forms of synaptic plasticity in multiple brain regions [223, 224]. However, it is reasonable to conclude that the current evidence suggests a predominantly post-synaptic locus of expression for NMDA-receptor mediated LTP that, under some experimental circumstances, may also include pre-synaptic enhancement [205, 206, 225, 226].

LTD, which acts to reduce synaptic efficacy, can be induced by repetitive low-frequency stimulation delivered alone, or in combination with a modest post-synaptic depolarization (***Figure 1.3a***) [227-229]. In comparison to LTP, there are very similar molecular mechanisms that underlie the expression of long-term depression (LTD) at glutamatergic cortical synapses. LTD is also input-specific and depends upon the synaptic activation of NMDA-receptors and calcium influx. However, it is thought that the magnitude and duration of post-synaptic calcium influx determines the transition of LTD to LTP [228, 230, 231]. For example, low-frequency pre-synaptic stimulation combined with a modest post-synaptic depolarization generates LTD, but when combined with a greater post-synaptic depolarization results in LTP [227]. It is thought that small rises in post-synaptic calcium predominantly activate calcineurin and protein phosphatase 1, which trigger the downstream signalling cascades leading to LTD. Meanwhile, large rises in calcium result in greater activation of CaMKII resulting in the generation of LTP [230, 232]. LTD causes the dephosphorylation and downregulation of synaptic AMPA-receptors through endocytosis and translocation, and therefore, in many respects LTD has been viewed as the inverse process of LTP (***Figure 1.3b***) [204, 233].

Although there is some evidence for the physiological occurrence of high-frequency activity patterns [234, 235], it is largely thought that the electrical stimuli typically used to induce LTP are unlikely to occur naturally. In contrast, the more recent discovery of spike-timing dependent plasticity (STDP), which relies upon low-frequency patterns of pre- and post-synaptic action potential firing to elicit changes in synaptic efficacy, is considered to be a more physiologically relevant form of synaptic plasticity. Furthermore, STDP was also the first identification of synaptic plasticity at the level of a single synaptic connection between a pair of connected neurons and, like classical LTP, was initially demonstrated in the hippocampus [209]. STDP relies upon the precise timing and order of pre- and post-synaptic spiking activity, which is reliably repeated over many pairings (~60-100), within a millisecond timeframe, to determine the sign and magnitude of synaptic plasticity. The most prevalent form at synapses between glutamatergic cortical neurons is Hebbian STDP, which generates LTP when the pre-synaptic cell reliably fires shortly before the post-synaptic cell fires an action potential (pre-post pairing). Whereas LTD is generated when the post-synaptic cell consistently fires before the pre-synaptic cell (post-pre pairing) (***Figure 1.4***) [236]. Spike-timing dependent LTP (tLTP) and LTD (tLTD) at glutamatergic cortical synapses is thought to

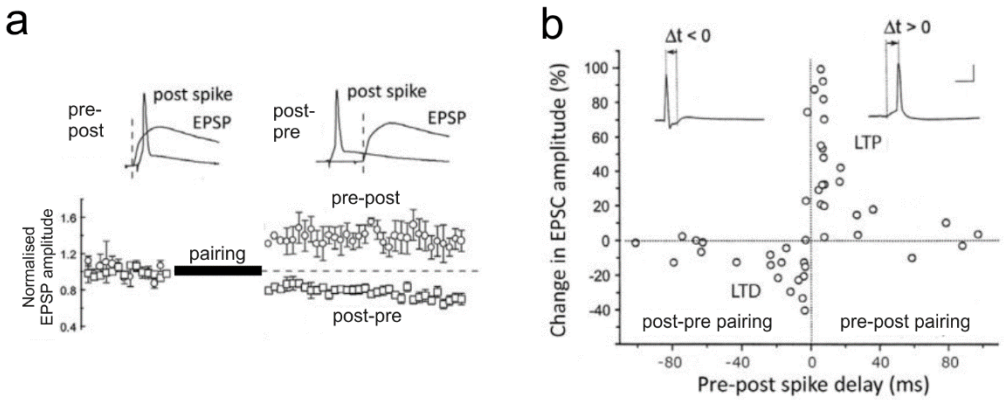

Figure 1.4. Spike-timing dependent plasticity (STDP). (a) In Hebbian STDP, the repetitive pairing of an action potential in the pre-synaptic neuron, which is shortly followed by an action-potential in the post-synaptic neuron (pre-post pairing), results in the bAP coinciding with the EPSP and leads to long-term potentiation of the synaptic response. In contrast, the repetitive pairing of action-potential firing where the post-synaptic neuron fires before the pre-synaptic neuron (post-pre pairing) leads to long-term depression of the synaptic response. Figure adapted from [237]. **(b)** The temporal window of Hebbian STDP described at glutamatergic synapses between dissociated rodent hippocampal neurons. The repetitive pairing of single pre- and post-synaptic action potential firing at short intervals (≤20 ms), induced a change in the amplitude of the post-synaptic response. Each point depicts a monosynaptic connection. Figure adapted from [236].

depend upon the same molecular mechanisms involved in the generation of classical frequency dependent LTP and LTD [237]. Similarly, tLTP and tLTD require NMDA-receptor activation and calcium influx that lead to changes in the expression and conductance of synaptic AMPA-receptors [236]. Sufficient post-synaptic calcium influx arises from the dendritic interaction of the EPSP with a back-propagating action potential (bAP) generated in the post-synaptic cell [238]. The short pre-post pairing interval enables the bAP to arrive at the dendrite at the peak of the NMDA-receptor current, which may combine with the inhibition of A-type K channels [239] or the activation of dendritic voltage-gated channels [236, 240, 241], to exert a large magnitude of calcium influx that induces LTP. In contrast, post-pre spiking causes the EPSP to coincide with the afterdepolarization potential phase of the bAP, thereby generating a moderate and slower calcium influx, which is associated with the generation of LTD [236, 238, 242].

Whilst the majority of what is known about the induction and expression of LTP has been learned from studies using hippocampal tissue, NMDA-receptor mediated LTP is also the predominant form of synaptic plasticity exhibited by excitatory synapses in the neocortex. High-frequency stimulation can be used to induce LTP in many cortical regions, although in some cases has required the pharmacological inhibition of GABAergic transmission [189, 243-245]. Likewise, STDP has also been demonstrated in the cortex within layer 2/3 [246], layer 5 [247, 248] and at layer 4 to layer 2/3 synapses [249, 250]. Interestingly, STDP at layer 5 synapses has often demonstrated frequency-dependent characteristics, such that pairing at ≥10 Hz has been required to induce LTP [247, 248]. Furthermore, unlike hippocampal synapses, cortical synapses often exhibit a wider time window for LTD generation compared to LTP, and have therefore shown a bias towards the generation of LTD [248, 250]. The generation of tLTD at some cortical synapses has been shown to be independent of post-synaptic NMDA-receptor activation and is expressed pre-synaptically [251, 252]. The mechanism at these synapses is believed to involve the binding of glutamate to post-synaptic metabotropic glutamate receptors, which leads to voltage-gated calcium channel activation and

the release of an endocannabinoid (eCB) retrograde messenger [251, 253]. The binding of eCB to presynaptic cannabinoid-1 receptors, plus the activation of pre-synaptic NMDA-receptors, results in a decrease of neurotransmitter release probability, thereby generating LTD [251, 252]. Studies have also indicated that the magnitude and time-course of NMDA-dependent LTP may differ slightly between cortex and hippocampus, whereby cortical LTP can exhibit a slower onset and lower degree of potentiation [254, 255]. In summary, it is evident that cortical synapses have the capacity to exhibit changes in synaptic efficacy in response to similar synaptic plasticity protocols that are used in the hippocampus, although in some cases the changes may differ in their extent and kinetics.

Experimental evidence for glutamatergic synaptic plasticity in humans

Unsurprisingly, the majority of synaptic plasticity studies have been performed in rodents. However, there are a limited number of reports describing synaptic plasticity in humans. These studies have demonstrated LTP and LTD in *in vitro* brain slices from tissue resected from patients with neurological conditions, and also *in vivo* LTP-like phenomena using non-invasive methods. The experiments performed *in vivo* have been limited to assessment of plasticity in the human visual, auditory and motor cortices. For the visual cortex, the response to a simple visual stimulus has been measured via EEG, whilst an LTP-like effect was induced by the presentation of the visual stimulus at high-frequency. This resulted in a long-lasting increase in the evoked response potential associated with the visual stimulus [256]. The same principles have been applied in the human auditory cortex to potentiate the evoked response potential elicited by a simple sound stimulus [257]. Meanwhile, motor-evoked potentials have exhibited potentiation following high-frequency transcranial magnetic stimulation (TMS) of the M1 area of the motor cortex, or by the pairing of low-frequency TMS with the stimulation of a peripheral nerve [80, 258-261]. Such LTP-like effects have also been prevented by NMDA-receptor blockade delivered via the systemic administration

of an NMDA-receptor antagonist [260], further demonstrating the similarities with LTP of excitatory cortical synapses *in vitro*.

Experiments using *in vitro* brain slices have provided direct evidence for LTP at human synapses. NMDA-receptor dependent LTP induced by high-frequency stimulation has been demonstrated in the human hippocampus and temporal cortex [262, 263]. Interestingly, LTP was impaired in slices derived from a cohort of patients with epilepsy who had neuropathological damage of the hippocampus that was clinically associated with memory impairment. Although indirect, this evidence supports the link between synaptic plasticity and human memory [262]. STDP has also been demonstrated in the human hippocampus, albeit with a different time window compared to that observed at rodent hippocampal synapses [264]. The temporal window for STDP in the hippocampus is considerably wider in humans than in rodents, and also has a negative shift in the time point for the transition from LTP to LTD [236, 264]. In rodents, reliable STDP is elicited by correlated spiking offset by ≤ 20 ms, whilst in humans, correlated spike timing that is offset by up to 130 ms exhibited STDP. Spike-timing LTP was observed by pre-post spike pairing at ≤ 20 ms, and post-pre pairing at ≤ 80 ms. Meanwhile LTD occurred at post-pre pairing intervals between 80-130 ms [264]. A similar temporal window was observed for STDP in human temporal cortex, with LTP occurring at spike-intervals of -100 ms to +10 ms, and LTD occurring at intervals of +10 to +40 ms [265]. The temporal window for STDP was similar in rodent temporal cortex although, in contrast, all pre-post spiking intervals (≤ 40 ms) generally exhibited LTP, not LTD [265]. The demonstration of tLTD [264, 265], alongside the low-frequency stimulation induced LTD in the cortex [263], illustrate that human excitatory synapses are able to exhibit both long-term potentiation and depression akin to that described in rodents, albeit with slight differences in the STDP rules.

Researchers have begun to investigate activity-dependent changes in synaptic transmission in human iPSC-derived neuronal cultures. To date, reports of synaptic plasticity-like phenomena in iPSC-derived neuronal cultures are limited (see section 7.1) [266-269]. These studies typically lack

direct evidence for a change in synaptic efficacy, use non-physiological induction protocols and can exhibit poor reproducibility. The use of iPSC-derived neurons as a platform to investigate synaptic plasticity requires further development and the characterization of excitatory synaptic connections. There is currently limited evidence that human iPSC-derived cortical neurons are equipped with the functional synaptic receptors necessary for synaptic plasticity, and therefore a system where these are robustly expressed would need to be established [162, 270-275]. In order to explore physiological forms of synaptic plasticity in a human iPSC-derived system, methods will also need to be developed to enable the reliable detection and manipulation of a stable evoked monosynaptic response between human iPSC-derived cortical neurons. Currently, evoked responses that may arise from a monosynaptic connection have been reported between rodent and human iPSC-derived neurons, and between a pair of human iPSC-derived neurons, but these accounts are rare and only qualitatively described [158, 276].

Studying glutamatergic synaptic plasticity in neuronal culture

In contrast to brain slice preparations and *in vivo* experiments, dissociated neuronal cultures lack the spatial organization of neuronal connectivity, which largely prohibits the classical LTP and LTD induction methods whereby many pre-synaptic afferent fibres are stimulated simultaneously. Instead, the induction of synaptic plasticity at excitatory synapses in rodent hippocampal cultures has typically been performed using electrical stimulation protocols on monosynaptically connected neuronal pairs, or by chemical methods. Many of these induction protocols were first established in slice preparations and were later adapted for use in culture. Consistent with the synaptic plasticity induced in hippocampal slice preparations, induction of LTP and LTD in dissociated hippocampal neurons is NMDA-receptor dependent and requires post-synaptic calcium signalling. LTP induction in dissociated neurons is commonly performed in the absence of external Mg^{2+} to promote NMDA-receptor activation [277-283].

Both LTP and LTD can be induced by electrical stimulation of pre- and post-synaptic neuronal activity in dissociated neurons. A substantial LTP of evoked-synaptic responses can be induced in monosynaptically connected neuronal pairs by high-frequency stimulation of the pre-synaptic neuron [207, 280], or low frequency pre-synaptic stimulation paired with post-synaptic depolarization to ≥0 mV [277]. Similarly, low-frequency pre-synaptic stimulation paired with modest post-synaptic depolarization to -50 mV, has been shown to generate LTD [284]. Meanwhile, extracellular high-frequency stimulation is associated with electrical artefacts that can obscure evoked synaptic responses, but has been used to induce LTP in the form of an increase in the frequency and amplitude of spontaneous EPSCs [281].

STDP has been robustly demonstrated in dissociated rodent cultures between pairs of synaptically connected excitatory pyramidal neurons [236]. The induction was NMDA-receptor dependent and required the repetitive pairing of single pre- and post-synaptic action potentials at 1 Hz for 60 s. Pre-post spiking, whereby the peak of the post-synaptic action potential occurred ≤ 20 ms after the EPSP onset, resulted in LTP that averaged a ~50 % increase in response amplitude [236]. However, the magnitude of LTP was dependent upon the initial response amplitude, with large responses (>500 pA) demonstrating little to no potentiation, thereby suggesting that synaptic efficacy at these synapses may already be maximal. Meanwhile, post-pre spiking at intervals ≤20 ms reliably induced LTD, which exhibited no correlation with the initial response amplitude, and caused a ~20 % reduction in response amplitude [236].

An alternative strategy for studies in culture has been to use chemical methods to induce widespread changes in synaptic efficacy. There are now a series of chemical methods that can induce NMDA-receptor dependent LTP in cultured rodent neurons. For instance, the brief (≤1 min) exposure to glutamate can increase the amplitude of evoked EPSCs and the frequency of spontaneous EPSCs by two-fold [279]. Similarly, acute exposure (3 x 1 s pulses delivered at 0.1 Hz) to high K^+ (90 mM) results in a long-term increase in the frequency of mEPSCs in rodent neuronal

cultures [282]. In rodent hippocampal slices, the short-term application (10 minutes) of the NMDA-receptor co-agonist glycine (10 mM), causes a two-fold increase in the amplitude of the field EPSP-response, which can be prevented by the previous induction of LTP by electrical stimulation [278, 285]. In dissociated rodent neurons, glycine (100-200 μM) exposure for 3 minutes results in an increase of both mEPSC amplitude and frequency, which was associated with an upregulation of AMPA receptors and was blocked by the inhibition of post-synaptic exocytosis [283]. In some cases, these protocols have been associated with changes in COV, failure rate, or spontaneous EPSC frequency, which may suggest the involvement of pre-synaptic mechanisms in the enhancement of synaptic efficacy [207, 277, 279].

A second group of chemical methods uses rolipram (0.1 μM) and forskolin (50 μM), often in combination with a $GABA_A$ antagonist (picrotoxin (50-100 μM) or bicuculline (20 μM)), to induce chemical LTP in the absence Mg^{2+} [286-288]. These protocols have been shown to have primarily a post-synaptic locus of expression [287, 288]. The adenylyl cyclase activator forskolin, and the phosphodiesterase inhibitor, rolipram, act in concert to raise cAMP levels by increasing production and decreasing degradation, respectively. Application of this chemical treatment for ~15 minutes is thought to generate a highly sensitized state and induce synchronous bursting activity that, together, provide sufficient stimulation for LTP induction [286, 288]. This has resulted in the persistent enhancement (~60 % increase) of an evoked EPSP in rodent neurons, which was associated with an increase in spine size and the upregulation of post-synaptic AMPA-receptors [286, 288]. In dissociated cultures this treatment can elicit an increase (~30 %) in mEPSC amplitude, with no effects upon mEPSC frequency [287].

Together, these studies demonstrate that NMDA-receptor dependent synaptic plasticity of excitatory glutamatergic synapses can be induced under cell culture conditions which, for some chemical LTP protocols, can generate widespread changes in synaptic efficacy. The properties of synaptic plasticity in neuronal culture appear to be consistent with *in vivo* and *in vitro* slice

experiments with intact neural circuity. Whilst the synaptic activation of NMDA-receptors is a requirement for most chemical LTP protocols, these induction methods are not physiological. However, the demonstration that the induction of LTP by electrical stimulation can occlude subsequent generation of chemical LTP [278], suggests shared underlying mechanisms are and therefore such methods can offer a simple approach to the study of synaptic plasticity.

1.8. Aims

As reviewed above, the vast majority of what has been learned about the pathogenesis of AD is from animal models, which are unable to fully recapitulate the disease. The lack of successful disease-modifying therapies that have been developed indicate that an alternative and more human-specific approach may be required. So far, the modelling of AD using iPSC technology has shown great potential in capturing the basic molecular changes that have been associated with AD. However, synaptic changes are thought to be fundamental in the generation of the key neurological symptoms of memory and cognitive impairment in AD. Whilst rodent studies point primarily to impairment of synaptic plasticity, it is uncertain how dysfunction at human synapses manifests in AD. Therefore, the development of methods that will enable the assessment of synapse function, and more specifically synaptic plasticity, in human iPSC-derived neurons would be highly advantageous. This will require the development of neuronal cultures that express functional, synaptic glutamate receptors, the generation of methods to enable the reliable detection of evoked monosynaptic responses, and a characterization of the properties and stability of these connections.

To that end, the aims of this thesis are:

1. To generate and characterize iPSC-derived cortical neurons from healthy control individuals and fAD patients
2. To assess the functional maturation state of iPSC-derived cortical neurons
3. To systematically compare methods for generating synaptically mature iPSC-derived cortical cultures
4. To characterize excitatory monosynaptic connections in iPSC-derived cortical cultures
5. To develop assays of synaptic plasticity in iPSC-derived cortical cultures

II: Materials and Methods

2.1. Materials

2.1.1. Mammalian cells

Primary rat cortical astrocytes were purchased from Gibco or made 'in house' (see section 2.2.4). HEK293T cells were a kind gift from Mariolina Salio, (Weatherall Institute of Molecular Medicine, University of Oxford). All hiPSC lines (see table below) were obtained from the StemBANCC consortium cell repository (http://stembancc.org/) and will be made available for future use through EBiSC. All hiPSC control cell lines were derived from individuals with no history of dementia, mental health problems, diabetes or migraine. iPS-NHDF-1 were derived from normal human dermal fibroblasts (Lonza; CC-2511) in the James Martin Stem Cell Facility, University of Oxford and have been described previously [289]. All cell lines were negative for mycoplasma as tested by PCR [290].

Genotype	Cell Line	Clone/s	Sex (M/F)	Age
Healthy control individuals	SBAd03	-01, -05	F	31
	SBAd02	-01	M	51
	SFC180-01	-01	F	60
	NHDF	-1	F	44
APP V717I	SFC809-03	-04	M	Unknown
PSEN1 M146I	SFC803-03	-01	F	Unknown
PSEN1 M139V	SFC805-03	-01	F	Unknown
PSEN1 Intron 4 Del	SFC808-03	-04	F	Unknown

2.1.2. Animals

P1 rats were purchased from Charles River Laboratories.

2.1.3. Media formulations

All media components were purchased from Life Technologies unless otherwise stated.

2.1.3.1. **Neural maintenance media (NMM/NMM-A)**

50 % v/v Neurobasal, 50 % v/v DMEM/F12 Glutamax medium containing 1x N2, 0.5x B27 + Vitamin A, 5 µg/mL insulin, 1 mM L-glutamine, 1x non-essential amino acids, 100 µM β-mercaptoethanol, 50 U/mL penicillin and 50mg/mL streptomycin. Neurobasal-A substitutes Neurobasal in NMM-A.

2.1.3.2. **BrainPhys™**

For BrainPhys™ Basic medium, BrainPhys™ Neuronal Medium (Stem Cell Technologies) [291] was supplemented with 1x N2 and 1x B27.

For BrainPhys™ with factors, BrainPhys™ Basic was supplemented with 20 ng/mL BDNF (Peprotech), 20 ng/mL GDNF (Peprotech), 1 mM dibutyryl cAMP (Sigma) and 200 nM ascorbic acid (Sigma).

2.1.3.3. **N2/DMEM**

DMEM/F12 + Glutamax medium containing 1x N2, 1x non-essential amino acids, 10 ng/mL BDNF (Peprotech), 10 ng/mL NT-3 (Peprotech), 1 µg/mL doxycycline (Sigma), 200 nM ascorbic acid (Sigma), 200 ng/mL laminin.

2.1.3.4. **NBA/B27**

Neurobasal A medium containing 1xB27 + VitA, 1x Glutamax, 50 U/mL penicillin and 50 mg/mL streptomycin, 10 ng/mL BDNF (Peprotech), 10 ng/mL NT-3 (Peprotech), 1 µg/mL doxycycline (Sigma), 200 nM ascorbic acid (Sigma), 200 ng/mL laminin.

2.1.3.5. **Astrocyte media**

Glial media (1): MEM containing 0.6 % w/v D-Glucose (Sigma), 50 U/mL penicillin and 50 mg/mL streptomycin, 10 % v/v horse serum.

Glial media (2); DMEM containing 15 % v/v fetal bovine serum (FBS).

2.1.3.6. **Rat neuron media**

Neurobasal-A with 1x B27, 1x Glutamax, 50 U/mL penicillin and 50 mg/mL streptomycin.

2.1.4. Buffers and solutions

All chemicals were purchased from Sigma unless otherwise stated. Solutions were made up in dH_2O and autoclaved or filtered sterilized where necessary.

2.1.5. Drugs

All drugs were purchased from Tocris unless stated otherwise. Stock solutions were stored at -20C.

Drug	Function	Final Concentration (µM)
TTX	Voltage gated Na-channel blocker	1
QX314 (Alomone Labs)	Use-dependent voltage gated Na-channel blocker	5000
CNQX	AMPA receptor blocker	40
Picrotoxin	GABA-A receptor blocker	100
Forskolin	Adenylyl cyclase activator	50
Rolipram	PDE4 inhibitor	0.1
AP5	NMDA receptor blocker	10
MK801	NMDA receptor blocker	50
Y-27632	ROCK inhibitor	10
SB431542	inhibitor of the TGF-β/Activin/NODAL pathway	10
Dorsomorphin	inhibitor of the BMP pathway	1

2.1.6. Lentiviral vectors

Vector	Virus	Source	Reference
FUdeltaGW-rtTA	LV-Ubiq-rtTA	FudeltaGW-rtTA was a gift from Konrad Hochedlinger (Addgene plasmid # 19780)	[292]
pTet-O-Ngn2-puro	LV-TetO-mNgn2-T2A-Puro	pTet-O-Ngn2-puro was a gift from Marius Wernig (Addgene plasmid # 52047)	[158]
pMD2.G	Encodes VSV-G viral envelope, 2nd generation lentivirus	pMD2.G was a gift from Didier Trono (Addgene plasmid # 12259)	
pCMV delta 8.91	Encodes viral packaging, 2nd generation lentivirus		
pLenti-Synapsin-hChR2(H134R)-EYFP-WPRE	LV-hSyn-ChR2-YFP	pLenti-Synapsin-hChR2(H134R)-EYFP-WPRE was a gift from Karl Deisseroth (Addgene plasmid # 20945)	[293]
pLenti-CaMKIIa-mKate2-WPRE	LV-CaMKIIa-mKate2	A kind gift from Ricardo Dolmetsch.	[162]
pLenti-CAG-YFP-WPRE	LV-CAG-YFP	A kind gift from Fred Gage.	

2.1.7. RT-PCR primers

Gene	Forward Primer Sequence (5'-3')	Reverse Primer Sequence (5'-3')
Foxg1	AGG AGG GCG AGA AGA AGA AC	TCA CGA AGC ACT TGT TGA GG
GAPDH	ATC CCA TCA CCA TCT TCC AG	CCA TCA CGC CAC AGT TTC C
Oct4	ACA TGT GTA AGC TGC GGC C	GTT GTG CAT AGT CGC TGC TTG
Otx1	GCC TCC CCT TCC AGT CTT TC	GGG CAG AAA CAC GCC AGT TA
Pax6	GTG TCC AAC GGA TGT GTG AG	CTA GCC AGG TTG CGA AGA AC

2.1.8. Primary antibodies for immunocytochemistry

Antibody	Raised in	Concentration	Supplier	Catalogue #
Ctip2	Rat	1:250	Abcam	ab18465
GAD65	Mouse IgG2a	1:250	Chemicon int. Inc.	MAB351
GAD65/67	Mouse IgG2a	1:400	Millipore	MAB5406
Homer1	Rabbit	1:500	Synaptic Systems	160003
MAP2A	Mouse IgG1	1:1000	Millipore	MAB378
Nkx2.1	Mouse IgG1	1:500	Millipore	MAB5460
Otx1/2	Rabbit	1:500	Abcam	ab9566
Pax6	Rabbit	1:500	Covance	PRB-278P
PSD95	Mouse IgG2a	1:2000	Millipore	MAB1596
Satb2	Mouse IgG1	1:200	Abcam	ab51502
Synaptophysin	Guinea Pig	1:1000	Synaptic Systems	101004
Tbr1	Rabbit	1:500	Abcam	ab31950
Tbr2	Rabbit	1:500	Abcam	ab23345
Tuj1	Mouse IgG2a	1:2000	Covance	MMS-435P

2.1.9. Secondary antibodies for immunocytochemistry

Antibody	Conjugate	Raised in	Concentration	Supplier	Catalogue #
Anti-mouse	Alexa Fluor 488/568	Goat	1:1000	Life Technologies	A11029/A11031
Anti-mouse	Alexa Fluor 633	Goat	1:500	Life Technologies	A21052
Anti-rabbit	Alexa Fluor 488/568	Goat	1:1000	Life Technologies	A11034/A11036
Anti-guinea pig	Alexa Fluor 488	Goat	1:400	Life Technologies	A11073
Anti-rat	Alexa Fluor 488	Goat	1:1000	Life Technologies	A11006
Anti-mouse IgG1	Alexa Fluor 488/568	Goat	1:1000	Life Technologies	A21121/A21124
Anti-mouse IgG2a	Alexa Fluor 488/568	Goat	1:1000	Life Technologies	A21131/A21134

2.1.10. Western blot antibodies

Antibody	Conjugate	Raised in	Concentration	Supplier	Catalogue #
Oct4		Rabbit	1:1000	Abcam	ab19857
Nanog		Mouse	1:1000	Cell Signalling	#4893
Tuj1		Mouse	1:2000	Covance	MMS-435P
GFAP		Mouse	1:1000	Millipore	MAB360
β-actin	HRP	Mouse	1:10,000	Sigma	A3854-200UL

2.2. Methods

2.2.1. hiPSC cell culture

Feeder-free human iPS cells were maintained in mTeSR1 medium (STEMCELL Technologies) on Geltrex (Gibco) coated plates. For coating, Geltrex was diluted 1/100 into cold KO-DMEM (Life Technologies) and incubated at 37 ^{o}C for 30 mins - 4 h. Pre-coated plates could be stored overnight at 4 ^{o}C. At 95 % confluency, cells were passaged as follows. Cells were washed with PBS then incubated in Versene-EDTA (Gibco) at 37 ^{o}C for 6 mins. Versene-EDTA was aspirated and cells were washed off and collected in mTeSR and supplemented with 10 µM Y-27632 (Tocris) overnight. Media was changed 100 % daily.

2.2.2. Coverslip preparation

13 mm glass coverslips thickness 0 (VWR) were soaked in 70% nitric acid for 48h before washing 5 x in dH_2O. Coverslips were briefly rinsed in 100 % ethanol to sterilize and dried overnight in an oven.

For poly-L-ornithine laminin coated coverslips: coverslips were incubated with 0.01 % poly-L-ornithine (Sigma) for 4 h to overnight, then replaced with 15 µg/mL laminin (Life Technologies) in DPBS + Mg^{2+}/+Ca^{2+} (Life Technologies) for 4 h to overnight. The coating solution was aspirated immediately prior to plating.

For poly-D-lysine coated coverslips: Poly-D-Lysine (Sigma) was applied to coverslips at 0.1 mg/mL diluted in dH_2O and incubated at 37 ^oC for 1-2 h. Coverslips were washed 3 x with dH_2O and allowed to dry at room temperature for 4-6 h before use.

2.2.3. Directed differentiation of hiPSCs into cortical neurons using defined factors

hiPSCs were grown to ~90 % confluency before passaging at a ratio of 2:1 onto 2 geltrex-coated wells of a 6 well plate (see section 2.2.1), in preparation for neural induction following a modified Shi et al., (2012) protocol [149]. After 24 h, the culture medium was changed to neural induction medium (NIM; NMM supplemented with 10 µM SB431542 (Tocris) and 1 µM dorsomorphin (Tocris)) which was changed daily for 12 days. At day 12 the cells form a dense, homogenous sheet with visible white spots. The sheet was scored using a needle into a 3x4 grid and 200 uL freshly filtered 10 mg/mL Dispase (Gibco) was added per well to the media and incubated at 37 ^oC. Plates were tapped frequently to encourage lifting. Sheets of cells lifted after 10-15 minutes. Cells were collected using into 10 mL NMM and pelleted by gravity, media was removed and this step repeated to wash out Dispase. Cells were plated onto 15 µg/mL laminin only coated wells in NIM overnight whilst maintaining large clumps of ~ 1 mm in size. 24 h later, the medium was changed to NMM supplemented with 20 ng/mL FGF2 (Peprotech) for 4 days to promote rosette formation. Rosettes

were cultured in NMM and were expanded 2-4 times using Dispase, as described, at a surface area ratio of 1:2 to 1:3 onto laminin only coated wells until the onset of neurogenesis, approximately day 25. For Dispase passaging media was changed 30 mins-4 h before and only stripettes were used to avoid cell shearing. At day 25, cells were passaged and plated onto laminin only coated wells at a surface area ratio of 1:2 using Accutase (Sigma) as follows. Cells were washed with PBS and incubated at 37 ^{o}C with 500 uL - 1 mL Accutase per well for 5 mins. Cells were triturated and collected into 9 mL NMM, centrifuged at 400 g for 5 minutes, and then the cell pellet was resuspended in NMM supplemented with 10 µM Y-27632 (Tocris), and plated onto laminin only coated wells. 100 % of the media was changed to NMM following day. After 2-3 days when neural NPCs were confluent cells were split again 1:2-1:3 with Accutase before being frozen down at 1.5 x 10^6 cells/vial between day 28-31 in 90 % v/v NMM, 10 % v/v DMSO and 20 ng/mL FGF2.

Frozen NPCs were fast-thawed at 37 ^{o}C, centrifuged at 400 g in a Heraeus Megafuge 8 centrifuge (Thermo Scientific), and plated onto laminin (15 µg/mL) coated plates in NMM with 10 µM Y-27632 and 10 ng/mL FGF2 overnight and cultured for 7 days. Cells were then lifted with Accutase for final plating onto rat astrocyte cultures, with the exception of control cultures (without rat astrocytes; ***Figure 4.1***) which were plated onto poly-L-ornithine laminin coated coverslips. Cells were plated at a density of 50-100,000 cells/cm^2 with 10 µM Y-27632 overnight.

If required, cells were transduced by adding lentiviral particles to the media overnight, 24-48 h after thawing. Cells were maintained in NMM-A for 50-90 days before analysis. Media was changed 90 % every 2-3 days and supplemented with 10 ug/mL laminin (Gibco) every 7 days.

2.2.4. Rat cortical astrocyte culture

P1 rat pups were killed by schedule 1 cervical dislocation and decapitation. Cortices were isolated and stripped of meninges in ice-cold CMF-HBSS containing 1x HBSS, 10 mM HEPES. Tissue was dissociated in 12 mL CMF-HBSS supplemented with 1.5 mL 2.5 % Trypsin (Gibco) and 1.5 mL 1 %

DNase for 5 mins at 37 ^{o}C before 10x trituration with a 10 mL stripette. The tissue suspension was further incubated for 10 mins at 37 ^{o}C with frequent agitation to resuspend tissue fragments. Following 10x trituration with a 5mL stripette, the cell suspension was put through a 70 µm cell strainer, centrifuged at 400 g and the cell pellet was resuspended in glial media (1). Cells derived from 2-3 brains were grown in one T75 flask (Nunc). 4 days post-dissociation, flasks were bashed several times to remove neurons, microglia and unwanted cell types leaving from the highly adherent astrocytes and 100 % of the media was changed. This was repeated every 3-4 days. Cells were grown until confluent before freezing 0.5 x 10^6 cell/vial in glial media (2) with 10 % v/v DMSO.

For astrocyte monolayer coverslips, cells were fast-thawed and resuspended in glial media (2) and plated as a 200 uL meniscus onto poly-D-lysine coated glass coverslips. After 10 minutes, media was topped up to 500 uL. Cells were grown until confluent with media changes every 3-4 days. In some cases rat astrocytes were acquired commercially (Gibco).

2.2.5. Culture in BrainPhys™ medium

iPSC-derived NPCs were thawed and maintained as described in section 2.2.3. NPCs were plated onto rat astrocytes in NMM. Two days after final plating media was changed by 50 % to NMM-A, BrainPhys™ Basic or BrainPhys™ with factors as appropriate. 50 % media changes were performed every 2-3 days and supplemented with 10 µg/mL laminin once a week. Neurons were assessed at 6-8 weeks post-final plating.

2.2.6. Co-culture of iPSC-derived cortical neurons with rat primary neurons

P1 rat pups were killed by schedule 1 cervical dislocation and decapitation, and cortices were isolated and stripped of meninges in ice-cold dissection media comprised of Neurobasal-A with 50 U/mL penicillin and 50 mg/mL streptomycin. Tissue was dissociated in dissection media with 100 uL Papain (P3125, Sigma) for 30 mins at 37 ^{o}C, DNase (100 µg/mL) was added for the final 5 mins.

The dissociated cell suspension was passed through a 70µm cell strainer, counted and plated at 50,000 live cells/cm^2 onto poly-ornithine and laminin-coated glass coverslips in rat neuronal media supplemented with 5 % horse serum overnight. Human NPCs were added in rat neuronal media at 50,000 cells/cm^2 onto rat primary cultures (according to section 2.2.4) the following day, and supplemented with 10 µM Y-27632 overnight. At 6 DIV cells were treated with 2 µM Ara-C followed by a half-media change the following day. Half-media changes were performed every 3-4 days.

2.2.7. Differentiation of hiPSCs into cortical neurons by induced neurogenin-2 expression (iPSC-mNgn2)

90 % confluent hiPSCs were lifted using Accutase and resuspended in mTeSR supplemented with 10 µM Y-27632. LV-Ubiq-rtTa and LV-TetO-mNgn2-T2A-Puro concentrated lentiviral particles, each at a dilution of 1/250, were added to the cell suspension, before plating onto Geltrex-coated plates and incubated overnight. Media was changed to N2/DMEM supplemented with doxycycline at 1 µg/mL (day 0) for 24 h before the addition of puromycin (Sigma) at 2 µg/mL for a further 48 h. Media was changed daily. Cells were lifted using Accutase on day 3 and plated onto rat astrocytes at 50,000-100,000 cells/cm^2 in NBA/B27 with 10 µM Y-27632 overnight. The total number of cells resuspended following Accutase treatment was divided by the total number of wells dissociated to obtain the cell yield.

Cultures were maintained to day 14-40 in NBA/B27 medium with 50 % media changes every 2-3 days. The media was supplemented with 2 % v/v horse serum (Gibco) every 7 days. On day 6 cultures were treated with 4 µM Ara-C (Sigma).

2.2.8. Differentiation of NPCs into cortical neurons by induced neurogenin-2 expression (NPC-mNgn2)

NPCs were fast-thawed and cells were resuspended in NMM supplemented with 10 µM Y-27632 and 10 ng/mL FGF2, as described in section 2.2.3. LV-Ubiq-rtTa and LV-TetO-mNgn2-T2A-Puro

lentiviral supernatants, each at a dilution of 1/4-1/8, were added to the cell suspension. NPCs were plated onto laminin (15 µg/mL) coated plates at 150,000 cells/cm^2. Media was changed the following day. After 3 days media was changed to NBA/B27 with doxycycline (day 0). On day 1 puromycin was added for 24 h at 2 µg/mL then increased to 2.5 µg/mL for a further 24 h. On day 3 cells were lifted using Accutase and plated onto rat astrocytes at 50,000 cells/cm^2 with 10 µM Y-27632 overnight.

To obtain the cell yield, the total number of cells resuspended following Accutase treatment was divided by the total number of wells dissociated. This value was multiplied by the average number of total NPCs generated at day 28-33, which were counted during freezing down, and that was divided by the number of wells of iPSCs used for neural induction.

Cultures were maintained for 14-53 days in NBA/B27 medium with 50 % media changes every 2-3 days. The media was supplemented with 2 % v/v horse serum (Gibco) every 7 days. On day 6 cultures were treated with 4 µM Ara-C (Sigma).

NPC-mNgn2 neurons were used for all experiments in Chapters VI and VII.

2.2.9. Lentiviral transductions and expression quantification

On day 1 of neurogenin-2 differentiation LV-CaMKIIα-mKate2, LV-hSyn-ChR2-YFP or LV-CAG-YFP lentiviral supernatants were added overnight at a dilution of 1/2-1/4 in media to separate wells, so that expression of each construct was mutually exclusive. Media was changed the following day. During final plating on day 3, the LV-CaMKIIα-mKate2 and LV-hSyn-ChR2-YFP or LV-CaMKIIα-mKate2 and LV-CAG-YFP transduced cell suspensions were combined before determining cell concentration and plating.

Live neuronal cultures were imaged on an EVOS FLoid Cell Imaging Station (ThermoFisher) at day 18-51. The approximate cell density was estimated under brightfield and the number of fluorescent cells were counted manually across 5 FOV.

2.2.10. Prolonged optogenetic stimulation

Day 33-35 neurogenin-2 NPC-derived neuronal cultures expressing LV-CaMKIIα-mKate2 and LV-hSyn-ChR2 or LV-CaMKIIα-mKate2 and LV-CAG-YFP, which were co-cultured with rat astrocytes, were activated in the incubator by 455 nm LED light pulses at an intensity of 2.4 mW/mm^2, achieved by a 500 mA power setting. The LED stimulation consisted of 5 flashes of 10 ms duration at 10 Hz delivered every 10 seconds for 2-4 days using a custom-built optogenetic chamber. This comprised four Rebel Star LEDs in Royal Blue LZ1-00B200 (Luxeon) that were covered with a Carclo 8 20 mm concentrator beam optic (Luxeon) and encased in light-impenetrable tubing (Thorlabs) which contained 40mm focal length biconvex lenses (Comar). To control the light pulses the optogenetic chamber was connected to a custom-built stimulator box via a Grass S48 stimulator (Grass Technologies).

2.2.11. Plasmid DNA purification

E. coli were streaked onto LB-Ampicillin plates from bacterial stabs or glycerol stocks. Alternatively, plasmids for amplification were transformed into One Shot™ Stbl3™ *E. coli* (Invitrogen) according to manufacturer's protocol. Lennox LB and Lennox LB-Agar were purchased from Invitrogen. A single colony was picked to generate a starter culture in 2 mL LB-Ampicillin media and shaken at 225 rpm for 8 hours at 30-37 ^{o}C, dependent on bacterial strain. 200 µL of starter culture was added to 150 mL of LB-Ampicillin media and shaken overnight at 30-37 ^{o}C. Bacteria were pelleted in a Fiberlite F14-6x250 fixed angle rotor (Thermo Scientific) in a Sorvall RC5C Plus centrifuge at 6000 g for 20 minutes at 4 ^{o}C. DNA was extracted using Qiagen Plasmid Maxi Kit according to

manufacturer's protocol, and each pellet was resuspended in 500 µL TE buffer (Invitrogen). DNA concentrations were determined using a NanoDrop spectrophotometer (Thermo Scientific).

2.2.12. Lentivirus production

HEK 293T cells were plated into a T75 flask at a density of 80,000 cells/cm^2 in 90 % DMEM, 10 % FBS, and grown to around 70 % confluency. Media was replaced and supplemented with 1x NEAAs preceding transfection. Cells were transfected with 100 µL Lipofectamine 2000 (Invitrogen), with 9.375 µg lentiviral vector DNA, 3.125 µg VSVg envelope DNA and 8.75µg Δ8.91 packaging DNA overnight. Lipofectamine was added to 1 mL Optimem and incubated at room temperature for 5 minutes. Separately, DNA was added to 1 mL Optimem then transferred to the Lipofectamine solution, inverting to mix contents. This was incubated for a further 25-30 minutes before adding to cell flasks. Transfection medium was replaced with fresh growth medium the following morning. Media was harvested after 24-48 h, centrifuged at 400 g for 5 minutes to remove cellular debris, and then passed through a 0.45 µm filter. Supernatant was either stored at -80 ^{o}C or further processed by ultracentrifugation to concentrate the viral particles. For ultracentrifugation, 8 mL supernatant was transferred into conical bottomed, heat sealable tubes (Beckman Coulter) and centrifuged at 65320 g (30,000 rpm) in a SW41TI swinging bucket rotor at 4 ^{o}C for 3 hours using a Beckman L8-70M Ultracentrifuge. The supernatant was removed and each viral pellet was resuspended in 20 µL Opti-MEM, 1:100 DNase I (1 U/µL stock concentration, Sigma Aldrich), and 8 µg/ml polybrene (hexadimethrine bromide, Sigma Aldrich) overnight at 4 ^{o}C, aliquoted and stored at -80 ^{o}C.

2.2.13. RNA extraction and RT-PCR

Cells were collected in PBS, pelleted, resuspended in RNAlater (ThermoFisher) and incubated at 4^{o}C overnight before long-term storage at -80 ^{o}C. For RNA extraction an equal volume of PBS was added to the RNAlater cell suspension and spun at 16,000 g for 5 minutes. RNA was extracted using TRIzol

Plus RNA Purification Kit (Invitrogen). In brief, the cell pellet was resuspended in 500 µL of TRIzol and incubated for 5 minutes. 100 µL chloroform was added, mixed vigorously and incubated for 2-3 minutes. Samples were centrifuged at 12,000 g for 15 minutes at 4 ^{o}C. An equal volume of 70 % ethanol was added to the RNA containing colourless upper aqueous solution and vortexed. The sample was transferred to a spin cartridge and centrifuged at 12,000 g for 15 minutes at 4 ^{o}C, the flow-through discarded, and repeated if necessary. The cartridge was washed twice by adding 500 µL of wash buffer II and centrifuging for 15 seconds at 12,000 g. After centrifuging at 12,000 g for 1 minute to dry the membrane, RNA was eluted by adding 35 µL of RNAse-free water, incubating for 1 minute, before centrifuging at 12,000 g for 2 minutes. RNA concentrations were determined using a NanoDrop spectrophotometer (Thermo Scientific).

RNA was reverse transcribed using SuperScript III First Strand Synthesis Supermix (Invitrogen), according to manufacturer's protocol. cDNA was amplified using Platinum Taq (Invitrogen) with the following thermocycling conditions; 94 ^{o}C for 1 minutes, 25 x cycles of (94 ^{o}C for 30 s, 60 ^{o}C for 30 s, 72 ^{o}C 1 minute), 72 ^{o}C for 1 minute and then held at 4 ^{o}C. The PCR product was run by gel electrophoresis on a 2 % w/v agarose in 1x TAE buffer (40 mM Tris acetate, 1 mM EDTA) containing 0.1 µg/mL ethidium bromide at 80-120 V. A 1 kb DNA ladder (Invitrogen) was run alongside DNA fragments and visualised using a UV trans-illuminator.

2.2.14. Immunocytochemistry

Neuronal cultures on coverslips were fixed in 4 % paraformaldehyde/ 4 % sucrose (w/v) in phosphate-buffered saline (PBS) solution and if not used immediately were stored at 4 ^{o}C in PBS containing 0.01 % w/v sodium azide. Cells were permeabilized in PBS with 0.4 % v/v Triton-X for 2 x 7 minutes at room temperature (RT) and blocked in PBS with 10 % v/v goat serum for 1-2 h at RT. Primary antibodies were diluted in PBS with 5 % v/v goat serum for 1 hour at RT or overnight at 4 ^{o}C. Secondary antibodies were diluted in 5 % v/v goat serum for 1 h at RT. Coverslips were washed

3 times for 5 minutes with PBS after each antibody application. Coverslips were rinsed in dH_2O before mounting in ProLong Gold or Diamond Antifade mountant (Life Technologies).

2.2.15. Imaging and quantification of immunocytochemistry

Coverslips were imaged using an Olympus BX40 epifluorescence microscope using Olympus UPlanFL 20X, 40X, 60X and 100X objectives. Images were acquired using an Orca-ER camera (Hamamatsu) and HCImage software (Hamamatsu). Images were processed using ImageJ software. Quantification was performed using CellProfiler custom made pipelines to identify positively-labelled cells based on size and intensity which were optimised separately for each image set and marker. Co-cultured astrocytes were excluded from quantification based on nuclear size and staining intensity. Random fields of view containing dissociated cells were identified under dapi fluorescence before subsequent channels were imaged.

2.2.16. Western blotting

Cells were lysed on ice for 20 minutes in treatment buffer (75 mM Tris-HCl pH 6.8, 3.8 % w/v SDS, 4 M Urea, 5 % v/v β-mercaptoethanol, 20 % v/v glycerol) and protein concentration determined by Bio-Rad DC protein assay (Bio-Rad).

An equal volume of 2x sample buffer (50 µL 1M DTT + 50 µL β-mercaptoethanol + 900 µL 2x Laemelli buffer (0.125 M Tris pH 6.8, 4 % w/v SDS, 20 % v/v Glycerol, 0.5 % w/v Bromophenol Blue)) was added to lysates and heated to 95 ^{o}C for 5 mins to denature. 8 µg of total lysate was run by SDS-PAGE on a 10 % v/v polyacrylamide gel at 80 V for 10 minutes, then resolved in running buffer (25 mM TRIS base, 192 mM glycine, 0.1 % SDS) at 150 V alongside Bio-Rad Precision Plus Protein Standards (161-0373). Bands were transferred in 4 ^{o}C transfer buffer (25 mM TRIS base, 192mM glycine) with 20 % v/v methanol, onto a nitrocellulose membrane at 85 V for 1 hour at 4 ^{o}C then blocked in 5 % w/v milk protein in TBS-T (150 mM NaCl, 20 mM Tris pH 7.5 with 0.1 % v/v Tween20).

Primary antibodies, see section 2.1.10, were incubated for 1 hour at room temperature in 5 % w/v milk protein in TBS-T. Membranes were washed 3x for 5 minutes with TBS-T. Secondary antibodies were species-specific HRP-conjugates (Jackson Labs) used at 1:3000. The membrane was washed 3x with 1x TBS-T then incubated with enhanced chemiluminescent western blotting substrate (Pierce) before exposure to photographic film for visualisation.

2.2.17. Sample preparation and measurement of Aβ-peptides

NPCs were thawed and maintained as described in section 2.2.3. For final plating cells were accutased and plated onto poly-L-ornithine and laminin coated 12 well plates (Corning) at 100,000 cells/cm^2, or 150,000 cells/cm^2 for neurogenin-2 differentiated NPCs (see section 2.2.8) with 10 µM Y-27632 overnight. Media was changed 48 hs prior to harvest at 50 days post final plating, or 25 days post-final plating for neurogenin-2 neurons.

Media was collected and centrifuged at 1000 g at 4 ^{o}C in an Eppendorf 5415R centrifuge (Eppendorf) for 5 minutes to remove cell debris. Halt combo inhibitor and EDTA 1:100 (ThermoFisher) and protease inhibitor cocktail (P8340 Sigma) 1:200 were added, and samples stored at -80 ^{o}C.

Cells were washed and collected in 4 ^{o}C PBS and pelleted at 5000 g for 5 minutes. Pellets were lysed for 20 minutes on ice in RIPA buffer (50 mM Tris pH 8, 150 mM NaCl, 1 % NP-40, 0.5 % NaDeoxycholate, 0.1 % SDS) containing Halt combo inhibitor and EDTA 1:100 (ThermoFisher) and protease inhibitor cocktail (P8340 Sigma) 1:200. Lysates was transferred to a QIAshredder column (Qiagen) and spun at 4 ^{o}C at 16000 g for 10 minutes. Supernatant was snap frozen and stored at -80 ^{o}C.

The Pierce BCA assay (Thermo Fisher) was used to determine sample protein concentration. In summary, 100 uL of BCA reagent was added to 8 uL of lysate in triplicate on a 96 well plate,

incubated for 30-60 minutes at 37 ^{o}C, and read at 562 nm. Dilutions of bovine serum albumin in RIPA buffer were used to generate a standard curve.

Amyloid-β measurements were performed with undiluted media using the V-PLEX Plus Aβ Peptide Panel 1 (6E10) Kit (Meso Scale Discovery) according to manufacturer's instructions. Aβ40 blocker was omitted. Total Aβ concentration was normalised to total cell lysate. Four separate wells were plated and analysed for each neuronal differentiation. The average of the four technical replicates was used to represent each individual for statistical comparison. For neurogenin-2 cells the total protein per well was below the limit of detection.

2.3. Electrophysiology

2.3.1. Recording conditions

Whole-cell patch clamp recordings were made with thin-wall borosilicate glass pipettes (resistance 5-8 MΩ) using a Sutter P-97 Flaming-Brown puller (Sutter Instrument Company), with cultures constantly perfused with external solution at 30^{o}C.

For the electrophysiology experiments performed in Chapter III, artificial CSF (1) bubbled with 95 % O_2 and 5 % CO_2 and internal (1) was used. In Chapter IV and thereafter, HEPES external solution (1) was used with internal solution (2), with the exception of experiments investigating tLTP induction and LTP induction using the pairing-protocol in which internal solution (3) was used.

Solution	Composition (mM)
aCSF (1)	126 NaCl, 2.5 KCl, 1.2 NaH_2PO_4, 26 $NaHCO_3$, 3 $CaCl_2$, 1 $MgCl_2$ and 10 glucose (made to pH 7.4 and 290 mosm)
HEPES external (1)	140 NaCl, 5 KCl, 2 $CaCl_2$, 2M gCl_2, 10 HEPES and 10 glucose (made to pH 7.4 and 290 mosm)
Internal (1)	130 K or Cs-gluconate, 10 NaCl, 1 EGTA, 0.133 $CaCl_2$, 2 $MgCl_2$, 10 HEPES, 3.5 Na_2ATP and 1 Na_3GTP (made to pH 7.3 and 290 mosm)
Internal (2)	140 K or Cs-gluconate, 6 NaCl, 1 EGTA, 10 HEPES, 4 MgATP and 0.4 Na_3GTP (made to pH 7.3 and 290 mosm)
Internal (3)	145 K-gluconate, 6 NaCl, 10 HEPES, 4 MgATP and 0.4 Na_3GTP (made to pH 7.3 and 290 mosm)

Drugs were dissolved in dH_2O where possible, or DMSO if necessary, and were bath applied. To prevent mixing of solutions 15 mL of perfusate was allowed to flow through before recycling when changing to or from a drug-containing solution.

2.3.2. Acquisition and analysis

Cells were viewed using a BX51WI microscope (Olympus) through a 20X/1.00NA XLUMPLFLN-W objective (Olympus) and iXon camera (Andor Technologies) with a 4X magnifier. Recordings were made with a Multiclamp 700B amplifier and Clampex software (Molecular Devices). Signals were sampled at 10 kHz and filtered at 2 kHz for voltage clamp recordings. Cells were clamped at -70 mV unless otherwise stated. Data was analysed using Clampfit software (Molecular Devices).

2.3.3. Intrinsic membrane properties and action potential firing

Automated measurements of capacitance and membrane resistance were generated through the Clampex membrane test function. Resting membrane potential was recorded upon entry into current clamp in the absence current injection and was not corrected for the liquid junction potential (calculated to be 14-18 mV). To assess voltage-gated currents, the membrane was held for 400 ms from -90 mV to +30 mV in 10 mV steps. For induced action-potential firing, current was injected in 5 pA steps from -20 pA to +55 pA. On occasions steps were increased to 10 pA if depolarization was not sufficient to reach action potential threshold.

The maximum sodium current was taken as the largest negative voltage-gated current generated in the voltage-steps protocol. The maximum potassium current was the largest positive voltage-gated current activated in the first 100 ms and captures the current generated from both A-type and delayed-rectifier potassium channels.

The number of consecutive action potentials was the greatest number of action potentials fired within one 400 ms depolarizing step of the current-steps protocol, whereby each action potential

must be at least half the amplitude of the preceding spike to be counted. The threshold was the lowest membrane voltage at which an action potential was triggered across the current-steps. The action potential amplitude was measured from resting membrane potential to action potential peak.

Cells exhibited an initial access resistance of 10-50 MΩ that did not increase by more than 40 %, and membrane capacitance and membrane resistance that did not deviate by more than 40 % throughout the recording.

2.3.4. Recording of spontaneous synaptic activity

All recordings of spontaneous synaptic activity were 2-5 minutes in duration. For EPSCs all recordings were made in voltage-clamp at -70 mV in the presence of picrotoxin using a K-based internal solution. Recordings of miniature excitatory post-synaptic events (mEPSCs) were performed in the presence of TTX and picrotoxin. For inhibitory synaptic events recordings were made in voltage clamp at 0 mV using a Cs-based internal solution.

A lowpass Bessel 8-pole filter at 1000 Hz was applied to all recordings. A template was generated in Clampfit by averaging 50-100 events and subsequently used to detect events in all recordings. Due to differing kinetics, templates were generated independently for AMPA-excitatory and GABA-inhibitory events, which exhibit fast and slow decay kinetics, respectively. Events were accepted or rejected manually and all were included in frequency and amplitude calculations.

In recordings from neurogenin-2 neurons, events were detected automatically using the Clampfit template with a fit 3-6 and subsequent post-hoc filtering was applied using criteria (amplitude > 7 pA, half width > 1 ms, rise time 10-90 % > 0.3 ms and < 2 ms, and decay time 90-10 % > 1.5 ms) which were designed to exclude false-positive events and were tested against manual detection.

The EPSC amplitude was determined by the generation of an average event per cell. Cells with an EPSC frequency <0.1 Hz were excluded from EPSC amplitude analysis.

Cells required an initial access resistance below 50 MΩ that did not increase by more than 40 %, and capacitance and membrane resistance that did not deviate by more than 40 % throughout the recording to be included in analysis.

2.3.5. Glutamate-evoked responses

Recordings were performed with Cs-based internal solution (2) supplemented with 5 mM QX-314 in HEPES external solution (1), supplemented with 10 µM glycine and 100 µM picrotoxin. Puffs of 600 µM L-glutamic acid dissolved in external solution were delivered by a Picospritzer III (IntraCel) at 20 psi for 10 ms at 10-20 µm from the cell soma. Puffs were delivered 8 s apart with ≥5 trials at -80 mV. The response at -80 mV was averaged and the maximum negative peak amplitude within 20 ms was taken as the AMPA-mediated response.

2.3.6. Assessment of monosynaptic connectivity

To assess excitatory monosynaptic connectivity pairs of NPC-mNgn2 neurons (whose soma were within 200 µm), were simultaneously whole-cell patch clamped in the presence of 100 µM picrotoxin. To simultaneously assess connectivity in both directions, cells were held in voltage-clamp and were depolarized by two 10 ms voltage steps, delivered 40 ms apart, to a voltage sufficient to evoke a voltage-gated sodium current. After 250 ms, a pair of depolarizing steps were delivered to assess connectivity in the opposite direction. Cells were also assessed with one cell in current-clamp whereby two steps of suprathreshold depolarizing current of 10 ms duration were injected 40 ms apart to elicit a pair of action potentials, whilst the other cell was held in voltage-clamp to detect a response. Trials were repeated at 0.1 Hz. Cells with a temporally-locked response ≤6ms from the action potential or voltage-gated sodium peak were considered to be connected.

For analysis of $EPSC_P$, responses were assessed from whole-cell and perforated patch clamp recordings performed in voltage-clamp from neurons between days 25-55. Paired-pulse stimulation was elicited by delivering two depolarizing 10 ms current pulses at a 40 ms interval to the pre-synaptic cell which was repeated at 0.1 Hz for 10-30 trials. A subset of paired-pulse recordings were performed using Cs internal solution (2). In all other assays, a single suprathreshold pre-synaptic stimulus was delivered at 0.1 Hz. The peak response amplitude, rise time 20-80 % and decay time 80-20 % were assessed from an averaged trace (excluding failures). The coefficient of variation (COV), latency and jitter (excluding failures), and the failure rate, were obtained across 10-30 trials, and averaged where appropriate. The latency was the time from the action potential peak to 5 % of the response amplitude, and values that were ± 1.5 x interquartile range (IQR) were considered to be outliers and therefore excluded. Trials that generated responses ≤7 pA were considered to be failures, as synaptic responses below this threshold could not be reliably detected above noise. Post-synaptic responses that had a latency of the median ±2 ms (determined for each individual connection) were also considered to be failures, as such events were likely to have been generated by polysynaptic connections or spontaneous activity. Trials with a response contaminated by large network events were excluded from analysis. On very rare occasions the post-synaptic response was suprathreshold and an action potential was triggered, these were excluded from analysis as the EPSC properties could not be clearly distinguished.

2.3.7. Characterization of ChR2-evoked activity

Optical responses were elicited using a 405 nm laser delivered through a 1000 µm fibre-optic and a 700DCXR dichroic.

For pre-synaptic assessment, ChR2-YFP fluorescent NPC-mNgn2 neurons (day 30-40) were targeted. The photocurrent was elicited by 500 ms light pulse delivered at 0.1 Hz. The action

potential threshold and number of action potentials fired was assessed in response to 10 ms light pulses delivered at 0.1 Hz. The latency and jitter were determined from 1-10 ms light pulses.

For post-synaptic assessment, mKate2-positive or non-fluorescent neurons (day 25-55) were targeted. Non-fluorescent cells with a current response latency of ≤1ms were confirmed to express low levels of ChR2 by the generation of a sustained photocurrent, and therefore were excluded. To assay light-evoked post-synaptic responses, light pulses of 0.1-10 ms up to a maximum intensity of 50 mW/mm^2 were delivered at 0.1 Hz. Cells with a reliable and temporally-aligned response within 10 ms of light onset were considered to have an $EPSC_L$. Recordings were made in the presence of 100 µM picrotoxin.

Analysis of $EPSC_L$ was performed as described for $EPSC_P$, in section 2.3.6.

2.3.8. AMPA/NMDA-ratio analysis

Recordings were performed from neurons at day 29-40 with Cs-based internal solution (2) in HEPES external solution (1) supplemented with 100 µM picrotoxin. Cells with an $EPSC_P$ or $EPSC_L$ were stimulated pre-synaptically at 0.1 Hz across ≥20 trials at -70 mV and +60 mV with single trials at intermediate voltages. The response at -70 mV was averaged and the maximum negative peak amplitude within 10 ms was taken as the AMPA-mediated response. The average of a 10 ms window across the peak ≥20 ms after EPSC onset was taken as the NMDA-mediated response. The average time for the AMPA-mediated current to decay to 5% was 13.1 ± 1.6 ms, and therefore at ≥20 ms after EPSC onset the NMDA-receptor mediated component will contribute ≥ 95 % of the current response. The holding potentials were adjusted for the access resistance using the following equation:

Actual holding potential (V) = Intended holding potential (V) - (Holding current (A) x Access resistance (Ω))

The current-voltage relationship was determined using single sweeps from intermediate voltages either side of the current reversal, where an extrapolated EPSP current = 0 pA was used as the response reversal potential (10.5 ± 1.2 mV, n = 19), calculated using the following equations where y = holding potential (mV), x = EPSP current (pA):

$$y = mx + C \qquad m = \frac{y2-y1}{x2-x1} \qquad C = y - mx$$

The AMPA and NMDA-receptor mediated peak current amplitudes were normalised to the driving force to determine the peak conductance using the following equations, before a ratio was calculated:

Driving force (mV) = Actual holding potential (mV) – reversal potential (mV)

Conductance, g (nS) = EPSP current amplitude (pA) / driving force (mV)

To determine the decay time constant of NMDAR-receptor mediated current component of evoked EPSCs, an exponential was fitted to the remaining portion of the current response from 20 ms after EPSC onset in order to avoid contamination from the AMPA-receptor mediated current. In some cases, EPSC recordings were of an insufficient duration or had an NMDA-receptor current decay phase contaminated by polysynaptic activity, and such were omitted from this analysis. The double exponential fit was described by the following equation, where τ describes the decay time constant and A describes the amplitude of the slow and fast components, where relevant:

Single exponential: : $A(t) = A\exp(-t/\tau)$

Double exponential: $A(t) = A_{slow}\exp(-t/\tau_{slow}) + A_{fast}\exp(-t/\tau_{fast})$

Subsequently the weighted time constant (τw) was determined for NMDA-receptor mediated currents fitted with a double exponential in accordance to that described by Cathala et al., 2000 [294]. The weighted time constant was calculated using the following equation:

$$\tau w = \tau slow[Aslow/(Aslow+ Afast)] + \tau fast[Afast/(Aslow+ Afast)]$$

2.3.9. Synaptic plasticity of monosynaptic connections

For all plasticity experiments, neurogenin-2 neurons were aged between day 25-55, and $EPSC_P$ and $EPSC_L$ were both included for population data. All recordings were performed in voltage clamp, with the exception of the plasticity induction period, as detailed in sections 2.3.6 and 2.3.7. Recordings were made using internal solution (3) and HEPES external solution containing 100 µM picrotoxin. In some cases the external Mg^{2+} concentration was decreased to 1 mM. Test stimuli were delivered at 0.1 Hz. A 5 minute baseline period was acquired immediately before applying the plasticity induction protocol, the average across this period is the response amplitude 'before'. Plasticity induction was performed within 15 minutes in whole-cell patch mode. The response was monitored for at least 20 minutes after plasticity induction. The average response 10-20 minutes following the plasticity induction was the response amplitude 'after'. Data was averaged across 1-minute bins and normalised to the average across the 5 minute-baseline period.

For perforated patch-clamping, a 40 mg/mL Amphotericin-B (Sigma) stock solution dissolved in DMSO and sonicated was prepared. The stock solution could be stored at -20 ^{o}C and used within 2 days. Amphotericin-B was further diluted to 80-120 µg/mL in internal solution (3), sonicated for 10s, vortex for 10s, then kept on ice and in the dark, and used within 3 hours. Perforated patch recordings with a sudden drop in access resistance were considered to have spontaneously ruptured and excluded from further analysis.

For control experiments the 'no pairing' period involved both cells receiving no stimuli for 60 s in voltage clamp. In some cases the post-synaptic cell was held in current clamp and stimulated to fire 60 x action potentials at 1 Hz. The pre-synaptic cell was not stimulated. 8/9 experiments were performed using perforated patch clamp.

For spike-timing LTP experiments the post-synaptic cell was held in current-clamp and induced to fire an action potential ≤ 20ms from pre-synaptic stimulus onset which was repeated for 60 trials at 1 Hz for LTP induction. 1/10 experiments was performed using perforated patch clamp.

For LTP induction using the pairing-protocol the post-synaptic cell was held in voltage-clamp and depolarized to 0 - +20mV whilst the pre-synaptic cell was stimulated at 2 Hz for 240-360 trials for LTP induction. In 3/8 experiments cells were pre-treated in the incubator with 1 µM TTX for 4-72 h, or 500 µM glycine or 500 µM glutamine was included in the external solution. All experiments were performed using perforated patch clamp.

To be included in analysis recordings required a stable 5 minute baseline with a response amplitude that deviated by ≤ 15 % and a COV ≤ 0.4. The 10-20 minute period post-induction must have an average access resistance and membrane resistance that did not change by ≥ 30 % of the 5 minute baseline average.

2.3.10. Chemical LTP

A chemical LTP solution (100 µM picrotoxin, 50 µM forskolin and 0.1 µM rolipram in HEPES external solution (1) without Mg^{2+}) was bath applied for 16 minutes at 30 ^{o}C to neurogenin-2 neurons, aged day 23-30. For control experiments, 0.2 % v/v DMSO was included in the external solution. After chemical LTP induction cells were perfused with picrotoxin (100 µM) and TTX (1 µM) and whole-cell recordings of mEPSCs were made using K- based Internal solution (2) for ≤ 120 mins. mEPSCs were analysed as described in section 2.3.4.

2.4. Statistics

Statistics were performed using GraphPad Prism software (GraphPad), bars show mean ± SEM, unless otherwise stated. Each dataset was tested for normality using the D'Agostino & Pearson omnibus normality test before applying an appropriate two-tailed statistical test, and was treated as unpaired, unless otherwise stated. Results were corrected for multiple comparisons. ns = not significant, * $p < 0.05$, ** $p < 0.01$, *** $p < 0.001$.

III: Generation and characterization of healthy control and familial AD-patient iPSC-derived cortical neurons

3.1. Introduction

The advent of iPSC technology provides the opportunity to investigate synaptic dysfunction in human neurons derived from patients clinically diagnosed with AD. Rodent models of AD have demonstrated synaptic deficits associated with cognitive and memory impairments [72, 295]. The development of human iPSC technology now enables such processes to be explored in a human model system and can provide a platform to validate how accurately rodent models capture synaptic dysfunction in AD and to investigate human-specific disease processes. Given the likely importance of synaptic dysfunction in causing the predominant disease symptoms, it is essential to understand how this manifests in human AD pathogenesis.

In order to investigate synaptic dysfunction in human neurons we must first generate functional cortical neurons from iPSCs derived from AD patients and healthy control individuals. As discussed in Chapter I, there are multiple publications describing human stem cell differentiation to neuronal sub-types. Differentiation into cortical neurons capitalises on the observation that excitatory cortical differentiation appears to be the default pathway following stem-cell patterning to neural ectoderm [148, 150, 161]. Specifically, the protocol developed by Shi et al., (2012) [149, 150] provides a number of advantages. Firstly, the protocol is a simple, monolayer differentiation that generates an expandable pool of cortical progenitor cells with high efficiency. Secondly, all sub-classes of cortical neuron are generated in a temporal sequence analogous with *in vivo* development, which form active excitatory synaptic networks. Thirdly, this protocol has successfully captured aspects of AD-pathology in neurons derived from patients with Down syndrome [167].

Whilst sAD accounts for the vast majority of patients, the origin of disease initiation is likely to be a complex combination of genetic and environmental factors that are challenging to study and are only beginning to be understood. The autosomal dominant and highly penetrant genetic mutations underlying the rare familial forms of AD offer a reliable initiation of disease pathogenesis. With the exception of disease-onset age, the familial and sporadic forms of AD are largely similar in terms of their disease presentation and pathology [296-298]. Therefore, insights gained from studying fAD-patient iPSC-derived neurons are likely to have implications for sAD.

Within this chapter I wanted to address the following questions:

- Can iPSCs from healthy control individuals and patients with fAD, which harbour mutations in *PSEN1* and *APP*, be differentiated into cortical neurons?
- Are the iPSC-derived cortical neurons functional and do they form active synaptic networks?
- Do the iPSC-derived cortical neurons derived from fAD patients' exhibit alterations in secreted Aβ-peptide composition?

3.2. Results

3.2.1. Human iPSCs from healthy controls can be directed towards a neural lineage to generate cortical neural progenitor cells and excitatory neurons

Human iPSCs from healthy control individuals were differentiated to cortical neurons using the protocol published by Shi et al., (2012) (***Figure 3.1a***) [149, 150]. Firstly, a monolayer of feeder-free iPSCs were induced to neural ectoderm by exposure to dual-SMAD inhibitors over a period of 12 days. By day 12 a dense neuroepithelial sheet was formed, which was lifted in large aggregates and replated with FGF2 to promote progenitor proliferation. Semi-quantitative RT-PCR was used to demonstrate that the formation of the neuroepithelial sheet was associated with the loss of mRNA expression for the pluripotency factor *OCT4,* and the upregulation of the cortical progenitor

transcription factors *PAX6*, *FOXG1* and *OTX1* (***Figure 3.1b***). From around day 16, neural rosette structures spontaneously formed. These rosettes were primarily comprised of Pax6-positive primary neural progenitor cells (NPCs) which self-organized into a polarized structure with a central lumen (***Figure 3.1a***). Tbr2-positve intermediate progenitor cells were also observed, predominantly on the periphery of rosettes (***Figure 3.1a***). The NPCs were dissociated and expanded several times, from day 20 onwards, during which newly-born neurons gradually appeared on the perimeter of rosettes. At approximately day 30, NPCs underwent a final plating and over time formed a dense MAP2-positive neuronal network (***Figure 3.1a***). Western blotting

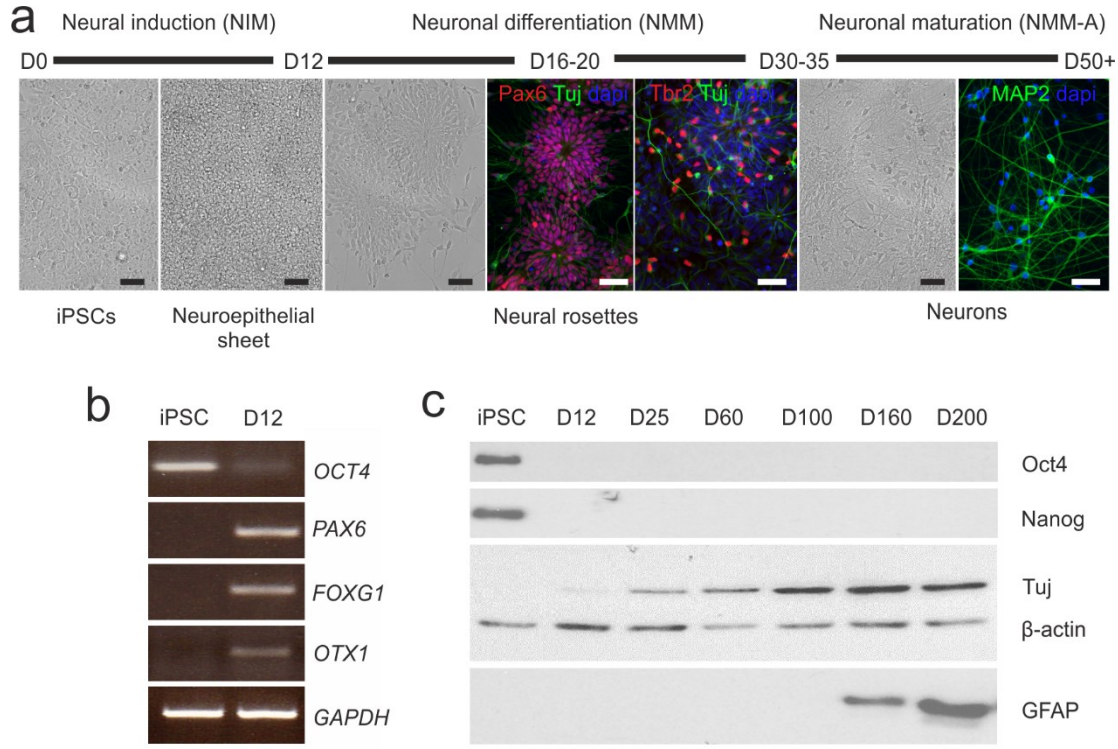

Figure 3.1. Differentiation of human iPSCs into cortical neurons results in loss of pluripotency markers and expression of neural markers. (a) Feeder free human iPSCs at day 0 (D0) were induced to a neuroepithelial sheet using the dual-SMAD inhibitors SB431542 and dorsomorphin for 12 days. After 16-20 days of neural induction, cells start to form polarized rosette structures and neurogenesis begins. NPCs underwent several rounds of expansion before a final plating between days 35-40. Neurons underwent a period of maturation out to 50 days or more to produce extensive neuronal networks. Scale bars 50 µm. **(b)** Semi-quantitative RT-PCR for the pluripotency marker *OCT4* expressed in iPSCs, and the markers of cortical neural progenitor cells *PAX6*, *FOXG1*, *OTX1*, and the control *GAPDH*. **(c)** Western blotting of protein lysates from control iPSCs and neuronal cultures of increasing differentiation age. iPSCs express the markers of pluripotency, Oct4 and Nanog, which are lost during neural induction. Tuj, the neuronal marker, increases with time of differentiation. At later time points the glial marker, GFAP, is present, indicative of the onset of gliogenesis. β-actin is the loading control.

was used to examine the developmental expression of the neuronal marker βIII-tubulin (Tuj) which was detected at day 25, corresponding with the onset of neurogenesis, and increased with time reflecting the continuous generation of neurons. At later stages, in accordance with a switch from neurogenesis to gliogenesis, expression of the glial marker GFAP was detected (***Figure 3.1c***).

In human development the extensive progenitor proliferation and prolonged period of neurogenesis are responsible for generating a large and diverse cerebral cortex. The neurons constituting the cortical layers are generated in an inside-out manner, a characteristic which is reproduced by this cortical differentiation protocol [150]. To assess the reliability of cortical induction, and to characterize the cell types generated, three healthy control cell lines were differentiated and analysed by immunocytochemistry at three time points. Following neural induction, all lines generated Pax6-positive cortical rosettes that were present at day 20-25 (***Figure 3.2a-c***). After the onset of neurogenesis, at day 45-60, subsets of cells expressing deep layer cortical markers, Tbr1 and Ctip2, could be observed (***Figure 3.2d-f***). The proportion of cells expressing either Tbr1 or Ctip2 was quantified and showed that, on average, at least 30% of the cellular population labelled positively for a deep-layer marker (***Figure 3.2j***). In some cases, Tbr1 and Ctip2 were found to be co-expressed, which may represent a stage of cortical projection neuron specification [299]. In older neuronal cultures (day 70-80), small clusters of cells positive for the upper layer cortical marker, Satb2, were detected (***Figure 3.2g-i***). At this stage the cultures had become very dense which, combined with the propensity for the cells to clump together, prohibited quantification of Satb2-positive cells. The sequential expression of deep to upper layer-specific markers is consistent with the progression of cortical differentiation *in vivo* [300].

During the rosette stage, small clusters of cells were occasionally observed that were not Pax6-positive, but instead expressed Nkx2.1, a marker predominantly associated with progenitors residing in the medial ganglionic eminences (MGE) (***Figure 3.2k***). The MGE is responsible for generating the majority of cortical interneurons, which migrate tangentially into the cortex [301,

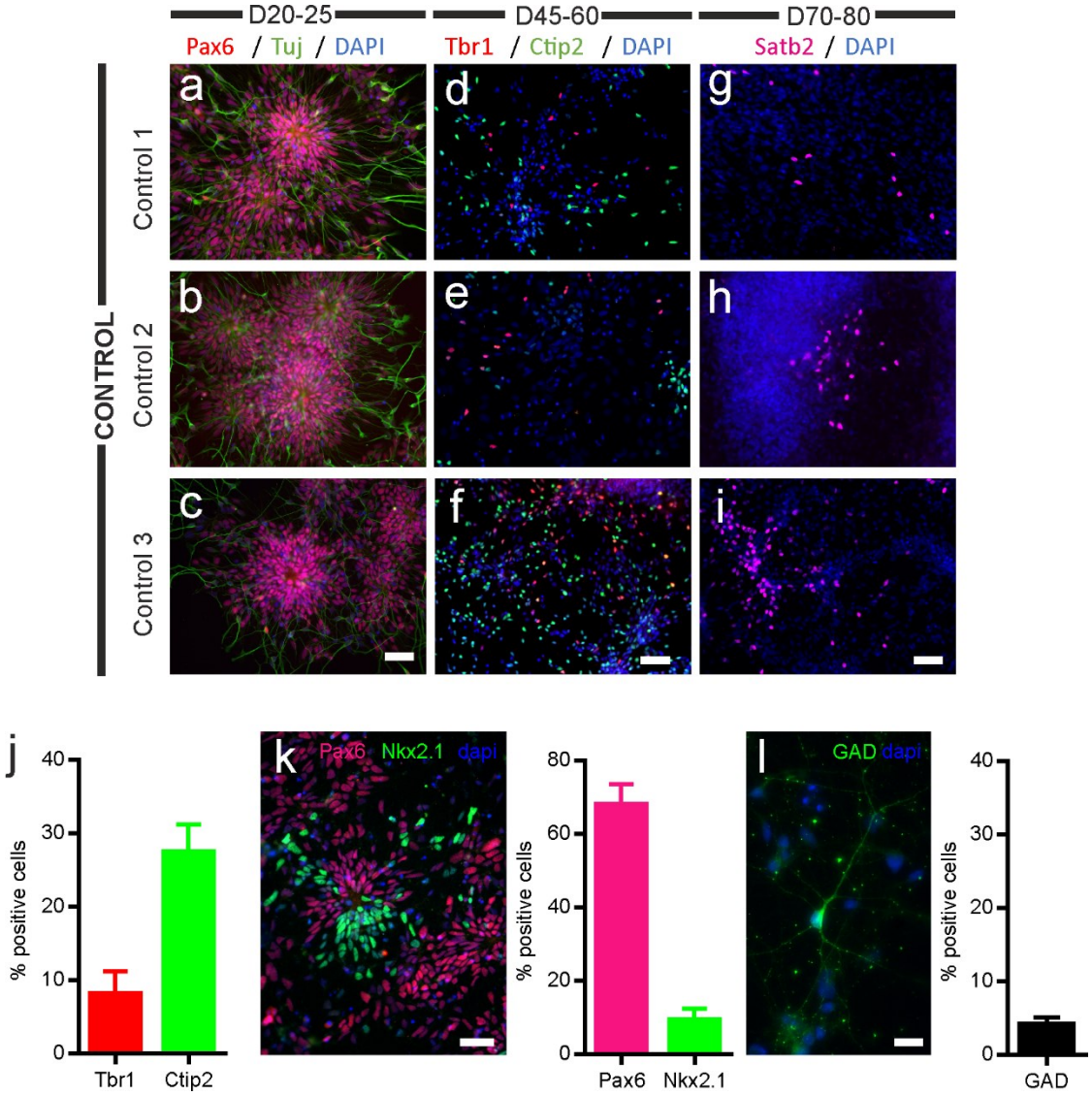

Figure 3.2. iPSC-derived neurons from healthy control individuals express predominantly excitatory cortical progenitor and layer specific markers. iPSC lines from three healthy control individuals were differentiated into cortical neurons. **(a-c)** At day 20-25, all lines generated cortical rosettes comprised of Pax6-positive progenitors that generated Tuj-positive neurons. **(d-f)** At day 45-60, subsets of human neurons labelled positively for the cortical layer 6 marker, Tbr1, and layer 5 marker, Ctip2. **(g-i)** At day 70-80, cells expressing the layer 2-4 marker, Satb2, could be observed. Scale bars 50 µm. **(j)** Quantification of Tbr1 and Ctip2 in day 45-60 cultures (n = 16 FOV, from 4 differentiations across 3 cell lines). **(k)** Example image of a region within a cortical culture containing Nkx2.1-positive cells. Scale bar 50 µm. **(l)** Quantification of Pax6-positive and Nkx2.1-positive cells at day 25 (n = 11 FOV from 1 differentiation). **(m)** Example image of a GAD-positive interneuron observed in an iPSC-derived cortical culture. Scale bar 20 µm. **(n)** Quantification of GAD-positive cells at day 50 (n = 12 FOV from 1 differentiation).

302]. Consistent with this, a very small proportion of cells (4.1 ± 1.0 %, n = 12 FOV; ***Figure 3.2l***) were positive for the GABAergic interneuron marker, GAD, at day 50. Nevertheless, the vast majority of the progenitor cells at day 20-25 were Pax6-positive, which is consistent with the expression of excitatory cortical neuronal markers following the onset of neurogenesis. These results are in line with those described in the original publication by Shi et al., (2012) and demonstrate that this protocol reproducibly generates predominantly excitatory cortical-like neurons.

3.2.2. iPSC-derived cortical neurons are functional and mature over time

A newly-born neuron undergoes a period of maturation, which includes the development of an excitable membrane and integration of the neuron into a synaptic network. To determine the extent of functional maturation, cortical cultures derived from one differentiation of a healthy control cell line were assessed using whole-cell patch clamp electrophysiology. Cells with multiple processes, consistent with a neuronal morphology, were targeted and their intrinsic membrane properties assayed at two time points: day 50 and day 80 (n = 12 and 10 cells, respectively; ***Figure 3.3a, b***). Neurons were subjected to a step-wise voltage clamp protocol (-90 mV to +30 mV, Δ10

Figure 3.3. (*cont. from previous page*) iPSC-derived cortical neurons differentiated from a control cell line that were assessed using whole-cell patch clamp electrophysiology at 50 ± 5 and 80 ± 5 days in culture. **(b)** Brightfield image of a patched iPSC-derived neuron at day 80. **(c)** Diagram showing the measurement of the voltage-gated sodium and potassium currents in voltage-clamp mode in response to a depolarizing voltage step. **(d)** Diagram showing the measurement of action potential firing properties in current clamp in response to a depolarizing current step. **(e)** Representative examples of voltage-gated currents (scale bar 200 pA, 100 ms) in response to a voltage-step protocol (-90 mV to +30 mV, Δ10 mV), and induced action potential firing (scale bar 20 mV, 100 ms) in response to a current-step protocol (-20 pA to +55 pA, Δ5 pA) recorded from day 50 and day 80 neurons. The intrinsic membrane properties from the young and old neurons and showed a trend towards increased maturity with time in culture, which in some cases reached significance: **(f)** resting membrane potential ($p = 0.7169$, M-W test), **(g)** membrane capacitance ($p = 0.0407$, M-W test), **(h)** membrane resistance ($p = 0.5822$, unpaired t-test), **(i)** maximum sodium current ($p = 0.0270$, unpaired t-test), **(j)** maximum potassium current ($p = 0.3767$, unpaired t-test), **(k)** number of consecutive action potentials ($p = 0.0573$, M-W test), **(l)** action potential threshold ($p = 0.6522$, unpaired t-test), and **(m)** action potential amplitude ($p = 0.0185$, M-W test). **(n)** The average current-voltage relationship (IV-plot) for voltage-gated sodium and potassium currents in day 50 (*blue*) and day 80 (*black*) neurons. n = 12 and 10 cells, from 1 differentiation, for day 50 and day 80, respectively. * $p < 0.05$.

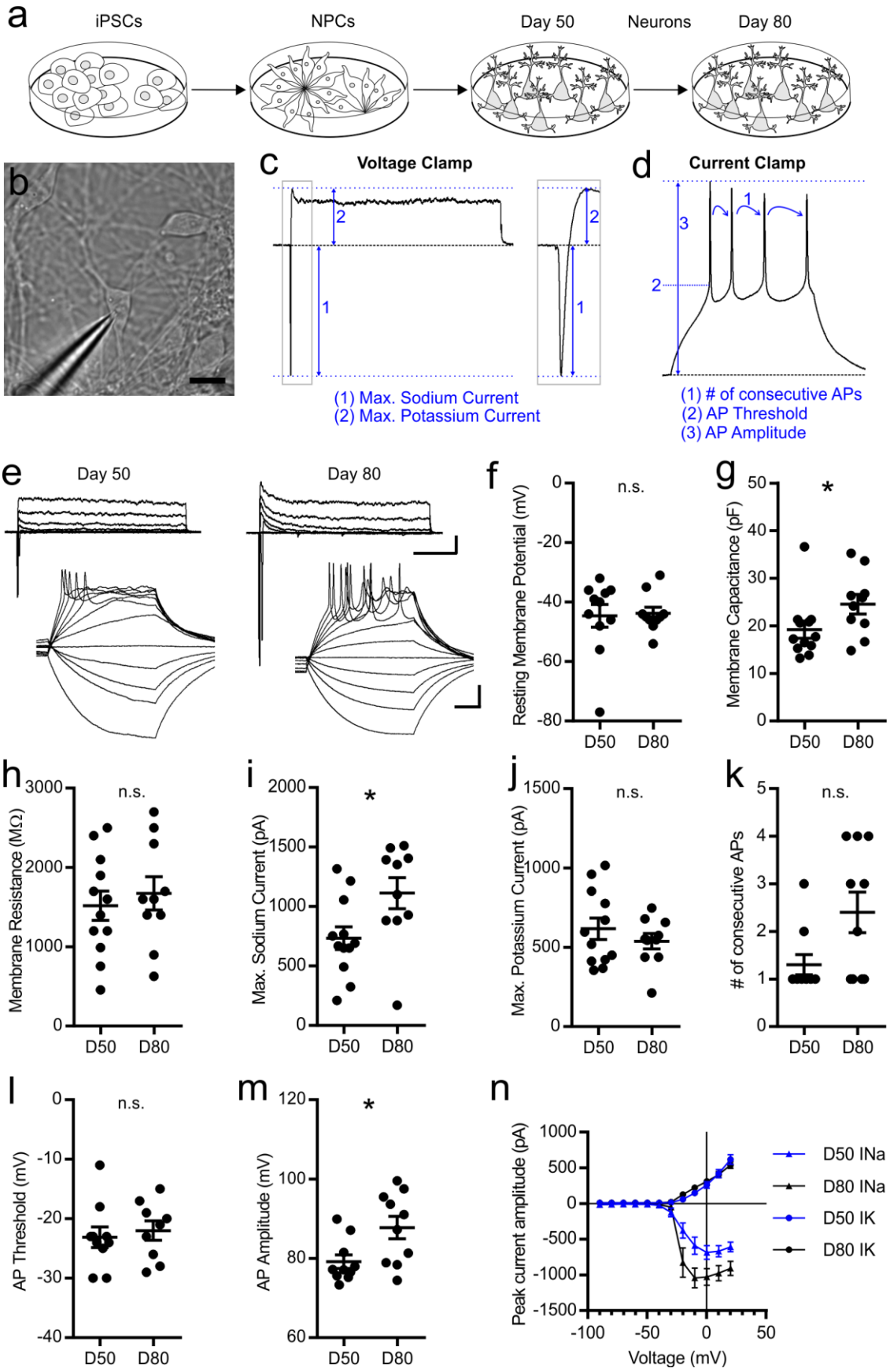

Figure 3.3. iPSC-derived cortical neurons are functional and their intrinsic membrane properties mature with time in culture. (a) Schematic of the experiment showing (*cont. on following page*)

mV), to determine the peak amplitudes of the inward voltage-gated sodium current and outward voltage-gated potassium current, and a step-wise current clamp protocol (-20 pA to +55 pA, Δ5 pA) to measure action potential firing properties (***Figure 3.3c, d***). At both time points assayed, neurons were able to demonstrate voltage-gated sodium and potassium currents and could generate an action potential (***Figure 3.3e***). Day 50 and day 80 neurons had a resting membrane potential, which did not differ significantly (-44.6 ± 3.8 mV for day 50, and -43.8 ± 2.0 mV for day 80, p = 0.7169, M-W test; ***Figure 3.3f***). Correction of these values for the liquid junction potential (see section 2.3.3) indicates that human iPSC-derived neurons have an average resting membrane potential of approximately -60 mV. Neurons from the older cultures had a significantly larger membrane capacitance (19.2 ± 1.8 pF for day 50, and 24.6 ± 2.1 pF for day 80, p = 0.0407, M-W test; ***Figure 3.3g***) indicative of more extensive processes. No difference was observed in the membrane resistance between the two time points (1517 ± 184 MΩ for day 50, and 1673 ± 210 MΩ for day 80, p = 0.5822, unpaired t-test; ***Figure 3.3h***). Day 80 neurons had significantly larger voltage-gated sodium currents (733 ± 95 pA for day 50, and 1112 ± 131 pA for day 80, respectively, p = 0.0270, unpaired t-test; ***Figure 3.3i***) reflecting the incorporation of a larger number of voltage-gated sodium channels into the membrane, whilst no difference was observed in the voltage-gated potassium current amplitude (616 ± 68 pA for day 50, and 539 ± 48 pA for day 80, p = 0.3767, unpaired t-test; ***Figure 3.3j***). Day 80 neurons showed a trend to fire an increased number of consecutive induced action potentials, although this did not reach significance (1.3 ± 0.2 for day 50, and 2.4 ± 0.4 for day 80, p = 0.0573, M-W test; ***Figure 3.3k***). The action potential threshold was comparable between day 50 and day 80 neurons (-23.1 ± 1.7 mV for day 50, and -22.0 ± 1.6 mV for day 80, p = 0.6522, unpaired t-test; ***Figure 3.3l***), equivalent to approximately -39 mV when corrected for the liquid junction potential. The voltage-gated sodium current generates the depolarizing phase of an action potential and consistent with this, day 80 neurons fired action potentials of a larger amplitude than those generated by day 50 neurons (79.2 ± 1.7 mV for day 50, and 87.8 ± 2.8 mV for day 80, p = 0.0185, M-W test; ***Figure 3.3m***). The current-voltage relationship

(IV-plot) (***Figure 3.3n***) demonstrates the activation of voltage-gated sodium channels at a voltage equivalent to the AP threshold determined in current clamp. The results are summarised in ***Table 3.1*** alongside the values reported for mature adult cortical neurons [303, 304]. Collectively, day 80 neurons exhibited more mature intrinsic neuronal properties than day 50 neurons, consistent with a progressive neuronal maturation over time. However, comparison of the intrinsic properties to those reported for mature adult human neurons indicates that human iPSC-derived neurons cultured for 80 days represent a relatively immature state. In addition, the distribution of each dataset demonstrates substantial variability of the intrinsic properties between cells within a culture.

Property	**hiPSC-derived cortical neurons**						**Mature adult neurons**	
	Day 50		**Day 80**				**Human (18-61 years)**	**Rat (P21 -36)**
	mean ± SEM	n (cells)	mean ± SEM	n (cells)	*p* value	Direction of change	Mean ± SEM	
Resting membrane potential (mV)	-44.6 ± 3.8	11	-43.8 ± 2.0	10	0.7169	↔	-73.2 ± 0.8	-76.5 ± 0.9
Membrane capacitance (pF)	19.2 ± 1.8	11	24.6 ± 2.1	10	0.0407*	↑	N/A	N/A
Membrane resistance (MΩ)	1517 ± 184	11	1673 ± 210	10	0.5822	↔	70 ± 6	70 ± 7
Max. Sodium current (pA)	733 ± 95	11	1112 ± 131	10	0.0270*	↑	N/A	N/A
Max. Potassium current (pA)	616 ± 68	11	539 ± 48	10	0.3767	↔	N/A	N/A
# of consecutive APs	1.3 ± 0.2	11	2.4 ± 0.4	10	0.0573	↗	Repetitive firing	Repetitive firing
AP Threshold (mV)	-23.1 ± 1.7	11	-22.0 ± 1.6	10	0.6522	↔	-40.6 ± 0.6	-54.8 ± 0.5
AP Amplitude (mV)	79.2 ± 1.7	11	87.8 ± 2.8	10	0.0185*	↑	139.8 ± 1.2	N/A

Table 3.1. Summary table of the intrinsic membrane properties of day 50 and day 80 neurons alongside the values reported by: Testa-Silva et al., 2014 [285] for mature adult human cortical layer 2/3 neurons in non-pathological samples derived from individuals aged 18–61 years (membrane potentials were not corrected for the liquid junction potential in this study), and Zhang 2004 [286] for wild-type rat layer V pyramidal neurons at postnatal day (P) 21-36 (membrane potentials were corrected for the liquid junction potential in this study). * $p < 0.05$

Having characterized the membrane properties of iPSC-derived cortical neurons and demonstrated the development of intrinsic excitability, I sought to determine whether these cells formed active synaptic networks. Firstly, the formation of physical synapses was assessed by immunocytochemistry. Neurons generated dense cultures of MAP2-posititve processes (***Figure 3.4a***), which were infrequently associated with punctate expression of the pan-synaptic marker synaptophysin, and the markers of glutamatergic and GABAergic synapses PSD95 and GAD-65, respectively. Short regions of MAP2-positive dendritic processes were co-localised with synaptophysin puncta, consistent with the formation of pre-synaptic compartments (***Figure 3.4b***). On occasion, GAD-65-positive puncta were associated with sections of MAP2-positive dendrite (***Figure 3.4c***), suggesting the formation of inhibitory pre-synaptic compartments, which is consistent with the small proportion of interneurons observed in the neuronal cultures (see ***Figure 2***). In general, the formation of spines was not observed, although on occasions, filopodic structures (considered to be immature precursors of spines [305]) could be observed. Furthermore, immunolabelling with markers of excitatory post-synaptic compartments, such as PSD95, revealed limited numbers of puncta (***Figure 3.4d***).

These data suggest that these cortical cultures exhibit immature synapse formation, although limitations in antibody specificity and sensitivity may preclude the accurate detection of excitatory synaptic markers. Therefore, to functionally assess the presence of excitatory synapses in these cultures, experiments were performed using whole-cell patch clamp electrophysiology. The majority of excitatory basal synaptic transmission in the cortex is mediated by AMPA-receptors. First, to determine whether iPSC-derived cortical neurons expressed functional AMPA receptors, cells were exposed to a short duration puff of glutamate directed towards the cell soma. This induced a rapid inward current with a fast rise phase, characteristic of an AMPA receptor mediated response. The slow decay phase was likely a result of the passive diffusion of the high concentration of glutamate. The application of the AMPA receptor antagonist CNQX entirely abolished the

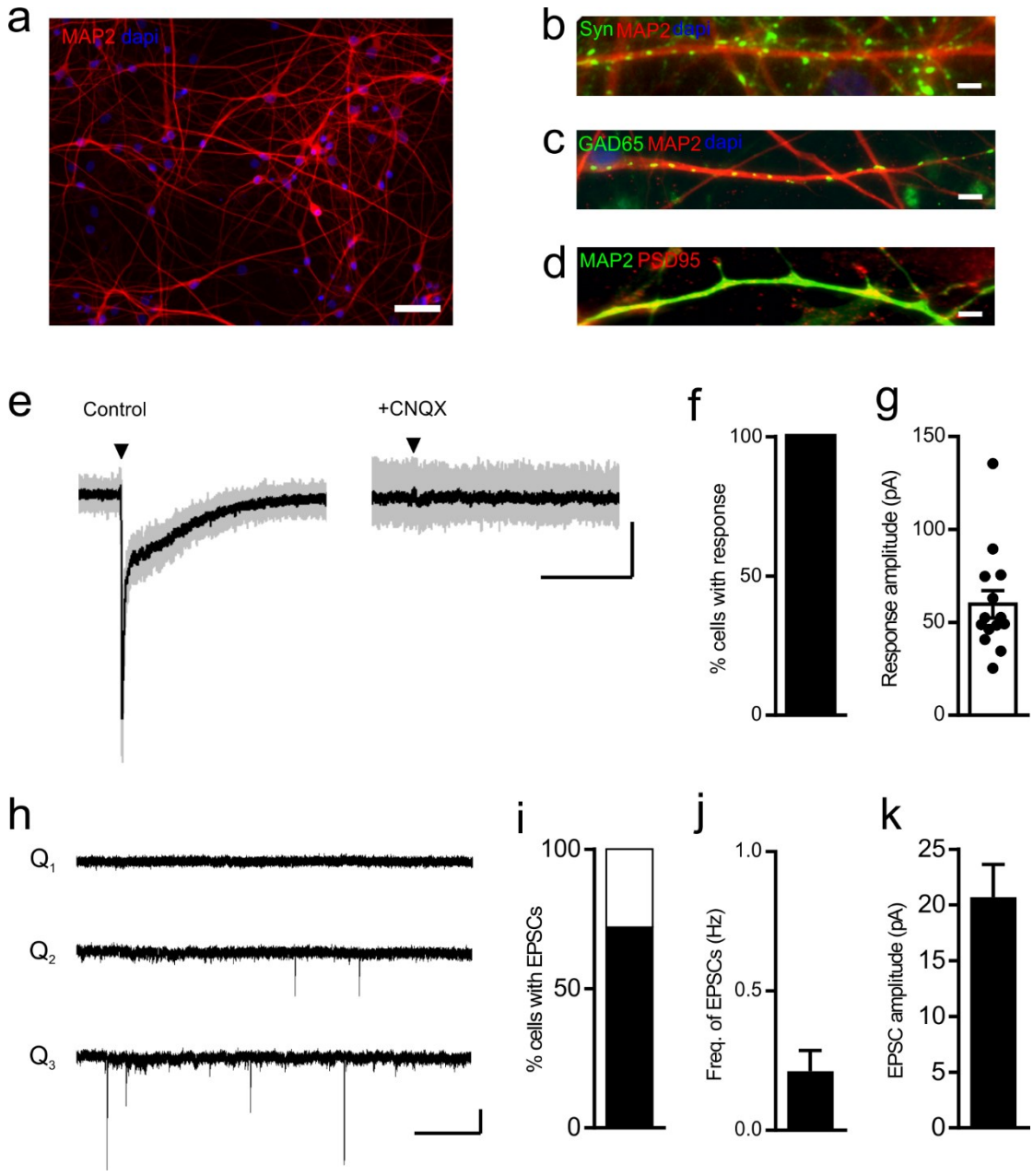

Figure 3.4. iPSC-derived neurons form functional glutamatergic synapses. (a) Example image of extensive MAP2-positve processes in iPSC-derived cortical cultures. Scale bar 50 µm. **(b)** Example image of synaptophysin-positive pre-synaptic puncta associated with a MAP2-positive dendrite. Scale bar 5 µm. **(c)** Example image of GAD65-positive pre-synaptic inhibitory puncta associated with a MAP2-positive dendrite. Scale bar 5 µm. **(d)** Example image of PSD95-positive puncta associated with a MAP2-positive dendrite. Scale bar 5 µm. **(e)** Day 90-110 iPSC-derived cortical neurons generated a rapidly activating excitatory current in response to a 10 ms duration puff of 600 µM glutamate onto the cell soma, whilst holding the neuron at V_m = -70 mV. The response was completely abolished by CNQX. The arrowhead (▼) denotes the onset of the glutamate puff. Scale bar 20 pA, 500 ms. **(f)** The proportion of cells responding to a glutamate puff, and **(g)** the amplitude of the response to a glutamate puff (n = 14 cells from 2 differentiations of 1 cell line). **(h)** Example recordings of spontaneous EPSCs recorded at V_m = -70 mV from day 75-105 neurons, representing the lower quartile (Q_1), median (Q_2), and upper quartile (Q_3) levels of activity. **(i)** The proportion of cells with EPSCs (n = 32 cells). **(j)** The frequency of EPSCs (n = 32 cells). **(k)** The amplitude of EPSCs (n = 23 cells) (From 4 differentiations of 1 cell line).

response, confirming that the response was mediated by AMPA receptors (***Figure 3.4e***). All neurons exposed to a glutamate puff demonstrated an inward current (100 %, 14/14 cells; ***Figure 3.4f***), which had an average peak amplitude of 59.79 ± 7.39 pA (n = 14 cells; ***Figure 3.4g***). Having established that neurons expressed some synaptic proteins and functional AMPA receptors, I explored whether they could exhibit spontaneous excitatory synaptic transmission. Neurons that were voltage-clamped at -70 mV displayed fast excitatory post-synaptic currents (EPSCs) (***Figure 3.4h***). EPSCs could be observed in the majority of cells (72 %, 23/32 cells; ***Figure 3.4i***) and had an amplitude of 20.71 ± 2.93 pA (n = 23 cells; ***Figure 3.4k***). However the frequency of these events was low (0.2 ± 0.07 Hz, n = 32 cells; ***Figure 3.4j***). Taken together, these data indicated that the human iPSC-derived cortical neurons expressed functional AMPA receptors and could exhibit spontaneous glutamatergic synaptic activity, albeit at low frequency.

3.2.3. iPSCs from fAD-patients can be differentiated into cortical neurons and have comparable intrinsic membrane properties to healthy controls

Having established that healthy control iPSCs could be differentiated into functional excitatory cortical neurons, I sought to investigate whether iPSCs derived from fAD patients also had the capacity to undergo cortical differentiation. To that end, human iPSCs from four patients with fAD, arising from mutations in *APP* or *PSEN1*, were subjected to neural induction to determine their capacity to generate excitatory cortical cultures. All cell lines generated cultures with Pax6-positive neural rosettes at day 20-25 (***Figure 3.5a-c***), and, following the onset of neurogenesis, gave rise to neurons positive for deep and upper layer cortical markers in the same manner as healthy controls (***Figure 3.5e-m***).

To determine whether a fAD genetic background has an impact on functional neuronal maturation, the intrinsic membrane properties of iPSC-derived cortical neurons from fAD patients and a healthy control were compared (***Figure 3.6a***). At day 80, fAD patient iPSC-derived cortical neurons could fire induced action potentials (***Figure 3.6b***) and were comparable to healthy control neurons in

their resting membrane potential (p = 0.6857), membrane capacitance (p = 0.3429), membrane resistance (p = 0.4857), maximum sodium current (p = 0.3429), maximum potassium current (p = 0.8857), number of consecutive action potentials (p = 0.2000), action potential threshold (p > 0.9999), and action potential amplitude (p = 0.3429) (n = 4 differentiations across 4 cell lines and 4 differentiations from 1 cell line for fAD and control, respectively; ***Figure 3.6c-j***). Overall, fAD neurons possessed equivalent intrinsic membrane properties to healthy control neurons at day 80.

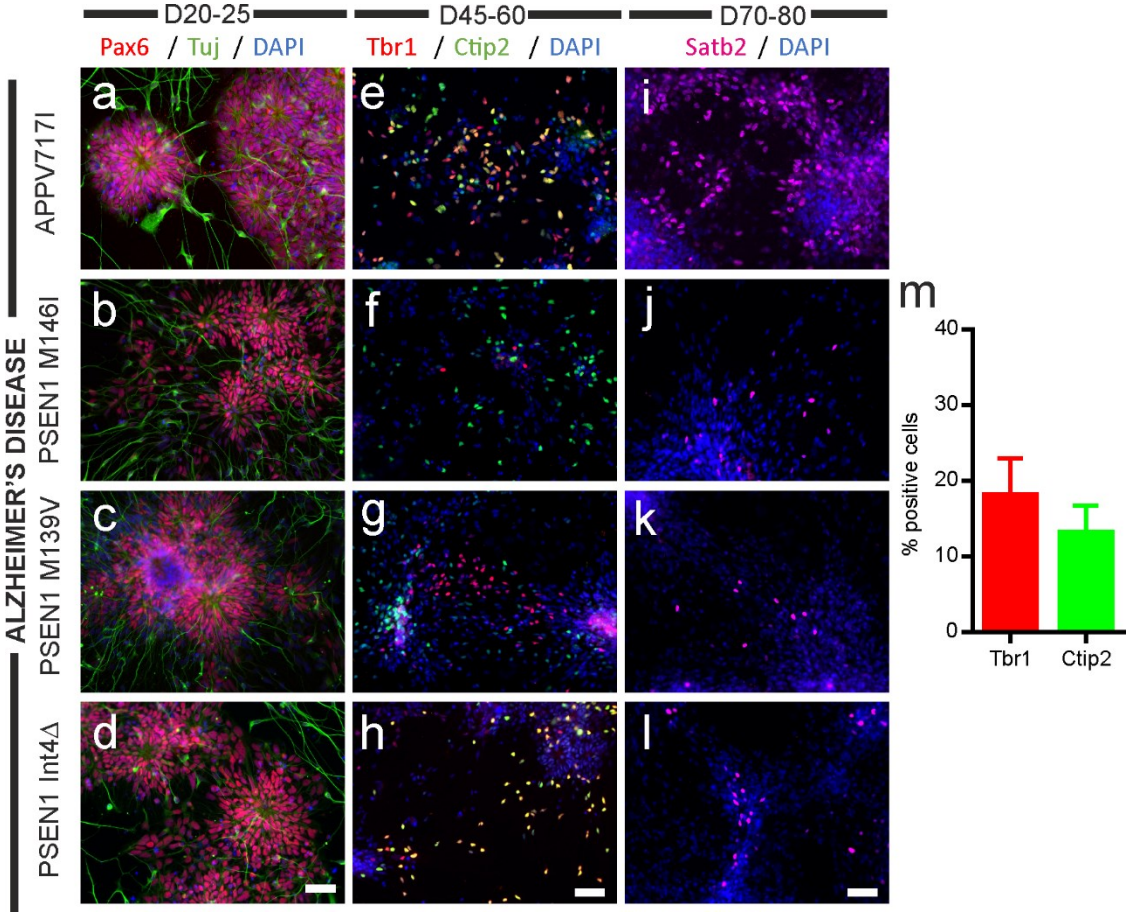

Figure 3.5. iPSC-derived neurons from patients with familial Alzheimer's disease express excitatory cortical progenitor and layer specific markers. iPSC lines from four patients with fAD were differentiated to cortical neurons. **(a-d)** At day 20-25 all lines generated cortical rosettes comprised of Pax6-positive progenitors that gave rise to Tuj-positive neurons. **(e-h)** At day 45-60 subsets of human neurons labelled positively for the cortical layer 6 marker, Tbr1, and layer 5 marker, Ctip2. **(i-l)** At day 70-80, cells expressing the layer 2-4 marker, Satb2, could be observed. Scale bars 50 µm. **(m)** Quantification of Tbr1 and Ctip2 in day 45-60 cultures (n = 16 FOV from 4 differentiations across 4 cell lines).

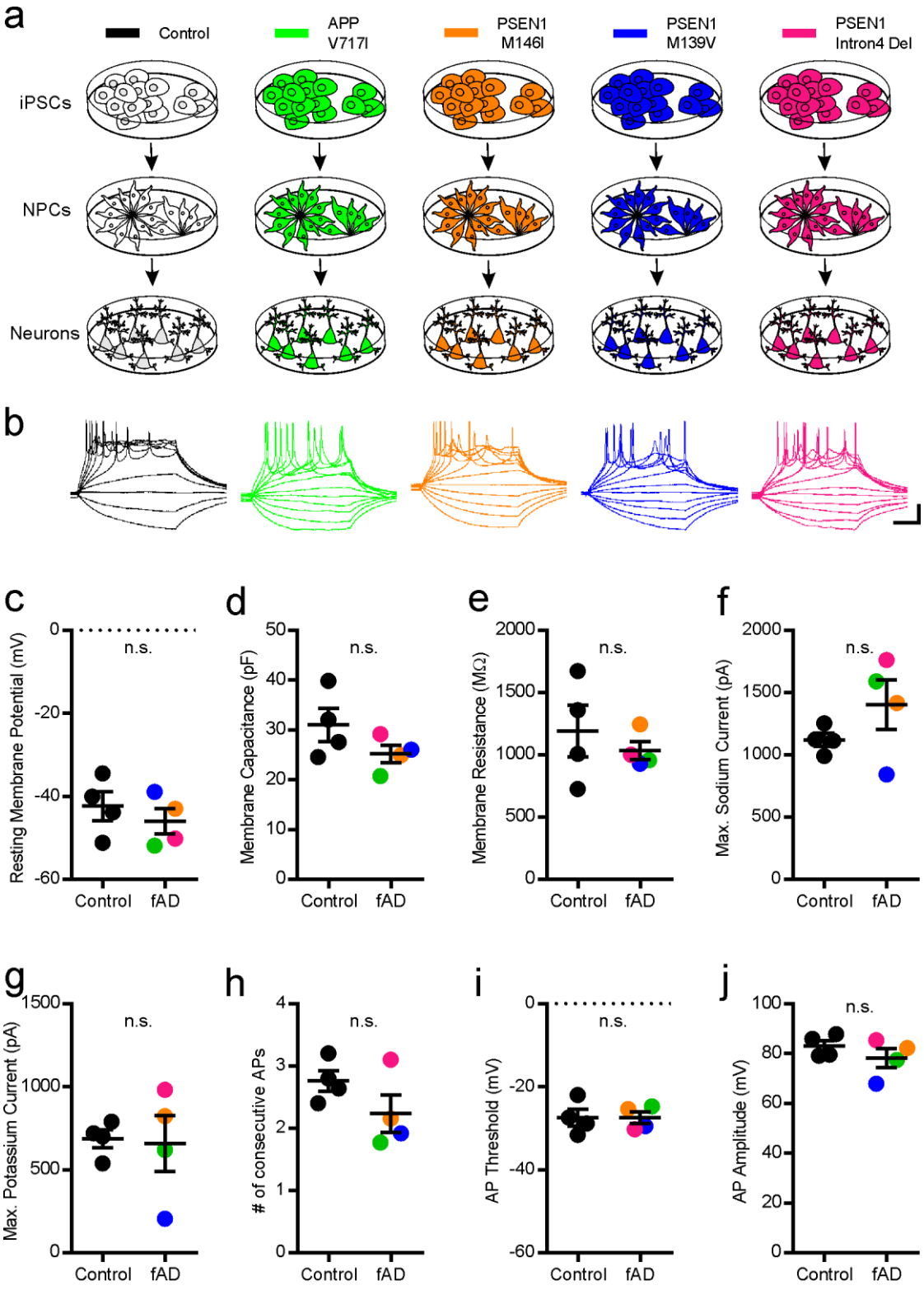

Figure 3.6. AD-patient iPSC-derived neurons are functional and have comparable intrinsic membrane properties to healthy control neurons. (a) Schematic of the experiment showing neurons derived from a healthy control and four fAD-patient iPSC- lines with mutations in *APP* or *PSEN1*. Neurons were cultured under comparable conditions until they were assessed at 80 ± 5 days. **(b)** Example traces of induced action potential firing from control and AD-patient iPSC-derived neurons. Scale bar 20 mV, 100 ms. Comparison of AD-patient neurons to those derived from a healthy control individual showed no differences across the intrinsic (*cont. on previous page*) membrane properties measured: **(c)** resting membrane potential ($p = 0.6857$), **(d)** membrane

3.2.4. iPSC-derived cortical neurons from fAD patients have altered Aβ-peptide secretion

The fAD-associated genetic mutations are believed to alter the processing of APP, and therefore affect the production of Aβ peptides [30]. Changes in the total Aβ peptide production or the ratios of Aβ-species have previously been reported in iPSC-models of AD [160, 164, 166]. To ascertain whether the fAD patient iPSC-derived cortical cultures generated here also exhibited alterations in secreted Aβ peptide species, media samples from day 80 cortical cultures were collected 48 hours after a full media change. The Aβ42:40 ratio exhibited a robust and significant increase ($p = 0.0061$, M-W test) in fAD cultures (n = 4 differentiations across 4 cell lines), relative to healthy controls (n = 7 differentiations across 3 cell lines) (***Figure 3.7a***). Meanwhile, no difference was detected in the total level of Aβ42 ($p = 0.2303$, M-W test) or Aβ40 ($p = 0.4121$, M-W test) produced by the cultures (***Figure 3.7b, c***). This demonstrates that the cortical cultures can exhibit AD associated alterations in Aβ peptides.

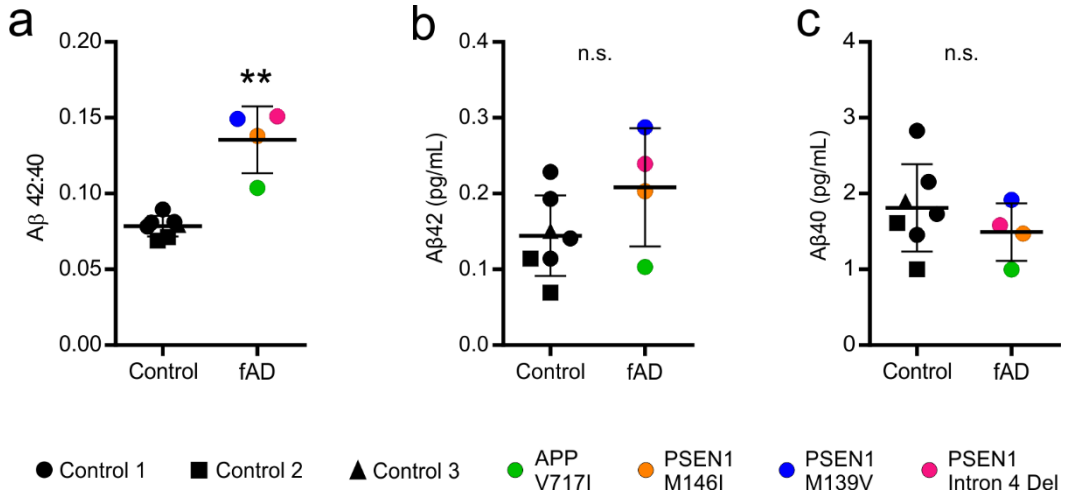

Figure 3.7. fAD patient iPSC-derived cortical cultures exhibit alterations in secreted amyloid-β peptides. Media samples from day 80 neurons were collected 48h following a full medium change and the secreted Aβ species were quantified using an MSD immunoassay and normalised to the total protein lysate. **(a)** fAD patient iPSC-derived cortical cultures had a significantly higher Aβ42:40 ratio than healthy controls ($p = 0.0061$). **(b)** There was no significant difference in the Aβ42 concentration ($p = 0.2303$), or **(c)** the Aβ40 concentration ($p = 0.4121$). n = 7 differentiations across 3 cell lines for control, and n = 4 differentiations across 4 cell lines for fAD, which were compared using a M-W test. ** $p < 0.01$

Figure 3.6. (*cont. from following page*) capacitance ($p = 3429$), **(e)** membrane resistance ($p = 0.4857$), **(f)** maximum sodium current ($p = 0.3429$), **(g)** maximum potassium current ($p = 0.8857$), **(h)** number of consecutive action potentials ($p = 0.2000$), **(i)** action potential threshold ($p > 0.9999$), and **(j)** action potential amplitude ($p = 0.3429$). n = 4 differentiations (5-13 cells per differentiation) from a control cell line and across 4 fAD cell lines. All properties were compared using a M-W test.

3.3. Discussion

Utilising a published protocol I have confirmed that I can generate excitatory cortical neurons from healthy control individuals and fAD patients. The resulting neuronal population acquired functional properties, which developed with increasing time in culture. The iPSC-derived cortical neurons acquired key aspects of neuronal function, including the ability to fire action potentials and mediate excitatory synaptic transmission. However, taken together, the intrinsic and synaptic properties reflect a relatively immature neuronal state. Neurons generated from fAD-patients displayed comparable cortical differentiation potential and possessed indistinguishable intrinsic membrane properties to healthy control neurons. Neuronal cultures generated from fAD-patient iPSCs also exhibited a robust elevation in the Aβ42:40 ratio of secreted Aβ peptide species. This demonstrates that the fAD patient iPSC-derived cortical neurons generated in this model have the ability to exhibit an AD-associated biochemical phenotype congruous with the hallmarks of AD pathology.

3.3.1. Differentiation of human iPSCs into cortical neurons

Neuronal differentiation of human iPSCs using the protocol developed by Shi et al., (2012) reliably generated neuronal cultures with a predominantly cortical identity from multiple cell lines. The vast majority of progenitors generated in these cultures expressed markers reminiscent of the cortical SVZ. However, the observation that a minority of progenitors expressed Nkx2.1, a marker of subcortical ventral progenitors, suggests a small degree of inefficient cortical patterning. This progenitor patterning is in accordance with the later observations that a large subset of cells expressed deep-layer excitatory markers with only a minority of GAD-positive interneurons. These GAD-positive cells are likely to have arisen from the ventralised progenitor population. Whilst, this was not reported by Shi et al., (2012), more extensive progenitor ventralisation has been described in similar cortical differentiation protocols [150, 178, 306].

3.3.2. Functional characteristics of human iPSC-derived cortical neurons

Newly-born neurons progressively develop functional properties over time [304, 307]. The generation of an excitable membrane requires the incorporation of ion transporters and channels, and consequently the generation of a hyperpolarized membrane potential. The changes to intrinsic membrane properties, observed from day 50 to day 80 neurons, suggests a continuous functional maturation of the cells. Considerable variability was detected amongst the membrane properties of the neurons at both ages, reflected by the large range of values observed within each parameter measured. For example, the maximum membrane resistance observed was five-fold greater than the minimum. This is likely to reflect heterogeneity in cell age that results from ongoing neurogenesis in the cultures. Whilst the neurons developed some functional properties, they were far from reminiscent of a mature adult neuron. For example, the membrane resistance differed by approximately 20-fold from that observed in mature rodent cortical neurons (see ***Table 3.1***). In addition, the majority of human iPSC-derived cortical neurons could not fire more than two successive action potentials and maintained a depolarized RMP relative to mature cortical neurons (see ***Table 3.1***), even after 80 days in culture. Over time the RMP is expected to become more hyperpolarized as a result of increasing expression of leak K^+ channels, which increase K^+ conductance at rest and thereby shift the RMP closer to the K^+ equilibrium potential [304, 308, 309]. Similarly the action potential threshold was relatively depolarized in comparison to mature cortical neurons, and is expected to become progressively more hyperpolarized during development, in parallel to the RMP, as a result of changes in sodium and potassium ion channel densities [304, 308]. The study of other model systems have demonstrated that whilst the RMP and action potential threshold hyperpolarize during development, the difference between these values remain relatively constant at approximately 20 mV [304, 308, 310, 311]. A similar magnitude difference was evident in the human iPSC-derived cortical neurons generated here. Whilst the neurons exhibited the capacity to respond to glutamate, excitatory synaptogenesis was clearly limited, as reflected by the very low levels of synaptic activity. In contrast, primary cortical cultures

derived from embryonic mice and plated at a comparable density have been shown to exhibit spontaneous frequencies four-fold greater at only 7 DIV, which subsequently increases to approximately 1.5 Hz by 14 DIV and is maintained in older cultures [312]. The amplitude of spontaneous EPSCs in the human iPSC-derived cultures was relatively small (≈ 20 pA) , consistent with that observed in primary cortical cultures at 7 DIV where 90 % of spontaneous EPSCs are ≤ 40 pA, with the majority ≤ 20 pA [312]. Following extensive synapse formation during development the amplitude of spontaneous EPSCs greatly increases by 14 DIV, with 85 % of events larger than 100 pA [312]. Similar findings have also been reported in acute slices of rodent cortical tissue during postnatal development [304]. Whilst EPSPs were not assessed, based upon the EPSCs observed excitatory synaptic inputs would be expected to exert a strong depolarization, largely due to the high membrane resistance, as determined by Ohm's Law. For example, this equates to an amplitude of 34.63 mV (V = IR; 20.71 pA x 1672 MΩ) in an "average" day 80 neuron, indicating that synaptic events are therefore likely to be suprathreshold. Indeed, newly born granule cells in the rodent hippocampus exhibit larger EPSPs relative to the EPSC than mature cells, and small somatic current injections as low as 10 pA can be sufficient to elicit an action potential [313-315]. However, further work would be required to determine the properties of EPSPs in the human iPSC-derived cortical neurons generated here. Overall, the human iPSC-derived cortical neurons possessed the key hallmarks of a functional neuron, but their functional characteristics were reflective of an immature state when compared to mature adult neurons. Consistent with this idea, single-cell analysis of cortical cultures at a similar age generated using the Shi et al., (2012) protocol, has shown that the iPSC-derived cortical neurons are most like human foetal, not adult, neurons [316].

Many studies, including the initial Shi et al., (2012) protocol, present largely descriptive functional characteristics that demonstrate the ability of iPSC-derived cortical neurons to acquire intrinsic electrical excitability and form excitatory synapses [118, 150, 163]. Meanwhile, studies that provide a more detailed and quantitative functional characterization of iPSC-derived neurons report

predominantly immature intrinsic and synaptic properties [159-161], which are consistent with the immature neuronal phenotype described in this chapter. Mouse stem cells have been successfully differentiated to mature functional cortical neurons in less than a month [317, 318]. However, corticogenesis in the human embryo occurs over nearly 100 days, compared to just 7 days in the mouse [319]. This developmental timing may well be reflected by the maturational differences observed in human compared to mouse stem-cell derived neurons. Whilst further culture time may enhance functional neuronal maturity, the current culture period of ~ 100 days already presents a substantial limitation on experimental throughput and is associated with long-term culture issues. For example, the increasing cell density and propensity for the cells to clump together, greatly impacts the suitability of the neuronal cultures for imaging studies and electrophysiological assessment. Moreover, studies investigating tau isoform expression in human iPSC-derived neuronal cultures have revealed primarily foetal tau isoform expression [320, 321]. In humans only 0N3R tau is expressed in the developing foetus, whilst in the adult all six tau isoforms are expressed, with 3R and 4R containing isoforms present at a 1:1 ratio [54]. Detection of 4R tau has been limited in control iPSC-derived neuronal cultures, and even after extensive culture periods (365 days) Sposito et al., (2015) reported that 3R and 4R were not expressed at equal proportions and foetal 0N3R tau remained the predominant isoform [320, 321]. Together, these data suggest that additional factors may be required to promote neuronal maturation or, alternatively, the development of methods that could selectively target more mature neuronal subpopulations that may exist within these heterogeneous cell cultures.

3.3.3. Properties of cortical neurons derived from fAD-patient iPSCs

Cortical cultures generated from four fAD patient iPSC lines were qualitatively comparable to healthy controls. Electrophysiological assessment revealed no differences in the intrinsic membrane properties and also indicated that fAD patient iPSC-derived cortical neurons reached a comparable level of functional maturation. This is perhaps unsurprising given that the major

functional phenotype associated with AD is alterations in excitatory synaptic transmission [51, 72, 79]. There have been a minority of studies reporting alterations in intrinsic neuronal excitability in rodent models of AD, which have included evidence of an increase in initial firing rate, a decrease in action potential width, an increase in the amplitude of the afterdepolarization potential, depolarization of the resting membrane potential and a decreased voltage-gated sodium current density [322-324]. However, these observations are not consistent across studies and the majority of intrinsic neuronal properties, including membrane resistance and membrane capacitance, are unaffected [322-326]. Therefore the results generated here are in line with the majority of findings in AD research models. However, it is possible that the detection of an intrinsic functional phenotype was not possible due to the immature state of the neuronal cultures, or that the protocols used were unable to detect more subtle differences.

Interestingly, the relative functional neuronal immaturity did not preclude the expression of a biochemical AD-associated phenotype. This manifested as a robust increase in the Aβ42:40 ratio of secreted peptides from fAD patient iPSC-derived cortical cultures. However, it was not possible to conclude which Aβ peptide species was responsible for driving this change, as there was no significant difference detected in the total levels of Aβ42 or Aβ40 produced by the cortical cultures. This contrasts with the elevation in total Aβ, Aβ42 and Aβ40 observed in human brain tissue samples derived from Alzheimer's disease patients relative to non-demented controls [327-329]. However the relative proportions of Aβ40 to Aβ42 in iPSC-derived cortical cultures was consistent with human brain tissue, whereby the shorter form is approximately 10 times more abundant [330]. Similarly, the altered composition of secreted Aβ peptides observed here is consistent with the findings from other cell and animal models, which report that the majority of fAD mutations cause an elevation of the Aβ42:40 ratio [30, 33]. Interestingly, the Aβ42:40 ratio determined using cellular models has been shown to correlate with the age of disease onset in fAD [33, 331]. Further work could determine whether this relationship is also evident in human fAD patient-iPSC derived cortical

cultures. Studies have demonstrated that even small changes in the Aβ42:40 can affect the conformation and aggregation of Aβ and result in detrimental synaptic effects [332]. Whether the soluble Aβ-species secreted by these cortical neuronal cultures exist in monomeric or oligomeric structures is currently unknown [333], and the presence of insoluble aggregated forms of Aβ were not examined. Numerous studies modelling fAD with iPSC-derived neurons have also demonstrated alterations in secreted Aβ peptides [160, 164, 166]. However, there have been limited reports of insoluble deposits [167] and indications that 3D neuronal cultures may be more suited to the demonstration of such phenotypes [181], perhaps because they can limit passive diffusion and wash-out of secreted proteins. Nonetheless, Hu et al., (2018) have shown that the composition of the Aβ-peptides secreted by fAD patient iPSC-derived cortical cultures, generated using the Shi et al., (2012) protocol, were able to impair rodent synaptic plasticity *in vivo* [333].

In summary, the neuronal cultures generated here may provide a sufficient platform for the interrogation of certain biochemical phenotypes in fAD patient iPSC-derived cortical neurons, but are limited in their potential to examine complex functional phenotypes. Investigation of synaptic phenotypes in human iPSC-derived cortical cultures requires enhancement of the functional neuronal properties. This will be explored in the following chapter.

IV: Examining methods to accelerate the maturation of glutamatergic synaptic transmission in iPSC-derived cortical neuronal cultures

4.1. Introduction

The generation of human iPSC-derived cortical neurons with immature functional properties, as described in Chapter III, is consistent with those described by others within the field. Many publications using iPSC-derived neurons present only minimal qualitative demonstrations of functional properties [118, 150, 163]. Meanwhile, those that quantitatively describe intrinsic and synaptic properties have reported similarly immature neuronal characteristics, such as low membrane capacitance, high membrane resistance and limited synaptic activity [159-162]. As a result, the investigation of complex functional phenotypes in human iPSC-derived neurons requires the development of methods that can promote neuronal maturation and the generation of active synaptic networks.

In animal studies, the major phase of synaptogenesis and synapse maturation begins late in embryonic development and has been shown to correlate with the onset of gliogenesis in multiple regions of the brain [334, 335]. The association between glia and synapse generation has been strengthened by numerous rodent studies, which have shown that glia can influence the formation and maturation of synapses *in vitro* and *in vivo* [336-339]. The formation of synapses with a normal ultrastructure can occur in the absence of glia, but the addition of glia induces a many-fold increase in the number of synapses and the levels of synaptic activity [336]. The glial-mediated effects upon synaptogenesis are exerted by both contact-dependent and independent mechanisms. The culture of rodent neurons in medium conditioned by astrocytes leads to an enhancement of synapse formation, however these effects are greatly increased by the direct culture of neurons with astrocytes [336-338]. The long-term maintenance of synapses is also affected by astrocytes, for example, the withdrawal of astrocyte-derived factors after synapse formation has been shown to result in a significant loss of synapses in rodent neuronal cultures [338].

Activity-dependent mechanisms also have a key role in neuronal circuit generation and synapse maintenance. Whilst rodent cortical synapses can form in the absence of neurotransmitter release, their numbers are greatly reduced [340]. The growth cones of developing axons can spontaneously release glutamate, a process thought to be involved in the induction of synapse formation [341, 342]. Accordingly, studies in rodents have demonstrated that increasing glutamate release, as a result of increased spontaneous neuronal firing, can significantly increase synapse number, albeit in a cell-type dependent manner [343]. The standard DMEM and neurobasal growth-media used in human iPSC-derived neuronal culture has been found to inhibit neuronal activity due its non-physiological ion composition [291], which was originally designed for the long-term maintenance of cell viability. Building upon this observation, Bardy et al., (2015) devised a media formulation, BrainPhys™, to support the long-term culture of neurons without impairing neuronal activity and synaptic transmission [291]. The authors report that iPSC-derived neurons cultured for several weeks in BrainPhys™ demonstrated comparable viability to those grown in a standard medium. However, the authors also observed that the neurons grown in BrainPhys™ had intrinsic properties that reflected improved maturity in comparison to neurons cultured in a standard medium. Furthermore, they found that within the neuronal population that were able to generate repetitive action potentials, the proportion of cells receiving synaptic inputs was increased [291]. This study demonstrates that modulating basal neuronal activity can affect intrinsic and synaptic maturation in iPSC-derived neurons.

The iPSC-derived cortical cultures are heterogeneous in cell age as a result of the long-term progenitor proliferation required for the generation of neurons from all cortical layers. Whilst the results in the previous chapter demonstrate that the neuronal population increased in maturity with time in culture, the variability in the intrinsic membrane properties at a single cell level indicates that it may be possible to target a subset of neurons with greater functional maturity. In animal studies, expression of CaMKIIα has been found only in excitatory neurons in the cortex, and

is strongly upregulated during neuronal development [344-346]. Furthermore, human iPSC-derived neurons with an active CaMKIIα promoter have a 12-fold enrichment of transcripts encoding a number of post-synaptic proteins [162]. Collectively, this suggests that the expression of a reporter gene that reflects the activity of a CaMKIIα promoter could be used to identify mature neurons that receive synaptic inputs.

Within this chapter I wanted to address the following questions:

- Does the co-culture of human iPSC-derived cortical neurons with rodent astrocytes promote the formation of active synaptic networks?
- Can factors modulating neuronal activity enhance synapse generation in human iPSC-derived cortical cultures?
- Does the expression of an active CaMKIIα promoter enable the selective targeting of human iPSC-derived cortical neurons with more mature functional properties?

4.2. Results

4.2.1. Rodent astrocytes promote the development of mature neuronal networks

Given the importance of glia in synaptic modulation, I sought to determine to what extent the addition of astrocytes could affect the levels of excitatory synaptic activity in iPSC-derived cortical cultures. The iPSC-derived cortical cultures can generate endogenous glia, however, these appear at late stages (see ***Figure 3.1***) and have unknown functional properties. Therefore, to explore the effects of glial introduction, and to benefit from both contact-dependent and contact-independent mechanisms, iPSC-derived NPCs (day 35-40) were plated either directly onto a confluent mono-layer of rat cortical astrocytes (***Figure 4.1***; *black*), or without astrocytes onto a poly-L-ornithine laminin substrate (***Figure 4.1***; *grey*) (***Figure 4.1a***). Following plating, neurons exhibited a qualitative increase in adherence, survival and neurite outgrowth when co-cultured with rat astrocytes. Neurons could be identified by positive immunolabelling for Tuj, whilst astrocytes

expressed GFAP, alongside marked differences in morphology between the two cell types (***Figure 4.1b***). The cortical cultures were maintained until day 75-105 for functional assessment using whole-cell patch clamp electrophysiology. The previously described protocols (see Chapter III) were applied to cells with a neuronal morphology to assess the levels of excitatory synaptic activity, voltage-gated currents and induced action potential firing (see ***Figure 4.1c*** for example traces).

The proportion of cells that received EPSCs was significantly higher in the human iPSC-derived cortical neurons co-cultured with rat astrocytes (41 %, 16/39 cells for without rat astrocytes, and 72 %, 23/32 cells for with rat astrocytes, p = 0.0160, Fisher's exact test; ***Figure 4.1***). However, the frequency (0.14 ± 0.04 Hz, n = 39 cells, for without rat astrocytes, and 0.21 ± 0.07 Hz, n = 32 cells, for with rat astrocytes, p = 0.5723, M-W test; ***Figure 4.1e***) and the amplitude (16.92 ± 1.44 pA, n = 16 cells for without rat astrocytes, and 20.71 ± 2.93 pA, n = 23 cells, for with rat astrocytes, p = 0.4203, M-W test; ***Figure 4.1f***) of the EPSCs did not significantly differ. The intrinsic membrane properties of the neurons with (n = 24-25 cells) and without (n = 19-23 cells) rat astrocytes were also assessed. Significant differences were identified in the resting membrane potential (-37.1 ± 1.8

Figure 4.1. (*cont. from following page*) plated onto a poly-L-ornithine laminin substrate (without rat astrocytes, *grey*) or a monolayer of rat cortical astrocytes (*black*). At day 75-105, spontaneous EPSCs and the intrinsic membrane properties were assessed. **(b)** Rat astrocytes stained positively for GFAP whilst neurons labelled for Tuj. **(c)** Representative traces of spontaneous EPSCs (*left*; scale bar 10 pA, 5 s), voltage-gated currents (*middle*; scale bar 500 pA, 100 ms), and induced action potential firing (*right;* scale bar 20 mV, 100 ms). **(d)** The proportion of cells receiving EPSCs was significantly higher on rat astrocytes (p = 0.0160, Fisher's exact test). **(e)** The frequency of EPSCs did not differ (p = 0.5723, M-W test) (n = 39 and 32 cells, for without rat astrocytes and with rat astrocytes, respectively, from 4 differentiations of 1 cell line). **(f)** The amplitude of EPSCs showed no significant difference (p = 0.4203, n = 16 and 23 cells, for without rat astrocytes and with rat astrocytes, respectively, M-W test). Analysis of the intrinsic membrane properties showed that **(g)** the resting membrane potential was significantly more hyperpolarized (p = 0.0084, unpaired t-test), **(h)** the membrane capacitance was significantly higher (p < 0.001, M-W test), **(i)** the membrane resistance was significantly lower (p = 0.0067, unpaired t-test), **(j)** the maximum sodium current was significantly increased (p = 0.0066, unpaired t-test), **(k)** the maximum potassium current was significantly increased (p < 0.001, unpaired t-test), **(l)** the number of consecutive action potentials fired was significantly increased (p < 0.001, M-W test) **(m)** the action potential threshold was significantly more hyperpolarized (p = 0.0045, M-W test), and **(n)** the action potential amplitude did not differ (p = 0.3838, unpaired t-test). n = 19-23 and 24-25 cells, for without rat astrocytes and with rat astrocytes, respectively, from 3 differentiations of 1 cell line. * p < 0.05, ** p < 0.01, ***

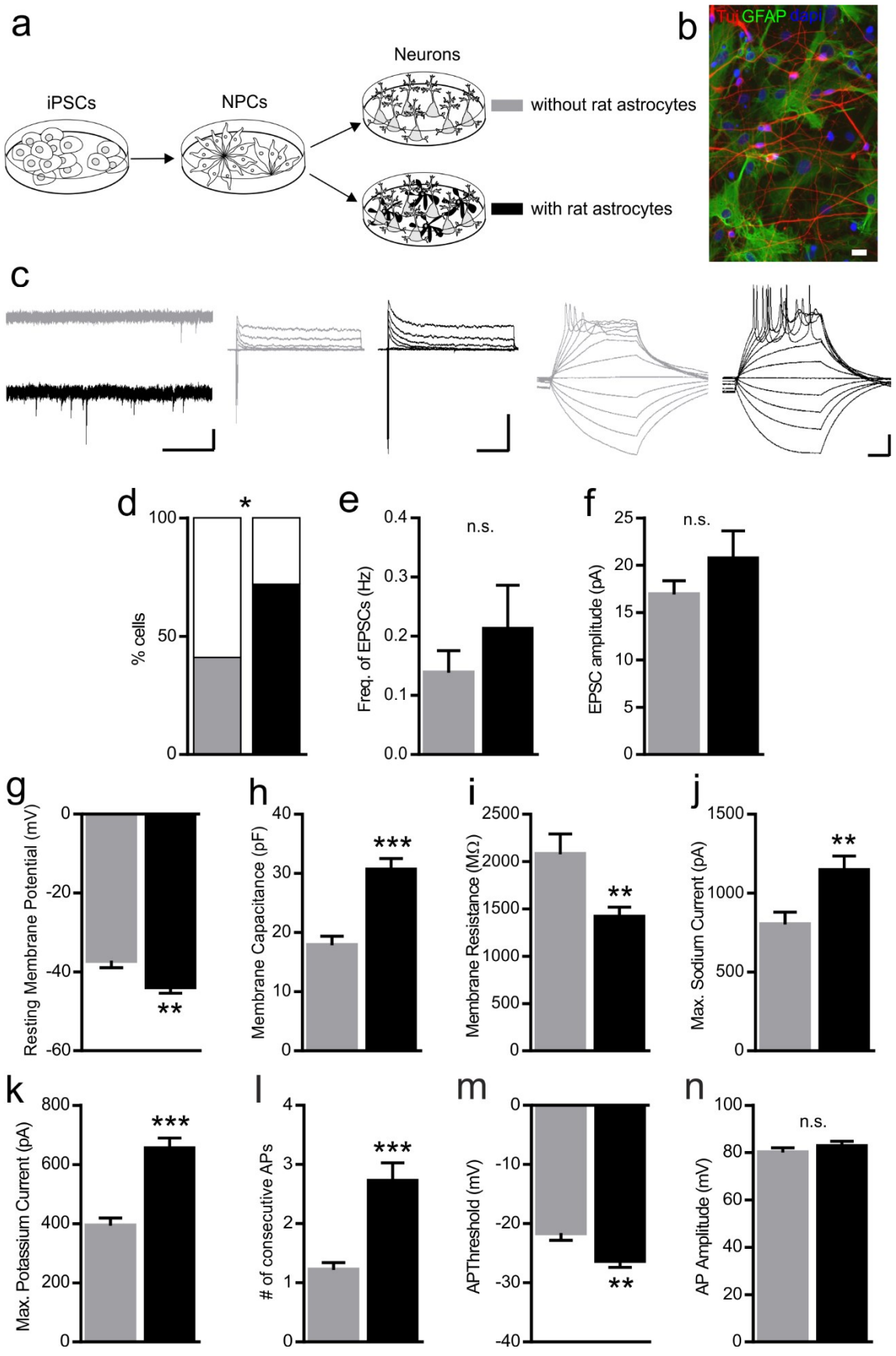

Figure 4.1. Co-culture of human iPSC-derived cortical neurons with rodent astrocytes accelerates the maturation of intrinsic neuronal properties and promotes the generation of active synaptic networks. (a) Schematic of the experiment in which day 35-40 NPCs were (*cont. on previous page*)

mV for without rat astrocytes, and -43.8 ± 1.6 mV for with rat astrocytes, p = 0.0084, unpaired t-test; ***Figure 4.1g***), the membrane capacitance (17.9 ± 1.5 pF for without rat astrocytes, and 30.6 ± 1.9 pF for with rat astrocytes, p < 0.001, M-W test; ***Figure 4.1h***), the membrane resistance (2077 ± 215 MΩ for without rat astrocytes, and 1414 ± 105 MΩ for with rat astrocytes, p = 0.0067, unpaired t-test; ***Figure 4.1i***), the maximum sodium current (821 ± 72 pA for without rat astrocytes, and 1163 ± 75 pA for with rat astrocytes, p = 0.0066, unpaired t-test; ***Figure 4.1j***), the maximum potassium current (393 ± 27 pA for without rat astrocytes, and 653 ± 36 pA for with rat astrocytes, p < 0.001, unpaired t-test; ***Figure 4.1k***), the number of consecutive action potentials (1.2 ± 0.1 for without rat astrocytes, and 2.7 ± 0.3 for with rat astrocytes, p < 0.001, M-W test; ***Figure 4.1l***) and the action potential threshold (-21.6 ± 1.2 mV for without rat astrocytes, and -26.3 ± 1.1 mV for with rat astrocytes, p = 0.0045, M-W test; ***Figure 4.1m***). The action potential amplitude did not differ (80.0 ± 2.0 pA for without rat astrocytes, and 82.7 ± 2.2 pA for with rat astrocytes, p = 0.3838, unpaired t-test; ***Figure 4.1n***). The functional properties are summarised in ***Table 4.1***. Collectively, the co-culture of human iPSC-derived cortical neurons with rat astrocytes significantly enhanced intrinsic cell maturity and had modest effects on the levels of excitatory synaptic activity.

Property	without rat astrocytes		with rat astrocytes			
	mean ± SEM	n (cells)	mean ± SEM	n (cells)	*p* value	Direction of change
% cells with EPSCs	41 %	16/39	72 %	23/32	0.0160*	↑
EPSC frequency (Hz)	0.14 ± 0.04	39	0.21 ± 0.07	32	0.5723	↔
EPSC amplitude (pA)	16.92 ± 1.44	16	20.71 ± 2.93	23	0.4203	↔
Resting membrane potential (mV)	-37.1 ± 1.8	23	-43.8 ± 1.6	25	0.0084**	↓
Membrane capacitance (pF)	17.9 ± 1.5	23	30.6 ± 1.9	25	< 0.001***	↑
Membrane resistance (MΩ)	2077 ± 215	23	1163 ± 75	25	0.0067**	↓
Max. Sodium current (pA)	821 ± 72	23	1163 ± 75	25	0.0066**	↑
Max. Potassium current (pA)	393 ± 27	23	653 ± 36	25	< 0.001***	↑
# of consecutive APs	1.2 ± 0.1	23	2.7 ± 0.3	25	< 0.001***	↑
AP Threshold (mV)	-21.6 ± 1.2	19	-26.3 ± 1.1	24	0.0045**	↓
AP Amplitude (mV)	80.0 ± 2.0	22	82.7 ± 2.2	25	0.3838	↔

Table 4.1. Summary table of the synaptic and intrinsic membrane properties of neurons cultured with and without rat astrocytes. * p < 0.05, ** p < 0.01, *** p < 0.001

4.2.2. Expression of a CaMKIIα reporter construct does not identify neurons of greater functional maturity

Having established that rodent astrocytes can promote functional neuronal maturation, I explored whether neurons that could actively drive the expression of a fluorescent reporter gene from a CaMKIIα promoter comprised a functionally more mature population from within a heterogeneous cortical culture. Day 28-33 NPCs were transduced with CaMKIIα-mKate2 lentivirus before plating onto rat astrocytes at day 35-40 (***Figure 4.2a***). The appearance of cells expressing the red fluorescent protein, mKate2, indicative of an active CaMKIIα promoter, began several days following plating (***Figure 4.2b***). Cortical cultures were maintained until functional assessment at day 75-105 whereby neurons that were mKate2-negative (control; *black*) and mKate2-positive (CaMKIIα-mkate2; *red*) were targeted for whole-cell patch clamp electrophysiology. The previously described protocols were applied to assess excitatory synaptic activity, voltage-gated currents and induced action potential firing (see ***Figure 4.2c*** for example traces). Analysis of the spontaneous EPSCs showed that neurons were comparable in the proportion of cells with EPSCs (33 %, 3/9 cells for mKate2-negative, 42 %, 5/12 cells for mKate2-positive, $p = 1.000$, Fisher's exact test; ***Figure 4.2d***), the frequency ($p = 0.9372$; ***Figure 4.2e***) and the amplitude ($p = 0.0714$; ***Figure 4.2f***) of EPSCs. Likewise, the intrinsic membrane properties of control and CaMKIIα-mKate2-positive neurons were equivalent in their resting membrane potential ($p = 0.3545$; ***Figure 4.2g***), membrane capacitance ($p = 0.9310$; ***Figure 4.2h***), membrane resistance ($p = 0.8928$; ***Figure 4.2i***), maximum sodium current ($p = 0.3470$; ***Figure 4.2j***), maximum potassium current ($p = 0.4491$; ***Figure 4.2k***), the number of consecutive action potentials ($p = 0.4140$; ***Figure 4.2l***), the action potential threshold ($p = 0.0540$; ***Figure 4.2m***) and the action potential amplitude ($p = 0.4048$; ***Figure 4.2n***). The functional properties are summarised in ***Table 4.2***. Taken together, the synaptic and intrinsic properties measured indicate that there is no difference in the functional properties of iPSC-derived cortical neurons that do and do not show activity of the CaMKIIα reporter construct.

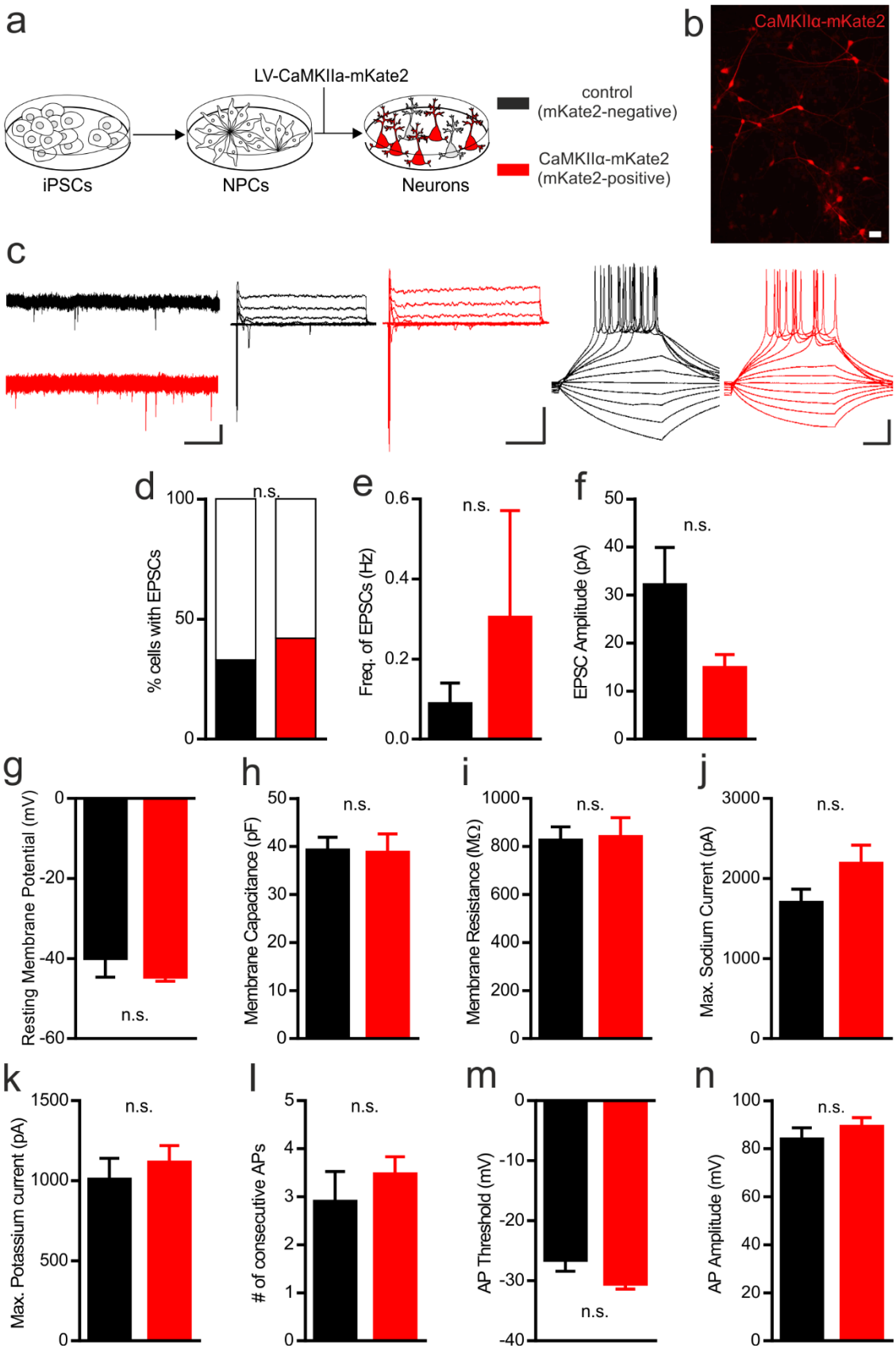

Figure 4.2. Targeting CaMKIIα-mKate2 positive cortical neurons does not identify a more mature neuronal population. (a) Schematic of the experiment in which day 28-33 NPCs were transduced with CaMKIIα-mKate2 lentivirus before plating onto rat astrocytes at (*cont. on following page*)

Property	Control		CaMKIIα-mKate2			
	mean ± SEM	n (cells)	mean ± SEM	n (cells)	*p* value	Direction of change
% cells with EPSCs	33%	3/9	42%	5/12	1.000	↔
EPSC frequency (Hz)	0.09 ± 0.05	9	0.30 ± 0.27	12	0.9372	↔
EPSC amplitude (pA)	32.04 ± 7.85	3	14.75 ± 2.89	5	0.0714	↔
Resting membrane potential (mV)	-39.8 ± 4.9	5	-45.5 ± 1.5	8	0.3543	↔
Membrane capacitance (pF)	39.1 ± 2.8	11	38.7 ± 4.0	16	0.9310	↔
Membrane resistance (MΩ)	823 ± 59	11	839 ± 82	16	0.8928	↔
Max. Sodium current (pA)	1691 ± 177	11	2183 ± 236	12	0.3470	↔
Max. Potassium current (pA)	1005 ± 135	11	1112 ± 107	12	0.4491	↔
# of consecutive APs	2.9 ± 0.6	9	3.5 ± 0.4	13	0.4140	↔
AP Threshold (mV)	-26.4 ± 2.0	9	-30.5 ± 0.9	13	0.0540	↘
AP Amplitude (mV)	83.7 ± 5.0	8	89.1 ± 3.9	11	0.4048	↔

Table 4.2. Summary table of the synaptic and intrinsic membrane properties of mKate2-negative control neurons and CaMKIIα-mKate2-positive neurons.

4.2.3. Long-term culture in BrainPhys™ medium does not enhance neuronal maturation

To determine whether disinhibiting neuronal activity during cell culturing could increase the maturational effects generated by rat astrocytes, and more specifically enhance levels of synaptic activity, I explored the use of BrainPhys™ medium. It is recommended that BrainPhys™ medium is supplemented with the additional factors BDNF, GDNF, cAMP and ascorbic acid. However, when added to standard culture medium these factors have already been reported to affect

Figure 4.2. (cont. from previous page) day 35-40. At day 75-105 the functional properties of mKate2-positive neurons (*red*) were compared to mKate2-negative (control; *black*) neurons. **(b)** Example image of neurons expressing mKate2 driven by the CaMKIIα promoter. Scale bar 20 µm. **(c)** Representative traces of spontaneous EPSCs (*left;* scale bar 10 pA, 5 s), voltage-gated currents (*middle;* scale bar 500 pA, 100 ms) and induced action potential firing (*right;* scale bar 20 mV, 100 ms). Analysis of spontaneous EPSCs showed that there was no significant difference in **(d)** the proportion of cells receiving EPSCs (p = 1.000, Fisher's exact test), **(e)** the frequency of EPSCs (p = 0.9372, M-W test), or **(f)** the amplitude of EPSCs (p = 0.0714, n = 3 and 5 cells for control and CaMKIIα-mKate2, respectively, M-W test) (From 1 differentiation). Assessment of the intrinsic properties showed no significant differences in **(g)** the resting membrane potential (p = 0.3543, n = 5 and 8 cells for control and CaMKIIα-mKate2, respectively, unpaired t-test), **(h)** the membrane capacitance (p = 0.9310, unpaired t-test) **(i)** the membrane resistance (p = 0.8928, unpaired t-test), **(j)** the maximum sodium current (p = 0.3470, M-W test), **(k)** the maximum potassium current (p = 0.4491 , M-W test), **(l)** the number of consecutive action potentials (p = 0.4140, unpaired t-test), **(m)** the action potential threshold (p = 0.0540, M-W test) or **(n)** the action potential amplitude (p = 0.4048, unpaired t-test). n = 8-11 and 11-16 cells for control and CaMKIIα-mKate2, respectively, unless otherwise stated, from 2 differentiations of 1 cell line.

synaptogenesis and maturation of rodent neurons [347-350]. Exogenous application of BDNF can induce the formation of both inhibitory and excitatory synapses and modulate axonal outgrowth and branching in dissociated rodent neurons [347]. Meanwhile, the addition of GDNF has been shown to exert neuroprotective effects on rodent cortical neurons [348]. The pharmacological activation of cAMP signalling pathways can promote the neuronal maturation of mouse NPCs, demonstrated by an enhancement of voltage-gated currents and the upregulation of pre-synaptic proteins [349]. The levels of the anti-oxidant ascorbic acid increase during embryonic brain development in rodents, and subsequently decrease postnatally [351]. Consistent with a role in neuronal development, supplementing culture media with ascorbic acid has been reported to enhance the neural conversion of mouse ESCs, which was associated with the upregulation of genes involved in neuron generation, maturation and synaptic transmission [350]. In order to separate the effects of enabling neuronal activity throughout the culture period, from the effects mediated by these additional factors, human iPSC-derived cortical cultures were maintained in either standard neuronal maintenance medium (control; *black*), BrainPhys™ without factors (BrainPhys™ Basic; *light blue*) or BrainPhys™ with factors (*dark blue*) (***Figure 4.3a***). Day 35-40 NPCs were plated

---

Figure 4.3. (*cont. from following page*) plated onto rat astrocytes and cultured in standard neuronal maintenance medium (Control; *black*), BrainPhys™ Basic (*light blue*) or BrainPhys™ with factors (*dark blue*) until functional assessment at day 75-105. **(b)** Representative traces of spontaneous EPSCs. Scale bar 10 pA, 5 s. **(c)** Representative traces of voltage-gated currents (*left;* scale bar 500 pA, 100 ms) and induced action potential firing (*right;* scale bar 20 mV, 100 ms). Assessment of spontaneous EPSCs showed no significant differences in **(d)** the proportion of cells receiving EPSCs ($p = 0.4438$, Chi-squared test), **(e)** the frequency of EPSCs ($p = 0.3958$, K-W test) or **(f)** the amplitude of EPSCs ($p = 0.2498$, n = 8, 5 and 3 cells for control, BrainPhys™ Basic and BrainPhys™ with factors, respectively, K-W test). Analysis of the intrinsic membrane properties showed that **(g)** the resting membrane potential was significantly higher in BrainPhys™ with factors ($p = 0.0210$, one-way ANOVA). The following properties showed no significant differences: **(h)** the membrane capacitance ($p = 0.0661$, one-way ANOVA), **(i)** the membrane resistance ($p = 0.3326$, one-way ANOVA), **(j)** the maximum sodium current ($p = 0.8421$, K-W test), **(k)** the maximum potassium current ($p = 0.3254$, K-W test), **(l)** the number of consecutive action potentials ($p = 0.2972$, one-way ANOVA), **(m)** the action potential threshold ($p = 0.3012$, one-way ANOVA) and **(n)** the action potential amplitude ($p = 0.1515$, one-way ANOVA). n = 20-22, 16-19 and 16 cells for control, BrainPhys™ Basic and BrainPhys™ with factors, respectively, unless otherwise stated, from 1 differentiation. All groups were tested for normality and then compared to the control group using a Kruskal-Wallis test or a one-way ANOVA with a Dunn's or Holm-Sidak's post-hoc test for multiple comparisons, respectively. * $p < 0.05$

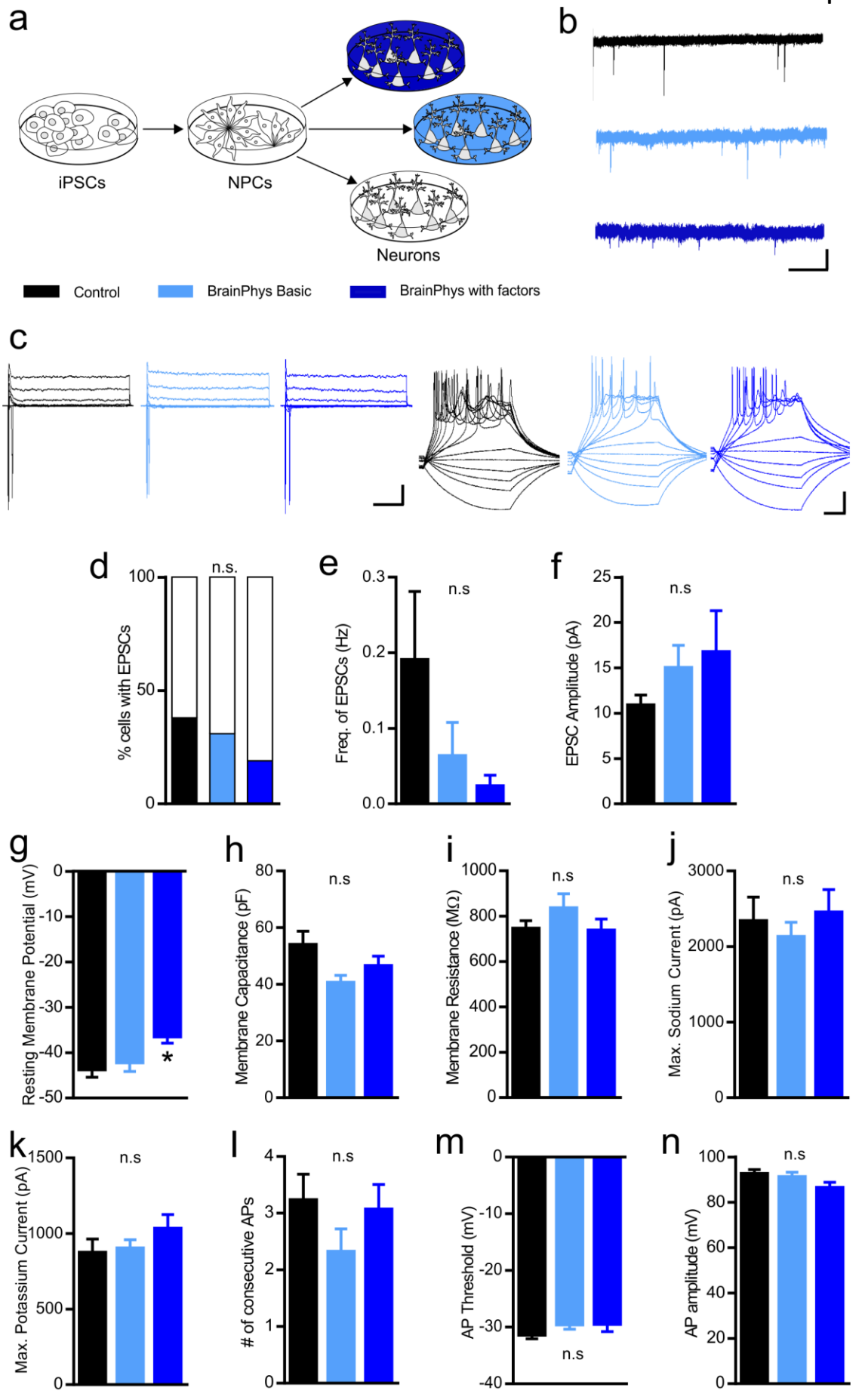

Figure 4.3. Long-term culture in BrainPhysTM medium does not improve functional neuronal maturity. (a) Schematic of experiment in which day 35-40 NPCs were (*cont. on previous page)*

onto rat astrocytes in standard neuronal maintenance medium which, through half-media changes, was gradually changed to BrainPhys™ medium, where appropriate. The human iPSC-derived cortical cultures were maintained until functional assessment at day 75-105 using the previously described electrophysiology protocols to assess excitatory synaptic activity, voltage-gated currents and induced action potential firing (see ***Figure 4.3b,c*** for example traces). The functional properties of iPSC-derived cortical neurons cultured in BrainPhys™ with and without factors were compared to the neuronal maintenance medium control group. Voltage-clamp recordings of EPSCs revealed no significant difference in the proportion of cells receiving spontaneous EPSCs (38 %, 8/21 cells for control, 31 %, 5/16 cells for BrainPhys™ Basic, and 19 %, 3/16 cells for BrainPhys™ with factors, p = 0.4438, Chi-squared test; ***Figure 4.3d***), or in the frequency (p = 0.3958; ***Figure 4.3e***) or amplitude (p = 0.2498; ***Figure 4.3f***) of the EPSCs. Assessment of the intrinsic membrane properties showed that neurons cultured in BrainPhys™ with factors had a significantly more depolarized

Property	**Control**		**BrainPhys™ Basic**		**BrainPhys™ with factors**		
	mean ± SEM	n (cells)	mean ± SEM	n (cells)	mean ± SEM	n (cells)	*p* value
% cells with EPSCs	38 %	8/21	31 %	5/16	19 %	3/16	0.4438
EPSC frequency (Hz)	0.19 ± 0.01	20	0.06 ± 0.04	16	0.02 ± 0.01	16	0.3958
EPSC amplitude (pA)	10.84 ± 1.18	8	14.98 ± 2.52	5	16.73 ± 4.57	3	0.2498
Resting membrane potential (mV)	-43.6 ± 1.8	22	-42.1 ± 2.1	17	-36.4 ± 1.5*	16	0.0210
Membrane capacitance (pF)	53.8 ± 5.0	22	40.4 ± 2.7	18	46.4 ± 3.5	16	0.0661
Membrane resistance (MΩ)	745 ± 36	22	834 ± 65	18	736 ± 51	16	0.3326
Max. Sodium current (pA)	2333 ± 323	22	2125 ± 195	19	2448 ± 304	16	0.8421
Max. Potassium current (pA)	871 ± 92	22	901 ± 58	19	1030 ± 96	16	0.3254
# of consecutive APs	3.2 ± 0.5	22	2.3 ± 0.4	19	3.1 ± 0.4	16	0.2972
AP Threshold (mV)	-31.3 ± 0.8	22	-29.5 ± 0.9	19	-29.4 ± 1.4	16	0.3012
AP Amplitude (mV)	92.4 ± 2.0	22	91.1 ± 2.2	19	86.3 ± 2.6	16	0.1515

Table 4.3. Summary table of the synaptic and intrinsic membrane properties of neurons cultured in NMM-A (control), BrainPhys™ Basic or BrainPhys™ with factors. * p<0.05

resting membrane potential (-43.6 ± 1.8 mV, n = 22 cells for control, -42.1 ± 2.1 mV, n = 17 cells for BrainPhys™ Basic, -36.4 ± 1.5 mV, n = 16 cells for BrainPhys™ with factors, p = 0.0210, one-way ANOVA; ***Figure 4.3g***). Otherwise, neurons were indistinguishable in their membrane capacitance (p = 0.0661; ***Figure 4.3h***), membrane resistance (p = 0.3326; ***Figure 4.3i***), maximum sodium current (p = 0.8421; ***Figure 4.3j***), maximum potassium current (p = 0.3254; ***Figure 4.3k***), the number of consecutive action potentials (p = 0.3413, ***Figure 4.3l***), the action potential threshold (p = 0.3012; ***Figure 4.3m***) and the action potential amplitude (p = 0.1515; ***Figure 4.3n***). The functional properties are summarised in ***Table 4.3***. Overall, the long-term culture in BrainPhys™ medium, with or without factors, did not further enhance the intrinsic or synaptic neuronal maturation of human iPSC-derived cortical neurons that were co-cultured with rat astrocytes.

4.2.4. Human iPSC-derived cortical neurons can integrate with a mature rodent neuronal network but this does not affect their intrinsic maturation

The culture of iPSC-derived cortical neurons with primary rodent neurons could offer an alternative route to promote activity-dependent synapse generation. Primary cultures generated from the dissociation of rodent cortex are comprised of excitatory glutamatergic neurons, inhibitory GABAergic neurons and astrocytes, and generate active synaptic networks within 7 DIV [312, 352]. GABAergic synapses are the first to develop and may be involved in the activity-dependent development of glutamatergic synapses [353]. The concurrent input from mature excitatory and inhibitory rodent neurons may stimulate activity-dependent processes that are involved in glutamatergic synapse maturation in co-cultured human iPSC-derived cortical neurons.

The effects of a surrounding active neuronal network on human iPSC-derived cortical neuron functional maturation was explored using rat primary cortical cultures. Firstly, primary cortical cultures were generated by the dissociation of P1 rat cortices and allowed to recover for 24 hours following plating. Meanwhile, human iPSC-derived NPCs were transduced with CaMKIIα-mKate2 to enable the distinction between rat and human neurons. Following transduction, day 40 human

iPSC-derived NPCs were plated onto either rat astrocytes alone (without rat neurons; *red*) or onto primary rat cortical cultures (with rat neurons; *red and black*) (***Figure 4.4a***). The primary rodent neurons could not remain viable for prolonged culture periods and therefore limited the functional assessment of the human iPSC-derived cortical neurons to an earlier time point than was used for the other experiments within this chapter. Consequently, the functional intrinsic and synaptic properties of mKate2-positive neurons, cultured with and without primary rat neurons, were assessed at day 58 using the previously described protocols (***Figure 4.4b***). Spontaneous EPSCs were not observed in any of the human neurons cultured without rat neurons. However, in the presence of rat neurons the majority of human neurons had EPSCs (0 %, 0/8 cells for without rat neurons, and 57 %, 4/7 cells for with rat neurons, p = 0.0256, Fisher's exact test; ***Figure 4.4c***). Synonymous with this observation, the frequency of EPSCs were significantly higher (0.00 ± 0.00 Hz, n = 8 cells for without rat neurons, and 0.16 ± 0.11 Hz, n = 7 cells for with rat neurons; ***Figure 4.4d***) and had an average amplitude of 17.98 ± 5.60 pA (n = 4 cells; ***Figure 4.4e***) in human iPSC-derived cortical neurons that were cultured with rat neurons. Whilst differences in synaptic properties were apparent between human neurons cultured with and without rat neurons, assessment of their intrinsic membrane properties demonstrated that they were comparable in their resting membrane

---

Figure 4.4. (*cont. from following page*) **(a)** Schematic of the experiment in which day 35 human NPCs were transduced with CaMKIIα-mKate2 lentivirus and plated at day 40 onto either rat astrocytes only (without rat neurons; *red*) or 1 DIV rat primary cortical cultures comprised of both rat neurons and rat astrocytes (with rat neurons; *red and black*). At day 58 (18 DIV) the functional properties of the human neurons, identified by the expression of mKate2, were assessed. **(b)** Representative traces of spontaneous EPSCs (*left;* scale bar 10 pA, 5 s), voltage-gated currents (*middle;* scale bar 500 pA, 100 ms) and induced action potential firing (*right;* scale bar 20 mV, 100 ms) from human iPSC-derived cortical neurons cultured with (*black*) and without (*red*) rat primary neurons. **(c)** Human neurons grown with rat neurons showed a significantly higher proportion of cells receiving EPSCs (p = 0.0256, Fisher's exact test). **(d)** Human neurons grown with rat neurons had a significantly higher frequency of EPSCs (p = 0.0256, M-W test). **(e)** The amplitude of EPSCs (with rat neurons, n = 4 cells). Assessment of the intrinsic membrane properties showed no significant difference in **(f)** the resting membrane potential (p = 0.4330, M-W test), **(g)** the membrane capacitance (p = 0.5358, M-W test), **(h)** the membrane resistance (p = 0.9781, M-W test), **(i)** the maximum sodium current (p = 0.3969, M-W test), **(j)** the maximum potassium current (p = 0.1520, M-W test), **(k)** the number of consecutive action potentials (p = 0.3095, M-W test), **(l)** the action potential threshold (p=0.6234, M-W test) or **(m)** the action potential amplitude (p = 0.3095, M-W test). n = 6-8 and 6-7 cells for without rat neurons and with rat neurons, respectively, unless otherwise stated, from 1 differentiation.* $p < 0.05$

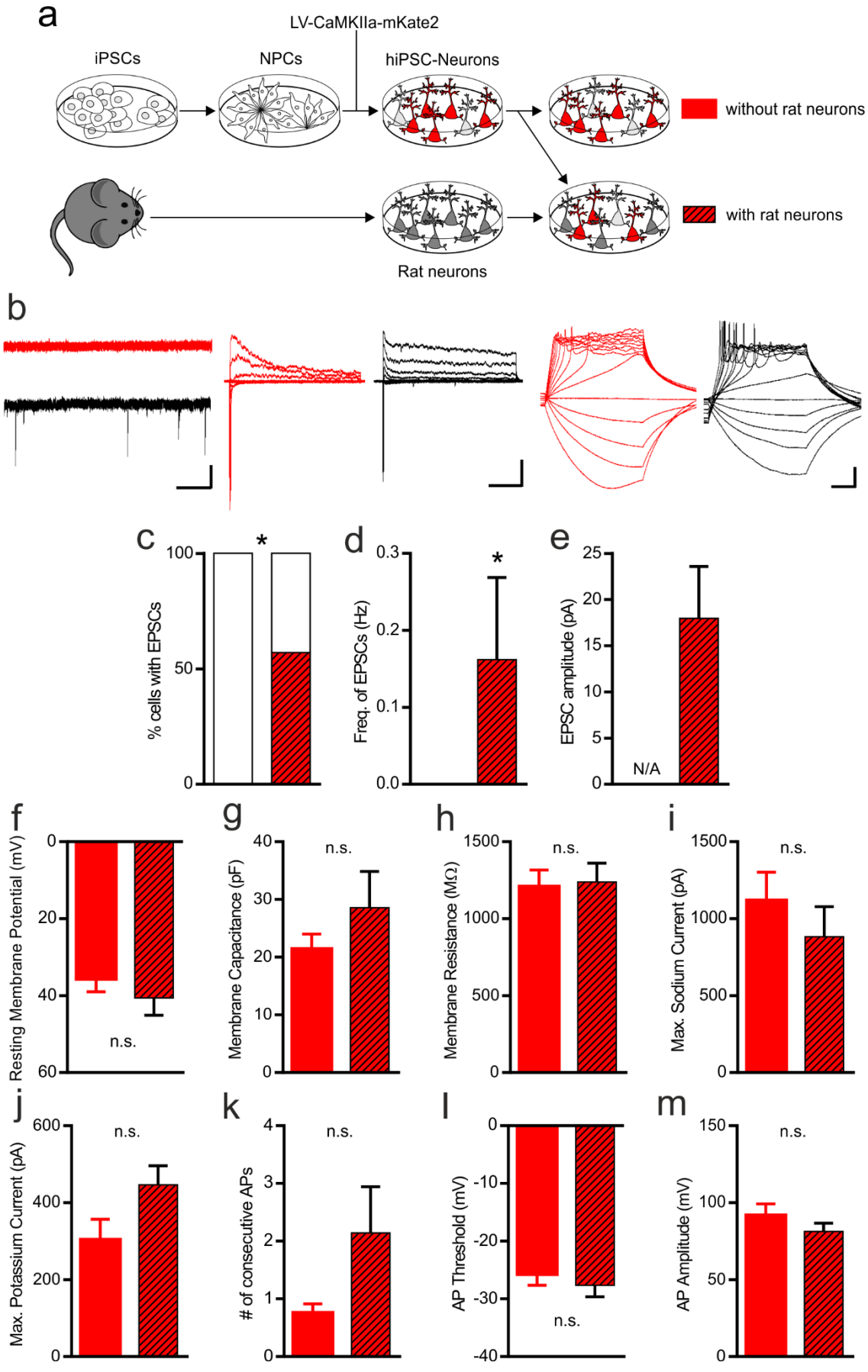

Figure 4.4. Human iPSC-derived cortical neurons can integrate with a network of rodent neurons but this does not affect their intrinsic functional maturity. (*cont. on previous page*)

potential (p = 0.4330; ***Figure 4.4f***), membrane capacitance (p = 0.5358; ***Figure 4.4g***), membrane resistance (p = 0.9781; ***Figure 4.4h***), maximum sodium current (p = 0.3969; ***Figure 4.4i***), maximum potassium current (p = 0.1520; ***Figure 4.4j***), the number of consecutive action potentials (0.2023; ***Figure 4.4k***), the action potential threshold (p = 0.6234; ***Figure 4.4l***) and the action potential amplitude (p = 0.3095; ***Figure 4.4m***). The functional properties are summarised in ***Table 4.4***. Altogether, these results suggest that the co-culture of human neurons with primary rat neurons can positively affect synaptic activity, but does not alter intrinsic functional maturation.

	without rat neurons		**with rat neurons**			
Property	mean ± SEM	n (cells)	mean ± SEM	n (cells)	*p* value	Direction of change
% cells with EPSCs	0 %	0/8	57 %	4/7	0.0256*	↑
EPSC frequency (Hz)	0.00 ± 0.00	8	0.16 ± 0.11	7	0.0256*	↑
EPSC amplitude (pA)	N/A	0	17.98 ± 5.60	4	N/A	N/A
Resting membrane potential (mV)	-35.6 ± 3.4	7	-40.6 ± 4.5	7	0.4330	↔
Membrane capacitance (pF)	21.4 ± 2.6	8	28.6 ± 6.3	7	0.5358	↔
Membrane resistance (MΩ)	1207 ± 109	8	1239 ± 122	7	0.9781	↔
Max. Sodium current (pA)	1116 ± 187	8	882 ± 196	7	0.3969	↔
Max. Potassium current (pA)	303 ± 54	8	446 ± 50	7	0.1520	↔
# of consecutive APs	0.8 ± 0.2	8	2.1 ± 0.8	7	0.2023	↔
AP Threshold (mV)	-25.7 ± 2.0	8	-27.7 ± 2.0	6	0.6234	↔
AP Amplitude (mV)	91.7 ± 7.5	8	81.3 ± 5.5	6	0.3095	↔

Table 4.4. Summary table of the synaptic and intrinsic membrane properties of neurons cultured with and without primary rat neurons. * $p < 0.05$

4.3. Discussion

Having identified in Chapter III that human iPSC-derived cortical neurons have immature functional properties, I explored methods to accelerate intrinsic and synaptic maturation or to target mature neurons in these heterogeneous cultures. To this end, I have demonstrated that the co-culture of human iPSC-derived cortical neurons with rat astrocytes can robustly improve intrinsic maturity and promote excitatory synaptic connectivity compared to neurons cultured on a poly-ornithine laminin substrate. Meanwhile, targeting cells with expression of a CaMKIIα-mKate2 reporter construct did not identify neurons with more mature functional properties. Long-term culture in

BrainPhys™ medium to enable neuronal activity did not accelerate functional maturation. This observation was irrespective of the addition of factors previously reported to affect functional neuronal development. When cultured with rat primary neurons, human iPSC-derived cortical neurons were able to exhibit enhanced excitatory synaptic activity, which was otherwise absent at this developmental stage. However, the presence of rat primary neurons did not affect the intrinsic membrane properties of human neurons.

4.3.1. Co-culture of human iPSC-derived cortical neurons with rodent astrocytes

The primary effect of co-culturing human iPSC-derived cortical neurons with rat astrocytes was the enhancement of the intrinsic membrane properties. Meanwhile, the increase observed in excitatory synaptic activity was only moderate. Co-culture with rat astrocytes enabled the majority of human neurons to receive excitatory inputs, but the frequency of these events remained low. It is likely that the enhanced intrinsic properties may have contributed to the changes observed in synaptic activity. The acceleration of the functional neuronal maturation of human iPSC-derived cortical neurons, achieved by the co-culture with rodent astrocytes, is an effect that has been described in similar studies [276, 354, 355]. As a result, functional studies of stem-cell derived neurons now frequently take advantage of the benefits associated with rodent astrocyte co-culture [162, 163, 356]. In the human cortex, glia are the predominant cell type comprising 80 % of the cellular population, whilst neurons represent only 20 % [357]. Taking this into consideration, it is unsurprising that astrocytes have many important functions that modulate neurotransmission, including extracellular ion buffering, neurotransmitter degradation and recycling, production of energy substrates and release of gliotransmitters [358]. As a result, astrocytes are essential for the long-term survival of neurons, evident by the observations of pronounced neuronal degeneration arising from the *in vivo* ablation of astrocyte subsets [359, 360]. Although I have demonstrated that astrocytes are beneficial in promoting the maturation of functional properties, they are also likely to be advantageous for long-term neuronal culture and the assessment of synaptic plasticity, given

their roles in neuronal survival and synapse modulation. Whilst the addition of rodent astrocytes is advantageous for electrophysiological analysis of iPSC-derived neurons, the direct co-culture approach could be prohibitive for bulk sample protein and RNA assays where the distinction of cell-type specific effects is required.

4.3.2. The utility of a CaMKIIα reporter construct as a marker of neuronal maturity

The activity of an active exogenous CaMKIIα promoter, as identified by the fluorescent reporter protein mKate2, did not identify neurons with greater functional maturity. Whilst the CaMKIIα-mKate2 reporter construct used here is predominantly expressed alongside markers of excitatory cortical neurons, the accuracy of this construct has not been quantitatively assessed [162]. In addition, the transduction efficiency must be considered, as neurons with an active endogenous CaMKIIα promoter that were not transduced by the lentivirus could contribute to the mKate2-negative control group and thereby prevent a clean comparison. It is also possible that differences in CaMKIIα-positive and negative neuronal populations have not yet developed at the stage of neuronal differentiation attained by the iPSC-derived cortical cultures generated here. During the course of this thesis, Nehme et al., (2018) have demonstrated that CaMKIIα expression can identify neurons enriched for neuronal and synapse-related genes, which also have a greater level of intrinsic functional maturity [275]. Through single-cell CaMKIIα expression analysis, Nehme et al., (2018) confirmed the reliability of their CaMKIIα-eGFP reporter construct and estimated that approximately 20 %-30 % of neurons with endogenous expression of CaMKIIα did not concurrently express eGFP. Nonetheless, they were able to observe a functional difference despite the potential CaMKIIα-expressing neuronal population contaminating the control group [275]. Here, and in the study by Nehme et al., (2018) the CaMKIIα promoter sequence used in the reporter construct was from the mouse CaMKIIα gene, and therefore species-specific differences in promoter sequences could not account for the difference in our observations. However, in comparison to the iPSC-derived cortical neurons described here, the overall level of neuronal maturity was greater in the

study by Nehme et al., (2018) [275]. Therefore, it is possible that the detection of maturational differences associated with the activity of the CaMKIIα promoter were hindered by the relatively immature state of the human iPSC-derived cortical neurons used here. Other studies have also sought to identify transcriptomic markers of functional maturity. Bardy et al., (2016) used PatchSeq, which combines whole-cell patch clamp electrophysiology with subsequent single-cell RNA Seq. This approach identified the expression of GDAP1L1 as a marker of functionally mature neurons within a human iPSC-derived neuronal culture [361]. However, GDAP1L1 promoter driven reporter constructs are not yet readily available to the wider scientific community.

4.3.3. Long-term culture in BrainPhys™ medium

The lack of a change in neuronal functional maturation following the long-term culture of iPSC-derived cortical neurons in BrainPhys™ medium contradicts the original study [291]. However, there are a number of key differences to acknowledge between the findings described here and those reported previously. Firstly, the cortical cultures assessed here were maintained in BrainPhys™ medium for 40-70 days in order to maintain consistency in the neuronal culture age between the maturational strategies undertaken. This time point is approximately one month longer than the duration used by Bardy et al., (2015) and, as a result, maturational differences may have occurred at earlier stages of differentiation or have been affected by long-term deterioration (although no obvious impact on cell viability was observed). Moreover, analysis of the same array of intrinsic and synaptic properties at an earlier time point did not reveal any differences (data not shown). Secondly, I pooled data derived from all recorded neurons, again for consistency within this chapter, whilst Bardy et al., (2015) enriched for neurons of greater maturity for their functional comparison by selecting only cells with multiple action potentials. Nonetheless, comparison of the average intrinsic membrane properties shows that the neurons described here are, on the whole, reflective of a more mature functional state than those demonstrated by Bardy et al., (2015). Albeit, I observed a lower proportion of cells with EPSCs and a lower EPSC frequency, which could possibly

be accounted for by a lack of cell selection for synaptic analysis, cell line variability [118] or cell density which could affect levels of synaptic activity [362]. Lastly, unlike Bardy et al., (2015) the iPSC-derived cortical neurons assessed here were grown on rat astrocytes. This suggests that BrainPhys™ media, with or without the additional factors, cannot exceed the effects achieved by rodent astrocyte co-culture. Furthermore, rodent astrocytes have been shown to secrete BDNF and GDNF [363], which can lead to downstream activation of cAMP signalling pathways [364], and the release of ascorbic acid [365]. This is consistent with the idea that the impact of BrainPhys™ with factors could have been limited by the endogenous activity of the rodent astrocytes.

4.3.4. Co-culture of human iPSC-derived cortical neurons with rodent neurons

The human iPSC-derived cortical neurons demonstrated integration with an active synaptic network of rodent neurons. However, this additional excitatory drive did not affect the intrinsic functional maturation over the time-frame assessed. The co-culture duration was limited by the survival of the rodent neurons, and therefore it was not possible to maintain the human iPSC-derived cortical neurons for a prolonged period under these conditions. In addition, the small number of cells assayed may have hindered my ability to detect subtle differences in intrinsic functional properties. Given the complete absence of excitatory synaptic activity amongst the human iPSC-derived cortical neurons cultured in the absence of rodent neurons, it seems unlikely that the EPSCs observed were derived from the rodent neuronal population. Indeed, similar studies have utilised optogenetic techniques to demonstrate the presence of functional synapses between rodent and human neurons [366, 367], which would be one further approach to assess the synapse directionality between the two species within these cultures. Nonetheless, the proportion of cells receiving excitatory inputs and their frequency was still very low, and did not surpass the effects obtained by rat astrocytes alone, whereby the origin of EPSCs from human neurons is certain.

In summary, the co-culture of human iPSC-derived cortical neurons with rodent astrocytes is clearly advantageous for electrophysiological studies. The intrinsic excitability of the iPSC-derived cortical neurons exhibited enhanced maturation compared to neurons cultured on a poly-ornithine laminin substrate, although the neurons were still unable to exhibit a level of maturation equivalent to mature adult neurons (see ***Table 3.1***). Specifically, the low levels of synaptic activity still pose a significant limitation to the investigation of synaptic phenotypes in these cells. Moreover, the ability of rodent stem-cell derived neurons to generate mature functional properties in less than a month without astrocytes [317, 318], suggests a species-specific temporal regulation of neuronal development and maturation that can only be modestly accelerated by exogenous factors within a reasonable time-frame. As a result, a different approach will be required to accelerate the generation of active and mature human synaptic networks for *in vitro* investigation. One alternative strategy that has been used to generate neurons is the induction of pro-neural transcription factor expression [152, 155, 158]. This option may provide a route to initiate or accelerate the transcriptional pathways associated with neuronal differentiation and maturation that may not have been modulated by the strategies explored here. The potential of this method in the generation of active synaptic networks will be investigated in the following chapter.

V: Using forced expression of neurogenin-2 to generate iPSC-derived cortical neurons with enhanced synaptic properties

5.1. Introduction

Recently, Zhang et al., (2013) took a new approach to generate functional neurons from human iPSCs and ESCs within a short-time frame [158]. Building upon previous direct conversion strategies [152, 154], Zhang et al., (2013) identified that the single transcription factor, neurogenin-2, could be expressed to convert human stem cells into neurons with an efficiency of nearly 100%. They also demonstrated similar results using NeuroD1. This method overcame the requirement for multiple transcription factor expression that was needed in previous neuronal transdifferentiation studies [152, 154, 155], and provided an expandable initial cell population through the use of stem cells. Furthermore, the conversion occurred over a rapid time-scale, as within just one week of neurogenin-2 expression cells expressed neuronal markers, and by three weeks exhibited functional synaptic networks [158].

Neurogenin-2 is a bHLH pro-neural transcription factor involved in the early specification of excitatory cortical neurons and the inhibition of ventral cell fates and gliogenesis [368]. The dorsal progenitor marker, Pax6, induces neurogenin-2 expression [369], which in turn activates a multitude of downstream transcriptions factors, such as Tbr2, NeuroD1 and VGlut1/2, to direct cortical neuronal differentiation [370]. The ablation of neurogenin-2 during development implicates this protein in many key aspects of cortical neuronal differentiation, including neuronal migration and acquisition of pyramidal cell morphology [370-372].

Using a lentiviral delivery strategy Zhang et al., (2013) enabled the inducible expression of mouse neurogenin-2 (mNgn2) in human stem cells [158]. The lentiviral construct contained eGFP as a marker of transduction, and conferred puromycin resistance to allow for the selection of transduced cells. Following three weeks of neurogenin-2 expression, the assessment of single-cell

transcriptional expression profiles indicated the generation of a largely homogenous neuronal population, consistent with a cortical layer 2/3 excitatory glutamatergic neuronal phenotype, which was reproduced across three cell lines. In line with the role of neurogenin-2 in embryonic development, Zhang et al., (2013) reported that none of the cells expressed markers of GABAergic interneurons or glia [158].

Most striking, were the functional properties of the neurogenin-2 neurons generated by Zhang et al., (2013) after just three weeks in culture [158]. The vast majority of cells demonstrated voltage-gated sodium currents, action potentials and robust excitatory AMPA-receptor mediated synaptic activity when co-cultured with mouse astrocytes. These results greatly exceeded the prevalence and frequency of excitatory synaptic activity previously described by many other iPSC-derived neuronal differentiation protocols [118, 161, 162, 373, 374]. Evidence of functional NMDA-receptor expression was apparent after four weeks in culture, congruent with the limited expression of transcripts encoding NMDA receptor subunits at earlier time points. With this new model, Zhang et al., (2013) demonstrated the capacity of neurogenin-2 neurons to express alterations in AMPA-receptor mediated synaptic activity following retinoic acid treatment or knockdown of the pre-synaptic protein, Munc18-1 [158].

A subsequent study by Ho et al., (2016) overexpressed neurogenin-2 in human iPSC-derived NPCs, which resulted in enhanced neuronal differentiation reflected by elevated MAP2A expression [375]. The resulting neuronal population was enriched for excitatory cortical neuronal markers, which occurred alongside a significant reduction in markers for other neuronal cell types and glia. Ho et al., (2016) demonstrated an increase in the mRNA expression of synaptic proteins and small increases in neuronal activity, despite the absence of glia, but did not perform an extensive functional characterization of the neurogenin-2 differentiated NPCs [375]. Therefore, it is uncertain whether earlier cortical patterning could enhance the neuronal differentiation and functional outcome of iPSC-derived neurons generated by the exogenous expression of neurogenin-2.

Within this chapter I aimed to determine the utility of induced neurogenin-2 expression in the differentiation of functional neurons directly from human iPSCs and from human iPSC-derived NPCs. More specifically, I wanted to address the following questions:

- Do human iPSC-derived neurons differentiated via neurogenin-2 expression maintain a cortical identity?
- Can neurogenin-2 expression be used to generate human iPSC-derived cortical neurons with enhanced functional properties that develop active synaptic networks?
- Does neurogenin2-mediated neuronal differentiation of human iPSCs conserve the fAD-associated phenotype in secreted Aβ-peptide species?

5.2. Results

5.2.1. Human iPSCs and NPCs can be differentiated into functional cortical neurons by induced expression of neurogenin-2

Two different strategies were taken in order to determine whether neurogenin-2 could be used to generate neurons with enhanced functional properties. The first approach was to generate neurons directly from iPSCs by expression of mNgn2, in line with the original protocol developed by Zhang et al., (2013) (***Figure 5.1a;*** termed iPSC-mNgn2) [158]. Whilst, it was predicted that this protocol would generate cortical neurons with robust functional properties, iPSCs are costly to culture and require daily feeding and frequent passaging during routine maintenance, which can result in karotypic abnormalities [376]. Furthermore, there is no intermediate expansion phase as iPSCs convert directly to post-mitotic neurons, which will limit the final yield of cells. Therefore, the second approach was to drive neurogenin-2 expression in iPSC-derived NPCs, previously differentiated according to Shi et al., (2012) (***Figure 5.1b;*** termed NPC-mNgn2) [149]. The proliferative nature of the NPCs generated through neural induction results in the production of a large number of cells from a small initial population of iPSCs, and therefore provides a plentiful supply of NPCs for neuronal differentiation. In both cases the initial cell population, iPSCs or NPCs,

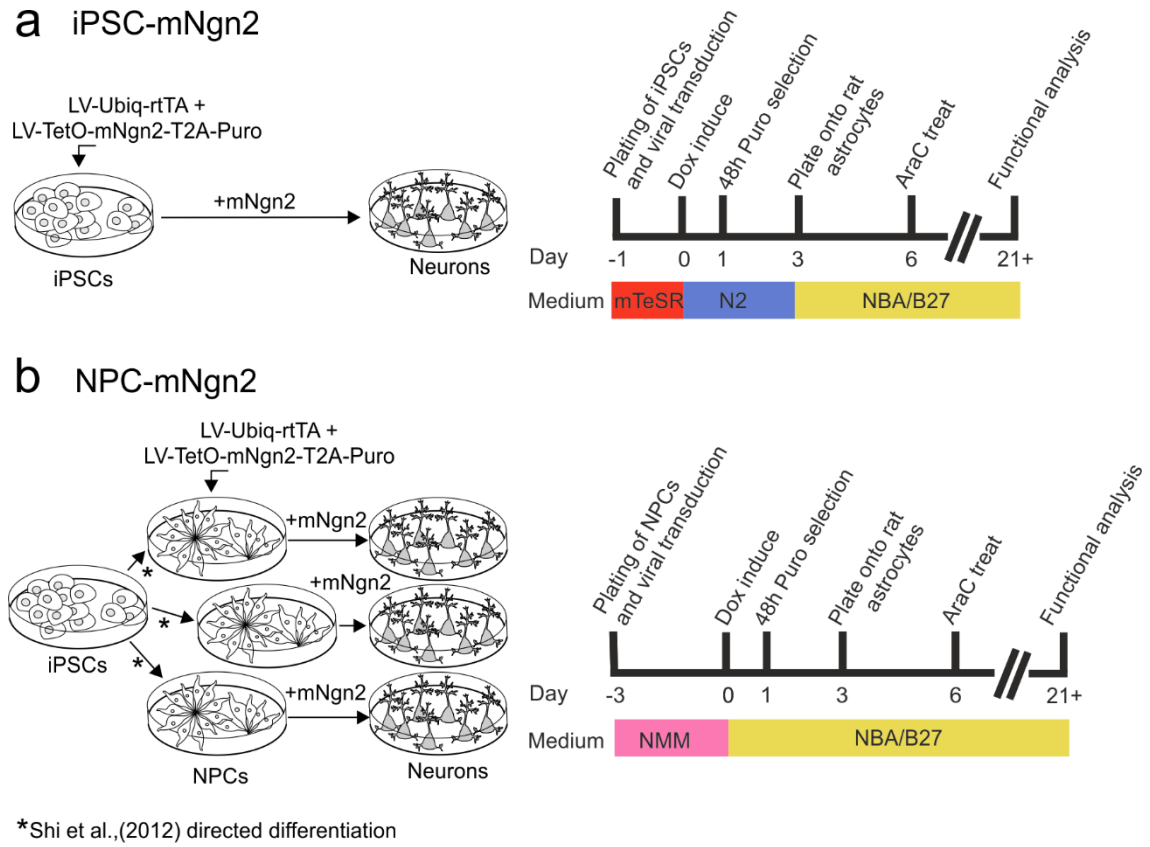

Figure 5.1. Experimental designs for neurogenin-2 neuronal differentiation from human iPSCs and NPCs. (a) Schematic of experiment (*left*) and timeline (*right*) for the differentiation of human iPSCs into cortical neurons by expression of neurogenin-2 (iPSC-mNgn2). Lentiviral transduction of iPSCs with the constructs Ubiq-rtTA and TetO-mNgn2-T2A-Puro will enable the inducible expression of mouse neurogenin-2 (mNgn2) in order to generate a direct conversion into post-mitotic neurons. **(b)** Schematic of experiment (*left*) and timeline (*right*) for the differentiation of day 28-33 human NPCs into cortical neurons by expression of neurogenin-2 (NPC-mNgn2). Human iPSCs are differentiated into NPCs using the Shi et al., (2012) neural induction protocol. The proliferative nature of the NPCs results in a considerable amplification of cell number throughout neural induction. The resulting NPCs can be transduced with the lentiviral constructs (Ubiq-rtTA and TetO-mNgn2-T2A-Puro) and then induced to express mNgn2 in order to accelerate neuronal differentiation. In each experimental paradigm, lentiviral transduction with both constructs is required for expression of mNgn2 and puromycin resistance. Following transduction, expression of the construct is induced by doxycycline (day 0) before a 2 day puromycin treatment period to select for the neurogenin-2 expressing cell population. Cells are replated onto rat astrocytes at day 3 to promote neuronal maturation and synapse formation and to enable control of cell density. Anti-mitotic treatment with AraC at day 6 eliminates any surviving proliferative cells, without affecting post-mitotic neurons.

required the successful transduction with two constructs, TetO-mNgn2-T2A-Puro and Ubiq-rtTA, in order to enable the inducible and simultaneous expression of mNgn2 and puromycin resistance. The Ubiq-rtTA generates constitutive expression of the reverse tetracycline transcriptional activator, which, only in the presence of tetracycline, can bind to the TetO promoter and activate gene transcription, thereby allowing for the temporal control of mNgn2 expression [377]. Here, doxycycline, a more efficacious derivative of tetracycline, was used [377]. The T2A peptide ensured that puromycin resistance would only be conferred upon cells that also express neurogenin-2 [378]. In these experiments a 2 day period of puromycin treatment was required to kill all untransduced cells. To enable a homogenous cell density across cultures, which would otherwise be influenced by transduction efficiency and viral toxicity, cells were lifted and replated at day 3 onto a monolayer of rat astrocytes. At day 3, cultures contained only mNgn2 expressing cells that were immature and without extensive neurite outgrowth, and therefore were less vulnerable to the mechanical stress of replating than mature neuronal populations. The anti-mitotic, AraC, was used to eliminate any surviving proliferative cells at day 6. No obvious adverse effects were observed in post-mitotic human neurons or rat astrocytes at the AraC concentration used.

Neurogenin-2 differentiated neurons were assessed at day 21 in order to determine their cellular identity and functional capacity. Immunolabelling for deep layer (Tbr1 and Ctip2) and upper layer (Satb2) cortical markers revealed positive cells in both iPSC-mNgn2 (***Figure 5.2a,c***) and NPC-mNgn2 (***Figure 5.2b,e***) neuronal cultures, indicating the generation of excitatory cortical neurons. However, as anticipated, the yield of cells at day 3 of neurogenin-2 differentiation was far greater for NPC-mNgn2 (32.44 ± 3.82 x10^6 cells, n=26 differentiations; ***Figure 5.2f***) than iPSC-mNgn2 (0.63 ± 0.17 x10^6 cells, n= 12 differentiations; ***Figure 5.2d***). This was a likely result of the considerable proliferation occurring throughout neural induction, which generated on average 21.40 ± 2.17 x10^6 NPCs (n=17 differentiations) at the point of freeze down on day 28-33. Whilst NPCs were readily transduced at high efficiency using lentiviral supernatants, iPSCs required single cell dissociation

and transduction in suspension using a concentrated lentiviral preparation in order to achieve reasonable transduction efficiencies. Even then, puromycin selection of the iPSC cultures was associated with considerable cell death, which was minimal in NPC cultures, further indicating the lower proportion of transduced cells and thereby affecting the cell yield. Following final plating onto rat astrocytes at day 3, whole-cell patch clamp electrophysiology at day 21 demonstrated that both

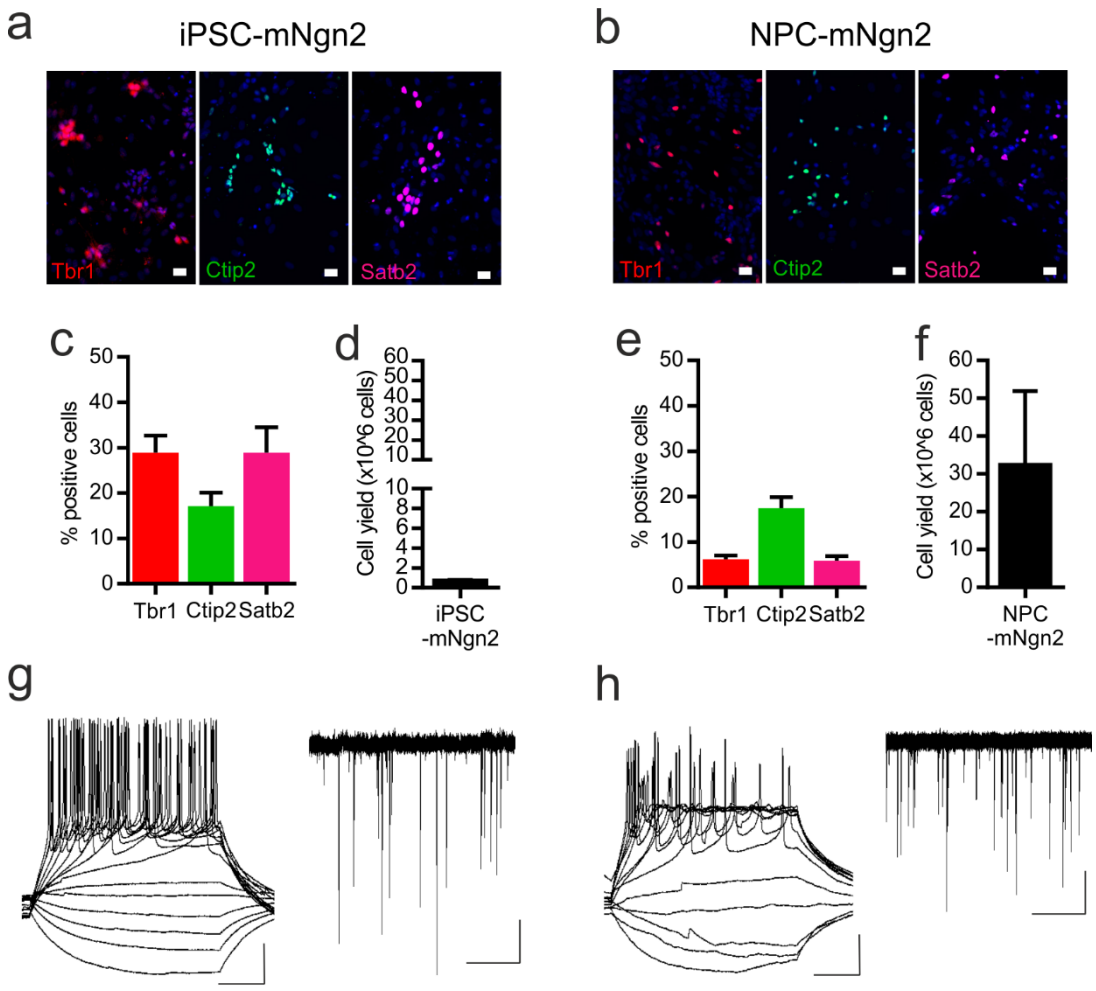

Figure 5.2. Functional cortical neurons can be generated in 3 weeks by induced-expression of neurogenin-2 in iPSCs or NPCs. Neurons differentiated by neurogenin-2 expression were assayed at day 21. **(a)** iPSC-mNgn2 and **(b)** NPC-mNgn2 neuronal cultured contained cells expressing deep layer, Tbr1 (*left*) and Ctip2 (*middle*), and upper layer, Satb2 (*right*) cortical markers (blue DAPI nuclei stain; scale bars 20 µm). **(c)** Quantification of cortical layer marker expression in neuronal nuclei only in iPSC-mNgn2 cultures (n = 21, 18, and 20 FOV for Tbr1, Ctip2 and Satb2, respectively, from 2 cell lines). **(d)** The yield of cells at day 3 of iPSC-mNgn2 neuronal differentiation from one well of iPSCs. **(e)** Quantification of cortical layer marker expression in neuronal nuclei only in NPC-mNgn2 cultures (n = 48, 50, and 40 FOV for Tbr1, Ctip2 and Satb2, respectively, from 3 cell lines). **(f)** The yield of cells at day 3 of NPC-mNgn2 neuronal differentiation, after the directed differentiation of iPSCs to NPCs, generated from one well of iPSCs. Example traces from **(g)** iPSC-mNgn2 and **(h)** NPC-mNgn2 neurons showing induced action potential firing (*left*; scale bars 20 mV, 100 ms) and spontaneous glutamatergic synaptic currents (*right;* scale bars 10 pA, 5 s).

iPSC-mNgn2 (***Figure 5.2g***) and NPC-mNgn2 (***Figure 5.2h***) neurons could fire multiple action potentials in response to current injection and received frequent excitatory synaptic inputs.

5.2.2. Neurogenin-2 neurons have enhanced functional maturity

Having established that neurogenin-2 differentiation of iPSCs and NPCs generated functional excitatory cortical neurons, I sought to determine whether the resulting neurons had enhanced intrinsic and synaptic functional properties compared to those generated by the Shi et al., (2012) protocol [149]. Neurogenin-2 neurons are cultured in NBA/B27, which has a different composition to standard neuronal maintenance medium. In addition to a different base medium, NBA/B27 also has a number of supplements (many described in Chapter IV) that have previously been reported to affect neuronal survival and maturation. To isolate the effects specifically associated with the induced expression of neurogenin-2, a subset of neurons derived using the Shi et al., (2012) protocol were also cultured in NBA/B27 medium. To this end, I performed a functional assessment at day 21 using whole-cell patch clamp electrophysiology to determine the parameters measured throughout Chapter IV. I compared neurons cultured under standard conditions (NMM-A; *pink*, n=19 cells), neurons cultured in NBA/B27 (*orange*; n=22-23 cells), NPC-mNgn2 neurons (*blue*; n=21 cells) and iPSC-mNgn2 neurons (*green*; n=24-25 cells), that were derived from two control cell lines (***Figure 5.3a***). The previously described protocols were applied to assess excitatory synaptic activity, voltage-gated currents and induced action potential firing (see ***Figure 5.3b-d*** for example traces). The functional properties of all experimental groups were compared to the NMM-A control group using an appropriate statistical test and a post-hoc multiple comparisons test. Analysis of the spontaneous EPSCs revealed a significant increase in the proportion of cells with EPSCs, whereby the vast majority of NPC-mNgn2 neurons received excitatory synaptic inputs. This represented a four-fold increase compared to the NMM-A control group (21 %, 4/19 cells for NMM-A, 32 % 7/22 cells for NBA/B27, 86 %, 18/21 cells for NPC-mNgn2, and 50 %, 12/24 cells for iPSC-mNgn2, $p < 0.001$, Chi-squared test; ***Figure 5.3e***). Expression of neurogenin-2 in iPSCs or NPCs also significantly

increased the frequency of EPSCs to more than twenty-fold greater than that observed in the NMM-A control group (0.04 ± 0.02 Hz for NMM-A, 0.18 ± 0.09 Hz for NBA/B27, 1.00 ± 0.27*** Hz NPC-mNgn2, and 0.91 ± 0.42* Hz for iPSC-mNgn2, $p < 0.001$, K-W test; ***Figure 5.3f***). The amplitude of EPSCs remained similar across the cultures (25.95 ± 7.60 pA, n=4 cells for NMM-A, 35.80 ± 13.66 pA, n=7 cells for NBA/B27, 25.09 ± 4.91 pA, n=18 cells for NPC-mNgn2, and 50.15 ± 10.00 pA, n=12 cells for iPSC-mNgn2, $p < 0.0200$, K-W test; ***Figure 5.3g***). Analysis of the intrinsic membrane properties showed that the maximum sodium current was also significantly increased in neurons expressing neurogenin-2 (1153 ± 101 pA for NMM-A, 1497 ± 153 pA for NBA/B27, 1819 ± 151* pA for NPC-mNgn2 and 2337 ± 244*** pA for iPSC-mNgn2, $p < 0.001$, one-way ANOVA; ***Figure 5.3j***). Expression of neurogenin-2 resulted in an increased membrane capacitance in NPC-mNgn2 neurons, but not iPSC-mNgn2 neurons (19.6 ± 1.5 pF for NMM-A, 21.2 ± 1.6 pF for NBA/B27, 27.8 ± 1.7** pF for NPC-mNgn2 and 20.6 ± 1.3 pF for iPSC-mNgn2, $p = 0.0015$, one-way ANOVA; ***Figure 5.3h***). Meanwhile, the following intrinsic membrane properties were significantly different only in iPSC-mNgn2 neurons, and were consistent with enhanced maturation: the resting membrane potential (-40.5 ± 1.8 mV for NMM-A, -39.8 ± 1.7 mV for NBA/B27, -38.8 ± 1.8 mV for NPC-mNgn2 and -47.7 ± 1.5* mV for iPSC-mNgn2, $p < 0.001$, one-way ANOVA; ***Figure 5.3g***), the membrane

Figure 5.3. Induced neurogenin-2 expression generates neurons that are functionally more mature. *(on following page)* **(a)** Schematic of the experiment showing neurons generated by directed differentiation and cultured in either NMM-A (*pink*) or NBA/B27 (*orange*), and neurons that were generated by induced neurogenin-2 expression from NPCs (NPC-mNgn2; *blue*) or directly from iPSCs (iPSC-mNgn2; *green*). Cells were plated onto rat astrocytes and functionally assessed at day 21-24. **(b)** Representative traces of spontaneous EPSCs. Scale bar 10 pA, 2 s. **(c)** Representative traces of voltage-gated currents (*upper;* scale bar 500 pA, 100 ms) and induced action potential firing (*lower;* 20 mV, 100 ms). Analysis of spontaneous glutamatergic synaptic currents showed significant differences in **(d)** the proportion of cells receiving EPSCs ($p = 0.0002$, Chi-squared test), **(e)** the frequency of EPSCs ($p < 0.001$, K-W test) and **(f)** the amplitude of EPSCs ($p = 0.0200$, n = 4, 7, 18 and 12 cells for NMM-A, NBA/B27, NPC-mNgn2 and iPSC-mNgn2, respectively, K-W test). The intrinsic membrane properties were assessed and showed significant differences in **(g)** the resting membrane potential ($p < 0.001$, one-way ANOVA), **(h)** the membrane capacitance ($p = 0.0015$, one-way ANOVA), **(i)** the membrane resistance ($p < 0.0001$, K-W test), **(j)** the maximum sodium current ($p < 0.001$, one-way ANOVA), **(k)** the maximum potassium current ($p = 0.0075$, K-W test), **(l)** the number of consecutive action potentials ($p < 0.001$, K-W test), **(m)** the action potential threshold ($p < 0.001$, one-way ANOVA) and **(n)** the action potential amplitude ($p < 0.001$, K-W test). n = 19,22-23, 21 and 24-25 cells, differentiated from 2 cell lines, for NMM-A, NBA/B27, NPC-mNgn2, and iPSC-mNgn2, respectively, unless otherwise stated. All groups were compared to the NMM-A control group using a K-W test or a one-way ANOVA with a Dunn's or Dunnett's post-hoc test for multiple comparisons, respectively. * $p < 0.05$, ** $p < 0.01$, *** $p < 0.001$

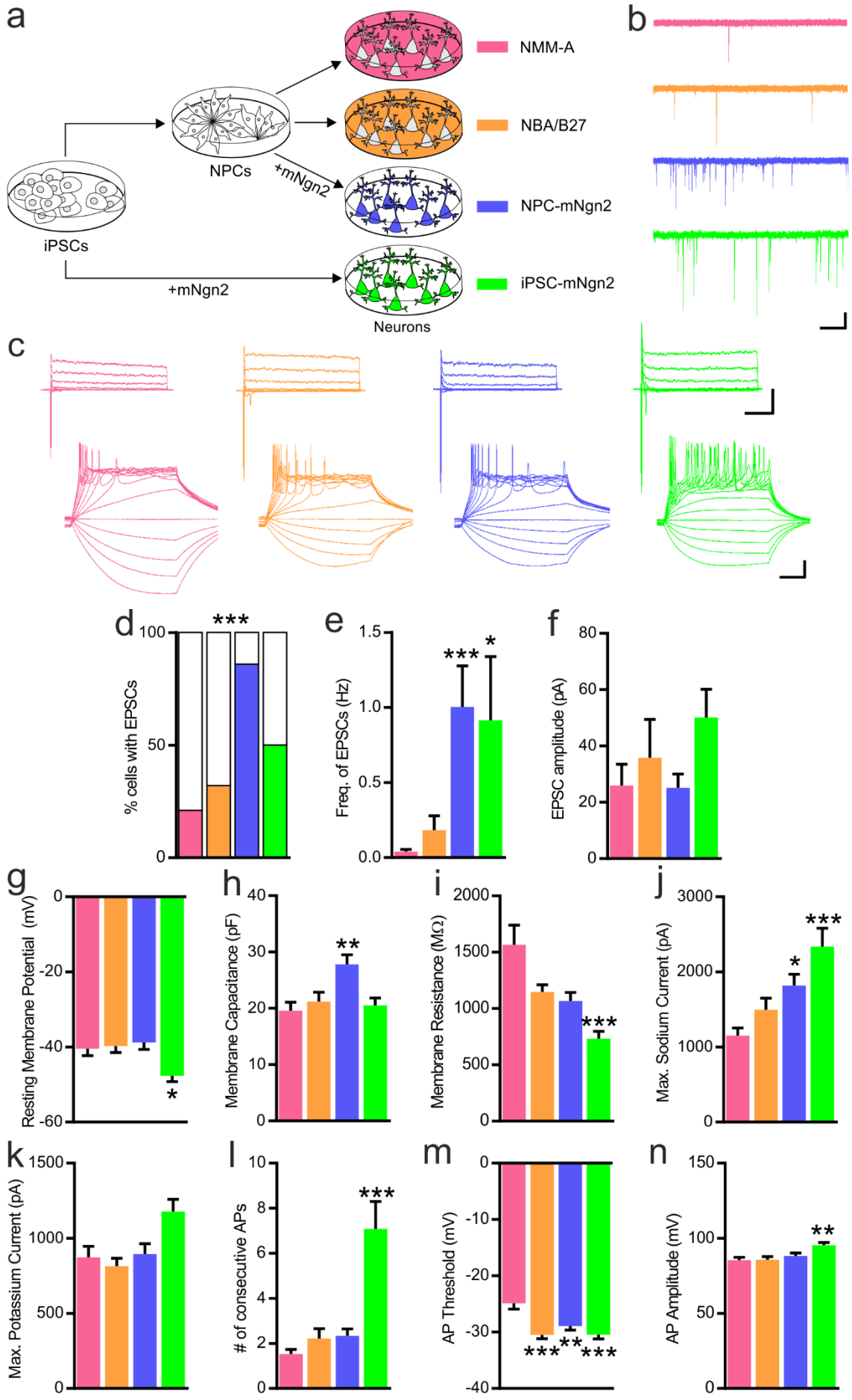
a
NMM-A
NBA/B27
NPC-mNgn2
iPSC-mNgn2
NPCs
+mNgn2
iPSCs
+mNgn2
Neurons
b
c
d
% cells with EPSCs
e
Freq. of EPSCs (Hz)
f
EPSC amplitude (pA)
g
Resting Membrane Potential (mV)
h
Membrane Capacitance (pF)
i
Membrane Resistance (MΩ)
j
Max. Sodium Current (pA)
k
Max. Potassium Current (pA)
l
# of consecutive APs
m
AP Threshold (mV)
n
AP Amplitude (mV)

resistance (1567 ± 173 MΩ for NMM-A, 1148 ± 63 MΩ for NBA/B27, 1066 ± 77 MΩ for NPC-mNgn2, and 732 ± 65*** MΩ for iPSC-mNgn2, $p < 0.001$, K-W test; ***Figure 5.3i***), the number of consecutive action potentials (1.5 ± 0.2 for NMM-A, 2.2 ± 0.4 for NBA/B27, 2.3 ± 0.3 for NPC-mNgn2, and 7.1 ± 1.2*** for iPSC-mNgn2, $p < 0.001$, K-W test; ***Figure 5.3l***) and the action potential amplitude (85.4 ± 2.0 mV for NMM-A, 85.8 ± 2.0 mV for NBA/B27, 88.3 ± 1.9 mV for NPC-mNgn2, and 95.4 ± 1.7** mV for iPSC-mNgn2, $p < 0.001$, K-W test; ***Figure 5.3n***). The action potential threshold was more hyperpolarized in all experimental groups relative to the NMM-A control group (-24.9 ± 1.0 mV for NMM-A, -30.5 ± 0.7*** mV for NBA/B27, -28.9 ± 0.7** mV for NPC-mNgn2, and -30.4 ± 0.8*** mV for iPSC-mNgn2, < 0.001, one-way ANOVA; ***Figure 5.3m***). The results are summarised in ***Table 5.1***. Taken together, these results demonstrate the most robust enhancement of the synaptic properties was demonstrated by NPC-mNgn2 neurons. These cells exhibited the largest proportion of synaptically integrated neurons, with events occurring at frequencies twenty-fold greater than NMM-A control neurons, and also exhibited an enhancement of intrinsic maturity. In contrast, iPSC-mNgn2 neurons exhibited considerable enhancement of intrinsic maturation, but still only 50 % of cells received synaptic inputs. Consistent with previous results (see Chapter IV), growth in NBA/B27 medium that was supplemented with factors previously reported to promote neuronal maturation, did not result in a significant enhancement of either the intrinsic or synaptic functional properties. Therefore, this indicated that the expression of neurogenin-2 was accountable for the enhanced functional properties observed in the iPSC-mNgn2 and NPC-mNgn2 neurons.

The enhanced synaptic properties, alongside the significantly higher cell yields, suggested that the NPC-mNgn2 neuronal differentiation would be most suitable for the future investigation of synaptic phenotypes. As a result, I performed additional characterization of the NPC-mNgn2 neuronal cultures. As previously described in Chapter III, neuronal cultures differentiated without neurogenin-2 generated a small proportion of Nkx2.1 progenitors and subsequently low numbers of GABAergic interneurons. During *in vivo* development, the expression of neurogenin-2 supresses

Property	NMM-A		NBA/B27		NPC-mNgn2		iPSC-mNgn2		
	mean ± SEM	n (cells)	mean ± SEM	n (cells)	mean ± SEM	n (cells)	mean ± SEM	n (cells)	*p* value
% cells with EPSCs	21 %	4/19	32 %	7/22	86 %	18/21	50 %	12/24	< 0.001
EPSC frequency (Hz)	0.04 ± 0.02	19	0.18 ± 0.09	22	1.00 ± 0.27***	21	0.91 ± 0.42*	24	< 0.001
EPSC amplitude (pA)	25.95 ± 7.6	4	35.80 ± 13.66	7	25.09 ± 4.91	18	50.15 ± 10.00	12	0.0200
Resting membrane potential (mV)	-40.5 ± 1.8	19	-39.8 ± 1.7	23	-38.8 ± 1.8	21	-47.7 ± 1.5*	25	< 0.001
Membrane capacitance (pF)	19.6 ± 1.5	19	21.2 ± 1.6	23	27.8 ± 1.7**	21	20.6 ± 1.3	25	0.0015
Membrane resistance (MΩ)	1567 ± 173	19	1148 ± 63	23	1066 ± 77	21	732 ± 65***	25	< 0.001
Max. Sodium current (pA)	1153 ± 101	19	1497 ± 153	23	1819 ± 151*	21	2337 ± 244***	25	< 0.001
Max. Potassium current (pA)	874 ± 73	19	814 ± 52	23	895 ± 68	21	1178 ± 80***	25	0.0075
# of consecutive APs	1.5 ± 0.2	19	2.2 ± 0.4	23	2.3 ± 0.3	21	7.1 ± 1.2***	25	< 0.001
AP Threshold (mV)	-24.9 ± 1.0	19	-30.5 ± 0.7***	23	-28.9 ± 0.7**	21	-30.4 ± 0.8***	25	< 0.001
AP Amplitude (mV)	85.4 ± 2.0	19	85.8 ± 2.0	23	88.3 ± 1.9	21	95.4 ± 1.7**	25	< 0.001

Table 5.1. Summary table of the synaptic and intrinsic membrane properties of iPSC-mNgn2 neurons, NPC-mNgn2 neurons, and neurons generated by directed differentiation cultured in NBA/B27 and the control NMM-A media. Asterisks denote the statistical significance following a post-hoc multiple comparisons test. *p < 0.05, ** p < 0.01, *** p < 0.001

the activation of transcriptional pathways that generate a GABAergic cell fate [379]. Therefore, I hypothesised that driving the expression of neurogenin-2 would abolish the generation of GABAergic interneurons in the NPC-mNgn2 neuronal cultures. To this end, immunolabelling for GAD65, a marker of GABAergic interneurons, was performed to determine the proportions of GABAergic neurons in NPC cultures that were differentiated without neurogenin-2 (- mNgn2) at day 53, and with neurogenin2 (+ mNgn2) at day 20-30 (***Figure 5.4a***). This revealed that low numbers of GAD65-positive cells were present in cultures differentiated both with and without mNgn2, and quantification demonstrated that the proportions did not differ significantly (4.2 ± 1.0 %, n = 12 FOV for without mNgn2, and 5.8 ± 1.1 %, n = 22 FOV for with mNgn2, p = 0.3011, unpaired t-test; ***Figure 5.4b***). Having rejected my hypothesis and established that subsets of inhibitory neurons are also present in cultures differentiated with mNgn2, I sought to assess the formation of functional inhibitory synapses using whole-cell patch clamp electrophysiology. Voltage-clamp recordings were performed at a holding potential of V_m = 0 mV, the approximate reversal potential for glutamatergic ionotropic receptors, in order to avoid detection of glutamatergic synaptic activity. These recordings revealed fast-onset outward currents with a slow decay phase that were consistent with $GABA_A$-receptor mediated inhibitory post-synaptic currents (IPSCs). The IPSCs were abolished by bath application of the $GABA_A$ receptor antagonist, picrotoxin (PTX), thereby confirming their nature (***Figure 5.4c***). Spontaneous IPSCs were observed in recordings from neurons in cortical cultures differentiated with and without mNgn2, indicative of functional inhibitory synapse formation (***Figure 5.4d***). Further analysis of spontaneous IPSCs revealed that comparable proportions of cells received IPSCs in cultures differentiated with and without mNgn2 (36 %, 5/14 cells for – mNgn2, and 58 % 14/24 cells for + mNgn2, p = 0.3133, Fisher's exact test; ***Figure 5.4e***). However, the frequency of IPSCs was significantly higher in mNgn2 neurons (0.01 ± 0.00 Hz, n = 14 cells for without mNgn2, and 0.27 ± 0.10 Hz, n = 24 cells for with mNgn2, p = 0.0233, M-W test; ***Figure 5.4f***), whilst the IPSC amplitude did not differ (10.07 ± 1.95 pA, n = 5 cells for without mNgn2, and 14.54 ± 1.85 pA, n = 15 cells for with mNgn2, p = 0.1418, M-W test; ***Figure 5.4g***). Taken

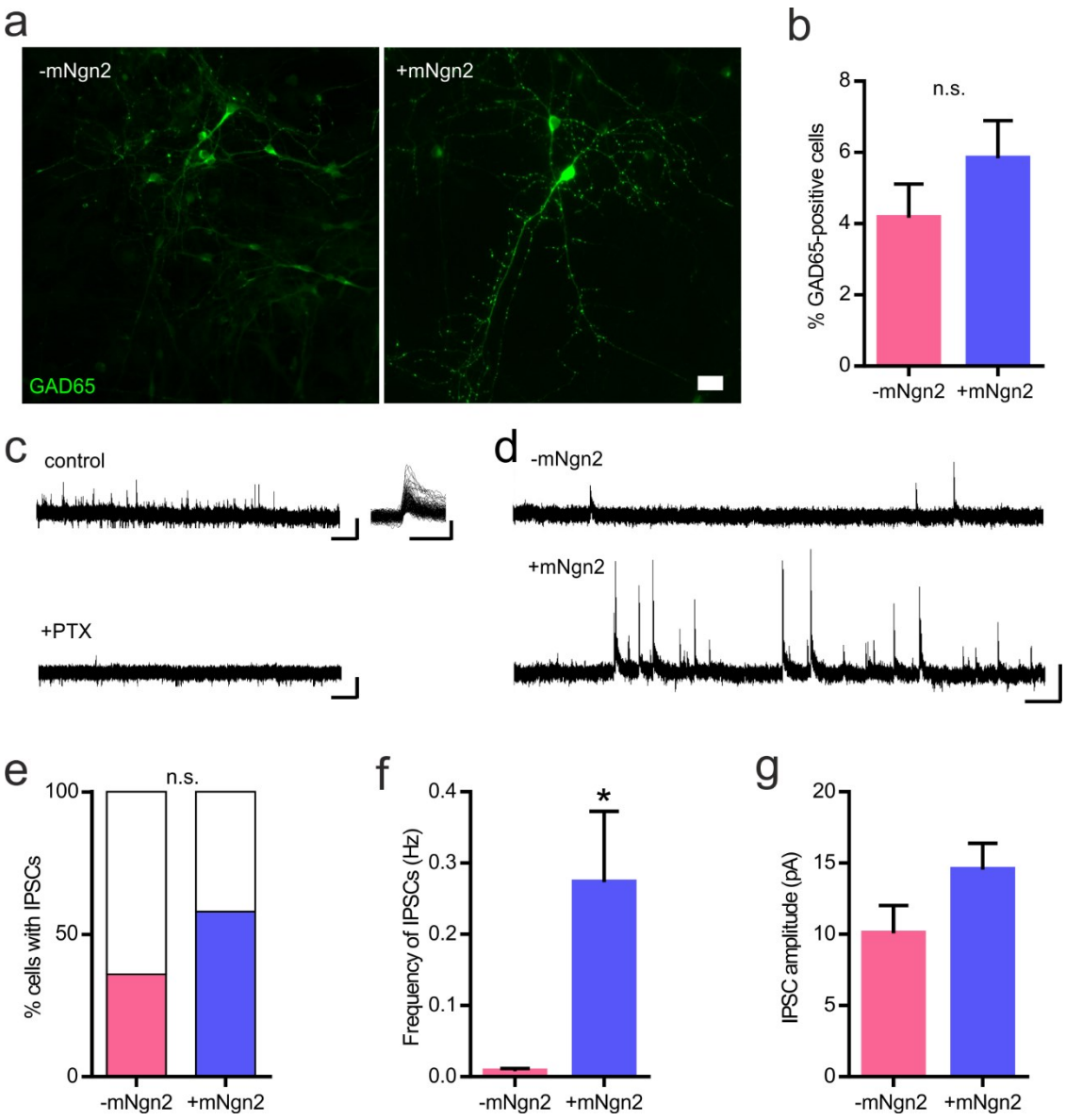

Figure 5.4. Neurogenin-2 neuronal cultures contain a small proportion of active interneurons. **(a)** Neuronal cultures generated without mNgn2 expression (-mNgn2; *left*) and with mNgn2 expression (+mNgn2; *right*) were labelled for the inhibitory interneuron marker GAD65. Scale bar 20 µm. **(b)** Quantification of GAD65 expression showed no difference in the proportion of positive-cells in cultures differentiated without mNgn2 (day 53) and with mNgn2 (day 20-30) ($p = 0.3011$, $n = 22$ and 12 FOV for without mNgn2 and with mNgn2, respectively, unpaired t-test). **(c)** Example recording at $V_m = 0$ mV showing IPSCs recorded under control conditions (*upper left;* scale bar 5 pA, 10 s), with overlaid detected events (*upper right;* scale bar 10 pA, 10 ms), and, following wash-in of picrotoxin (PTX), the blockade of all IPSCs (*lower;* scale bar 5 pA, 10 s). **(d)** Example traces of IPSCs from neurons differentiated without mNgn2 (day 80-90) and with mNgn2 neurons (day 20-30). Scale bar 10 pA, 2 s. **(e)** The proportion of neurons receiving IPSCs did not differ significantly ($p = 0.3133$, $n = 14$ and 24 cells for differentiated without mNgn2 and with mNgn2, respectively, Fisher's exact test). **(f)** The frequency of IPSCs was significantly increased in cultures differentiated with mNgn2 ($p = 0.0233$, $n = 14$ and 24 cells for without mNgn2 and with mNgn2, respectively, M-W test). **(g)** No difference was observed in the IPSC amplitude ($p = 0.1418$, $n = 5$ and 15 cells for without mNgn2 and with mNgn2, respectively, M-W test) (From 1 cell line). * $p < 0.05$

together, this data demonstrates that comparable proportions of GABAergic interneurons are generated by neuronal differentiation of NPCs with and without neurogenin-2. Likewise, similar proportions of cells receive inhibitory inputs, but the frequency of IPSCs are significantly higher in neuronal cultures differentiated with mNgn2, reflective of increased inhibitory network activity.

5.2.3. Neurogenin-2 neurons from a fAD patient have altered Aβ-peptide secretion

As shown in Chapter III, neurons differentiated without neurogenin-2 from fAD patient-derived iPSCs demonstrate a robust increase in the Aβ42:40 ratio compared to healthy controls. To determine whether this phenotype was conserved in NPC-mNgn2 neurons, the secreted Aβ peptides were measured in media samples from cortical cultures of a healthy control and a fAD patient with the PSEN1 Intron 4 Del mutation that were differentiated from NPCs with and without neurogenin-2. Media samples were collected 48 hours after a full medium change from day 25 cultures differentiated with mNgn2, and from day 85 cultures differentiated without mNgn2, and the Aβ-species were quantified using an MSD immunoassay to calculate the Aβ42:40 ratio. In

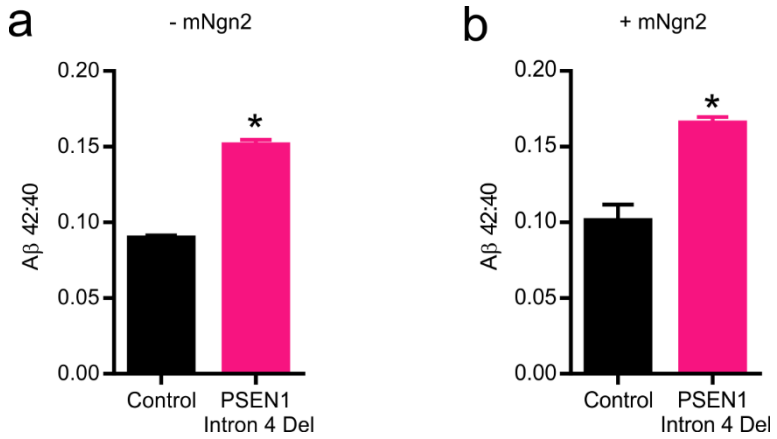

Figure 5.5. Neurogenin-2 neurons conserve the Alzheimer's disease associated phenotype in secreted Aβ peptides. Cortical NPCs, from a control individual and a fAD patient with a PSEN1 Intron 4 deletion, were differentiated without (-mNgn2) or with mNgn2 (+mNgn2) expression. Media samples were collected 48 h following a full medium change from day 85 cultures differentiated without mNgn2, and from day 25 cultures differentiated with mNgn2, and then the Aβ species were quantified using an MSD immunoassay. **(a)** Cortical cultures derived from a fAD patient that were differentiated without mNgn2 had a significantly higher Aβ42:40 ratio relative to a healthy control ($p = 0.0286$, M-W test). **(b)** Cortical cultures derived from a fAD patient that were differentiated with mNgn2 also had a significantly higher Aβ42:40 ratio relative to a healthy control ($p = 0.0286$, M-W test). n = 4 technical replicates from 1 differentiation for control and PSEN1 Intron 4 Del. * $p < 0.05$

comparison to cultures differentiated without mNgn2, the total Aβ42 and 40 in cultures differentiated with mNgn2 could not be determined as the cell lysate protein concentration, required for normalisation, was below the level of detection. As expected, the ratio of secreted Aβ42:40 peptides was significantly increased in PSEN1 Intron 4 Del media samples from day 85 cultures differentiated without mNgn2, in line with previous observations (0.09 ± 0.0 for control, 0.15 ± 0.0 for PSEN1 Intron 4 Del, p = 0.0286, M-W test; ***Figure 5.5a***). Similarly, the ratio of secreted Aβ42:40 peptides in media samples from day 25 PSEN1 Intron 4 Del cultures differentiated with mNgn2 was also significantly increased (0.10 ± 0.01 for control, 0.17 ± 0.0 for PSEN1 Intron 4 Del, p = 0.0286, M-W test; ***Figure 5.5b***). This confirms that the biochemical changes leading to altered Aβ peptide composition also occur in neurons differentiated with neurogenin-2.

5.3. Discussion

Two approaches were explored that took advantage of inducible neurogenin-2 expression with the aim to further enhance the functional properties of iPSC-derived cortical neurons above that achieved by co-culture with rodent astrocytes (see Chapter IV), and to generate neurons with functional properties more similar to mature adult neurons (***Table 3.1***). Neurogenin-2 expression was induced in iPSCs or NPCs and, in both cases, generated functional cortical neurons after 21 days. However, the cell yield was far larger for NPCs compared to iPSCs. An electrophysiological comparison of the functional properties revealed that the greatest enhancement in excitatory synaptic activity was observed in NPC-mNgn2 neurons. Meanwhile, iPSC-mNgn2 neurons demonstrated significantly more mature intrinsic properties, yet only half of the neurons assayed received excitatory synaptic inputs. As a result, NPC-mNgn2 neuronal differentiation was considered most appropriate for further study. The expression of neurogenin-2 did not appear to affect interneuron generation, as comparable proportions of GAD-positive neurons were observed in NPC-derived cultures differentiated with and without neurogenin-2. Neuronal differentiation with neurogenin-2 resulted in more than twenty-fold increases in the levels of inhibitory and

excitatory synaptic activity. However, the frequency of excitatory activity was four times greater than the frequency of inhibitory activity, suggesting that NPC-mNgn2 neuronal cultures are predominantly comprised of glutamatergic cortical neurons. Furthermore, fAD-patient derived NPC-mNgn2 neuronal cultures reproduced the Aβ42:40 phenotype previously described in Chapter III, indicating that Aβ processing was unaffected by neurogenin-2 mediated differentiation of NPCs.

5.3.1. Functional cortical neuron generation from iPSCs and NPCs using neurogenin-2

In this chapter I described two neuronal differentiation strategies that took advantage of an inducible neurogenin-2 construct with the aim to promote functional maturity. The first was to drive the direct conversion of iPSCs to cortical neurons (iPSC-mNgn2) based upon the protocol by Zhang et al., (2013) [158], and the second was to accelerate neuronal differentiation of pre-patterned cortical NPCs (NPC-mNgn2), in a similar manner to Ho et al., (2016) [375]. In each case, the induction of neurogenin-2 expression was intended to drive the starting cell type towards a more mature cortical neuronal phenotype than previously achieved by neurons generated by directed differentiation. Both iPSC-mNgn2 and NPC-mNgn2 differentiation protocols generated neurons with cortical identities that were able to fire multiple induced action potentials and received frequent excitatory synaptic inputs following 21 days of neurogenin-2 expression. Comparable to neurons generated by directed differentiation, neurogenin-2 neurons expressed the deep-layer markers Ctip2 and Tbr1, and the upper layer marker Satb2. Interestingly, the iPSC-mNgn2 neuronal cultures contained a greater proportion of cells expressing these markers than the NPC-mNgn2 neuronal cultures, which may suggest NPC-mNgn2 cultures contain a greater diversity of cell types. Subsequent analysis revealed that a small subset of NPC-mNgn2 neurons expressed the GABAergic interneuron marker GAD65, although this did not fully account for the unlabelled population. Single cell transcriptomic techniques could provide a method to determine the cellular identities within this population. This may reveal the expression of cortical-layer specific markers that were not tested here, or could reveal alternative neural cell types previously identified in

directed differentiation cultures, such as NPCs or glia. The presence of cells expressing markers of NPCs, even following 28 days of neurogenin-2 expression, have been reported in some neurogenin-2 differentiation studies [275]. In contrast to my observations, others utilising neurogenin-2 for neuronal differentiation describe minimal or complete absence of Ctip2 expression or markers of inhibitory neurons [158, 275, 375, 380, 381]. Interestingly, despite the rare detection of Tbr1 mRNA, Nehme et al., (2018) showed that the majority of neurons immunolabelled positively for the Tbr1 protein [275]. This discrepancy could indicate detection errors at either the mRNA or protein level. Meanwhile, the generation of high proportions of neurons expressing the upper-layer cortical markers Brn2, Cux1 and Satb2 have been frequently reported in neurogenin-2 derived neuronal cultures [158, 275, 381]. However, the expression of Brn2 and Cux1 has not yet been determined in the cultures generated here as a result of inconclusive immunofluorescence for these markers. The presence of GAD65 positive interneurons within the NPC-mNgn2 neuronal cultures could have arisen from the pre-patterning of iPSCs towards a neural fate. Whilst, neurogenin-2 expression has been reported to prevent the GABAergic neuronal differentiation of ventral progenitors *in vitro* [382], it is possible that the level of ectopic neurogenin-2 expression achieved here was insufficient to redirect the cell fate of this population. Nonetheless, there was no difference in the proportion of GAD65-positive cells compared to cultures differentiated without neurogenin-2, indicating that the NPC-mNgn2 neuronal cultures retain a predominantly excitatory cortical neuronal composition.

The lower time and cost investment required for the culture of human iPSC-derived NPCs, compared to iPSCs, makes the NPC-mNgn2 protocol a more attractive option. This is underscored further by the significantly higher cell yields achieved with the NPC-mNgn2 protocol. NPCs are efficiently transduced with simple viral supernatant preparations, whereas iPSCs required transduction whilst in suspension and the use of ultracentrifuged viral preparations, which still did not enable a comparable transduction efficiency. Others have explored the generation of cell lines with integrated rtTA and TetO-mNgn2 through stable transfection, or with gene editing techniques

that can enable integration at specific target sites associated with high transgene expression and minimal impact upon endogenous gene expression [380, 381]. Whilst both of these strategies would reduce the variability of transgene expression, they would require extensive time investment during cell line generation. Therefore, the NPC-mNgn2 approach is particularly scalable, both within and across cell lines, which could be particularly beneficial to higher throughput drug discovery and phenotyping studies.

5.3.2. The functional properties of neurogenin-2 neurons

Most important, for the aims of this thesis, was the generation of mature and active synaptic networks. To this end, the functional properties of iPSC-mNgn2 neurons, NPC-mNgn2 neurons and neurons generated via directed differentiation, which were cultured in neurogenin-2 neuronal medium or standard media, were assayed at day 21. Neuronal culture in NBA/B27 medium was not associated with significant changes in intrinsic or synaptic properties with the exception of a lower action potential threshold. This result further supports the idea that media supplementation with neurotrophins and other factors for several weeks, does not significantly enhance the functional maturation of the iPSC-derived cortical neurons in the cultures generated here. By contrast, neurogenin-2 expression robustly changed the functional properties of the neurons. Interestingly, NPC-mNgn2 neuronal cultures formed highly active excitatory synaptic networks where the majority of neurons were synaptically integrated and the intrinsic properties were modestly enhanced. Meanwhile, iPSC-mNgn2 neurons exhibited considerably more mature intrinsic properties but had variable synaptic properties: whilst some iPSC-mNgn2 neurons showed frequent synaptic inputs, half of the cells assayed demonstrated no excitatory synaptic network integration. Thus the more consistent synaptic properties of day 21 NPC-mNgn2 neurons suggested that this differentiation protocol was the most suitable for synaptic phenotyping studies within a short time-frame.

It is possible that the interaction of neurogenin-2 expression with already active neuronal transcriptional pathways in NPCs can focus the effects of neurogenin-2 expression more specifically towards the upregulation of synapse-related genes. Comparatively, the absence of neuronal gene expression in iPSCs may drive the upregulation of transcription factors associated with neuronal differentiation and the acquisition of intrinsic membrane excitability. The BAM (*Brn2, Ascl1*, and *Myt1l*) transcription factor mediated neuronal conversion protocol indicates the potential functional effects of interactions between different transcription factor signalling cascades [152]. This published work showed that whilst the expression of Ascl1 alone could convert mouse fibroblasts to cells with a neuronal phenotype, the resulting neurons show relatively immature intrinsic properties in comparison to those differentiated via the simultaneous co-expression of *Ascl1, Brn2* and *Myt1l* [152]. This demonstrates the capacity for different transcription factors to act synergistically in the generation of functional neuronal properties. A temporal analysis of the transcriptomic profiles of iPSC-mNgn2 and NPC-mNgn2 cultures could help to elucidate the pathways leading to the functional differences observed here.

Interestingly, concurrent with the enhancement of excitatory synaptic activity was an increase in IPSC frequency. The lack of a simultaneous increase in the proportion of GABAergic neurons suggests a specific increase in interneuron activity. This may also have occurred in parallel with an increase in the total number of GABAergic synapses, which could be determined through quantification of GABAergic synaptic puncta and assessment of miniature IPSCs. The changes observed in excitatory synaptic activity suggests that there was an increased excitatory drive onto inhibitory interneurons, which would be expected to increase their synaptic output. Meanwhile, the IPSC amplitude suggests that the strength of these synapses remains unchanged. These observations demonstrate that NPC-mNgn2 cultures contain functionally active GABAergic interneurons. However, the level of excitatory activity is nearly four-fold higher, further supporting the predominantly glutamatergic nature of these neuronal cultures.

5.3.3. An AD-associated phenotype in neurogenin-2 neurons

The previously observed fAD-patient associated phenotype showing an elevation in the Aβ42:40 ratio of secreted Aβ-peptides ***(Figure 3.7)*** was conserved by NPC-mNgn2 neuronal cultures, indicating that disease relevant Aβ peptide processing was unchanged by neurogenin-2 expression. To my knowledge, the neurogenin-2 neuronal differentiation method has yet to be used for the assessment of disease-associated phenotypes from patient derived cells. Therefore, this is the first demonstration of an Alzheimer's disease associated phenotype in patient-derived neurons differentiated using neurogenin-2. As a result of the enhanced maturational state of the synaptic networks, the NPC-mNgn2 differentiation approach offers the potential for the investigation of synaptic phenotypes in fAD-patient derived cultures.

In summary, neurogenin-2 can drive the generation of functional cortical neurons from both NPCs and iPSC in 21 days. However, the superior synaptic properties, extensive cell yield and ease of NPC culture, support the use of NPC-mNgn2 neurons for synaptic phenotyping assays and consequently, will be the method of choice for further synaptic characterization and manipulation in this thesis. From this chapter, it is evident that excitatory synaptic inputs can be frequent at a population level. However, the animal literature has shown that some of the best controlled synaptic plasticity assays require the isolation and temporal control of a single monosynaptic connection. Therefore, the extent of interconnectivity and the functional properties of excitatory synapses in NPC-mNgn2 neuronal cultures will be explored in the following chapter.

VI: Isolation and characterization of monosynaptic connections in iPSC-derived cortical networks

6.1. Introduction

Synaptic connections form the foundation of functional neuronal circuitry and the basis for information processing. The ability to study and manipulate a monosynaptic connection can provide huge insights into the complex molecular mechanisms underlying signal transduction in the brain. The isolation and interrogation of monosynaptic connections is largely performed using simultaneous whole-cell patch clamp recordings from a connected pair of neurons. Such recordings enable the investigation of basal synaptic transmission, such as pre-synaptic release probability, synaptic efficacy and the functional properties of post-synaptic receptors, at a unitary connection in isolation without interference from polysynaptic activity [383-385]. Dual-patch recordings were used for the first demonstration of synaptic plasticity at the level of a single connection [209], and have enabled further investigations into the pre- and post-synaptic alterations that result in changes to synaptic efficacy. For example, pharmacological manipulations can be selectively delivered to only the pre- or post-synaptic neuron by inclusion in the patch pipette solution, thereby allowing researchers to probe the cellular processes involved in synaptic plasticity [252, 386]. This approach also enables the interrogation of synaptic connectivity between defined cell types, which can be specifically targeted or identified by reporter gene expression, anatomical location, morphology or intrinsic membrane properties. For example, STDP has been shown to be reliably generated between pairs of cultured excitatory rodent hippocampal neurons, but was not demonstrated by excitatory synaptic connections to inhibitory neurons [236]. Dual-whole cell patching enables the manipulation and precise temporal readout of pre- and post- synaptic activity, which can be used to monitor both the short and long-term kinetics of synaptic transmission. Whilst this approach offers a high level of control over both the pre- and post-synaptic neurons, it is a slow and laborious method that can be limited by connection probability.

The use of optogenetic tools, such as ChR2, can provide a faster and more efficient approach to the study of synaptic connectivity. ChR2 can drive single and high-frequency trains of action potentials with precise temporal control [192]. As a result, ChR2 is often used to control neuronal activity without the need for extracellular or intracellular electrical stimulation. In addition, ChR2 can circumvent the problem of large artefacts that are often associated with extracellular electrical stimuli, which can obscure responses with short latencies. Moreover, the expression of ChR2 in neurons does not appear to have adverse effects upon neuronal membrane properties or cell viability [192]. The use of transgenic approaches to drive ChR2 expression in a subpopulation of neurons can enable the selective and specific activation of a genetically defined population of cells [387]. The activation of ChR2 in pre-synaptic cells can generate light-evoked synaptic responses, and therefore, many animal studies have utilised ChR2 to investigate synaptic circuitry in the brain [388-391]. Activation of many ChR2-expressing axonal fibres can generate an optically evoked field post-synaptic potential, in a manner similar to extracellular electrical stimulation [193]. Similarly, pre-synaptic ChR2 activation can also be used to generation a monosynaptic response that can be detected using whole-cell patch-clamp recordings in a post-synaptic neuron [201]. Optically evoked ChR2-responses strongly resemble those generated by pre-synaptic somatic current injection, and have also demonstrated the ability to undergo synaptic plasticity [201]. However, ChR2-activation can evoke axonal action potential generation, which can trigger neurotransmitter release at the synapse in the absence of a somatic action potential. This can be advantageous for the assessment of long-range projections in slice preparations whereby the axonal connection to the soma can be severed [388]. However, this property of ChR2 expression has the potential to pose limitations to the assessment of monosynaptic connections, where light stimulation could promote the generation of polysynaptic activity through the activation of nearby axonal projections. Moreover, the absence of a whole-cell patch on a pre-synaptic ChR2-expressing neuron prohibits the direct measure of electrical activity or intracellular pharmacological manipulation to the patched post-synaptic neuron only.

The probability of identifying a pair of synaptically connected neurons is variable within the rodent cortex. Intra-laminar connection probabilities have been reported to range from 3-15 % in layer 5 [248, 385, 392], 5-20 % in layer 2/3 [392-394] and up to 24 % in layer 4 [395]. Interestingly, several of these studies have reported that the proportion of bidirectional connections was greater than anticipated from the unidirectional connectivity probability [396], which suggests that non-random patterns of local connectivity occur in the cortex [248, 385, 397]. Meanwhile, inter-laminar connection probabilities have been reported from 1-20 %, dependent on the direction of connectivity [392, 393]. The distance between neuronal soma strongly influences the connection probability, whereby neurons situated further apart are less likely to be connected [398]. These connection probabilities were assessed in acute rodent brain slice preparations and are therefore likely to be an underestimate due to axon severance [385, 399]. Comparatively, in rodent cortical slice culture, where axonal outgrowth occurs and new synaptic connections are established, the connection probability is higher [400]. This is particularly evident in the hippocampus, where acute hippocampal slice preparations show typical connection probabilities of 2-13 % [401, 402], whilst hippocampal slice cultures show connection probabilities of up to 56 % [399, 403, 404]. The connection probabilities reported from dissociated rodent hippocampal cultures are more variable and depend upon developmental age [405], cell density [362, 406], and neuronal activity [405]. In general, mature dissociated hippocampal cultures can exhibit relatively high levels of connectivity, on the order of 30-40 % [362, 405]. Although, an equivalent connectivity assessment has not been reported for dissociated cortical cultures.

The properties of intra- and inter-laminar monosynaptic connections in rodent cortex have been described using simultaneous whole-cell patch clamp recordings in slice preparations. In all studies the intracortical monosynaptic connections are reported to have a very short latency to the onset of the post-synaptic response, that averages 0.9-2.1 ms, and has been associated with minor (<1 ms) increases for longer (>250 µm) connection distances [383-385]. In addition, the temporal jitter

of the post-synaptic response onset is very minimal [383-385]. Monosynaptic connections have smooth kinetics, indicative of the activation of a single pre-synaptic neuron, with a fast rise phase and a slow decay phase [383-385]. Intracortical connections have been reported to have low failure rates that average 5-7 %, indicating that rodent neurons form reliable synaptic connections. Furthermore, these connections typically have low coefficients of variation (0.27-0.52), reflecting a relatively consistent post-synaptic response magnitude across stimulations [383-385], and exhibit paired-pulse depression, which is thought to reflect a high neurotransmitter release probability [384]. In general, monosynaptic connections in rodent cortex exhibit relatively small post-synaptic response amplitudes [383-385]. Whilst each neuron in the brain receives thousands of synaptic inputs [407], anatomical assessments in rodent cortex have estimated that connections between excitatory pyramidal neurons are comprised of only 2-8 putative synaptic contacts [383-385]. The number of putative synaptic contacts between pairs of connected excitatory neurons has been found to exhibit a weak positive correlation with the amplitude of the post-synaptic response [383]. While there have been limited characterizations of human synapses in excised tissue, the properties of excitatory cortical synapses that have been described, such as latency and short-term plasticity, are largely consistent with those described in rodent tissue [303, 408, 409]. However, differences in the behaviour of human and rodent synapses have been observed, for example human synapses have been reported to exhibit a faster recovery following short-term synaptic depression [303]. Overall, the study of synapses between cortical neurons has demonstrated that their monosynaptic nature can be defined by a short latency and low temporal jitter, and that intracortical synapses between excitatory neurons typically exhibit short-term depression, high reliability and low variability [383-385, 409]. Furthermore, excitatory monosynaptic connections in rodent cortex have been shown to exhibit changes in synaptic efficacy induced by spike-timing dependent plasticity protocols [246-250].

The generation of synaptically-connected human neuronal networks via neurogenin-2 mediated differentiation, described in Chapter V, enables the further investigation of synaptic interconnectivity and the properties of excitatory synaptic connections in human iPSC-derived cortical neurons. To this end, I wanted to address the following questions within this chapter:

- Can monosynaptic connections be isolated between pairs of human iPSC-derived cortical neurons?
- What are the functional characteristics of excitatory monosynaptic connections?
- Can the optogenetic tool, ChR2, be used to study monosynaptic connections between human iPSC-derived cortical neurons?

6.2. Results

6.2.1. Reliable excitatory monosynaptic connections can be identified between pairs of iPSC-derived cortical neurons

To determine the probability of finding an excitatory monosynaptic connection in iPSC-derived cortical cultures, dual whole-cell patch clamp recordings were made from pairs of iPSC-derived cortical neurons whose somas were within 200 µm. The $GABA_A$ antagonist, picrotoxin, was included in the extracellular solution to prevent any contamination by inhibitory synaptic connections. Connectivity was primarily assessed by holding one neuron in current clamp and inducing a pair of action potentials by injecting depolarizing current, whilst holding the other neuron in voltage clamp at V_m = -70 mV to record post-synaptic responses. Dual voltage-clamp recordings were occasionally used to determine synaptic connectivity (see Chapter II). Connectivity was assessed in both directions at low frequency (0.1 Hz) to avoid the induction of any activity-dependent synaptic changes across trials. Cells that generated short-latency (≤6 ms) post-synaptic responses, which were temporally-locked to the pre-synaptic action potential were considered to be monosynaptically connected (***Figure 6.1a***). On occasions, trains of high-frequency action potential firing were elicited in the pre-synaptic neuron, which revealed short-term depression of excitatory

post-synaptic currents (***Figure 6.1b***). A total of 436 putative connections were assayed from 218 neuronal pairs, which revealed a 7 % (29/436) synaptic connection probability (***Figure 6.1c***) and showed that the majority of neuronal pairs were not connected (88 %; 191/218 pairs) (***Figure 6.1d***). Neuronal pairs that were monosynaptically connected demonstrated predominantly unidirectional connectivity (93 %; 25/27 connected pairs), whilst bidirectional connections were rare (7 %; 2/27 connected pairs). The prevalence of bidirectional connectivity (0.92 %; 2/218 pairs) was similar to the expected value if all putative connections had equal probability (0.07 x 0.07 = 0.49 %) suggesting that there was no bias towards the formation of bidirectional connections. Given the developmental increase in synaptic connectivity described for rodent cultures [405], the connection probability was compared between young (day 14-27) and old (day 28-40) cultures, which revealed a more than two-fold increase at the later time point (4 %, 8/195 for D14-27, and 10 % 25/251 for D28-40, p = 0.0273, Fisher's exact test; ***Figure 6.1e***). Overall, neuronal pairs with a monosynaptic excitatory connection were relatively infrequently detected and were predominantly unidirectional. The synaptic connection probability increased with age, and thereby increased the likelihood of detecting a synaptically connected pair in older neuronal cultures.

Having established that monosynaptically connected neuronal pairs could be identified, albeit at low frequency, I sought to characterize the properties of these connections using whole-cell and perforated patch clamp recordings. For each monosynaptic connection, a single pre-synaptic action potential was repeatedly evoked at low frequency (0.1 Hz) to generate a post-synaptic response for 10-30 trials (***Figure 6.2a***). Action potentials could be reliably evoked, and demonstrated minimal temporal jitter (0.20 ± 0.03 ms, n = 27 cells; ***Figure 6.2b***), thereby enabling consistent pre-synaptic activation across trials. The average latency was determined from across trials and measured as the time from the pre-synaptic action potential peak to 5 % of the post-synaptic response amplitude. Consistent with monosynaptic connectivity, the latencies were short (2.0 ± 0.2 ms, n = 29 connections; ***Figure 6.2c***) and showed minimal temporal jitter of the EPSC onset (0.24 ± 0.04 ms, n

= 29 connections; ***Figure 6.2d***). An average post-synaptic response was generated from 10-30 trials to determine the response amplitude and kinetics. As expected for excitatory monosynaptic connections, the kinetics of the response showed a fast 20-80 % rise time (0.95 ± 0.04 ms; ***Figure 6.2e***) and a slower 80-20 % decay time (5.53 ± 0.63 ms; ***Figure 6.2f***).

The efficacy, variability and reliability of the monosynaptic connections between human iPSC-derived cortical neurons was assessed to ascertain whether these excitatory synapses had comparable properties to intracortical synapses in rodent cortex. All post-synaptic responses (n =

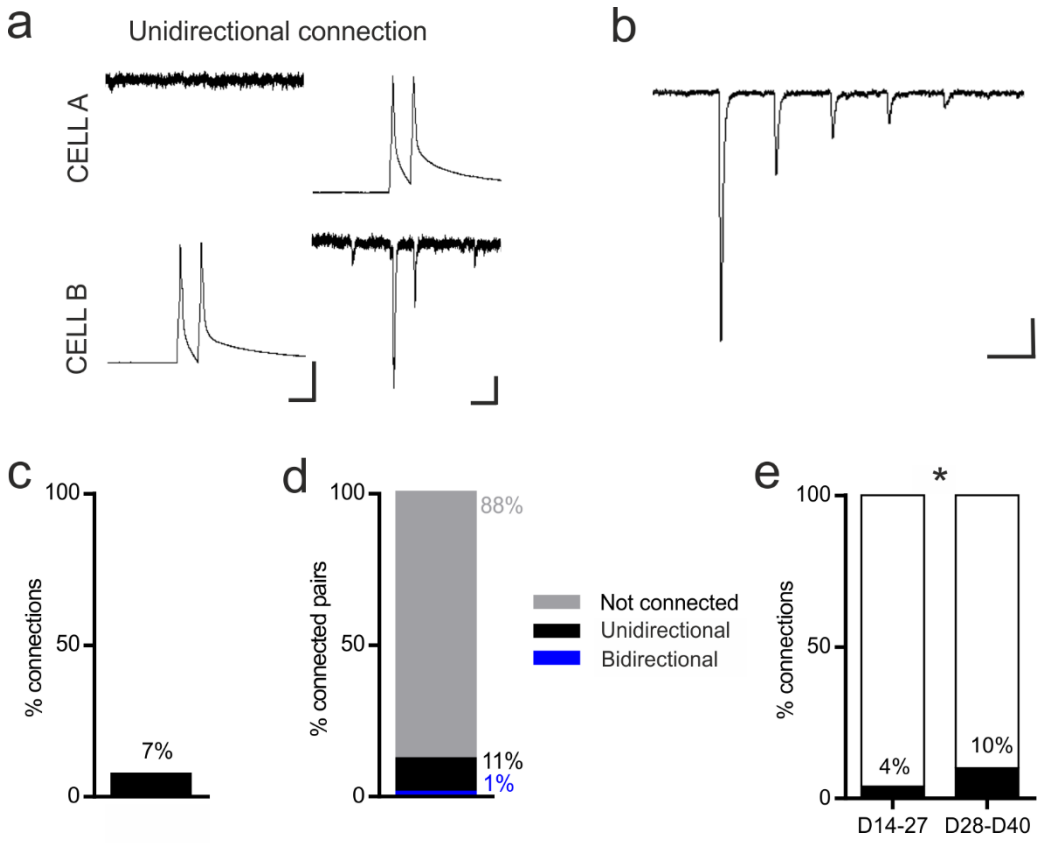

Figure 6.1. Whole-cell dual patch recordings reveal pairs of monosynaptically connected human iPSC-derived cortical neurons. (a) Example recording from a pair of neurons, whose soma were within 200 µm. When cell A was stimulated a temporally aligned post-synaptic current was observed in cell B in response to each action potential. When cell B was stimulated to fire a pair of action potentials, no response was observed in cell A, thus demonstrating a unidirectional synaptic connection. Scale bars 40 mV, 20 pA, 50 ms. **(b)** Representative average trace of post-synaptic currents exhibiting short-term depression in response to high-frequency pre-synaptic action potential firing. Scale bar 20 pA, 50 ms. **(c)** The probability of finding a synaptic connection as a proportion of all putative connections assayed (n = 436). **(d)** The proportion of bidirectional, unidirectional and unconnected neuronal pairs (n = 218). **(e)** The probability of observing a monosynaptic connection significantly increased with the age of the neuronal culture ($p = 0.0273$, n = 195 and 251 putative connections for D14-27 and D28-40, respectively, Fisher's exact test) (From 8 differentiations across 2 cell lines). * $p < 0.05$

30 connections) generated an inward current which had an average peak amplitude of 138.8 ± 30.2 pA. The histogram of response amplitudes showed that connections between human iPSC-derived cortical neurons were skewed towards smaller amplitude responses, reflected by the difference between the mean and median (IQR), which was 63.2 pA (23.9 pA to 209.9 pA) (***Figure 6.2g***). The post-synaptic response amplitude is considerably greater than the amplitude of the miniature EPSCs (mEPSCs) detected in these cultures, see Chapter VII. mEPSCs are thought to be generated by spontaneous quantal release at a single synaptic bouton, and may suggest that, like rodent cortical neurons [383-385], monosynaptic connections between human iPSC-derived cortical neurons consist of a small number of synaptic contacts. The peak amplitude could vary from trial-to-trial and had a coefficient of variation (COV) of 0.26 ± 0.02 (***Figure 6.2h***). The failure rate was determined on a trial-by-trial basis by the assessment of the response amplitude and latency. Assessment of the failure rate demonstrated that responses were reliably evoked and failures were rare (5.3 ± 1.7 %; ***Figure 6.2i***). The repetitive firing of a pre-synaptic cell can result in the short-term decrease (depression) or increase (facilitation) of the post-synaptic response amplitude, termed short-term plasticity [410]. The paired-pulse ratio (P2/P1) was assessed to determine whether the excitatory synapses undergo short-term plasticity. Pairs of pre-synaptic action potentials were evoked 40 ms apart and the post-synaptic response was averaged across 6-20 trials (***Figure 6.2j***).

Figure 6.2. Characterizing monosynaptic connections between pairs of iPSC-derived cortical neurons. *(on following page)* **(a)** An example of a dual whole-cell patch recording from a pair of monosynaptically connected neurons showing an EPSC in response to a pre-synaptic action potential (*black*: averaged traces, *grey:* individual trials; scale bar 20 pA, 10 ms). **(b)** The jitter of the presynaptic action potential in response to suprathreshold current injections from across 10-30 trials (n = 27 connections). **(c)** The EPSC latency from the action potential peak. **(d)** The jitter of the EPSC onset time. An averaged post-synaptic response was generated from 10-30 trials and the following properties were analysed: **(e)** the rise time (20-80 %), **(f)** the decay time (80-20 %), and **(g)** the amplitude of the response. Across 10-30 trials **(h)** the coefficient of variation (COV), and **(i)** the failure rate were assessed. **(j)** A representative trace of a post-synaptic response showing synaptic depression in response to two pre-synaptic action potentials stimulated 40 ms apart (*black*: averaged traces, *grey:* individual trials; scale bar 20 pA, 10 ms). **(k)** The paired-pulse ratio of post-synaptic responses (P2/P1) determined from an average of 6-20 trials (n = 27 connections). Population data are presented as frequency histograms with inset bar graphs (n = 30 connections). The response amplitude showed a significant inverse correlation with **(l)** the COV ($p = 0.0032$, $r^2 = 0.2715$) and **(m)** the failure rate ($p = 0.0499$, $r^2 = 0.1304$) (n = 30 connections, Pearson's correlation coefficient) (From 9 differentiations across 3 cell lines). * $p < 0.05$, ** $p < 0.01$

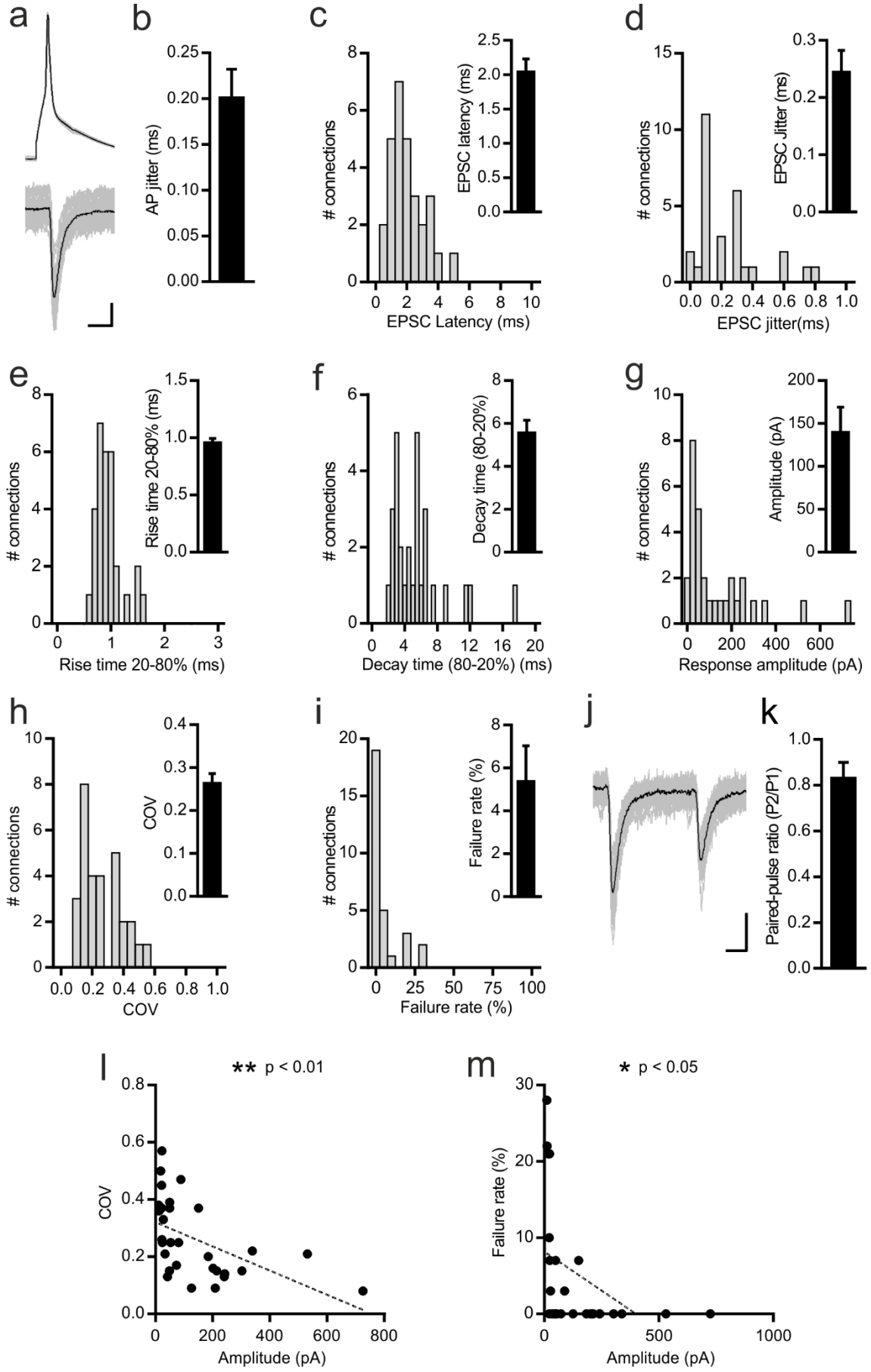
a
b
AP jitter (ms)
c
connections
EPSC Latency (ms)
EPSC latency (ms)
d
connections
EPSC jitter(ms)
EPSC Jitter (ms)
e
connections
Rise time 20-80% (ms)
Rise time 20-80% (ms)
f
connections
Decay time (80-20%) (ms)
Decay time (80-20%)
g
connections
Response amplitude (pA)
Amplitude (pA)
h
connections
COV
COV
i
connections
Failure rate (%)
Failure rate (%)
j
k
Paired-pulse ratio (P2/P1)
l
** p < 0.01
COV
Amplitude (pA)
m
* p < 0.05
Failure rate (%)
Amplitude (pA)

Overall, excitatory synaptic connections had a tendency to demonstrate short-term depression (0.83 ± 0.07, n = 27 connections, p = 0.0013, Wilcoxon signed-rank test; ***Figure 6.2k***). However, some connections exhibited an inconsistent paired-pulse ratio between trials and one connection showed robust facilitation. The response amplitude showed a significant inverse correlation with the COV (p = 0.0032, r^2 = 0.2715; ***Figure 6.2l***) and the failure rate (p = 0.0499, r^2 = 0.1304; ***Figure 6.2m***), indicating that smaller amplitude connections were more variable and more prone to failure. Overall, the characteristics of the excitatory synaptic responses generated by pairs of human iPSC-derived cortical neurons were consistent with the activation of a monosynaptic connection. The monosynaptic connections exhibited a skewed distribution of response amplitudes, a low failure rate, minimal response variability and paired-pulse synaptic depression. In general, the properties of monosynaptic connections between human iPSC-derived cortical neurons were similar to those described at excitatory synapses between neurons in the rodent cortex [383-385].

6.2.2. The optogenetic tool, ChR2, can be used to study monosynaptic connections between iPSC-derived cortical neurons

The assessment of synaptic transmission and the manipulation of synaptic efficacy requires not only the detection of a monosynaptic connection, but also the ability to maintain viable and stable patch-clamping of the pre- and post-synaptic neurons over a prolonged time period. Given that the connection probability is low in iPSC-derived cortical cultures, the evaluation of synaptic properties and the execution of physiological synaptic plasticity experiments solely using dual-patched neuronal pairs is challenging. Dual-patching only allows for the assessment of two putative connections, which can be exponentially increased by simultaneously patching additional neurons, although this would be a difficult and laborious approach. Therefore, I sought to develop another method that would enable the isolation of a monosynaptic connection at greater frequency. The expression of ChR2 in a subset of neurons enables the simultaneous activation of a larger number

of potential pre-synaptic partners in comparison to dual-patching. To this end, separate wells of iPSC-derived cortical cultures (on day 1 of neurogenin-2 expression) were transduced with lentivirus to deliver either hSyn-ChR2-YFP or CaMKIIα-mKate2, thereby ensuring that expression of these constructs was mutually exclusive. Subsequently, the two neuronal populations were pooled together during final plating onto rat astrocytes. The red fluorescent marker, mKate2, was used to facilitate the identification of neurons that did not express ChR2-YFP, as low levels of ChR2-YFP expression could not be detected by fluorescence microscopy, but could result in the generation of small photocurrents. The ChR2-YFP expressing neurons represented the putative pre-synaptic population that could be activated by light, whilst the mKate2 neurons received light-evoked synaptic inputs that were not contaminated by the generation of an endogenous photocurrent (***Figure 6.3a***). Robust endogenous expression of cytoplasmic mKate2 and membrane-localised YFP,

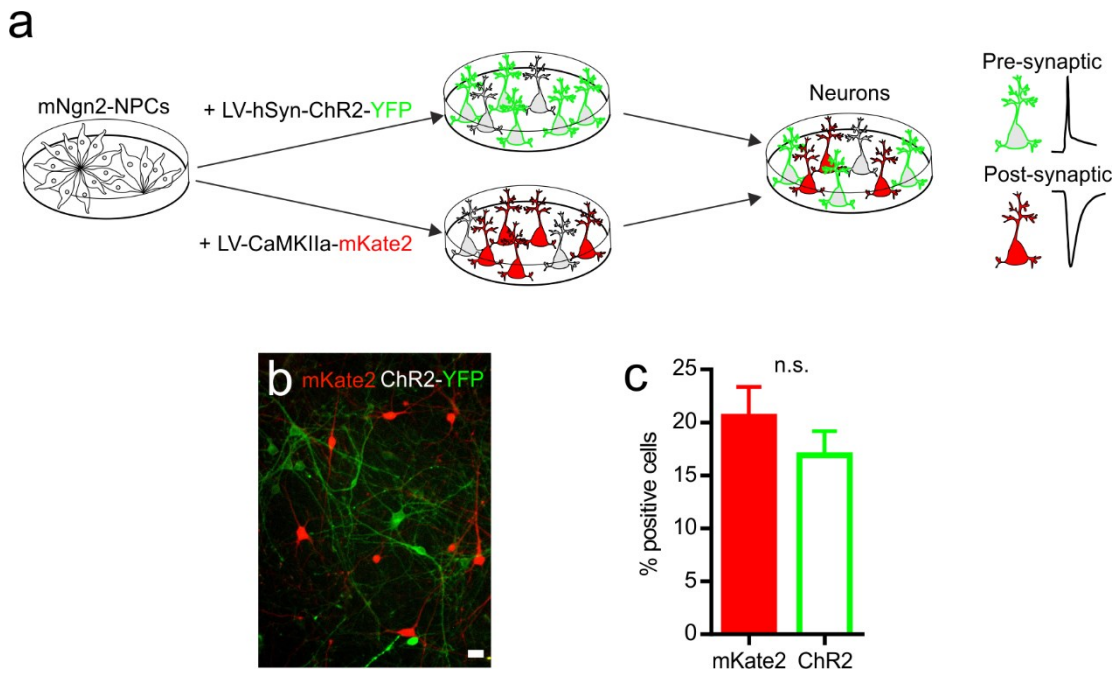

Figure 6.3. Using ChR2 as a tool to study monosynaptic connections between iPSC-derived cortical neurons. (a) Schematic of the generation of ChR2-YFP and mKate2 co-cultures. Human iPSC-derived cortical cultures (on day 1 of neurogenin-2 expression) were separately transduced with lentivirus containing either hSyn-ChR2-YFP or CaMKIIα-mKate2 on day 1 of doxycycline treatment. On day 3, cells were pooled and plated onto rat astrocytes. ChR2-YFP expressing cells represent the pre-synaptic population that can be activated by light. Whilst the mKate2-positive cells do not express ChR2 and represent the putative post-synaptic population that can receive light-activated synaptic inputs. **(b)** Representative image of a ChR2-YFP/mKate2 co-culture. Scale bar 20 µm. **(c)** The proportion of mKate2 and ChR2-YFP expressing cells are similar within each co-culture ($p = 0.1421$, $n = 21$ cultures, from 9 differentiations across 2 cell lines, paired t-test).

indicative of the incorporation of ChR2-YFP molecules into the membrane, were detected in neuronal cultures (***Figure 6.3b***). On average, 37 % of cells expressed a fluorescent marker, which was comprised of relatively equal proportions of mKate2 and ChR2-YFP expressing cells within cultures (20.5 ± 2.8 % for mKate2, and 16.9 ± 2.3 % for ChR2-YFP, n = 21 cultures, p = 0.1421, paired t-test; ***Figure 6.3c***).

To explore the utility of ChR2 as a method of activating putative pre-synaptic neurons, whole-cell patch clamp recordings were performed on ChR2-YFP expressing iPSC-derived cortical neurons (***Figure 6.4a***). Recordings in voltage-clamp demonstrated that all ChR2-YFP-positive neurons assessed could generate a photocurrent in response to light pulses delivered by a 405 nm laser. The photocurrent was sustained for the duration of the light pulse and increased in amplitude with increasing light intensity (***Figure 6.4b;*** *upper*). Similarly, current-clamp recordings revealed that increasing the light intensity generated an increased neuronal depolarization which could trigger an action potential (***Figure 6.4b;*** *lower*). Short (1-10 ms), high intensity light pulses were sufficient to evoke an action potential. However, increasing the duration from 1 to 10 ms was associated with an increase in network activity (***Figure 6.4c***). Reliable light-evoked action potential firing could be sustained at high-frequency in response to 10 Hz trains of short duration, high intensity light pulses, whereby 100 % of cells assayed fired in response to every pulse (14/14 cells; ***Figure 6.4d***). Increasing the light intensity resulted in a larger proportion of cells reaching the threshold to fire an action potential, until an action potential was triggered in all cells assayed (100 %, 24/24; ***Figure 6.4e***). The reliability of action potential firing was assessed over 10 trials at three different light intensities and light durations. The probability of action potential firing was improved by increasing either light intensity or light duration. Mid to high light intensities (8 and 50 mW/mm^2) were sufficient to evoke an action potential on every trial in response to a 10 ms duration light pulse. Moreover, high intensity (50 mW/mm^2) light pulses of only 1 ms duration could reliably trigger an action potential in the vast majority of cells (***Figure 6.4f***). On average, short 1-10ms high intensity

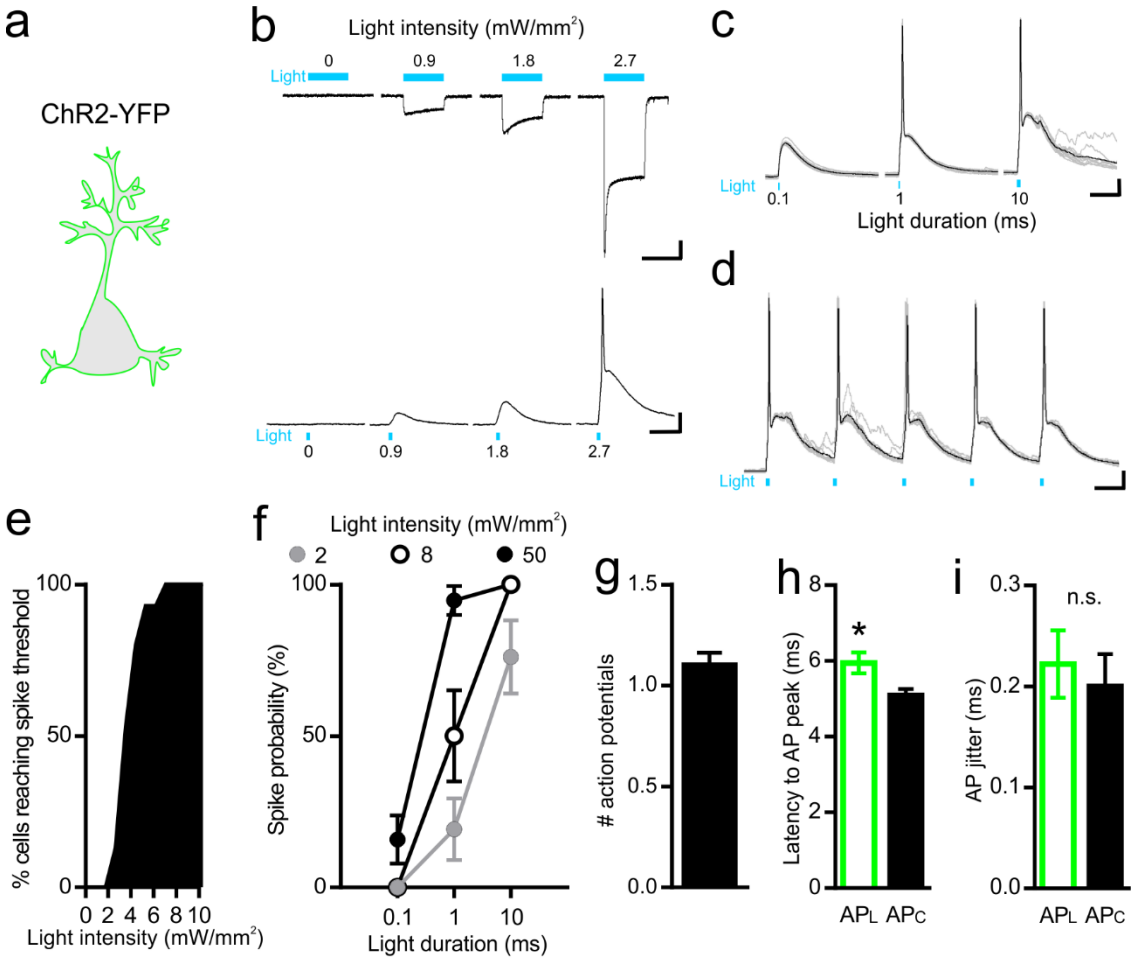

Figure 6.4. ChR2 can reliably and efficiently drive pre-synaptic action potentials in iPSC-derived cortical neurons. (a) Whole-cell patch clamp recordings were performed on ChR2-YFP expressing neurons. **(b)** Example voltage-clamp recording *(upper)* from a ChR2-YFP expressing neuron showing a photocurrent in response to 1 s light pulses delivered by a 405nm laser. The photocurrent is comprised of an initial peak and a sustained current that increase in amplitude with increasing light intensities (*upper*; scale bar 100 pA, 1 s). An example recording in current-clamp *(lower)* showing the effect of brief (10 ms) light pulses, which can trigger an action potential when the light intensity is sufficient (*lower;* scale bar 10 mV, 50 ms). **(c)** Reliable action potential firing in response to short light pulses (*black:* averaged trace, *grey:* individual trials; scale bar 10 mV, 50 ms). **(d)** Reliable light evoked action potential firing in response to 10 Hz light-stimulation *(black:* averaged trace, *grey:* individual trials; scale bar 10 mV, 50 ms). **(e)** The proportion of cells reaching spike threshold from a 10 ms light pulse of varying intensities (n = 24 cells). **(f)** The probability of spiking across 10 trials relative to light duration and intensity (n = 13, 13 and 19 cells for 2, 8, and 50 mW/mm^2, respectively). **(g)** The number of action potentials evoked by a 1-10ms light pulse (n = 19 cells). **(h)** The latency to the action potential peak from the light onset (AP_L) was ~20 % slower compared to an action potentials elicited by somatic current injection (AP_C) (p = 0.0168, unpaired t-test). **(i)** The jitter in the action potential timing was comparable between light and current-evoked action potentials (p = 0.8617, M-W test) (n = 36 and 27 cells for AP_L (from 2 differentiations of 1 cell line) and AP_C (from 9 differentiations across 3 cell lines), respectively). * $p < 0.05$

light pulses, generated a single light-evoked action-potential (AP_L) (1.1 ± 0.1, n = 19 cells, ***Figure 6.4g***) with a latency to peak that was ~20 % slower than action-potentials that were evoked by somatic current injection (AP_C) (5.9 ± 0.3 ms, n = 36 cells for AP_L, and for 5.1 ± 0.2 ms, n = 27 cells for AP_C, p = 0.0168, unpaired t-test; ***Figure 6.4h***). However, the temporal jitter was comparable between light and current-evoked action potentials (0.22 ± 0.03 ms, n = 36 cells for AP_L, and for 0.20 ± 0.03 ms, n = 27 cells for AP_C p = 0.8617, M-W test; ***Figure 6.4i***). Collectively, the activation of ChR2 with high intensity, short-duration light pulses could reliably generate single action potentials with high temporal precision in all neurons tested. This indicated that ChR2 could provide an alternative strategy to control the activity of pre-synaptic iPSC-derived cortical neurons, and was largely comparable to whole-cell patch clamping.

Having established that ChR2 could be used to reliably activate pre-synaptic neurons, I explored whether light-evoked monosynaptic responses could be detected in the co-cultured ChR2-negative neurons. To this end, whole-cell and perforated patch clamp recordings were performed on ChR2-negative neurons, predominantly those expressing mKate2. Short-light pulses were able to evoke excitatory post-synaptic currents ($EPSC_L$; *blue*) with a short latency and kinetic properties that were qualitatively comparable to those generated within a pair of dual-patched connected neurons ($EPSC_P$; *black*) (***Figure 6.5a***). Light-evoked responses that had frequent failures, long-latencies and high temporal jitter were also observed. These responses were assumed to be poly-synaptic in origin and therefore excluded from further analysis. The proportion of cells that received a monosynaptic $EPSC_L$ was three-fold greater than those receiving an $EPSC_P$ (34 %, 33/98 cells for $EPSC_L$, and 10 %, 23/231 cells for $EPSC_P$, p < 0.001, Fisher's exact test; ***Figure 6.5b***). The properties of $EPSC_L$ responses (n = 49 cells) in response to a single light-pulse, were assessed and compared to $EPSC_P$ responses (n = 29-30 cells). The latency from time 0 (t0) denotes the time of light-onset for

---

Figure 6.5. *(cont. from following page)* responses to pre-synaptic stimuli delivered 40 ms apart. Scale bar 10 ms. **(k)** The average paired-pulse ratio was lower for $EPSC_L$ (n = 31 cells) compared to $EPSC_P$ (n = 27 cells) (p = 0.0063, unpaired t-test). (n = 49 and 30 cells for $EPSC_L$ and $EPSC_P$, respectively) (From 11 differentiations across 3 cell lines). * p < 0.05, ** p < 0.01, *** p < 0.001

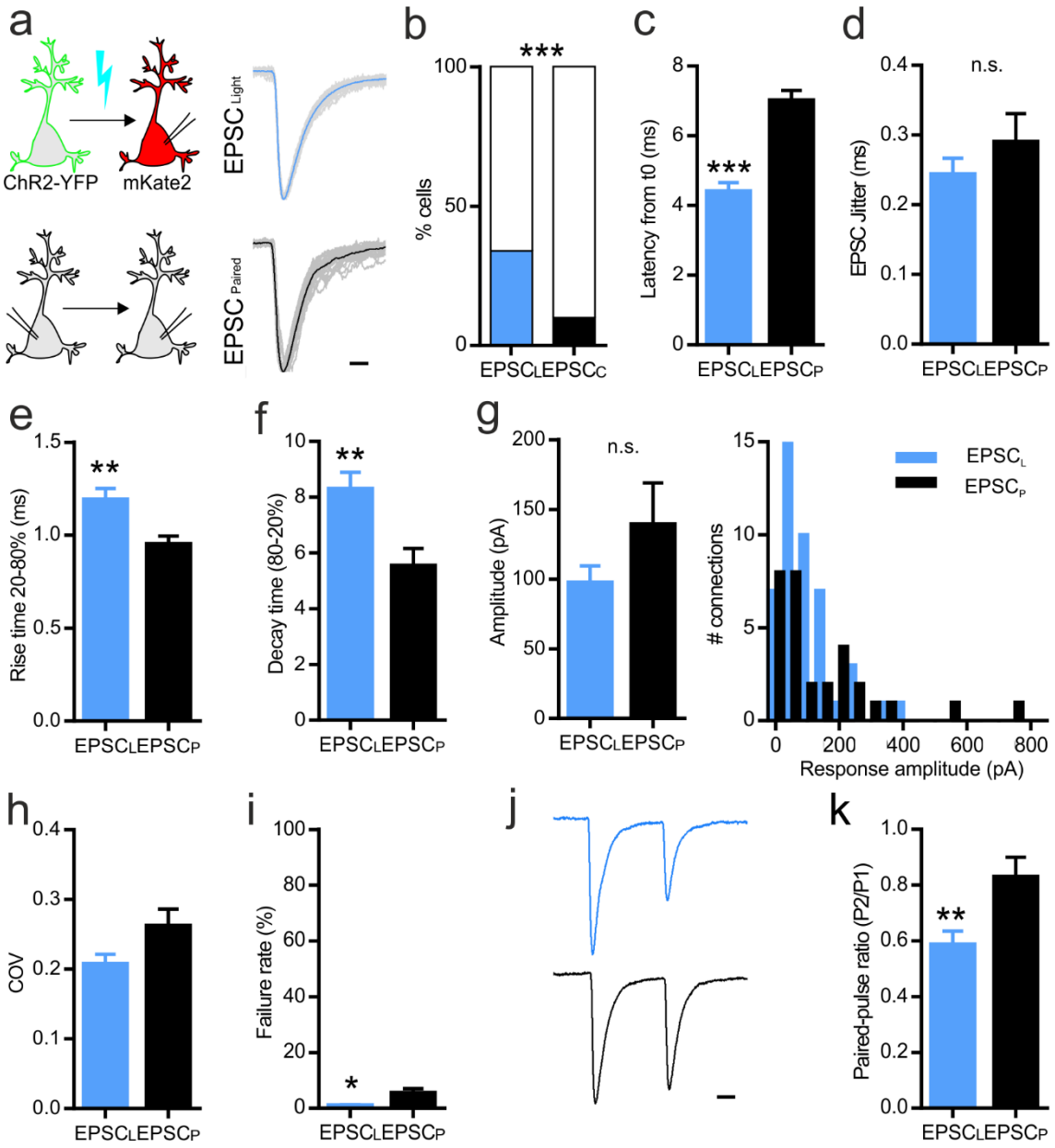

Figure 6.5. Light-evoked monosynaptic responses offer advantages for studying monosynaptic connections. (a) Whole-cell patch clamp recordings were made from ChR2-YFP-negative neurons, which were typically mKate2-positive neurons (*left*). Scaled representative traces of a monosynaptic EPSC evoked by short, single 0.1-10 ms light pulses ($EPSC_{Light}$; *upper right - blue*) and an EPSC evoked by electrically activating a monosynaptically connected pre-synaptic neuron ($EPSC_{Paired}$; *lower right - black*). Scale bar 10 ms. **(b)** The proportion of cells that exhibited a monosynaptic $EPSC_L$ (n = 98 cells) was significantly higher than those showing an $EPSC_P$ (n = 231 cells) ($p < 0.0001$, Fisher's exact test). **(c)** The EPSC latency from light onset or current injection onset, denoted as time 0 (t0), shows that the EPSC latency was significantly shorter for $EPSC_L$ compared to $EPSC_P$ ($p < 0.001$, M-W test), whilst **(d)** the jitter in the timing of the EPSC showed no difference ($p = 0.6358$, M-W test). Averaged recordings showed that **(e)** the rise time (20-80 %) was significantly longer ($p = 0.0029$, M-W test), and **(f)** the decay time (80-20 %) was significantly longer ($p = 0.0019$, M-W test), whilst **(g)** the response amplitude (bar graph; *left* and frequency histogram; *right*) showed no difference ($p = 0.8213$, M-W test). Analyses from across trials showed that **(h)** the coefficient of variation did not significantly differ ($p = 0.0949$, M-W test), and **(i)** the failure rate was significantly lower ($p = 0.0110$, M-W test). **(j)** Scaled representative traces of paired-pulse post-synaptic *(cont. on previous page)*

$EPSC_L$ responses, and the time of pre-synaptic current injection for $EPSC_P$ responses. As described in ***Figure 6.4h***, light-evoked action potential firing was slightly slower than current-evoked action potential firing, and therefore it was anticipated that the onset latency for $EPSC_L$ would be longer than for $EPSC_P$. Unexpectedly, the latency was significantly shorter (4.39 ± 0.26 ms for $EPSC_L$, and 7.00 ± 0.30 ms for $EPSC_P$, $p < 0.001$, M-W test; ***Figure 6.5c***). However, the temporal reliability of $EPSC_L$ was indistinguishable from $EPSC_P$, as demonstrated by the EPSC jitter (0.24 ± 0.02 ms for $EPSC_L$ and 0.29 ± 0.04 ms for $EPSC_P$, $p = 0.6358$, M-W test; ***Figure 6.5d***). $EPSC_L$ responses had a fast rise phase and a slower decay phase although, in contrast to $EPSC_P$, these were significantly longer by a small degree (rise time 20-80%: 1.19 ± 0.06 ms for $EPSC_L$ and 0.95 ± 0.04 ms for $EPSC_P$, $p = 0.0029$, M-W test; ***Figure 6.5e***, decay time 80-20%: 8.28 ± 0.62 ms for $EPSC_L$ and 5.53 ± 0.63 ms for $EPSC_P$, $p = 0.0019$, M-W test; ***Figure 6.5f***). Meanwhile, there was no difference in the average amplitude of the post-synaptic responses (97.15 ± 12.24 pA for $EPSC_L$ and 138.8 ± 30.35 pA for $EPSC_P$, $p = 0.8213$, M-W test; ***Figure 6.5g***; *left*), and like $EPSC_P$, smaller $EPSC_L$ response amplitudes were more common (***Figure 6.5g***; *right*). Whilst the variability of $EPSC_L$ responses was comparable to $EPSC_P$, reflected by the COV (0.21 ± 0.01 for $EPSC_L$ and 0.26 ± 0.02 for $EPSC_P$, $p = 0.0949$, M-W test; ***Figure 6.5h***), the reliability of $EPSC_L$ responses was significantly greater, indicated by a decreased failure rate (0.88 ± 0.38 % for $EPSC_L$ and 5.53 ± 0.63 % for $EPSC_P$, $p = 0.0110$, M-W test; ***Figure 6.5i***). Similar to $EPSC_P$, paired-pulse stimulation of $EPSC_L$ also resulted in short-term depression (***Figure 6.5j***). However, the paired-pulse ratio was significantly lower, indicating a greater extent of depression

Property	$EPSC_{Light}$		$EPSC_{Paired}$			
	mean ± SEM	n (cells)	mean ± SEM	n (cells)	*p* value	Direction of change
% cells with EPSC	34 %	33/98	10 %	23/231	< 0.001***	↑
Paired-pulse ratio (P2/P1)	0.59 ± 0.05	31	0.83 ± 0.07	27	0.0063**	↓
Amplitude (pA)	97.15 ± 12.24	49	138.80 ± 30.15	30	0.8213	↔
Rise time 20-80 % (ms)	1.19 ± 0.06	49	0.95 ± 0.04	30	0.0029**	↑
Decay time 80-20 % (ms)	8.28 ± 0.62	49	5.53 ± 0.63	29	0.0019**	↑
COV	0.21 ± 0.01	49	0.26 ± 0.02	30	0.0949	↓
Failure rate (%)	0.88 ± 0.38	49	5.33 ± 1.70	30	0.0110**	↓
Latency from t0 (ms)	4.39 ± 0.26	49	7.00 ± 0.30	30	< 0.001***	↓
EPSC jitter (ms)	0.24 ± 0.02	49	0.29 ± 0.04	30	0.6358	↔

Table 6.1. Summary table of the properties of $EPSC_{Light}$ and $EPSC_{Paired}$ responses. * $p < 0.05$, ** $p < 0.01$, *** $p < 0.001$

for $EPSC_L$, in comparison to $EPSC_P$ (0.59 ± 0.05, n = 31 cells for $EPSC_L$, and 0.83 ± 0.07, n = 27 cells for $EPSC_P$, p = 0.0063, unpaired t-test; ***Figure 6.5k***). The properties of $EPSC_L$ and $EPSC_P$ are summarised in ***Table 6.1***. The enhancement of paired-pulse depression in $EPSC_L$ is indicative of an increase in the probability of neurotransmitter release [411], which is further supported by the increased reliability of transmission. Overall, the expression of ChR2 in a subset of cells within iPSC-derived cortical cultures could enable the detection of a monosynaptic response in one-third of cells assayed. In combination with dual-patching, this approach allowed for the study of excitatory monosynaptic responses in almost 50 % of all cells patched, thereby making population studies more achievable.

6.2.3. iPSC-derived cortical neurons express functional synaptic AMPA and NMDA receptors

Induction of STDP at glutamatergic cortical synapses requires synaptic activation of NMDA-receptors [236, 248, 250]. Having developed methods to enable the study of monosynaptic synapses, I set out to investigate whether these connections possessed the functional synaptic machinery required for the generation of glutamatergic synaptic plasticity. Monosynaptic $EPSC_P$ (*black*) and $EPSC_L$ (*blue*) were assessed in voltage-clamp to detect AMPA and NMDA-receptor mediated currents. At Vm = -70 mV post-synaptic responses had a fast-onset and fast-decay that were predominantly generated by AMPA-receptors, as NMDA-receptors are largely inhibited by the voltage-dependent Mg^{2+} block at this membrane potential [412]. Wash-in of the NMDA-receptor antagonist, DL-AP5, had minimal effect on the response at Vm = -70 mV, whereas application of the AMPA-receptor antagonist, CNQX, completely abolished the response. Depolarization of the membrane potential to Vm = +60 mV relieved the NMDA-receptor Mg^{2+} block and generated an outward current with a fast-onset and slow-decay, suggestive of a compound response formed of AMPA and NMDA-receptor mediated currents. Wash-in of DL-AP5 removed the slow-component, leaving the fast AMPA-only component, which could be abolished by the addition of CNQX (***Figure 6.6a***). Pharmacology was performed only on a small subset of monosynaptic responses to confirm

the presence and kinetics of the AMPA and NMDA-receptor mediated components. Subsequently, the AMPA-receptor current (I_{AMPA}) component was defined as the peak inward current at -70 mV, whilst the NMDA-receptor current (I_{NMDA}) was taken as the peak outward current at +60 mV occurring at ≥ 20 ms, whereby the majority of the AMPA component had largely decayed and contributed ≤ 5 %. The majority of monosynaptic connections had both AMPA and NMDA-receptor mediated currents (89 %, 17/19; ***Figure 6.6b***), although two connections were found to have negligible I_{NMDA} (≤ 7 pA) and were excluded from further analysis. AMPA and NMDA currents were each adjusted for the driving force to determine the peak conductance (*g*), before the calculation

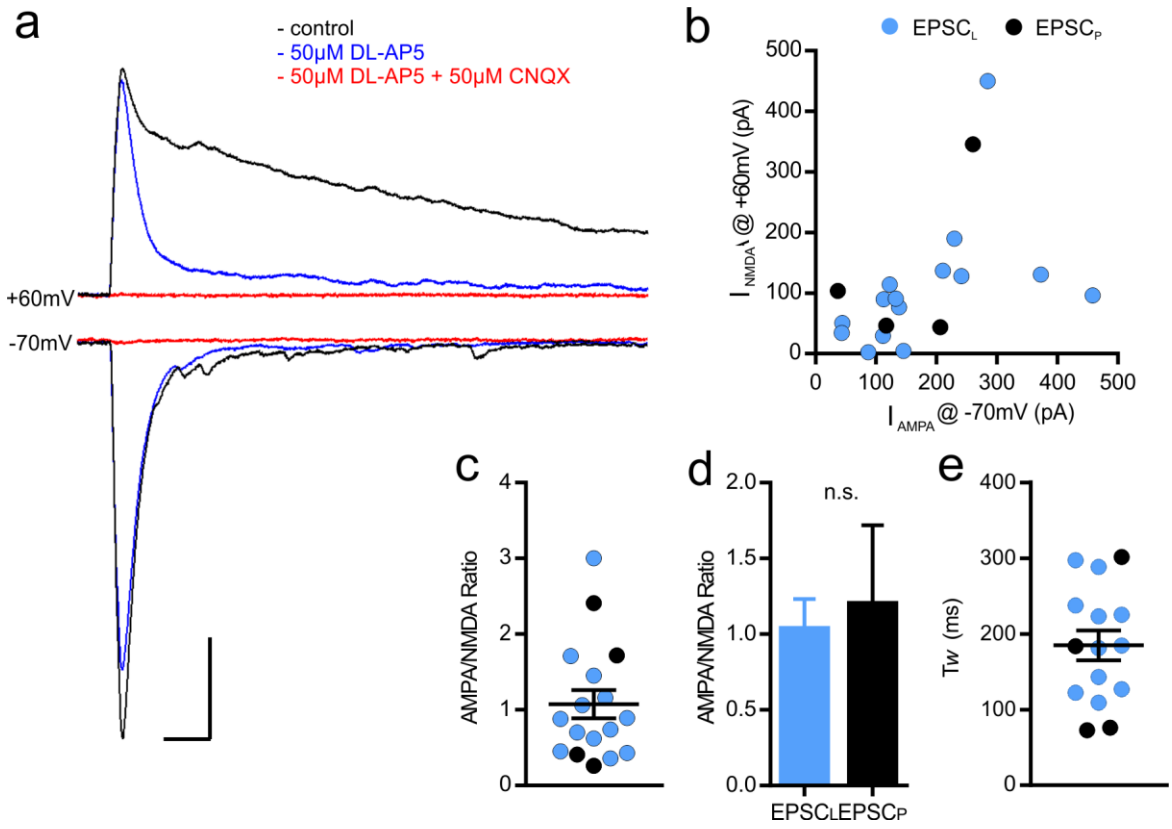

Figure 6.6. Human iPSC-derived cortical neurons express functional synaptic AMPA and NMDA receptors. (a) Example recording of an $EPSC_L$ averaged across 20 trials per condition. Recording at V_m = -70 mV shows an AMPA-receptor only mediated response abolished by the AMPA antagonist CNQX. At V_m = +60 mV the slower kinetic NMDA-receptor component is evident and can be blocked by the antagonist DL-AP5. Scale bar 100 pA, 20 ms. **(b)** The relationship between AMPA and NMDA-receptor mediated currents for individual cells recorded as either light-evoked post-synaptic responses ($EPSC_L$*; blue*) or electrically-evoked post-synaptic responses ($EPSC_P$*; black*) (n = 19 connections). **(c)** The AMPA/NMDA ratio of peak conductance determined for cells that had detectable AMPA and NMDA-receptor mediated currents (n = 17 connections). **(d)** The average AMPA/NMDA ratio was comparable for $EPSC_L$ (n = 13 connections) and $EPSC_P$ (n = 4 connections) (p = 0.9563, M-W test). **(e)** The weighted time constant (τw) determined by an exponential fit to the decay of the NMDA-receptor mediated current component (n = 14 connections). (From 4 differentiations across 2 cell lines)

of the AMPA/NMDA ratio, which was 1.07 ± 0.19 (n = 17 connections; ***Figure 6.6c***). This demonstrates that the peak AMPA and NMDA-receptor mediated conductance is equal during glutamatergic synaptic transmission at V_m = + 60 mV in iPSC-derived cortical cultures. The AMPA/NMDA ratio did not differ significantly between $EPSC_L$ and $EPSC_P$ responses (1.04 ± 0.20, n = 13 connections for $EPSC_L$, and 1.20 ± 0.52 n = 4 connections for $EPSC_P$, p = 0.9563, test; ***Figure 6.6d***). NMDA-receptors in the cortex are predominantly comprised of the NR1 subunit in combination with NR2A and NR2B subunits. NMDA-receptors undergo developmental changes in receptor subunit composition, whereby the NR2B subunit is highly expressed during development, but NR2A is most prevalent in the adult [413, 414]. The NMDA receptor subunit composition affects the kinetics of the NMDA-receptor mediated current, whereby receptors containing NR2A subunits mediate a current with a 5-fold faster decay (≈ 50ms) than those containing NR2B subunits (≈ 300ms) [415]. To gain insight into the likely subunit composition of the synaptic NMDA-receptors an exponential fit was applied to the NMDA-receptor mediated current component, which revealed an average weighted decay time constant (τw) of 184.8 ± 19.8 ms (n = 14 connections) (***Figure 6.6e***). This duration of decay suggests that the glutamatergic synapses contain NMDA-receptors largely comprised of NR2B subunits. Collectively, these results demonstrate that the majority of synapses have functional AMPA and NMDA-receptors and therefore possess the synaptic receptors required for the induction of LTP. The AMPA/NMDA ratio for $EPSC_L$ and $EPSC_P$ was comparable, indicating that these methods of pre-synaptic neuronal stimulation activate synapses with equivalent glutamatergic receptor properties.

6.3. Discussion

Having previously developed the NPC-mNgn2 neuronal differentiation protocol that significantly enhanced excitatory synaptic activity (see Chapter V), I sought to determine the monosynaptic connection probability and further characterize the properties of excitatory synapses. Dual whole-cell patch clamping experiments demonstrated predominantly unidirectional monosynaptic connections that were detected at a low frequency, which was increased by culture age. The monosynaptic connections were very reliable, had a short latency, low variability and exhibited paired-pulse depression. The optogenetic tool, ChR2, was recruited with the aim of enhancing the frequency of detecting monosynaptic responses. The expression of ChR2-YFP enabled temporally precise and reliable light-evoked action potential firing in iPSC-derived cortical neurons. As a result, light-evoked monosynaptic responses could be observed in ChR2-negative neurons that were co-cultured with hSyn-ChR2-YFP neurons. Whilst the overall characteristics of $EPSC_L$ were very similar to $EPSC_P$ responses, the pre-synaptic activation of ChR2 resulted in the following changes to the properties of the monosynaptic response: $EPSC_L$ responses exhibited a greater degree of paired-pulse depression, marginally slower kinetics, increased reliability, and the detection of light-evoked responses was three-fold more frequent than responses evoked by pre-synaptic somatic current injection in neuronal pairs. In combination, these approaches enabled the study of monosynaptic responses in almost half of the cells assayed. Further analysis of monosynaptic responses showed that 89 % of cells had functional synaptic AMPA and NMDA-receptors. Calculation of the AMPA/NMDA ratio demonstrated a relatively equal AMPA and NMDA-receptor conductance during glutamatergic synaptic transmission at V_m = +60 mV. Moreover, the AMPA/NMDA ratio was comparable between $EPSC_L$ and $EPSC_P$ responses.

6.3.1. The properties of excitatory synaptic connections

The level of connectivity that was demonstrated by the iPSC-derived cortical cultures was within the physiological range previously reported between cortical neurons in the rodent cortex [248,

385, 392-395]. Furthermore, the age-dependent increase in connection probability was consistent with the increased connectivity observed in developing rodent cortical neurons [405]. In human development the process of synaptogenesis gradually increases the number of synapses, whilst the total number of neurons remains relatively stable, and thereby increases interconnectivity. Synaptic density peaks postnatally at approximately 12 months, before subsequently declining through synaptic pruning and refinement [416, 417]. It is uncertain whether the iPSC-derived cortical cultures used had reached peak connectivity, but to avoid extensive culture periods, older cultures were not tested. However, it would be interesting to explore whether manipulation of the cell density may increase the connection probability within this time period [362].

The extent of bidirectional connectivity was similar to that expected if the connection probability was uniform across synapses and independent of direction. However, studies in rodent cortex have demonstrated that bidirectional connections occur at greater than expected probabilities [383, 385, 397]. This may suggest that the human iPSC-derived neuronal networks demonstrate a more random local connectivity pattern than that observed in rodent cortex [397], alternatively, it could be a reflection of the developmental stage [396]. High-levels of bidirectional connectivity have been reported in very low-density rodent neuronal cultures, which may have been induced by the artificial conditions [236]. In rodent cortical slices, bidirectional connections are common within layers, but are rarely observed between layers [383-385]. It is uncertain whether such patterns of inter- and intra-laminar connectivity are preserved in culture where cortical neurons from all layers are randomly dispersed, although there is evidence from rodent studies which suggests that preferential synapse formation, consistent with *in vivo* circuitry, can occur in culture to some extent [418].

The properties and kinetics of human excitatory synapses between iPSC-derived cortical neuronal pairs was found to be very similar to those reported between excitatory neurons in rodent cortex [383-385, 419]. The iPSC-derived cortical neurons exhibited reliable pre-synaptic neuronal

activation, which enabled consistent low frequency synaptic stimulation across trials. The short latency and minimal jitter are strongly indicative that the synaptic connections observed here were monosynaptic in nature, in contrast to polysynaptic connections, which have a longer delay, greater onset jitter, higher variability and are more prone to failure [383]. In general, rodent connectivity studies, which are performed in cortical slice preparations, assess the properties of excitatory post-synaptic potentials measured in current-clamp, whereby the equivalent current response would be dependent upon the neuronal membrane resistance as defined by Ohm's Law. The positively skewed EPSC amplitudes observed here, whilst not directly comparable, are in line with these studies, which report that small post-synaptic responses are more prevalent than larger amplitude potentials [383, 385]. The median response amplitude was relatively small, and when compared to the mEPSC amplitude, is indicative of a small number of synaptic contacts. This is in line with the number of synapses that have been estimated to occur between rodent cortical neurons [383-385]. The small number of connections with large post-synaptic response amplitudes indicates that some neurons in iPSC-derived cortical cultures are strongly connected. Overall, the EPSC amplitudes were consistent with those reported for synapses between excitatory neurons in human cortical slice preparations [408], and also for excitatory monosynaptic connections in dissociated rodent hippocampal cultures [236, 406]. The excitatory monosynaptic connections between human iPSC-derived cortical neurons exhibited short-term paired-pulse depression similar to that observed at rodent cortical synapses [384, 385, 419]. Furthermore, this supports studies in human excised tissue which suggest that short-term depression is a feature shared by both human and rodent excitatory cortical synapses [303]. The human cortical synapses also displayed low variability and high reliability, reflected by the COV and failure rate, respectively, that were within the range reported for rodent cortical synapses [383-385]. The inverse correlation that was observed between the EPSC amplitude and the COV, or the failure rate, has consistently been observed for intra-cortical synapses in rodent cortex [383-385]. This has largely been explained by a simple binomial model of synaptic transmission, whereby the pre-synaptic neurotransmitter release probability is the main

determinant of the EPSC amplitude, although this model commonly excludes a small proportion of monosynaptic connections that have large amplitudes [383-385]. The temperature maintained during recording can influence the response variability, reliability and the kinetic properties of synaptic transmission to a small degree, and therefore must be considered when making direct comparisons between studies [383, 420]. However, the temperature maintained during the recording of connections between human iPSC-derived cortical neurons in these experiments (30^{o}C) was similar to that used in rodent studies (21 – 37^{o}C) [383-385]. Taken together, these data suggest that the properties of excitatory synaptic connections between human iPSC-derived cortical neurons are very similar to those in rodent cortex.

6.3.2. Optogenetic interrogation of excitatory synaptic connectivity

The expression of ChR2 was used to increase the probability of isolating a monosynaptic connection in human iPSC-derived cortical cultures. ChR2 and similar variants have frequently been used to control neuronal electrical activity and generate light-evoked post-synaptic responses in rodent models [192]. More recently, this strategy has also been applied to human stem cell-derived neuronal cultures [158, 270, 421, 422]. In this chapter, the expression of hSyn-ChR2-YFP in iPSC-derived cortical neurons enabled reliable and temporally precise light-evoked action potential firing in response to short duration, high intensity light pulses. The selective targeting of CaMKIIα-mKate2 neurons that were co-cultured with hSyn-ChR2-YFP neurons facilitated the detection of light-evoked monosynaptic responses, which occurred at a greater frequency than achieved by dual-patching. Approximately 20 % of neurons visibly expressed ChR2-YFP, but this is likely to be an underestimate, as subsets of neurons with no detectable YFP fluorescence were found to elicit small photocurrents. Increasing the proportion of cells with ChR2-YFP expression could increase the probability of $EPSC_L$ detection, but is also likely to increase light-evoked polysynaptic activity as a greater proportion of neurons would be activated. This effect could be counteracted by illuminating a smaller area, although this may require higher expression levels of ChR2 in the cells to ensure

action-potential threshold is reached, as activation of a smaller area of neuronal membrane will generate reduced photocurrents.

The thorough characterization of light-evoked monosynaptic response properties in iPSC-derived cortical neurons, and their comparison to those evoked by pre-synaptic current injection, highlighted a number of differences. However, these differences are consistent with those described for ChR2-mediated light-evoked responses at mature rodent synapses [201, 423]. For example, the shorter than predicted latency of the $EPSC_L$ has previously been observed [201], and may suggest that the absence of a whole-cell patch on ChR2-YFP-positive neurons results in a quicker neuronal depolarization to action-potential threshold, or alternatively that the $EPSC_L$ was not generated by a somatic action potential. Evidence for the axonal generation of action potentials have been described in studies using ChR2 to evoke synaptic transmission [201, 388, 423]. Nonetheless, pre-synaptic activation was temporally reliable across trials, reflected by the minimal jitter, which was comparable to $EPSC_P$ responses.

Previous studies in rodents have also demonstrated the enhancement of short-term depression in ChR2-evoked synaptic responses [201, 423, 424]. This has been shown to: 1) be affected by the method used for transgene expression, 2) demonstrate variability between synaptic pathways, and 3) be dependent upon the location of light-stimulation [423]. Commonly, these studies have stimulated large proportions of cells or axonal bundles [423, 424], and therefore this observation could be due to failures in pre-synaptic action potential firing, which has been demonstrated for the ChR2 (H134R) variant used here [425]. However, ChR2-YFP expressing human iPSC-derived cortical neurons demonstrated robust and reliable light-evoked pre-synaptic action potential firing at high frequency, and $EPSC_L$ responses had very low failure rates, thereby suggesting that failures of pre-synaptic action potential firing were unlikely. It is also probable that the majority of $EPSC_L$ responses observed were generated by a single pre-synaptic cell, not the summation of multiple inputs, considering the following: 1) only a small area was exposed to light-stimulation, 2) only ~30

% cells generated $EPSC_L$ responses, and 3) the amplitude of $EPSC_L$ and $EPSC_P$ responses were comparable. Alternatively, the enhanced paired-pulse depression has been suggested to arise from an increased release probability [201, 423], as a result of enhanced Ca^{2+} influx via the ChR2-mediated activation of voltage-gated calcium channels [201]. An increased release probability would also account for the reduction in failures that was observed for $EPSC_L$ responses, relative to $EPSC_P$. The difference in rise time, albeit significant, was just a fraction of a millisecond, and therefore it is uncertain whether this would have any physiological implications. It is possible that the pre-synaptic currents activated by ChR2, or the possible lack of a somatic action potential, could have caused subtle alterations in the kinetics of neurotransmitter release, although such effects have not been reported by others. Alternatively, this could indicate that light stimulation of ChR2 has a tendency to activate more distal synaptic inputs [249, 389]. The longer decay time could have been caused by ChR2-evoked polysynaptic activity, which was rarely observed for $EPSC_C$, consistent with the suprathreshold stimulation of a single neuron, but more common for $EPSC_L$, whereby multiple putative pre-synaptic neurons were simultaneously activated by light. Although $EPSC_L$ responses with large spontaneous current responses occurring during the decay phase were excluded, many $EPSC_L$ responses demonstrated multiple, small poly-synaptic currents that would have slowed neuronal repolarization.

Overall, these observations suggest that the majority of $EPSC_L$ responses are likely to be generated by the light activation of a single pre-synaptic cell, and that the differences between $EPSC_L$ and $EPSC_P$ responses are probably caused by changes in the pre-synaptic neurotransmitter release probability. Nonetheless, rodent studies have demonstrated robust LTP of light-evoked responses [200, 201], suggesting that pre-synaptic ChR2 activation does not impact the induction of glutamatergic synaptic plasticity. Therefore, the expression of ChR2 in a subset of iPSC-derived cortical neurons may provide a reliable and efficient method to evoke monosynaptic responses for the study of synaptic plasticity.

6.3.3. The functional assessment of AMPA and NMDA glutamatergic synaptic receptors

The assessment of the AMPA/NMDA ratio at monosynaptic $EPSC_P$ and $EPSC_L$ revealed the presence of AMPA and NMDA-mediated current components in the majority of human iPSC-derived cortical neurons, and thereby demonstrated the expression of functional synaptic AMPA and NMDA-receptors. Whilst AMPA-mediated synaptic activity has been reported by numerous studies utilising human stem cell-derived neurons, the demonstration of robust and functional NMDA receptor expression has not been evident. Studies exploring NMDA receptor function in human iPSC-derived neurons have predominantly used the exogenous application of glutamate or NMDA to evoke currents [162, 270-275]. NMDA-receptor responses evoked by this method confirm the presence of functional surface NMDA-receptors, but cannot demonstrate synaptic localisation and function. For example, some studies have presented evidence that glutamatergic synaptic transmission is purely AMPA-receptor mediated, despite the presence of exogenously evoked NMDA-receptor currents [270, 275]. This is not surprising as non-synaptic functional AMPA and NMDA receptors can be expressed on the surface of neural progenitor cells and new-born neurons [426, 427]. Others have demonstrated NMDA-receptor contribution to spontaneous [274] and evoked synaptic currents [158, 162] in human iPSC-derived neurons. However, the NMDA-receptor mediated synaptic currents, which were evoked by extracellular electrical stimulation were small, despite the likely activation of multiple pre-synaptic neurons. In contrast, I have demonstrated that 89 % of excitatory monosynaptic connections between human iPSC-derived cortical neurons have functional synaptic NMDA-receptors and can exhibit large NMDA-receptor mediated synaptic currents.

The induction of post-synaptic potentiation at excitatory glutamatergic cortical synapses is an NMDA-receptor dependent process [200, 236, 248]. Therefore, the functional NMDA-receptor responses observed in human iPSC-derived cortical neurons indicate that the vast majority of excitatory connections possess the synaptic machinery required for LTP induction. Furthermore,

the comparable AMPA/NMDA ratio observed between $EPSC_L$ and $EPSC_P$ indicates that the pre-synaptic expression of ChR2 does not impact the post-synaptic expression of glutamatergic receptors. The presence of a small proportion (11 %) of synapses that exhibited AMPA-receptor only mediated synaptic responses is consistent with observations in developing rodent neuronal cultures, which have found subsets of synapses solely comprised of AMPA-receptors [428, 429]. The AMPA/NMDA ratio has been shown to increase with developmental age and reflects the maturation of glutamatergic synapses [430, 431]. The range of AMPA/NMDA ratios across synaptic connections suggests a varying degree of synapse maturation in human iPSC-derived neuronal cultures. This is further supported by the NMDA-receptor current decay time constant, which is indicative of a largely NR2B subunit composition and is consistent with glutamatergic receptor subunit expression patterns observed at relatively early stages of cortical development in rodents [413]. Similar findings have been reported by Zhang et al., (2016) who functionally demonstrated a primarily NR2B subunit composition in human iPSC-derived cortical neurons that were exposed to a brief application of NMDA. The predominance of NR2B subunits was inferred by the NMDA current response kinetics and confirmed pharmacologically. To further confirm the functional NMDA-receptor subunit composition of the human iPSC-derived cortical neurons generated in this thesis, similar experiments could be performed utilising the NR2A and NR2B-subunit specific antagonists NVP-AAM077, and Ro 25-6981 or ifenprodil, respectively. Assessment of the NMDA-receptor mediated current decay described in this chapter is likely to have been minimally influenced by the AMPA-receptor mediated current, which has a fast decay. Nonetheless, further functional assessment of NMDA-receptor mediated currents should be performed in the presence of AMPA-receptor antagonists to eliminate any influence of AMPA-receptor activation on the EPSC.

In summary, monosynaptic connections were detected at low frequency between pairs of iPSC-derived cortical neurons. The expression of ChR2 in a subset of neurons enabled the reliable light-evoked generation of monosynaptic responses at a frequency three-fold higher than that achieved

by dual-patching. Post-synaptic responses generated by either pre-synaptic somatic current injection or light activation demonstrated high reliability, low variability and the robust expression of functional synaptic AMPA and NMDA receptors in the majority of cases. Together, these approaches have enabled the exploration of synaptic plasticity in human iPSC-derived cortical neurons, which is described in the following chapter.

VII: Assaying glutamatergic synaptic plasticity in iPSC-derived cortical networks

7.1. Introduction

To date, there have been a small number of studies reporting LTP-like changes in human iPSC-derived neurons [266, 267, 269]. Kirwan et al., (2015) [269] assessed changes in the calcium transients generated by cortical neuronal cultures following a chemical LTP (cLTP) induction, which consisted of a 5 minute exposure to 100 µm glycine in the absence of Mg^{2+}. This resulted in NMDA-receptor dependent changes to the synchronous calcium activity 50 minutes after cLTP induction, whereby the amplitude of the calcium transients was increased and bursting became more frequent [269]. In rodent cortical neurons the brief application of glycine has been reported to increase the amplitude and frequency of synaptic responses. However, in the study by Kirwan et al., (2015) it is unknown what changes in synapse function may have responsible for driving the alterations in calcium activity.

Meanwhile, Odawara et al., (2016) [266] assessed network activity on microelectrode arrays in response to focal high-frequency stimulation. They observed widespread changes in the number of spikes and the firing rate, which were maintained for up to 1 hour post-HFS and occasionally after 24 hours [266]. However, there was considerable variability in the time-course and direction of change between cultures, which may have been influenced by age, and the sensitivity to NMDA-receptor blockade was not tested. Furthermore, the interpretation of data presented in this study is limited by the small sample size and inconsistent changes.

Most recently, Fink et al., (2017) [267] reported NMDA-receptor dependent changes in spontaneous synaptic activity following the transient exposure of cells to a cLTP cocktail comprised of 50 µM forskolin, 0.1 µM rolipram and no Mg^{2+} for 15 minutes. In comparison to the baseline period, the frequency, but not the amplitude, of spontaneous synaptic activity was increased for

up to 60 minutes following cLTP induction. In addition, the cLTP treatment also caused an increase in the frequency of calcium transients [267]. The response generated by the human iPSC-derived neurons in this study contrasts with those described in rodent neurons, whereby the amplitude, not the frequency of mEPSCs were enhanced [286-288]. However, this may be as a result of differing experimental methods used to assess the LTP-induced changes. The frequency and amplitude of mEPSCs, which are not generated by pre-synaptic action potentials, can reflect the number of synapses and their strength, respectively. Meanwhile, Fink et al., (2017) detected changes in spontaneous EPSC frequency, which would primarily arise from action potential-dependent synaptic release, and thereby could indicate an increase in pre-synaptic excitability [432]. In contrast to their previous study, Fink et al., (2018) have since reported that control neurons can exhibit an increase in both the amplitude and frequency of spontaneous EPSCs in response to the cLTP cocktail [268], which suggests that changes in synaptic efficacy were involved. It is possible that the latter study detected the small degree of amplitude change (~10 %) by increasing the sample size, although the authors do not comment on their conflicting results. In comparison to the described changes in amplitude, the effects of the cLTP induction upon spontaneous EPSC frequency appear to be robust [268].

The majority of these studies in human iPSC-derived neurons have shown alterations in the patterns of network activity that are suggestive of LTP, but have not reproducibly demonstrated a change in the post-synaptic response amplitude, akin to classical LTP. Furthermore, the methods that were used for LTP induction were non-physiological. In addition, the cultures used in these studies required extensive culture periods of up to 25 weeks [266, 267, 269].

In this thesis, I have described the isolation of monosynaptic excitatory connections (see Chapter VI), which will enable the investigation of physiological LTP induction at unitary connections. Specifically, STDP protocols are an attractive option for the induction of LTP at synapses between human iPSC-derived cortical neurons. Firstly, STDP has been robustly demonstrated at excitatory

synapses in rodent cortex and in excised human cortical tissue [246-248, 250, 264]. Secondly, STDP has been reliably induced in dissociated rodent neurons, which indicates that such changes can occur in a simple neuronal network [236]. And thirdly, these protocols are simple and can involve the pairing of single pre- and post-synaptic action potentials at low frequency for a short period of time. This is beneficial as the assessment of induced action potential firing (see Chapter V) suggests that NPC-mNgn2 neurons may not be able to sustain the high firing rates that are required for pre-synaptic tetanus induced LTP between neuronal pairs [207, 277, 280].

The human iPSC-derived neuronal cultures generated by Kirwan et al., (2015) and Fink et al., (2017), required lengthy culture periods for the demonstration of cLTP [267, 269]. However, it is uncertain whether iPSC-derived cortical neurons differentiated with neurogenin-2, which formed active synaptic networks in just a month, can undergo network wide changes in synaptic efficacy. In addition, rodent studies have demonstrated that LTP is a developmentally regulated process [433-435] and that the underlying molecular mechanisms also change in association with postnatal age [436]. Therefore, it would be interesting to determine whether the intrinsic maturity of human iPSC-derived neurons correlates with the capacity to undergo synaptic plasticity.

To this end, I wanted to address the following questions within this chapter:

- Can monosynaptic connections between iPSC-derived cortical neurons undergo LTP?
- Can spontaneous excitatory network activity undergo LTP in iPSC-derived cortical neurons?
- Does the level of functional maturation affect the capacity for iPSC-derived cortical neurons to exhibit synaptic plasticity?

7.2. Results

7.2.1. The amplitude of evoked monosynaptic excitatory currents in iPSC-derived cortical neurons remains stable throughout sustained low-frequency stimulation

In order to assess the impact of synaptic plasticity induction protocols, the ability for monosynaptic connections to generate a stable EPSC under control conditions must be ascertained. Monosynaptic responses were generated by pre-synaptic somatic current injection in synaptically connected pairs ($EPSC_P$), or by light-activation of pre-synaptic neurons expressing ChR2 ($EPSC_L$), as described in Chapter VI. To avoid activity-dependent changes in synaptic efficacy, $EPSC_P$ and $EPSC_L$ responses were evoked by test stimuli delivered at a low frequency (0.1 Hz). The monosynaptic EPSCs were recorded in response to test stimulation for a baseline period of 5 minutes and then, at time 0, both pre- and post-synaptic cells were subjected to a control period of 60 seconds in which no stimulation was applied. Subsequently, the test stimulation was resumed for a further 20 minutes (***Figure 7.1a***). The amplitude of the EPSC that was generated in response to each test stimulation was measured (***Figure 7.1bi***), and then the values were averaged from the 5 minute baseline period 'before' the no stimulation control period, and 10-20 minutes 'after' (see ***Figure 7.1bii*** for example traces). The amplitude of the EPSCs before the control period ranged from 18 to 699 pA, which after the control period had changed on average by 9.3 ± 11.9 % (n = 8). Across the eight control experiments that were performed there was no significant change in the response amplitude after

---

Figure 7.1. iPSC-derived cortical neurons are able to sustain a stable evoked monosynaptic response. *(on following page)* **(a)** Excitatory post-synaptic currents were evoked by either **(i)** pre-synaptic somatic current injection in a pair of monosynaptically connected neurons, $EPSC_P$, or **(ii)** light stimulation of a ChR2-expressing pre-synaptic neuron, $EPSC_L$. In order to assess the stability of recordings, a 5 minute baseline period was acquired using 0.1 Hz pre-synaptic test stimulation before connections were subjected to a control period of 60 seconds in which no stimulation was provided. Test stimulation was then resumed for a further 20 minute period. **(b)(i)** Example $EPSC_P$ response recorded under control conditions. **(ii)** Averaged traces from 5 minutes 'before' and 10-20 minutes 'after' no-stimulation. Scale bar 100 pA, 20 ms. **(c)** Across all experiments there was no significant change in the response amplitude after the control period of no stimulation ($p = 0.4351$, n = 8 cells, paired t-test). Summary data of all no stimulation experiments demonstrate that **(d)** the response amplitude, **(e)** the rise slope of the response **(f)** the access resistance and **(g)** the membrane resistance remained stable throughout the duration of the experiment. Raw data was averaged across 1-minute bin sizes and normalized to the average of the 5 minute baseline period. From 4 differentiations across 2 cell lines.

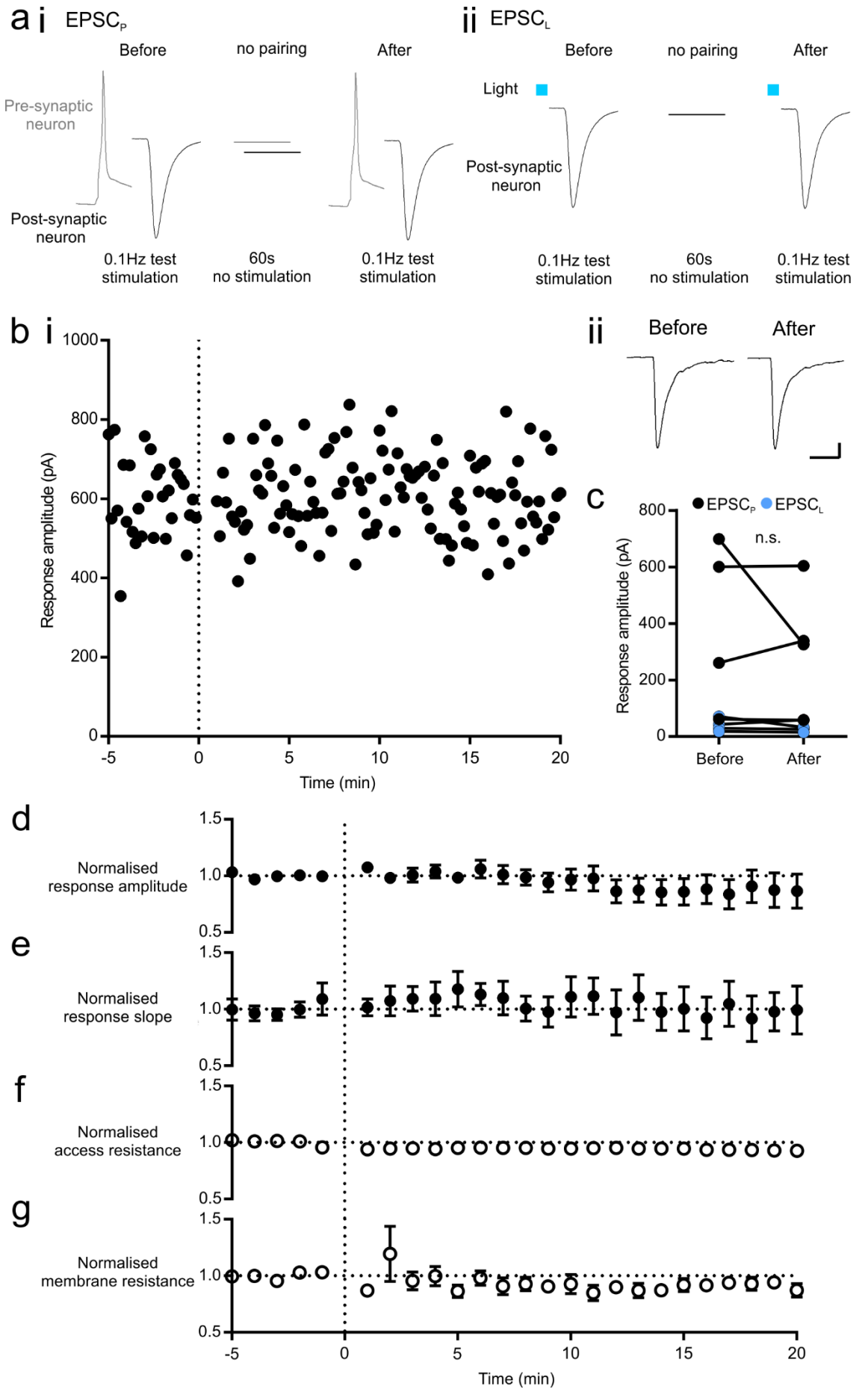
a i EPSC$_P$
Before
no pairing
After
Pre-synaptic neuron
Post-synaptic neuron
0.1Hz test stimulation
60s no stimulation
0.1Hz test stimulation
ii EPSC$_L$
Before
no pairing
After
Light
Post-synaptic neuron
0.1Hz test stimulation
60s no stimulation
0.1Hz test stimulation
b i
Response amplitude (pA)
Time (min)
ii
Before
After
c
EPSC$_P$ EPSC$_L$
n.s.
Response amplitude (pA)
Before
After
d
Normalised response amplitude
e
Normalised response slope
f
Normalised access resistance
g
Normalised membrane resistance
Time (min)

the no stimulation control period (p = 0.4351, n = 8 cells, paired t-test; ***Figure 7.1c***). Measurements from these experiments were grouped into 1 minute bin sizes and normalised to the mean of the baseline in order to generate summary data. Summary data indicated that the EPSC amplitude (***Figure 7.1d***) and the response slope (20-80 % rise slope; ***Figure 7.1e***) remained stable throughout the duration of the recording. The response slope is commonly measured in classical LTP experiments as it reflects the monosynaptic EPSC size and is less likely to be contaminated by polysynaptic activity. The access resistance affects the ability to measure or induce electrical changes in the patched neuron. Large increases in access resistance can introduce errors into recordings by filtering response kinetics and reducing the ability to detect small events, whilst the inverse is true for decreases in access resistance. Meanwhile, the membrane resistance is indicative of the membrane integrity and thus reflects cell viability. Summary data of the access resistance (***Figure 7.1f***) and membrane resistance (***Figure 7.1g***) show that these properties did not change throughout the course of the experiments, and therefore were unlikely to have influenced the EPSC amplitude. These data indicate that stable monosynaptic EPSCs can be evoked at low-frequency for a prolonged duration, and thereby enable the investigation of synaptic plasticity at unitary connections.

The stability of the response during the baseline period, recording stability and cell viability were evaluated in all experiments assessing monosynaptic connections (sections 7.2.1-3). In order to be included for analysis, each experiment was required to meet specific criteria, which were in line with rodent studies assessing synaptic plasticity [221, 248]. These criteria were devised to eliminate recordings that were unstable or underwent changes in cell viability which could impact the detection or expression of activity dependent changes. As a result, less than half of all monosynaptic connections identified were included for further analysis of synaptic efficacy.

7.2.2. Monosynaptic excitatory connections between iPSC-derived cortical neurons cannot undergo spike-timing dependent plasticity

At excitatory synapses in rodent cortex [247, 248, 250], human cortex [264] and dissociated rodent hippocampal cultures [236], the repetitive pairing of pre- before post-synaptic action potential firing at short intervals induces LTP, which is reflected by an increase in the evoked post-synaptic response amplitude. In order to determine if human iPSC-derived cortical neurons could exhibit similar spike-timing dependent changes in synaptic efficacy, monosynaptic connections ($EPSC_P$ and $EPSC_L$) were assessed using whole-cell patch clamp electrophysiology. As described in section 7.2.1, EPSCs were evoked using low frequency test stimuli (0.1 Hz) for a 5 minute baseline period. However, at time 0, a tLTP protocol was applied which involved the repetitive pairing of single pre- and post-synaptic action potential firing. The repetitive pairing consisted of the induction of a single post-synaptic action potential <20 ms after a single pre-synaptic action potential, which was repeated at 1 Hz for a total of 60 pairings. Following tLTP induction the test stimulation was resumed for 20 minutes (***Figure 7.2a***). An example EPSC recording is shown in ***Figure 7.2b***. The EPSC amplitude was compared before and after the tLTP induction, which demonstrated that the response amplitude did not change significantly ($p = 0.8438$, $n = 10$ cells, Wilcoxon signed-rank test; ***Figure 7.2c***). The initial EPSC amplitude before ranged from 31 to 460 pA and had changed on average by 12.8 ± 6.9 % following tLTP induction. Summary data indicated that throughout the duration of the recording the response amplitude (***Figure 7.2d***) and response slope (***Figure 7.2e***) were stable and did not deviate from the baseline values. The access resistance (***Figure 7.2f***) and membrane resistance (***Figure 7.2g***) also remained constant during the recordings and therefore were unlikely to have affected the detection of activity dependent changes in the EPSC amplitude. These data indicate that the application of a short pre- post- spike-pairing protocol, which has been shown to induced synaptic changes in other experimental systems, does not result in changes of monosynaptic connection efficacy in human iPSC-derived cortical neurons.

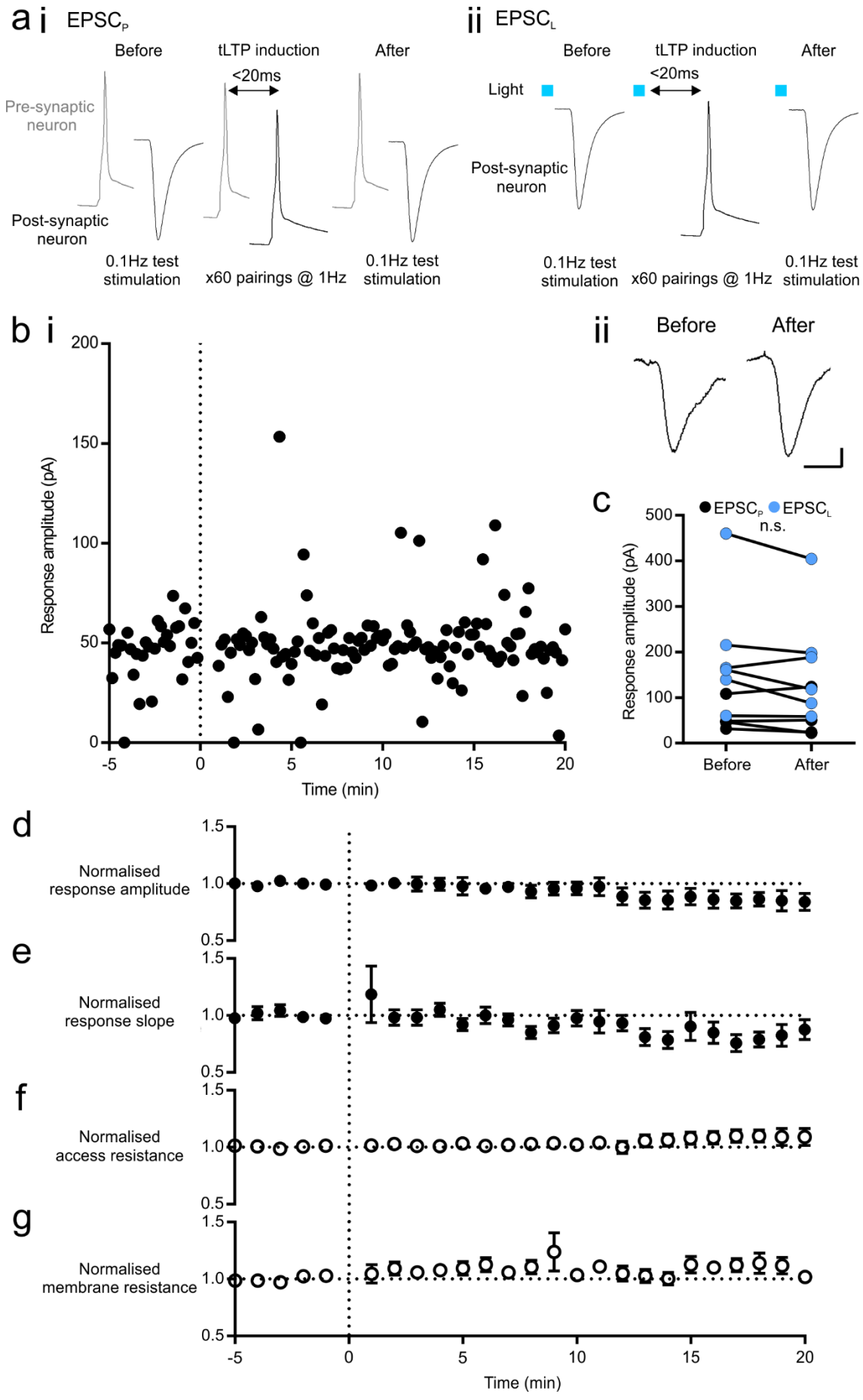
a i EPSC$_P$
Before
tLTP induction
After
<20ms
Pre-synaptic neuron
Post-synaptic neuron
0.1Hz test stimulation
x60 pairings @ 1Hz
0.1Hz test stimulation
ii EPSC$_L$
Before
tLTP induction
After
<20ms
Light
Post-synaptic neuron
0.1Hz test stimulation
x60 pairings @ 1Hz
0.1Hz test stimulation
b i
Response amplitude (pA)
Time (min)
ii
Before
After
c
EPSC$_P$ EPSC$_L$
n.s.
Response amplitude (pA)
Before
After
d
Normalised response amplitude
e
Normalised response slope
f
Normalised access resistance
g
Normalised membrane resistance
Time (min)

7.2.3. Monosynaptic excitatory connections between iPSC-derived cortical neurons do not exhibit synaptic plasticity in response to a LTP-pairing protocol

Experiments investigating synaptic plasticity in a single post-synaptic neuron are sometimes performed using perforated patch clamp electrophysiology [236, 437], and some studies have reported that LTP could not be induced using whole-cell patch clamping [207]. This may be due to the gradual dialysis of cell contents with the intracellular recording solution, which could 'wash out' soluble molecular messengers involved in synaptic plasticity [207]. Intracellular dialysis may have contributed to the absence of STDP at monosynaptic connections between iPSC-derived cortical neurons, as these experiments were performed using whole-cell patch clamping. In addition, the generation of a single post-synaptic spike may not have induced sufficient dendritic depolarization and calcium influx to activate signalling pathways involved in synaptic plasticity.

As a result, the aims of this experiment were two-fold: 1) to avoid intracellular dialysis, and 2) to provide strong post-synaptic depolarization in order to drive robust calcium influx. To this end, monosynaptic EPSCs ($EPSC_P$ and $EPSC_L$) were recorded from iPSC-derived cortical neurons using perforated patch-clamp electrophysiology. Using this method the membrane is not ruptured, but instead perforated by an anti-biotic, which is added to the intracellular solution in the patch pipette. In this case, amphotericin-B was used, which forms pores in the membrane that are only permeable

Figure 7.2. iPSC-derived cortical neurons do not exhibit spike-timing dependent long-term potentiation (tLTP). *(on previous page)* Excitatory post-synaptic currents were evoked by either **(i)** pre-synaptic somatic current injection in a pair of monosynaptically connected neurons, $EPSC_P$, or **(ii)** light stimulation of a ChR2-expressing pre-synaptic neuron, $EPSC_L$. A 5 minute baseline period was acquired using 0.1 Hz pre-synaptic test stimulation before connections were subjected to a tLTP induction protocol. tLTP induction consisted of 60 pairings at 1 Hz, whereby an action potential was induced in the post-synaptic cell with the peak occurring no later than 20 ms after the pre-synaptic action potential peak. Test stimulation was then resumed for a further 20 minute period. **(b)(i)** Example recording of $EPSC_P$ amplitude for a monosynaptic connection obtained from a pair of dual-patched neurons undergoing tLTP induction at time 0. **(ii)** Averaged traces from 5 minutes 'before' and 10-20 minutes 'after' tLTP induction. Scale bar 10 pA, 10 ms. **(c)** Across all experiments there was no significant change in the response amplitude after tLTP induction ($p = 0.8438$, $n = 10$ cells, Wilcoxon signed rank test). Summary data of all tLTP experiments demonstrate that **(d)** the response amplitude and **(e)** the rise slope of the response did not change after tLTP induction. **(f)** The access resistance and **(g)** the membrane resistance remained stable throughout the duration of the experiment. Raw data was averaged across 1-minute bin sizes and normalized to the average of the 5 minute baseline period. From 3 differentiations from 1 cell line.

to monovalent ions, thereby preventing dialysis of intracellular signalling molecules [438]. Following perforation, monosynaptic EPSCs were evoked by low frequency test stimulation (0.1 Hz) for a 5 minute baseline period, which was then resumed for 20 minutes after the delivery of a pairing-protocol for LTP induction at time 0 (***Figure 7.3a***). The pairing-protocol consisted of the stimulation of 360 pre-synaptic action potentials evoked at a frequency of 2 Hz, whereby the post-synaptic cell was held at V_m = +20 mV for the duration of the pairing. An example EPSC recording is shown in ***Figure 7.3b***. Comparison of the EPSC response amplitude before and after the pairing-protocol revealed that there was no significant difference after LTP induction (p = 0.1259, n = 8 cells, paired t-test; ***Figure 7.3c***). The amplitude of EPSCs before LTP induction ranged from 24 to 305 pA, and were changed by 6.1 ± 4.6 % on average. Summary data indicated that the response amplitude (***Figure 7.3d***) and the response slope (***Figure 7.3e***) did not change throughout the recording. Similarly, as in previous experiments, the access resistance (***Figure 7.3f***) and the membrane resistance (***Figure 7.3g***) also remained constant. These data demonstrate that a strong LTP pairing-protocol delivered to cells that were recorded using perforated patch clamping was unable to induce synaptic plasticity.

Figure 7.3. iPSC-derived cortical neurons do not exhibit long-term potentiation in response to synaptic stimulation paired with post-synaptic depolarization. *(on following page)* Excitatory post-synaptic currents were evoked by either **(i)** pre-synaptic somatic current injection in a pair of monosynaptically connected neurons, $EPSC_P$, or **(ii)** light stimulation of a ChR2-expressing pre-synaptic neuron, $EPSC_L$. A 5 minute baseline period (before) was acquired using 0.1Hz pre-synaptic test stimulation before connections were subjected to LTP induction using a pairing-protocol. The pairing-protocol used for LTP induction consisted of 360 pairings at 2 Hz whereby the post-synaptic cell was depolarized to +20 mV for the duration of the pairings. Test stimulation was resumed for a further 20 minute period. **(b)(i)** Example $EPSC_L$ amplitude undergoing LTP induction using the pairing protocol at time 0. **(ii)** Averaged traces from 5 minutes 'before' period and 10-20 minutes 'after' no-stimulation. Scale bar 20pA, 10ms. **(c)** Across all experiments there was no significant change in the response amplitude after using the pairing protocol (p = 0.1259, n = 8 cells, paired t-test). Summary data of all LTP experiments demonstrate that **(d)** the response amplitude and **(e)** the rise slope of the response did not change after LTP induction. **(f)** The access resistance and **(g)** the membrane resistance remained stable throughout the duration of the experiment. Raw data was averaged across 1-minute bin sizes and normalized to the average of the 5 minute baseline period. From 5 differentiations across 2 cell lines.

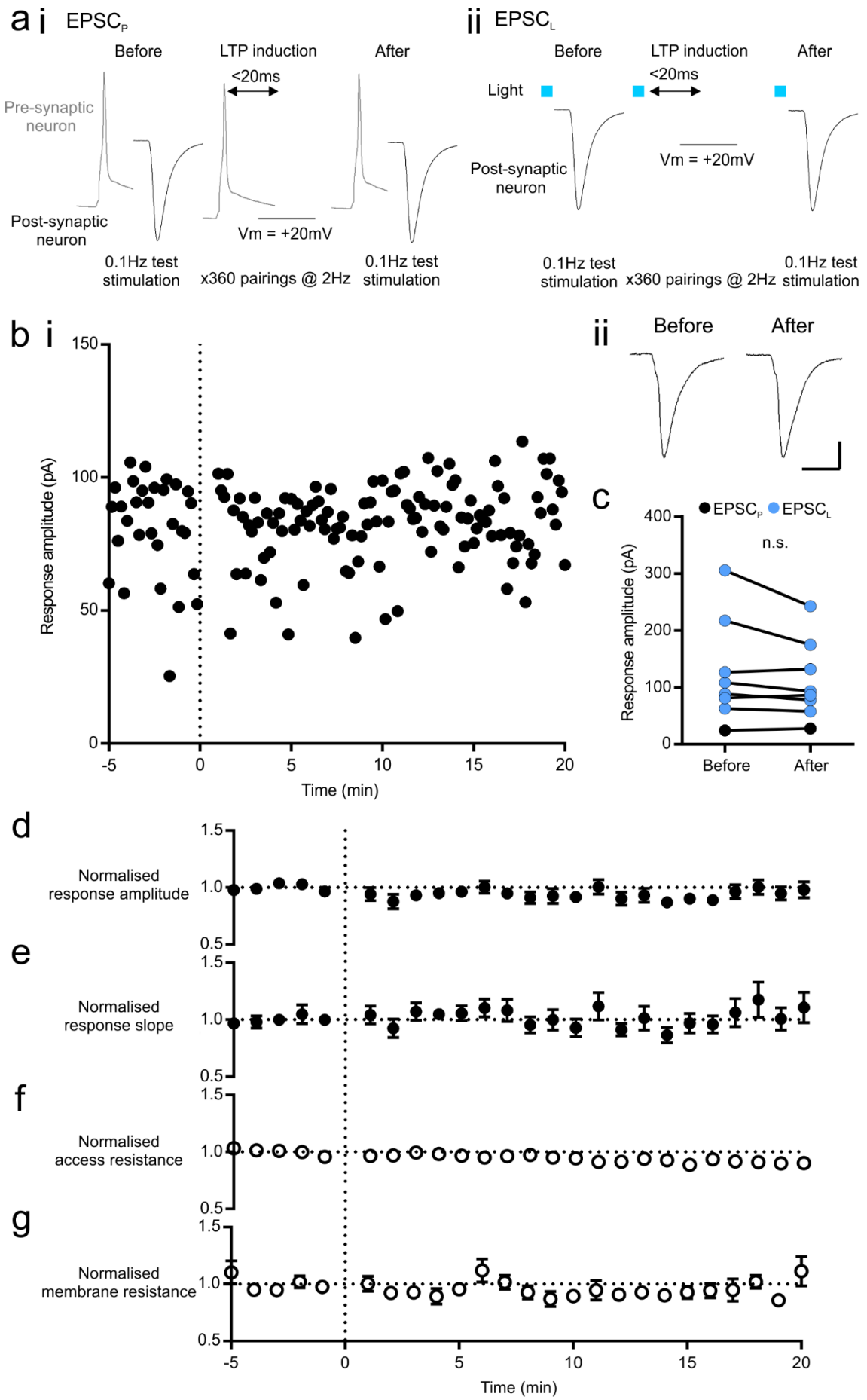
a i EPSC$_P$
Before
LTP induction
After
<20ms
Pre-synaptic neuron
Post-synaptic neuron
Vm = +20mV
0.1Hz test stimulation
x360 pairings @ 2Hz
0.1Hz test stimulation
ii EPSC$_L$
Before
LTP induction
After
Light
<20ms
Post-synaptic neuron
Vm = +20mV
0.1Hz test stimulation
x360 pairings @ 2Hz
0.1Hz test stimulation
b i
Response amplitude (pA)
Time (min)
ii
Before
After
c
EPSC$_P$ EPSC$_L$
n.s.
Response amplitude (pA)
Before
After
d
Normalised response amplitude
e
Normalised response slope
f
Normalised access resistance
g
Normalised membrane resistance
Time (min)

7.2.4. $EPSC_P$ and $EPSC_L$ had comparable stability and responsivity to LTP induction

In Chapter VI, a number of differences were identified between monosynaptic EPSCs that were evoked by pre-synaptic somatic current injection and those evoked by light-activation of ChR2. To determine whether the method used to evoke a pre-synaptic action potential affected either the long-term stability of the post-synaptic response, or the capacity for LTP induction, the changes in EPSC amplitude for $EPSC_P$ and $EPSC_L$ were compared. For control experiments, where no stimulation was given at time 0 (see section 7.2.1), the change in EPSC amplitude was indistinguishable between $EPSC_P$ and $EPSC_L$ responses (0.93 ± 0.17, n = 4 cells for $EPSC_P$, and 0.88 ± 0.19, n = 4 cells for $EPSC_L$, p = 0.6857, M-W test; ***Figure 7.4a***). Similarly, for LTP experiments, undergoing either a tLTP or pairing-protocol at time 0 (see section 7.2.2-3), the change in EPSC amplitude was also comparable between $EPSC_P$ and $EPSC_L$ (0.92 ± 0.13, n = 5 cells for $EPSC_P$, and 0.89 ± 0.04, n = 13 cells for $EPSC_L$, p = 0.5663, M-W test; ***Figure 7.4b***). Given that the change in response amplitude was no different for $EPSC_P$ and $EPSC_L$, these groups were pooled in order to assess whether the initial EPSC amplitude

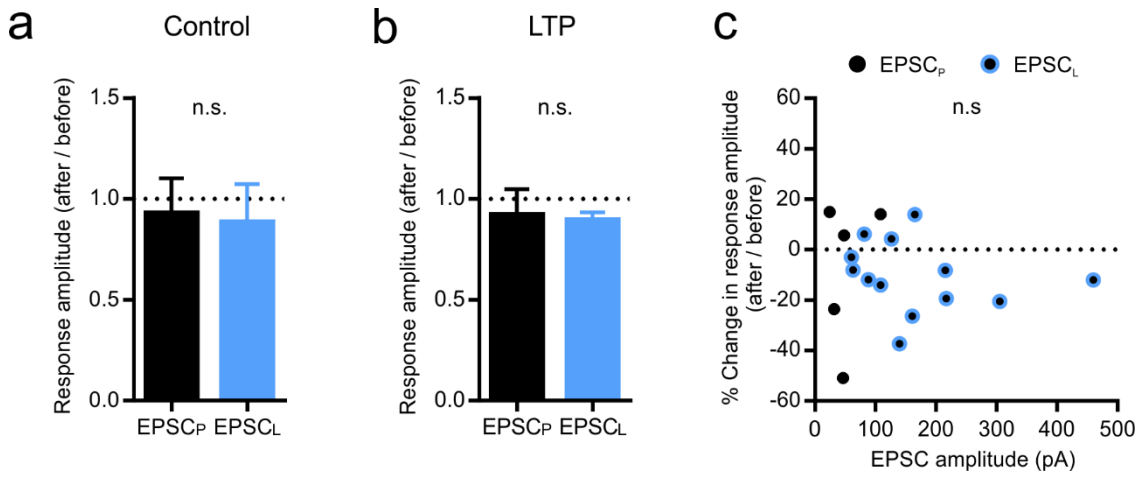

Figure 7.4. Monosynaptic EPSCP and EPSCL responses do not differ in their stability or responsivity to LTP induction. (a) The monosynaptic response amplitude (after / before) following control experiments, where no stimulation was given for 60 s at time 0, was comparable for $EPSC_P$ and $EPSC_L$ (p = 0.6857, n = 4 cells for both $EPSC_P$ and $EPSC_L$, M-W test). **(b)** The monosynaptic response amplitude (after / before) following LTP induction at time 0 using a tLTP protocol or pairing-protocol, was also comparable for $EPSC_P$ and $EPSC_L$ (p = 0.5663, n = 5 and 13 cells for $EPSC_P$ and $EPSC_L$, respectively, M-W test). **(c)** LTP experiments using $EPSC_P$ and $EPSC_L$ were pooled and showed that there was no significant correlation between the initial response amplitude and the change (%) in the monosynaptic response amplitude following LTP induction (tLTP and pairing-protocol) (p = 0.6364, r^2 = 0.0143, n = 18 cells, Pearson's correlation coefficient). From 6 differentiations across 2 cell lines.

affected the ability to undergo changes in synaptic efficacy when using a LTP induction protocol (tLTP or pairing-protocol). This revealed that there was no correlation between the initial EPSC amplitude and the percentage change following LTP induction ($p = 0.6364$, $r^2 = 0.0143$, $n = 18$ cells, Pearson's correlation coefficient; ***Figure 7.4c***). Overall, the monosynaptic response stability or responsivity to LTP induction was unaffected by the method used to evoke pre-synaptic action potential firing. Furthermore, the initial response amplitude did not impact the sign or magnitude of the change in response amplitude following an LTP induction protocol.

7.2.5. Miniature excitatory synaptic transmission in iPSC-derived cortical cultures is unaffected by a chemical LTP induction protocol

The investigation of synaptic plasticity at monosynaptic connections was limited to a relatively small number of cells and involved a short induction protocol. Therefore I sought to explore whether synaptic changes in iPSC-derived cortical neurons could be generated by a chemical LTP induction protocol, which would stimulate synapses across the entire culture and pharmacologically stimulate changes involved in LTP induction. The cLTP protocol involved the application of forskolin, rolipram, and picrotoxin, in the absence of Mg^{2+}, for 16 minutes and has been shown to upregulate post-synaptic AMPA receptors at rodent synapses, which can be reflected by changes in mEPSC amplitude [286-288].

To assess the effects of cLTP induction on human iPSC-derived neurons, cortical cultures were treated with the cLTP drug cocktail, or with a DMSO (0.2%) control, for 16 minutes. Subsequently, cultures were perfused with standard extracellular solution and mEPSCs were recorded from cells using whole-cell patch clamp electrophysiology for a period of up to 2 hours following induction (***Figure 7.5a***). In comparison to recordings of spontaneous EPSCs, which are action-potential dependent, the detection of mEPSCs offers a cleaner method to investigate synapse strength and number. Each miniature excitatory synaptic current represents the spontaneous quantal release at a single synaptic bouton and therefore changes in mEPSC amplitude reflect a change of synapse

strength, whilst changes in mEPSC frequency reflect alterations in the number of functional synapses. Assessment of mEPSC frequency showed that there was no difference between control and cLTP conditions (2.2 ± 0.3 Hz, n = 73 cells for control, and 2.6 ± 0.3 Hz, n = 68 cells for cLTP, p = 0.4385, M-W test; ***Figure 7.5b***). Similarly, no difference was detected in the mEPSC amplitude (15.5 ± 0.9 pA, n = 71 cells for control, and 17.0 ± 1.6 pA, n = 67 cells for cLTP, p = 0.5925, M-W test; ***Figure 7.5c***). Taken together, this data indicates that the cLTP induction did not affect the efficacy of miniature excitatory synaptic transmission in human iPSC-derived cortical cultures.

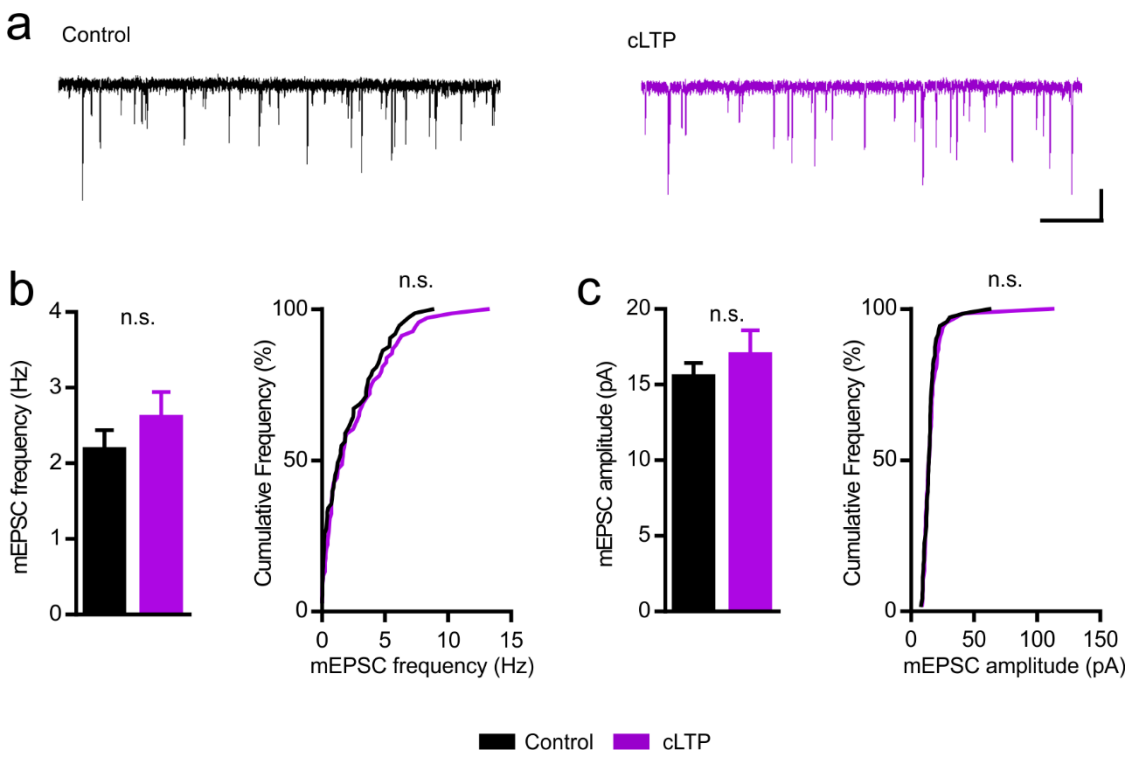

Figure 7.5. iPSC-derived cortical neurons do not exhibit chemical LTP. iPSC-derived cortical cultures were treated with a DMSO control or a chemical LTP (cLTP) solution for 16 minutes. Following cLTP induction, mEPSCs were recorded in standard HEPES external. **(a)** Representative traces of mEPSCs recorded following control (*left*) or cLTP induction (*right*). Scale bar 10 pA, 2 s. **(b)** Summary bar graph and cumulative distribution of the frequency of mEPSCs showing no significant difference between control and cLTP treatments (p = 0.4385, n = 73 and 68 cells for control and cLTP, respectively, M-W test). **(c)** Summary bar graph and cumulative distribution of the amplitude of mEPSCs showing no significant difference between control and cLTP treatments (p = 0.5925, n = 71 and 67 cells for control and cLTP, respectively, M-W test) (From 3 differentiations across 2 cell lines).

7.2.6. Prolonged optogenetic activation of pre-synaptic iPSC-derived cortical neurons can induce a potentiation of miniature excitatory synaptic transmission

The absence of plasticity induced by relatively short protocols suggested that long-term pre-synaptic stimulation may be required to generate activity-dependent changes in synaptic efficacy. Therefore, I sought to determine if prolonged pre-synaptic stimulation, delivered over several days, could generate synaptic plasticity at excitatory synapses in iPSC-derived cortical neurons. The establishment of iPSC-derived cortical cultures where pre-synaptic ChR2-expressing neurons can be activated by light (see Chapter VI) provides the opportunity for prolonged pre-synaptic stimulation without electrodes. Using a custom-built LED set-up, 10 Hz trains of 10 ms duration light flashes were delivered every 10 s to iPSC-derived cortical cultures in the incubator for a period of 2-4 days. To assess the impact of pre-synaptic ChR2 activation, the LED stimulation protocol was delivered to co-cultures comprised of CaMKIIα-mKate2 neurons co-cultured with either hSyn-ChR2-YFP neurons or CAG-YFP neurons, to generate 'activated' and 'control' cultures, respectively (***Figure 7.6a,b***). To determine whether the LED stimulation resulted in phototoxicity, cell cultures that had and had not been subjected to prolonged light stimulation were stained with propidium iodide to assess cell death. This revealed minimal levels of necrotic cell death, which was no different between iPSC-derived cultures containing either hSyn-ChR2-YFP-positive neurons or CAG-YFP-positive neurons, and was not affected by exposure to prolonged light stimulation (0.4 ± 0.2 % for hSyn-ChR2-YFP-containing cultures with light, and 0.3 ± 0.2 % without light, 0.1 ± 0.1 % for CAG-YFP-containing cultures with light, and 0.1 ± 0.1 % without light, n = 10 FOV for each experimental group, p = 0.2539, one-way ANOVA). In order to specifically address the impact of pre-synaptic ChR2 activation on synaptic efficacy, mEPSCs were recorded from CaMKIIα-mKate2-positive cells (***Figure 7.6c***). This revealed that the mEPSC-frequency was unaffected (1.0 ± 0.2 Hz, n = 49 cells for control, and 1.5 ± 0.3 Hz, n = 68 cells for activated, p = 0.4648, M-W test; ***Figure 7.6d***). However, the distribution of mEPSC amplitudes in activated cultures was shifted towards larger values and was significantly different from control cultures (18.9 ± 1.5 pA, n = 40 cells for control, and 21.1 ± 1.2

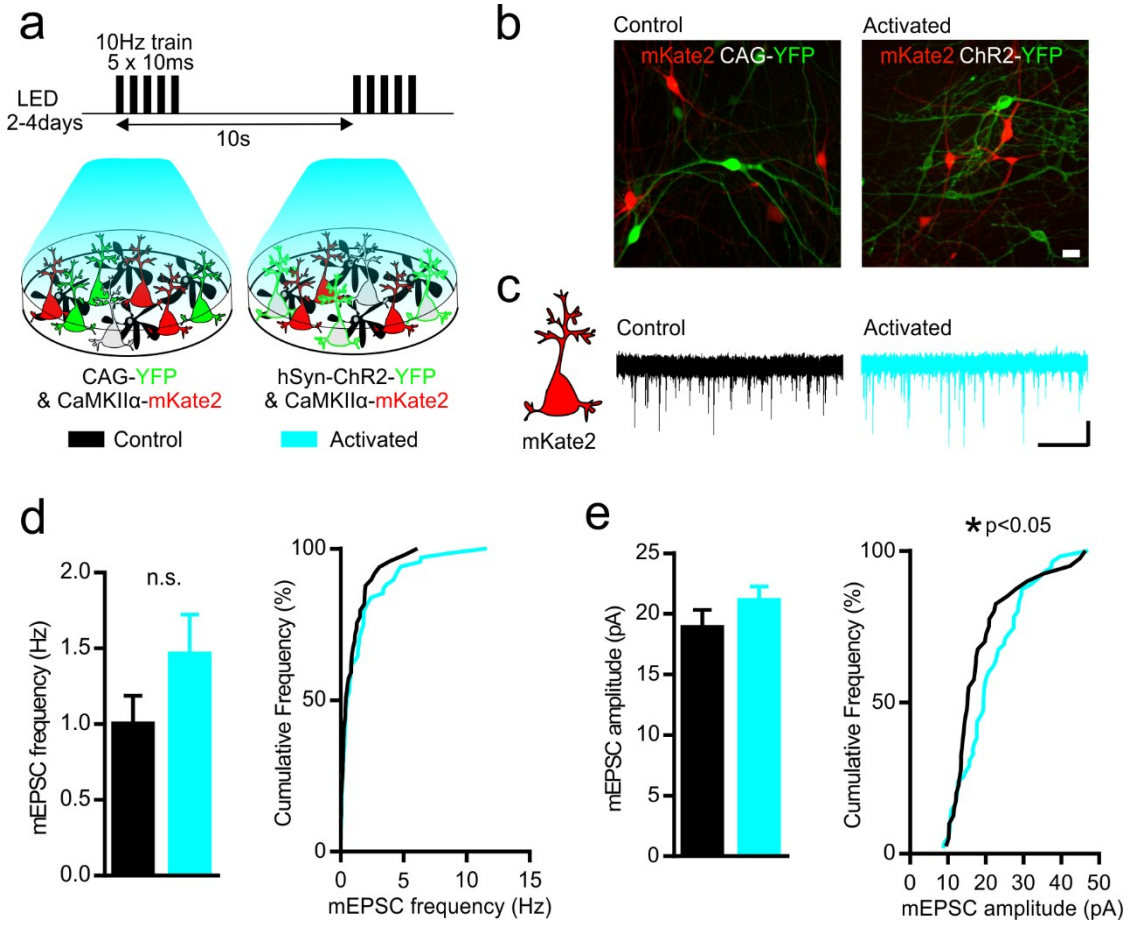

Figure 7.6. iPSC-derived cortical neurons demonstrate post-synaptic potentiation in response to long-term optogenetic pre-synaptic activation. (a) Schematic of the experimental set-up. 'Control' co-cultures, comprised of CAG-YFP and CaMKIIα-mKate2 expressing neurons, and 'Activated' co-cultures, comprised of hSyn-ChR2-YFP and CaMKIIα-mKate2 expressing neurons, were subjected to 2-4 days LED stimulation during culturing. The LED stimulation consisted of 5 flashes of 10 ms duration at 10 Hz delivered every 10 s. **(b)** Example images of control (*left*) and activated (*right*) neuronal cultures. Scale bar 20 µm. **(c)** Representative traces of mEPSCs recorded from mKate2-positive neurons from control (*left*) and activated (*right*) cultures. **(d)** Summary bar graph and cumulative distribution of the frequency of mEPSCs showing no significant difference between control and activated cultures ($p = 0.4648$, $n = 49$ and 68 cells for control and activated, respectively, M-W test). **(e)** Summary bar graph and cumulative distribution of the amplitude of mEPSCs demonstrating a significant difference in the distribution between activated and control cultures ($p = 0.0448$, $n = 40$ and 55 cells for control and activated, respectively, K-S test) (From 4 differentiations across 3 cell lines). * $p < 0.05$.

pA, n = 55 cells for activated, p = 0.0448, K-S test; ***Figure 7.6e***). Taken together, this data suggests that the prolonged optogenetic stimulation of pre-synaptic neurons can result in an activity-dependent potentiation of synaptic transmission.

7.2.7. The synaptic potentiation induced by prolonged optogenetic activation of pre-synaptic neurons is only expressed by mature post-synaptic iPSC-derived cortical neurons

Given the developmental regulation of synaptic plasticity, I set out to determine whether the expression of synaptic potentiation induced by prolonged pre-synaptic optogenetic stimulation was universally expressed by all iPSC-derived cortical neurons, or whether it was influenced by the relative degree of functional maturity. Membrane capacitance is a passive membrane property that can be reliably measured in electrophysiological recordings and, in rodent neurons, has been demonstrated to predict morphological and synaptic maturity [439]. The potential for membrane capacitance to reflect the degree of functional maturity in human iPSC-derived cortical neurons was therefore explored. To that end, the relationship between membrane capacitance and other intrinsic properties that are affected by neuronal maturation was assessed [304]. Membrane resistance, which decreases with neuronal maturation, demonstrated a highly significant inverse correlation with membrane capacitance ($p < 0.001$, $r^2 = 0.5018$, n = 44 cells; ***Figure 7.7a***). Meanwhile, sodium and potassium voltage-gated currents, which are increased during neuronal maturation, showed a similarly strong positive correlation with membrane capacitance (maximum sodium current: $p < 0.001$, $r^2 = 0.3905$, n = 44 cells; ***Figure 7.7b***; maximum potassium current: $p = 0.0077$, $r^2 = 0.1573$, n = 44 cells; ***Figure 7.7c***). Likewise, the number of induced action potentials was also positively correlated with membrane capacitance ($p = 0.0361$, $r^2 = 0.1004$, n = 44 cells; ***Figure 7.7d***). In addition, rodent neurons with a larger membrane capacitance also have a higher frequency of synaptic inputs, and their synapses exhibit more mature characteristics [439]. In human iPSC-derived cortical neurons the frequency of mEPSCs demonstrated a strong positive correlation with membrane capacitance ($p < 0.001$, $r^2 = 0.3557$, n = 73 cells; ***Figure 7.7e***). However,

the amplitude of mEPSCs did not correlate with membrane capacitance ($p = 0.7615$, $r^2 = 0.0013$, n = 71 cells; ***Figure 7.7f***). Overall, the membrane capacitance was robustly correlated with markers of intrinsic neuronal maturity. Meanwhile, the correlation of mEPSC frequency, but not amplitude, with membrane capacitance suggests that a greater number of synapses are formed onto larger, more mature iPSC-derived cortical neurons, but that these synapses do not differ in strength.

Having established that membrane capacitance could be used as an indicator of relative neuronal maturity, I investigated whether there was a relationship between functional maturity and the capacity to demonstrate synaptic potentiation in response to prolonged optogenetic stimulation.

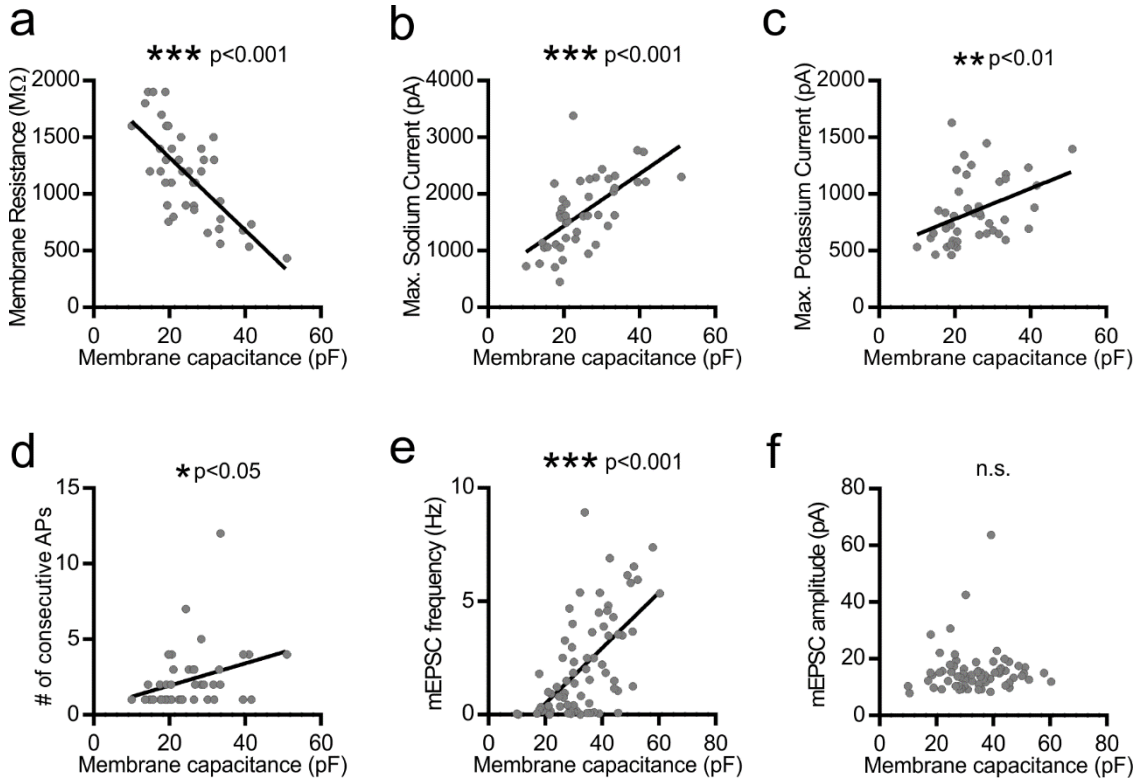

Figure 7.7. The membrane capacitance of the post-synaptic neuron strongly correlates with markers of intrinsic functional maturation and mEPSC frequency. (a) Membrane capacitance showed a significant inverse correlation with membrane resistance ($p < 0.001$, $r^2 = 0.5018$, n = 44 cells). **(b)** Membrane capacitance has a significant positive correlation with maximum sodium current ($p < 0.001$, $r^2 = 0.3905$, n = 44 cells), **(c)** maximum potassium current ($p = 0.0077$, $r^2 = 0.1573$, n = 44 cells) and **(d)** the number of consecutive action potentials ($p = 0.0361$, $r^2 = 0.1004$, n = 44 cells) (From 2 differentiations across 2 cell lines). Membrane capacitance showed a significant positive correlation with **(e)** mEPSC frequency ($p < 0.001$, $r^2 = 0.3557$, n = 73 cells) but not **(f)** mEPSC amplitude ($p = 0.7615$, $r^2 = 0.0013$, n = 71 cells) (From 3 differentiations across 2 cell lines). The relationship between all properties was assessed using Pearson's correlation coefficient. * $p < 0.05$, ** $p < 0.01$, *** $p < 0.001$.

To that end, the neurons that were assessed in ***Figure 7.6*** were ranked according to their membrane capacitance (***Figure 7.8a***). Neurons with membrane capacitance values in the 1st quartile represented the most immature neuronal subpopulation, whilst those in the 4th quartile were from the subpopulation of neurons with the greatest functional maturity (***Figure 7.8b***). The membrane capacitance of control and activated neurons within these two subpopulations was comparable (1st quartile: 39.7 ± 1.2 pF, n = 13 cells for control, and 38.6 ± 1.8 pF, n = 17 cells for activated, p = 0.9671, M-W test; 4th quartile: 99.8 ± 5.4 pF, n = 13 cells for control, and 94.1 ± 5.9 pF, n = 18 cells for activated, p = 0.2107, M-W test). Interestingly, neurons in the 1st quartile showed no difference in either mEPSC frequency (0.7 ± 0.4 Hz, n = 13 cells for control, and 0.9 ± 0.3 Hz, n = 17 cells for activated, p = 0.8773, M-W test; ***Figure 7.8c***), or mEPSC amplitude (23.2 ± 4.7 pA, n = 10 cells for control, and 21.3 ± 3.3 pA, n = 11 cells for activated, p = 7564, M-W test; ***Figure 7.8d***) following the prolonged optogenetic activation of pre-synaptic neurons. Similarly, neurons in the 4th quartile also showed no difference in mEPSC frequency (1.1 ± 0.3 Hz, n = 13 cells for control, and 1.6 ± 0.7 Hz, n = 18 cells for activated, p = 0.8668, M-W test; ***Figure 7.8e***). In contrast, neurons in the 4th quartile had a significantly increased mEPSC amplitude, which was ~30 % larger, for activated cultures compared to controls (16.8 ± 1.6 pA, n = 10 cells for control, and 27.2 ± 2.2 pA, n = 13 cells for activated, p = 0.0016, unpaired t-test; ***Figure 7.8f***). Taken together, this data suggests that a subset of more mature post-synaptic neurons are largely responsible for the synaptic potentiation elicited by prolonged optogenetic activation of pre-synaptic neurons. Meanwhile, neurons with relatively immature properties do not undergo changes in synaptic efficacy in response to this protocol.

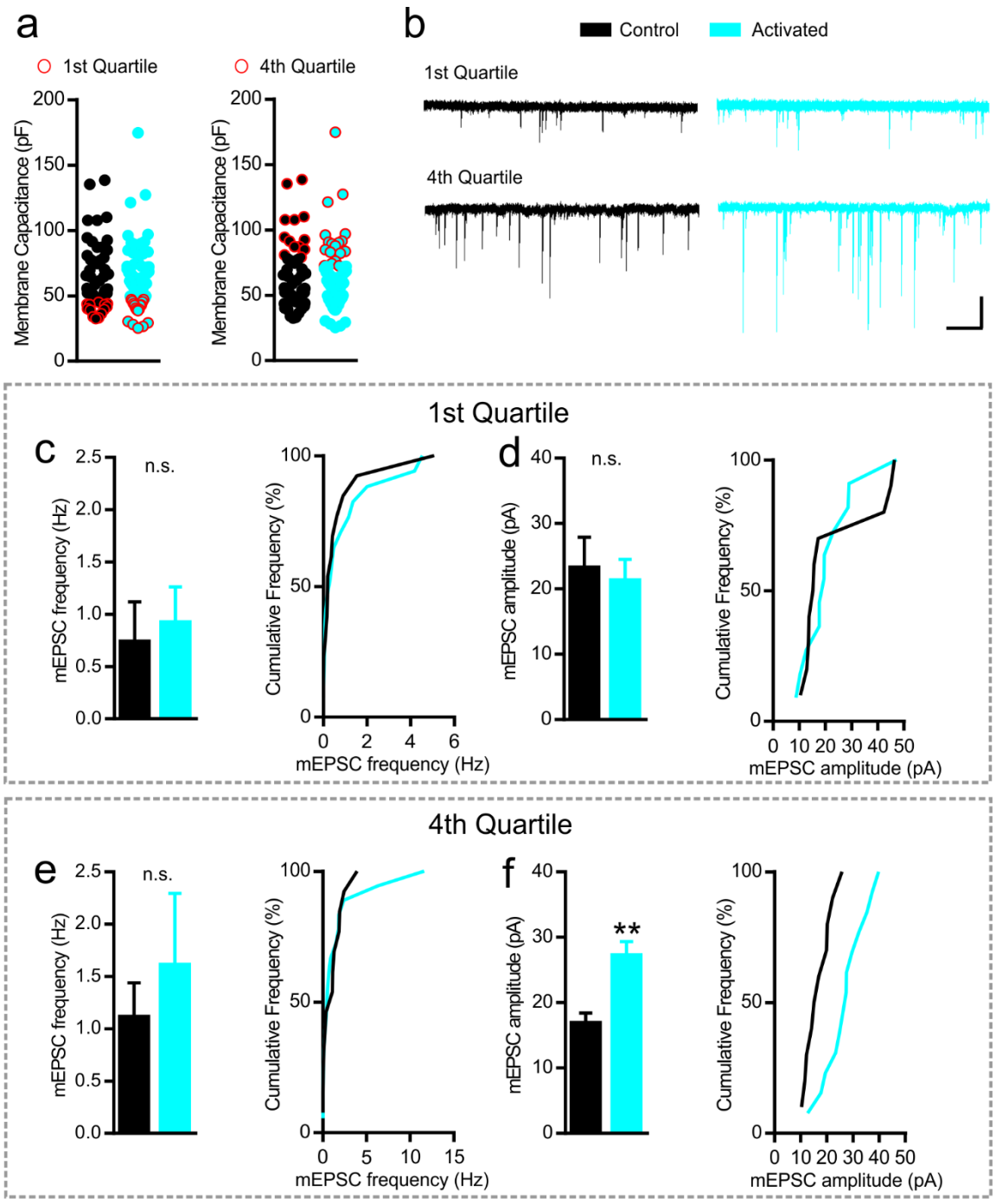

Figure 7.8. A mature subpopulation of post-synaptic neurons are responsible for driving the post-synaptic potentiation observed in response to prolonged optogenetic pre-synaptic activation. **(a)** Neurons were ranked according to their membrane capacitance and those with values in the 1st quartile and 4th quartile were taken for further analysis. **(b)** Representative traces of mEPSCs from neurons in the 1st quartile (*upper*) and 4th quartile (*lower*) from control (left) and activated (*right*) cultures. Scale bar 20 pA, 2 s. For neurons with lower membrane capacitance (1st quartile), summary bar graphs and cumulative distributions show that control and activated cultures did not differ in **(c)** the frequency of mEPSCs ($p = 0.8773$, $n = 13$ and 17 cells for control and activated, respectively, M-W test), or **(d)** the amplitude of mEPSCs ($p = 0.7564$, $n = 10$ and 11 cells for control and activated, respectively, M-W test). For neurons with high membrane capacitance (4th quartile), summary bar graphs and cumulative distributions show that control and activated *(cont. on following page)*

7.3. Discussion

In this chapter, I sought to assess the ability for excitatory synaptic connections to undergo synaptic plasticity utilising the methods established in Chapter VI. I first set out to determine whether monosynaptic excitatory connections could undergo spike-timing dependent plasticity. Stable monosynaptic EPSCs, generated by pre-synaptic electrical current injection ($EPSC_P$) or light activation of ChR2 ($EPSC_L$), could be evoked throughout the duration of recordings in response to low frequency test stimuli. However, a STDP protocol comprising repetitive pre- post-spike pairing at short intervals was unable to induce changes in synaptic efficacy. In order to elicit stronger post-synaptic depolarization than that induced by pre- post-spike pairing, a classical LTP induction protocol that combined pre-synaptic stimulation with sustained post-synaptic depolarization was assessed. However, this pairing-protocol also failed to generate changes in synaptic efficacy. As these protocols manipulate only a single synaptic connection, the capacity for iPSC-derived cortical cultures to undergo widespread changes in synaptic efficacy was also evaluated. To assess changes in excitatory synaptic transmission the mEPSC frequency and amplitude were analysed. Neither of these properties were significantly changed following the application of a cLTP induction protocol. With the aim to provide prolonged bursts of synaptic activity, co-cultures of hSyn-ChR2-YFP and CaMKIIα-mKate2 neurons were subjected to prolonged LED stimulation over several days. Assessment of synaptic transmission was performed in CaMKIIα-mKate2-positive neurons, which receive synaptic inputs from light-activated hSyn-ChR2-YFP neurons. This revealed that the amplitude, but not the frequency, of mEPSCs were significantly different in 'activated' cultures compared to 'control' cultures. Further interrogation revealed that the effect was largely driven by neurons with greater levels of maturity, whilst relatively immature neuronal subpopulations were unaffected by the stimulation protocol. This demonstrates that iPSC-derived cortical neurons are able to exhibit activity-dependent synaptic plasticity, but not via classical LTP or STDP protocols.

Figure 7.8. *(cont. from previous page)* neurons showed no difference in **(e)** the frequency of mEPSCs ($p = 0.8668$, $n = 13$ and 18 cells for control and activated, respectively, M-W test) but had a significant increase in **(f)** the amplitude of mEPSCs ($p = 0.0016$, $n = 10$ and 13 cells for control and activated, respectively, unpaired t-test) (From 4 differentiations across 3 cell lines). ** $p < 0.01$

7.3.1. The influence of post-synaptic maturity on LTP induction

The absence of classical LTP or STDP at monosynaptic connections, alongside the finding that only more mature subsets of post-synaptic human iPSC-derived cortical neurons exhibited synaptic potentiation following prolonged optogenetic activation of pre-synaptic neurons, strongly implicates maturity as a contributing factor. In the sections below, I will discuss the potential impact of neuronal maturity and other contributing factors on each of the synaptic plasticity protocols used here.

7.3.2. Synaptic plasticity at monosynaptic excitatory connections using classical LTP and STDP protocols

Control recordings revealed that monosynaptic responses did not exhibit any consistent long-term changes in EPSC amplitude throughout the duration of recordings (~30 minutes). Similarly, monosynaptic responses did not show any changes in EPSC amplitude following a STDP or classical LTP protocol at a population level. The characterization of $EPSC_P$ and $EPSC_L$ (see Chapter VI) had identified some differences arising from the use of ChR2-activation to evoke pre-synaptic action potential firing, which may have influenced the induction or expression of synaptic plasticity. Although, these were consistent with observations made in rodent studies, which had also reported that $EPSC_L$ responses were capable of undergoing LTP [201]. Comparison of the changes in response amplitude for $EPSC_P$ and $EPSC_L$ in human iPSC-derived cortical neurons revealed that the previously identified differences in monosynaptic response properties had no apparent impact on either the long-term stability or responsivity to LTP induction. This data suggests that it was unlikely that the absence of LTP was due to the grouping of experiments that used different methods to evoke a pre-synaptic action potential.

The failure to induce STDP at monosynaptic connections between human iPSC-derived cortical neurons may have been a result of insufficient post-synaptic calcium influx. Others have demonstrated that both LTP and LTD have a calcium threshold that must be surpassed in order for

synaptic plasticity to occur [231]. In the case of STDP, the co-incidence of the back-propagating action potential (bAP) with the EPSP results in the non-linear summation of calcium transients [238]. The amplitude of the bAP decreases with distance from the soma [238, 440, 441]. Factors that affect bAP propagation, such as morphology and voltage-gated channel activation [441], could have resulted in limited bAP-mediated voltage changes in the post-synaptic dendrite, which would be particularly pronounced for more distal inputs. Whilst the efficacy of action potential back-propagation within trains is inversely affected by frequency, the overall magnitude of dendritic calcium flux is greater than that evoked by single action potentials [442]. Moreover, the initiation of post-synaptic high-frequency action potential bursts has been shown to induce synaptic plasticity at connections where the pairing of single action potentials was insufficient [386]. Therefore, plasticity protocols using post-synaptic bursting could be explored in human iPSC-derived cortical neurons.

The depolarizing after-potential (DAP), which follows an action potential, also influences dendritic calcium transients by providing a more sustained period of depolarization and has been associated with the activation voltage-gated calcium channels (VGCCs) [265]. The DAP is thought to contribute to the associativity of STDP and has been shown to be essential for STDP generation in human and rodent neurons [265]. The characteristics of the DAP change with developmental age, such that DAPs in more mature neurons have a longer duration and larger calcium transients. The gradual developmental increase in DAP-associated calcium influx also correlates with the emergence of LTP in rodents [443]. The properties of DAPs in human iPSC-derived neurons have not been reported, and could not be assessed in the recordings here due to contamination of the depolarizing voltage step with the decay-phase of the action-potential. However, should iPSC-derived cortical neurons possess poorly developed DAPs, this could present a limiting factor to increases in post-synaptic calcium. The kinetics of an action potential induced by ChR2 activation have been reported to differ from those generated by somatic current injection. In rodent neurons, ChR2-induced action

potentials have a larger, slower DAP and are associated with larger calcium transients, which are thought to be caused by the activation of VGCCs rather than direct calcium influx through ChR2 [201]. Therefore, it would be interesting to explore whether promoting post-synaptic calcium influx by driving post-synaptic firing using ChR2-activation could result in potentiation of a monosynaptic response when using tLTP induction protocols. Such protocols have been successfully used to induce LTP at excitatory synapses between pairs of synaptically connected neurons in rodent hippocampal slice preparations [200].

Despite these considerations, the failure of the classical LTP pairing-protocol suggests that insufficient post-synaptic depolarization may not be responsible for the lack of synaptic plasticity observed with the tLTP protocol. In the LTP pairing-protocol, the post-synaptic neuron is depolarized for 3 minutes, which represents a very intense membrane depolarization. Although it should be remembered that, whilst the voltage at the soma was successfully maintained at depolarized potentials, the extent of dendritic depolarization achieved during this protocol was unknown. Others have used caesium-based internal solutions to block potassium channels and thereby enable better spatial clamping of the membrane voltage to promote the induction of synaptic plasticity [190, 220, 250]. Nevertheless, providing post-synaptic depolarization alone does not result in changes to synaptic efficacy, but still requires the generation of associative calcium signals induced by synaptic activation [444]. Previous work has demonstrated spike-pairing induced LTP in rodent cortical neurons, whilst a pairing-protocol delivered in TTX to prevent action potential firing failed to have an effect. This also suggests that the coincidence of a bAP with an EPSC can be important for LTP induction at some synapses [247].

A feature of synaptic plasticity is that it can be saturated [228, 246]. The magnitude of LTP at rodent synapses has been shown to inversely correlate with the initial response amplitude, which may indicate that large responses are already maximally potentiated [201, 219, 236]. However, in recordings from iPSC-derived cortical neurons there was no correlation in the initial response

amplitude and the magnitude or direction of change following a LTP induction protocol at monosynaptic connections. Furthermore, the range of initial response amplitudes was similar to those observed at monosynaptic connections in dissociated rodent hippocampal neurons, which could undergo LTP. Therefore, there was no evidence for a limit on the initial response amplitude for synaptic plasticity.

The expression of LTP can be associated with a decrease in synaptic failure rate (see Chapter I). However, the characterization of monosynaptic connections between human iPSC-derived cortical neurons (see Chapter VI) revealed relatively low variability, a low failure rate and a high probability of neurotransmitter release, which suggests that these properties may not be able to undergo further enhancement. Indeed, the ability to induce LTP in rodent hippocampal slices has been shown to inversely correlate with release probability [433]. Over the same period that rodent hippocampal neurons start to express LTP, their excitatory synapses switch from exhibiting paired-pulse depression (PPD) to paired-pulse facilitation (PPF), thereby reflecting changes in neurotransmitter release probability [433]. Meanwhile, decreasing the extracellular calcium concentration, which can artificially decrease release probability, can reveal LTP earlier in development [433]. Similar developmental changes in release probability have also been observed at synapses in rodent cortex [445]. Therefore, it is possible that the saturation of neurotransmitter release probability may have prohibited the expression of synaptic plasticity at monosynaptic connections between human iPSC-derived cortical neurons.

GABAergic synaptic transmission has also been demonstrated to affect LTP induction, and some studies have been unable to induce LTP in rodent cortex without the blockade of inhibitory transmission [243, 245]. In addition, there is evidence that the threshold for LTP induction in immature neurons may be lower, although this is thought to be due to developmental changes in GABAergic inhibition [437, 446]. In the first two weeks of life, GABAergic synaptic inputs have been found to be depolarizing in rodents as a result of elevated intracellular chloride concentrations

[447]. Therefore, the simultaneous activation of GABAergic inputs with glutamatergic inputs could promote post-synaptic depolarization and the induction of LTP. However, changes in chloride homeostasis, which is maintained throughout adult life, cause GABA to become hyperpolarizing. Subsequently, simultaneous activation GABAergic inputs can counteract depolarization induced by glutamatergic synapses activation, and thereby increase the threshold for LTP [437]. This developmental regulation of GABAergic synaptic transmission has also been observed in human iPSC-derived neurons [448]. Although the influence of GABAergic synaptic inputs is likely to have been limited (see Chapter V), the $GABA_A$ receptor antagonist picrotoxin was included throughout all monosynaptic plasticity experiments. Therefore, the influence of GABAergic synaptic transmission could not account for the absence of synaptic plasticity.

7.3.3. Chemical LTP induction in iPSC-derived cortical cultures

The cLTP protocol that uses the combined application of forskolin, rolipram and picrotoxin in the absence of Mg^{2+}, has been shown to induce changes in excitatory synaptic transmission. In rodent neurons the application of this cLTP treatment has been shown to increase the amplitude of evoked synaptic responses and the amplitude, but not the frequency, of mEPSCs [286-288]. In contrast, Fink et al., have reported a robust increase in the frequency of spontaneous EPSCs, and in some cases this was associated with an increase in spontaneous EPSC amplitude [267, 268]. The effects observed by Fink et al., in human iPSC-derived neurons manifested as alterations in synaptic activity recorded without TTX, and were therefore likely to be primarily action-potential dependent synaptic events [267, 268]. In comparison, the excitatory currents assessed here (***Figure 7.5***) are action-potential independent, and therefore some effects, such as changes in pre-synaptic excitability, would not be detected. In contrast to this previous work, I did not observe any changes in the excitatory synaptic activity of human iPSC-derived cortical neurons in response to this cLTP protocol.

The application of this cLTP cocktail has been reported to cause large increases in synaptic activity and drive synchronous bursting [267, 288]. The simultaneous and repetitive activation of synapses is thought to result in the strong activation of NMDA-receptors and the generation of LTP. Here, it is unknown to what extent spontaneous excitatory transmission was increased during the period of cLTP induction. This protocol is likely to rely upon the simultaneous activation of convergent inputs in order to drive sufficient post-synaptic calcium influx for LTP induction. Therefore it is possible that, in the human iPSC-derived cortical neurons assessed here, the cLTP protocol was unable to produce the network drive and synchronous bursts of activity, which are required for LTP. Application of the cLTP drug cocktail in the presence of Mg^{2+} has been demonstrated to induce a sensitized state that is then able to undergo LTP in response to minimal, low-frequency synaptic stimulation [286]. Therefore, it would be interesting to determine whether combining this cLTP cocktail with a stimulation protocol that could drive synchronous synaptic activation, such as bursts of optogenetic stimulation, would enable the generation of LTP.

The frequency of mEPSCs in the cultures used for cLTP induction was higher than has been observed in other experiments using NPC-mNgn2 neuronal cultures, which is likely due to culture variability. However, as discussed in section 7.3.2, LTP can be saturated, and it is therefore possible that the synapses in these culture could not have been further potentiated. However, the mEPSC amplitude was similar to that observed in neurons following prolonged LED stimulation, which may suggest that this is not the case. In comparison to experiments assessing the effects of prolonged LED stimulation, which specifically targeted CaMKIIα-mKate2 neurons, no cell selection was performed for electrophysiological recordings following cLTP induction. As has been shown by Nehme et al., (2018) using iPSC-derived neurons differentiated with neurogenin-2, the CaMKIIα-mKate2-positive neurons may represent a subset of neurons with different properties, such as greater functional maturity [275]. Such differences may also include an increase in the capacity for CaMKIIα-mKate2-

positive neurons to undergo LTP, and therefore may have contributed to the differences observed between cLTP and prolonged LED stimulation experiments.

7.3.4. Changes in synaptic efficacy induced by prolonged optogenetic pre-synaptic activation

Prolonged optogenetic activation of pre-synaptic neurons delivered during cell culturing was found to result in a potentiation of glutamatergic synaptic strength, which was primarily mediated by effects in a subpopulation of more mature post-synaptic neurons. Therefore, this study provides direct evidence for an activity-dependent change in synaptic transmission in iPSC-derived cortical neurons. Importantly, because this effect was observed in CaMKIIα-positive neurons, which were post-synaptic to the optically activated pre-synaptic ChR2 neurons, this shows a clear requirement for synaptic transmission.

It seems reasonable to propose that it was the different temporal and spatial patterns of activity evoked by prolonged optogenetic stimulation that resulted in the synaptic potentiation of the human glutamatergic synapses. For example, the whole-field illumination would be expected to cause the simultaneous activation of multiple ChR2-expressing pre-synaptic neurons, which would elicit synchronous light-evoked post-synaptic responses in the CaMKIIα-mKate2 neurons. As a result, the prolonged LED stimulation protocol could satisfy the cooperative aspects of LTP, whereby the activation of single 'weak' monosynaptic connections is insufficient, and rather the simultaneous activation of many inputs is required to induce LTP [77, 248]. This mechanism would also be consistent with the demonstration of potentiation only in post-synaptic neurons with a high membrane capacitance, as this property was associated with a greater frequency of mEPSCs, indicating that these neurons received larger numbers of synaptic inputs. Taken together, these experiments reveal that human iPSC-derived cortical neurons can support synaptic plasticity, but that this critically depends upon the maturational state of the post-synaptic neuron.

STDP at some cortical synapses in rodents has been shown to be frequency-dependent, such that spike-pairing at low frequencies (< 10 Hz) failed to induce LTP [247, 248]. The potentiation that was observed in response to the 10 Hz bursts of LED stimulation, which did not occur in the LTP experiments performed at 1-2 Hz at monosynaptic connections, could suggest that synaptic plasticity at human iPSC-derived cortical neurons may also be dependent upon the frequency of stimulation. Furthermore, it is uncertain whether the prolonged stimulation was necessary for the induction of potentiation in these cultures, and therefore it would be interesting to determine whether the same pattern of LED stimulation could induce changes in excitatory synaptic transmission when delivered for short periods during electrophysiological recordings.

The induction of LTP at cortical excitatory synapses is an NMDA-receptor dependent process [77, 236, 250, 449]. The culture of neurons in the presence of an NMDA-receptor antagonist, during the delivery of LED stimulation, could provide one method to ascertain whether the potentiation induced by prolonged optogenetic stimulation also required the activation of NMDA-receptors. The change in mEPSC amplitude (***Figure 7.8***), but not frequency, is indicative of a post-synaptic locus of expression. LTP is typically associated with changes of AMPA-receptor mediated responses, whilst NMDA-receptor mediated synaptic transmission undergoes little to no change [190, 219, 220, 222]. Here an increase was detected in the amplitude of AMPA-mediated mEPSCs, but it remains to be determined whether the LED stimulation also induced changes in NMDA-receptor mediated transmission.

Overall, the induction of LTP in human iPSC-derived cortical neurons proved to be challenging. Neither STDP, nor a classical pairing-protocol that resulted in more intense depolarization, were able to induce changes in monosynaptic connection efficacy. Similarly, a cLTP protocol also failed to alter miniature excitatory synaptic transmission. However, providing bursts of pre-synaptic stimulation over several days during cell culture induced the potentiation of mEPSC amplitude. This effect was largely driven by a relatively mature neuronal subpopulation, whilst neurons with

immature properties were unaffected. Synaptic plasticity is a complex process that can be affected by many factors. However, the findings presented here suggest that the degree of maturity is likely to be critical when exploring synaptic plasticity in human iPSC-derived cortical cultures.

VIII: Discussion

The principal aim of this thesis was to develop methods for the investigation of phenotypes in synaptic transmission and synaptic plasticity in fAD patient iPSC-derived neurons. Specifically, I sought to: (1) characterize the molecular and functional properties of iPSC-derived cortical neurons generated from healthy control individuals and fAD patients; (2) to explore methods to generate active and mature synaptic networks; and (3) to develop assays of glutamatergic synaptic plasticity. In this chapter I will briefly review how these aims were addressed experimentally and summarise the major experimental findings. I will discuss the potential applications of the techniques developed here, and the aspects that could be further refined. I will then consider the limitations of the methodological approaches that have been used, and the broader challenges associated with iPSC-derived models of AD.

8.1. Summary of experimental findings

In ***Chapter III*** I generated cortical neurons from iPSCs derived from a healthy control and four patients with fAD using a protocol previously published by Shi et al., (2012), which recapitulates many aspects of *in vivo* cortical development. In line with the published protocol, neuronal differentiation of control and fAD patient iPSC monolayers resulted in the generation of primarily excitatory neurons that expressed deep and upper layer cortical markers. Examination of the intrinsic membrane properties at two time points showed that increasing the culture duration could enhance functional neuronal maturity. Nonetheless, functional assessment of the control iPSC-derived cortical neurons, following 2 - 4 months of culture, revealed that the functional properties of neurons were heterogeneous and that the majority of cells fired only a single action potential and exhibited minimal or absent excitatory synaptic transmission. Similarly, fAD patient derived cortical neurons demonstrated comparable intrinsic membrane properties to healthy control neurons. Despite the relative functional immaturity, cortical cultures derived from fAD-patient iPSCs had a significant elevation in the Aβ42:40 ratio of secreted peptides, thereby demonstrating

that these cells could exhibit biochemical phenotypes in line with disease pathology. Whilst the neurons acquired key functional neuronal properties, they were not reminiscent of mature, adult cells, which is consistent with the physiology reported in other studies using iPSC-derived neurons. Therefore, the level of functional maturity demonstrated by these cultures was not conducive to the assessment of complex functional phenotypes.

Having established that neurons were functionally immature, I then set out in ***Chapter IV*** to explore methods that may promote neuronal maturation and the formation of active synaptic networks, or enable the targeting of functionally mature subsets of neurons. The co-culture of human iPSC-derived cortical neurons with rat astrocytes was found to significantly enhance intrinsic neuronal maturity and promote the formation of excitatory synaptic networks. As a result, neuronal co-culture with rat astrocytes was consistently used for all functional studies in this thesis. Although rat astrocytes increased the proportion of cells with excitatory synaptic inputs, the frequency of EPSCs remained low and therefore other strategies were tested. I determined that the expression of a CaMKIIα-mKate2 reporter construct was unable to identify neurons of greater functional maturity within these heterogeneous cultures. The culture of neurons in BrainPhys™ medium alone, or supplemented with additional factors, was also found to have no effect upon neuronal maturation. Meanwhile, recordings from human iPSC-derived cortical neurons co-cultured for several weeks with primary rodent cortical neurons exhibited low levels of synaptic activity, but demonstrated immature intrinsic maturation and had a limited culture duration due to rodent neuron viability. Therefore, whilst the benefits of rat astrocytes were clearly demonstrated in this chapter, it was apparent that a different approach was required for the generation of mature human synaptic networks.

In ***Chapter V***, I investigated whether the exogenous expression of neurogenin-2, in either iPSCs or NPCs, could generate active synaptic networks of cortical neurons. Both experimental approaches generated functional neurons with cortical identities within a few weeks. However NPCs

differentiated with neurogenin-2 exhibited a greater enhancement of excitatory synaptic activity, whereby the majority of cells had excitatory inputs (86 %), which occurred at a twenty-fold higher frequency (~1 Hz) than the control group (~0.05 Hz), and also generated a much higher cell yield. Furthermore, the elevated Aβ42:40 phenotype previously identified in fAD-patient derived neurons was still evident in the neurogenin-2 cultures. These data demonstrated that exogenous expression of neurogenin-2 could be used to accelerate the functional maturation of human iPSC-derived cortical neurons, whilst conserving biochemical phenotypes. As a result of the enhanced synaptic properties, the neurogenin-2 differentiation of NPCs was used for the experiments in Chapters VI and VII.

The aim of ***Chapter VI*** was to optimise the detection and isolation of excitatory monosynaptic connections between human iPSC-derived cortical neurons, and to characterize the properties of these unitary connections. Dual whole-cell patch clamp experiments demonstrated the detection of primarily unidirectional monosynaptic connections at low frequency (7 %). The excitatory monosynaptic connections exhibited paired-pulse depression, low variability and high reliability, and had very similar properties to excitatory synapses in rodent cortex. The optogenetic tool, ChR2, was recruited with the aim of increasing the probability of detecting a monosynaptic connection. Human iPSC-derived cortical neurons expressing ChR2 could reliably generate light-evoked action potentials at high frequencies and with minimal temporal jitter. In co-cultures of ChR2-YFP and CaMKIIα-mKate neurons (used to facilitate the targeting of ChR2-negative neurons), 34 % of ChR2-negative neurons were found to generate light-evoked monosynaptic responses, which were qualitatively similar to those evoked in connected neuronal pairs. Assessment of the AMPA/NMDA ratio at monosynaptic connections revealed that the vast majority (89 %) displayed functional AMPA and NMDA receptors, which are critical for the induction and expression of synaptic plasticity.

I set out in ***Chapter VII*** to determine whether human iPSC-derived cortical neurons could exhibit synaptic plasticity. I ascertained that stable monosynaptic responses could be evoked by test stimuli under control conditions. Neither a STDP protocol nor a LTP pairing-protocol induced changes in synaptic efficacy. The initial response amplitude or the method used to evoke a pre-synaptic action potential had no apparent effect upon the outcome of these experiments. Similarly, a cLTP protocol also failed to alter miniature excitatory synaptic transmission. In contrast, an optogenetic strategy, in which ChR2-expressing cultures were stimulated over a period of days, did produce synaptic plasticity effects. Neurons post-synaptic to ChR2-expressing neurons exhibited a significant potentiation of mEPSC amplitude. The observed potentiation of synaptic efficacy was primarily driven by a subset of neurons with greater maturity, which exhibited a ~30 % increase in mEPSC amplitude, whilst relatively immature neurons were unaffected. Together, these data provide direct evidence for an activity-dependent change in synaptic efficacy in a subset of human iPSC-derived cortical neurons, but suggest that neuronal maturity remains a major limiting factor in the synaptic phenotypes that can be explored in these cultures. Further interrogation into the mechanisms underlying optogenetic induced synaptic plasticity may offer important insights for future investigations in iPSC-derived cortical cultures.

8.2. Establishing the potential of an iPSC-derived cortical neuronal platform for the study of excitatory synaptic transmission

An important contribution of this thesis is the development of a well-characterized iPSC-derived cortical neuronal platform that can be used to interrogate excitatory synaptic transmission at the level of a single connection. The methods developed in this thesis present the opportunity to investigate pre- and post-synaptic alterations following experimental manipulations or in patient iPSC-derived neurons, and thus have broad applications for the study of neurological disorders. Furthermore, the refined neurogenin-2 differentiation protocol offers a scalable approach for the generation of active synaptic networks within a short time period. The optogenetic strategy developed in this thesis provides the reliable and frequent detection of monosynaptic responses,

thereby increasing experimental throughput, and is a method that could be further refined for studies of monosynaptic connectivity.

The methods developed in this thesis will enable further investigations of excitatory synaptic transmission in iPSC-derived models of AD. Specifically, rodent models with fAD mutations have exhibited alterations in basal excitatory synaptic transmission, alongside changes in synaptic plasticity [51, 78, 79]. The phenotypes that have been reported include decreased amplitudes of evoked glutamatergic synaptic responses, changes in short-term plasticity and alterations in AMPA/NMDA ratios [51, 78, 79]. Given the species-specific differences in Aβ, tau and the synaptic proteome between mice and humans [53, 55, 97], it is uncertain whether the effects upon glutamatergic synapses that have been observed in rodents also manifest in human neurons with fAD mutations. Now these synaptic properties could be explored in a human-specific model. The conservation of the Aβ phenotype in neurogenin-2 neurons further supports the use of this method for the investigation of excitatory synaptic transmission in fAD patient iPSC-derived neurons.

To date, 85 human central nervous systems diseases have been associated with mutations in 82 genes encoding post-synaptic proteins placing synaptic dysfunction central to a substantial number of neurological disorders [450]. As a result, the experimental approaches developed in this thesis could also support the study of other neurological disorders where excitatory synaptic transmission is thought to be impaired, such as autism and schizophrenia. A multitude of mutations affecting genes encoding proteins involved in synapse structure and function result in neurological disorders associated with intellectual disability and autism, for example *SHANK3* mutations which cause Phelan-McDermid Syndrome [451]. Shank proteins are highly expressed in cortical neurons and are localised to the post-synaptic density [452]. Rodent models exploring the function of Shank3 have implicated this protein in basal synaptic transmission, synaptic plasticity, AMPA receptor trafficking and regulation of dendritic spine morphology [453, 454]. Specifically, alterations in miniature excitatory glutamatergic synaptic transmission, paired-pulse ratio and evoked AMPA-receptor

mediated synaptic responses have been reported in *Shank3* mutant mice and could now be explored in a human-specific system using the methods developed in this thesis [454]. Similarly, Rett syndrome is a genetic form of autism caused by mutations in *MECP2* that disrupt the function of the protein as a transcriptional repressor [455]. Loss of *Mecp2* function in rodents has been associated with reductions in glutamatergic cortical synaptic connectivity, decreased mEPSC frequency and increased short-term synaptic depression [456-458]. There is also evidence for altered glutamatergic synaptic connectivity in the cortex of patients with schizophrenia. For example, studies using post-mortem tissue and animal models have reported decreases in dendritic spine density, altered PSD95 expression and NMDA receptor hypofunction [459-461]. Schizophrenia is a complex psychiatric disorder that commonly manifests in adolescence; a time when major synapse remodelling occurs [462]. Schizophrenia exhibits high heritability and GWAS studies, which have implicated ≈ 600 genes in the disorder, suggest that the genetic risk arises from the complex interactions of multiple genetic variants [463, 464]. This complex genetic background and the difficulties associated with modelling psychiatric disorders in animal models make human iPSC technology an attractive model for investigating disease pathogenesis in schizophrenia. Several studies have generated iPSC-derived neurons from patients with Rett Syndrome [465, 466], Phelan-McDermid Syndrome [162], and schizophrenia [163, 467], but investigations into synapse function have often been limited by the immature properties of the iPSC-derived neurons generated. Therefore, the enhanced synaptic connectivity and functional synaptic assays developed in this thesis could be easily applied to such studies.

Given the relatively low connectivity in iPSC-derived cortical cultures, the greatly enhanced probability of light-activated monosynaptic responses make ChR2 a powerful tool in the investigation of unitary connections in these cultures. This ChR2 approach could be further refined and utilised as a high-throughput method to probe connectivity from putative pre-synaptic neurons. Others have developed techniques that can promote the generation of a somatic action-

potential and limit axonal stimulation through the spatial restriction of light exposure or ChR2 expression [468-471]. This may produce more physiological pre-synaptic activation and enable the activation of a single pre-synaptic neuron, rather than a population that are activated by wide-field illumination. The use of a narrow diameter fibre-optic can enable the generation of a small <5 µm light spot, which can be focussed onto the soma of a putative pre-synaptic neuron to evoke an action potential [468]. This would reduce the direct activation of axonal fibres and therefore the generation of polysynaptic activity. Similar methods have also been devised using two-photon activation of ChR2, which can limit light scatter and enhance the cellular specificity of ChR2 activation [469, 470]. However, these approaches are limited to only high ChR2 expressing cells and require longer light-durations in order to reach action potential threshold as a result of the activation of a smaller area of membrane, which generates a smaller photocurrent [468, 469]. Alternatively, the use of ChR2 that has been genetically tagged to target expression to the soma and proximal dendrites would similarly promote somatic action potentiation generation and prevent direct axonal activation [471].

ChR2 could be used to probe pre- and post-synaptic mechanisms, in a similar manner to dual-patching. As described in this thesis, the reliable generation of optically evoked monosynaptic responses allows the assessment of variability, failure rate, short-term plasticity and the properties of post-synaptic receptors. Therefore, ChR2 can enable a detailed interrogation of synaptic function and insights into the locus of change following a manipulation. ChR2 could also be used to probe synaptic changes in a disease context using co-cultures of patient and control neurons that are transduced separately with ChR2-YFP or mKate2 constructs. Similar cultures were generated by Shcheglovitov et al., (2013) and used the expression of fluorescent reporter constructs to distinguish between patient and control neurons in order to reduce the impact of culture variability in an iPSC-derived model of autism [162]. I have shown that it is possible to combine this method with ChR2 in order to specifically activate control pre-synaptic neurons and record from patient

post-synaptic neurons, or the inverse. This experimental design will facilitate investigations into the locus of any synaptic alterations.

The demonstration of an activity-dependent change in excitatory synaptic transmission using prolonged optogenetic stimulation provides a foundation for the future investigation into synaptic plasticity in iPSC-derived cortical neurons. Further experiments could be performed to identify molecular mechanisms involved in the potentiation of synaptic transmission. Delivery of the optogenetic stimulation in the presence of NMDA-receptor antagonists would ascertain whether the potentiation is dependent upon NMDA-receptor activation. Meanwhile, the delivery of the LED stimulation paradigm for a brief period during electrophysiological recordings could determine the importance of the duration and spatiotemporal pattern of the optogenetic stimulation protocol.

8.3. Methodological considerations and broader challenges associated with the study of excitatory synaptic transmission in an iPSC-derived cortical neuronal platform

In this section I will consider the methodological approaches used and how these could have influenced the outcome of the experiments conducted in this thesis. I will also discuss the broader challenges that are associated with investigations into excitatory synaptic transmission and plasticity in an iPSC-derived cortical neuronal platform, with a specific focus on the factors that are most relevant for the study of AD.

8.3.1. Were the recording conditions optimal for the induction and detection of synaptic plasticity at monosynaptic connections?

An important question is how the recording conditions and protocols used during my assessment of synaptic plasticity in human iPSC-derived cortical neurons may have influenced the properties of excitatory synapses and the induction or detection of classical LTP. The extracellular recording solution has been primarily designed to reproduce the *in vivo* extracellular ion composition of the brain. Small adjustments to the extracellular concentration of ions such as Ca^{2+} and Mg^{2+} can affect

synaptic plasticity. For example, decreasing extracellular Ca^{2+} concentration during the induction period can significantly impair LTP, whilst raising Ca^{2+} can facilitate LTP by increasing the calcium influx in response to stimulation [472]. Comparatively, the extracellular Mg^{2+} concentration influences NMDA receptor activation and has been shown to negatively correlate with LTP magnitude [472, 473]. However, the complete absence of Mg^{2+} increases neuronal excitability and can induce spontaneous LTP-like changes that potentiate synaptic activity and prohibit subsequent LTP induction [474]. The concentration of Ca^{2+} and Mg^{2+} in the extracellular solution was similar to other studies of synaptic plasticity and was comparable to the levels found in the culture medium used during the prolonged optogenetic stimulation [209, 249, 250, 264]. Therefore the concentrations of Ca^{2+} and Mg^{2+} are unlikely to account for the failure to induce classical forms of LTP.

In development, newly generated glutamatergic synapses are thought to be initially 'silent', due to the presence of only NMDA receptors in the post-synaptic membrane, which are largely inactive at resting membrane potential [353]. Rodent studies in slice preparations and cultured neurons have demonstrated that neurons can be connected by only silent synapses, and that the proportion of these silent connections decreases with developmental age [216, 217, 219, 220, 405, 475, 476]. In this thesis, synaptic connectivity between human iPSC-derived cortical neurons was assayed at V_m = -70 mV in a Mg^{2+} containing extracellular recording solution, and therefore only AMPA-mediated responses would have been detected. Therefore, neurons connected by purely silent synapses would not have been identified under the recording conditions used here, and instead would require removal of Mg^{2+} or depolarization to a positive membrane potential. The mechanism of unsilencing appears to be analogous to LTP, whereby the activation of NMDA receptors, coupled to post-synaptic depolarization, leads to the insertion of AMPA receptors [216, 217, 220, 477]. The relative immaturity of the human iPSC-derived cortical neurons may suggest that there is a high probability that silent connections could be present in these cultures. In rodent neurons classical

LTP-pairing protocols have similar effects on silent connections as they do on AMPA-containing synaptic connections, however, instead of potentiating an existing AMPA component they result in the generation of an AMPA-mediated response [217]. The very nature of silent synapses suggests that they provide a synaptic state with the greatest capacity for potentiation. Thus, the investigation of silent synapses would be an interesting avenue for future exploration in human iPSC-derived cortical neurons, and could provide a further opportunity for the interrogation of LTP.

In patch-clamp electrophysiology experiments, cells were targeted that had a neuronal morphology and appeared healthy, but the neuronal subtype of the patched cell was unknown. In experiments where CaMKIIα-mKate2 positive cells were targeted the neuron is expected to be glutamatergic [346], albeit with an unknown regional identity. Comparatively, the hSyn-ChR2-YFP construct has a pan-neuronal promoter and therefore would be expressed by all neuronal subtypes [478]. As a result, patched neurons or activated ChR2-YFP-positive cells are likely to have represented a range of cortical identities and may have included a subset of GABAergic neurons. In rodent cortex, GABAergic neurons are highly connected to glutamatergic neurons, and in some regions these inhibitory connections have been found to be 10 times more prevalent than connections between excitatory connections, and are frequently bidirectional [479, 480]. Furthermore, studies have reported that glutamatergic connections onto some subtypes of GABAergic neurons cannot undergo synaptic plasticity [236, 481, 482]. Although only half of the neurons assayed exhibited spontaneous GABAergic synaptic activity, it is possible that excitatory monosynaptic connections onto GABAergic interneurons could have been detected, but are likely to represent a minority of the connections assayed.

As outlined above, a number of factors associated with the recording conditions and protocols used could be altered to facilitate classical LTP induction and expression in future experiments. However, it seems unlikely that these factors could account for the complete absence of monosynaptic plasticity observed in this thesis.

8.3.2. Could alternative differentiation methods or further protocol refinement generate iPSC-derived neuronal networks with enhanced maturity?

I have demonstrated that the expression of neurogenin-2 can enhance neuronal maturation. However, the observation that functional maturity is likely to still represent a limiting factor in the investigation of excitatory synaptic plasticity, indicates that alternative differentiation methods or further protocol refinements may be necessary. In this thesis, 2D monolayer cultures were used due to their simplicity and amenability for functional assessment. The directed differentiation of iPSCs into neurons in either 2D or 3D cultures can recapitulate many aspects of *in vivo* cortical development [144, 145, 150, 151]. However, 3D cultures are thought to better recreate the cytoarchitecture of the brain and can exhibit some degree of cortical layer formation [144, 151]. This poses the question: can the 3D culture environment promote functional maturation? There have been limited reports describing the electrophysiological characterization of neurons in 3D cultures [151, 483]. Pasca et al., (2015) generated 3D cultures comprised of progenitor cells and neurons expressing cortical markers, which they termed cortical spheroids [151]. After prolonged time periods (> 130 days), these cultures were functionally assessed following dissociation and short-term culture (akin to primary neuronal cultures), or in acute slice preparations. In both cases, most cells had a relatively hyperpolarized resting membrane potential, were capable of induced action potential firing and received excitatory inputs, albeit at relatively low frequency [151]. Extracellular electrical stimulation of slices appeared to evoke primarily polysynaptic activity, which, taken together, suggest that these cultures exhibit relatively low connectivity even after extensive cell culture periods. Similar results were also obtained by Li et al., (2017) in human iPSC-derived organoid cultures [483]. Furthermore, the transcriptome of 3D cultures, like 2D cultures, maps to foetal tissue, not adult tissue [144, 151, 316]. Therefore, the data generated by these studies suggests that 3D cultures do not offer advantages for neuronal maturation and synaptic network formation.

During the course of this thesis, there have been a number of studies describing modified 2D differentiation protocols designed to generate mature cortical neurons within a short-time period [275, 484]. The Studer laboratory have adapted their 2D monolayer neuronal differentiation protocol to include the addition of several small molecules in order to accelerate neuronal differentiation and maturation [148, 484]. This protocol generated primarily post-mitotic neurons after 13 days however, these cultures were predominantly comprised of deep-layer Tbr1-positive neurons. The generation of upper-layer neurons required the removal of small molecules that promoted differentiation, and thereby compromised functional maturation, which required more than double the culture time to achieve similar electrophysiological properties [484]. Comparatively, Nehme et al., (2018) combined dual-SMAD inhibition with neurogenin-2 expression which generated neurons primarily expressing upper layer markers, similar to the original neurogenin-2 publication [158, 275]. They identified that CaMKIIα-expressing neurons demonstrated more mature functional properties, and in transcriptome analysis, this subset of cells were found to cluster with both foetal and adult human neurons [275]. In this study, following 28 days of culture, electrophysiological characterization of the CaMKIIα-positive population showed that the majority of neurons received synaptic inputs at frequencies of ~1 Hz, and overall, had similar properties to the 21 day NPC-mNgn2 neurons described in this thesis [275]. Overall, the membrane properties and electrical activity of the neurons generated by these studies are largely comparable to those observed in the NPC-mNgn2 neurons, described in Chapter V, and indeed were achieved using similar methods: anti-mitotic treatment, directed differentiation to a neural lineage, and neurogenin-2 expression. Nonetheless, these protocols are still unable to generate iPSC-derived neurons that fully resemble adult human neurons which, for example, have a many-fold lower membrane resistance and a more hyperpolarized membrane resistance [303]. Therefore, alternative neuronal differentiation protocols do not appear to be more appropriate for the generation of mature neurons than the strategies used here. However, as discussed in Chapter VII, there are a number of intrinsic properties that could impact the ability of a neuron to change

synaptic strength in response to plasticity protocols. One outstanding question from the current work is whether the enhanced intrinsic maturity observed in iPSC-mNgn2 neurons (see Chapter V) could enable these neurons to undergo synaptic plasticity.

The use of inducible neurogenin-2 constructs enabled the temporal control of neurogenin-2 expression. However, this method requires high viral efficiency as it is necessary for cells to be transduced independently with both rtTa and TetO-mNgn2-T2A-Puro lentivirus. Low copy number of integrated transgenes can linearly correlate with transgene expression, however, high viral transduction efficiency, as was typically observed in NPCs, results in a wide variation in the transgene copy number per cell and can result in considerable variability in transgene expression between cells [485]. Indeed, the functional properties of neurogenin-2 neurons were heterogeneous, which may reflect transgene expression variability. Further investigation would be required to determine whether the relative level of neurogenin-2 expression correlates with neuronal maturation. In addition, doxycycline was added on day 0 and maintained during the culture period to induce neurogenin-2 expression throughout the experiment. Whilst this was consistent with the original protocol from Zhang et al., (2013), Ho et al., (2015) reported that only a short period of neurogenin-2 induction was sufficient to upregulate the expression of genes associated with neuronal differentiation. Although this was assessed after only 14 days and differences arising from the limited duration of neurogenin-2 expression may manifest later [375]. Further work is required to establish whether prolonged neurogenin-2 expression is required for the functional effects, or whether the expression of this pro-neural transcription factor is detrimental to long-term neuronal maturation, as neurogenin-2 is not expressed by mature adult neurons [486]. There are also questions regarding the artificial nature of the manipulations used to promote the generation of mature neurons, which may result in the acquisition of neuronal characteristics that do not exist *in vivo*. For example, the mechanism by which exogenous neurogenin-2 expression promotes neuronal maturation is unknown, and may simply accelerate

the transcriptional timeline of development. Alternatively, exogenous neurogen-2 may bypass the activation of developmental signalling pathways that are required for functional maturation.

At present, the electrophysiological characterization of neurons derived from alternative differentiation protocols suggest that other current strategies are unlikely to enhance neuronal maturation above that achieved by the neurogenin-2 differentiation described in this thesis. Whilst the pro-maturational consequences of neurogenin-2 expression are beneficial, further investigations may be necessary to determine how closely neurogenin-2 neurons resemble those found *in vivo*.

8.3.3. How may cortical cell types that are not present in iPSC-derived cortical cultures contribute to neuronal function and disease pathology?

The modelling of AD using human iPSC-derived cortical cultures that contain primarily glutamatergic neurons is somewhat simplistic. The cortex is comprised of diverse, interacting cell types, which include GABAergic neurons, astrocytes and microglia. Some of these occur in low numbers in the iPSC-derived cortical cultures, whilst others are entirely absent. Furthermore, these cell types have been reported to have a role in the modulation of excitatory synaptic maturation or an involvement in AD pathology. Below, I will discuss each of these cell types in turn, considering how they might impact iPSC-based investigations into synaptic phenotypes in the context of AD.

Astrocytes

The pro-maturational effects that astrocytes have on iPSC-derived neurons, as demonstrated in Chapter IV, has resulted in the increasing use of astrocyte co-culture in iPSC studies [162, 163, 356]. Given the abundance of astrocytes in the brain, the inclusion of this cell type seems necessary for a physiologically-relevant iPSC-derived cortical model. Whilst the benefit of rodent astrocytes upon neuronal function are evident, the use of human astrocytes may better promote neuronal maturation and the support of synaptic plasticity [487-490]. This idea is supported by studies in in

a human glial chimeric mouse, which displayed enhanced LTP and learning [491]. In comparison to rodent astrocytes, human astrocytes span a larger area, have more extensive processes and faster calcium transients [492]. Researchers are exploring methods to generate human astrocytes from iPSCs, which typically required extensive culture periods and the resulting cells can exhibit immature properties [487-490]. Future experiments exploring the impact of substituting rat astrocytes for human iPSC-derived astrocytes could determine whether there are species-specific effects associated with astrocyte co-culture that can enhance neuronal maturation. However, it would be important to first establish an iPSC-derived astrocyte differentiation protocol that generates astrocytes with mature functional properties in order to assess the full potential of incorporating this cell type into iPSC-derived cortical cultures.

The generation of human iPSC-derived astrocytes would also be advantageous for the investigation of non-cell autonomous effects, as this approach would enable the generation of neuron-astrocyte co-cultures derived from the same individual. A study using rodent ESCs has shown that the co-culture of healthy motor neurons with astrocytes that express an ALS-associated SOD1 mutation results in decreased survival of motor neurons [493]. This was the first account demonstrating the importance of the astrocyte genotype on neurotoxicity in a model of ALS [493]. Non-cell autonomous effects mediated by astrocytes may also contribute to pathogenesis in AD. In AD astrocytes acquire an activated phenotype and have been found to associate with Aβ-plaques [494]. Astrocytes have the ability to uptake and degrade Aβ [495] and whilst this response may be protective, at least initially, the accumulation of Aβ in astrocytes can promote astrocyte-mediated Aβ-secretion and cause an impairment of astrocyte function [496, 497]. The application of Aβ to rodent primary cultures containing astrocytes has been shown to enhance neuronal toxicity, which may be partly caused by a decreased ability for the astrocytes to sustain neuronal viability [496, 498]. A human iPSC-derived model of AD has also reported aberrant properties in iPSC-derived astrocytes which harboured the PSEN1 ΔE9 mutation and, when co-cultured with healthy control

neurons, caused a reduction of neuronal calcium transient amplitude in response to exogenous neurotransmitter application [499].

Typically, as in this thesis, the assessment of Aβ-peptide secretion is performed on iPSC-derived neurons that have been cultured alone [164-166, 500]. However, the co-culture of human ESC-derived neurons with rodent astrocytes has been shown to abolish ApoE isoform associated differences in Aβ peptide secretion that were detected in neurons cultured alone [501]. Additional experiments comparing the composition of secreted Aβ peptides in medium from cell cultured alone and with rat astrocytes would establish whether the Aβ phenotype observed in fAD patient iPSC-derived neurons is affected by the presence of astrocytes. This should be ascertained before the assessment of synaptic phenotypes in fAD patient-iPSC derived cortical cultures, which are thought to be downstream of alterations in Aβ [8].

GABAergic neurons

Excitatory glutamatergic neurons are the predominant neuronal cell type in the cortex, accounting for approximately 80 % of the neuronal population, whilst GABAergic neurons comprise the remaining 20 % [502]. Functional GABAergic neurons were present in the iPSC-derived cortical cultures described in this thesis however, the number of GABAergic neurons was below physiological levels. GABAergic neurons have important roles in both the developing and adult cortex, and their incorporation into human iPSC-derived models is likely to be crucial for complex patterns of synaptic transmission. In the adult cortex, GABAergic neurons have a largely inhibitory action and are highly connected to pyramidal cells, thereby exerting a strong influence over excitatory output [479, 503]. GABAergic neuronal populations are diverse and vary in their spatial patterns of innervation onto excitatory neurons, and as a result have many functional roles [503]. GABAergic neurons can regulate excitatory neuronal firing, prevent runaway excitation, shape oscillatory activity and modulate synaptic plasticity. The balance between excitation and inhibition

(E/I balance) is essential for normal circuit function, whilst an aberrant E/I balance can lead to pathological activity, such as epileptogenesis [503].

Animal studies have identified that in the developing cortex GABA actually has a primarily depolarizing action and can often excite target neurons [504-506]. Furthermore, GABAergic neurons not only mature before glutamatergic neurons, but also form the first synapses [439, 505]. Studies have also shown that GABA-mediated depolarizing input is critical for normal glutamatergic synapse formation [506, 507]. In rodents where GABA had been artificially converted to exert a hyperpolarizing effect, the frequency of spontaneous excitatory transmission in cortical neurons was greatly reduced [507]. The enabling effect that GABA has on functional excitatory synapse formation is thought to occur through the unsilencing of synapses. It has been suggested that GABA acts synergistically with glutamate to provide a sufficient depolarization to relieve the NMDA receptor voltage-dependent block, and thereby trigger an LTP-like mechanism that causes the insertion of synaptic AMPA receptors [353, 507]. Interestingly, the promotion of excitatory synapse formation elicited by BDNF and NT-3 in rodent cultured neurons affects the morphological properties of GABAergic neurons, not glutamatergic neurons, suggesting a key role for this cell type in mediating the effects of neurotrophic factors [347].

There have been several reports describing the directed differentiation of human iPSCs to a ventral fate and the subsequent generation of a neuronal population enriched for GABAergic neurons, which occurs over a protracted time period [508-513]. Alternatively, GABAergic neurons can also be generated by expressing a combination of transcription factors [422]. Some studies have begun to explore the interactions between iPSC-derived GABAergic and glutamatergic neurons by combining the two populations in 3D and 2D cultures, which have demonstrated functional synapse formation between these cell types and GABAergic involvement in network activity patterns [422, 513]. In contrast to findings in animal studies, a small number of human iPSC-derived neuronal studies have reported that spontaneous excitatory synaptic transmission was observed before

inhibitory synaptic activity in cultures containing glutamatergic and GABAergic neurons [276, 514]. Further work is needed to determine how closely iPSC-derived GABAergic neurons resemble mature adult interneurons, or whether their presence affects excitatory synapse formation.

Microglia

Microglia are not derived from a neural lineage, but instead are generated in the yolk-sac and migrate into the brain during development. Microglia are considered to be the resident immune cells of the brain and are involved in the phagocytosis of cellular debris, synaptic pruning, and can become activated in response to injury or disease and release proinflammatory factors [515]. The identification of several genes as risk factors for sporadic AD that are highly expressed by microglia, such as *TREM2* and *ABCA7*, has generated increased interest in the role of these cells in AD [43, 516-518].

Microglia have also been shown to modulate and refine synaptic connectivity in animal studies [519]. In early postnatal development, immature microglia have been reported to promote spine and synapse formation in rodent cortical neurons *in vitro* and *in vivo* [520, 521]. Later in development, microglia have a key role in refining neuronal circuitry through the remodelling and elimination of synapses, known as synapse pruning [522]. Several protocols have been developed for the differentiation of microglia from iPSCs, which have been reported to adopt a dynamic and mature morphology when co-cultured with iPSC-derived cortical neurons [523-527].

As briefly reviewed above, interactions between different cell types is likely to be important for the generation of mature phenotypes and disease modelling. As a result, iPSC-derived models are increasingly combining multiple cell types to investigate these interactions. For example, a recent study used a 3D microfluidic chamber that contained a tri-culture of human neurons, astrocytes and microglia as a platform for the study of AD-associated inflammation [528]. Currently, such models are in their infancy and further work is required to establish culture conditions for the

growth of multiple cell types and to determine the impact of other cortical cell types upon excitatory synaptogenesis and maturation and disease pathogenesis.

8.3.4. What factors limit the functional maturation of iPSC-derived neurons and how might they be overcome?

There is mounting evidence that the differentiation and maturation of human iPSC-derived models is strictly governed by a species-specific developmental timeframe. The *in vivo* timing of cortical development in humans is more than 10 times longer than in mice [319]. Protocols that use directed differentiation of stem cells, which aim to mimic the patterning signals that occur in development, quite clearly capture this species-specific timeline [149, 161, 317, 318, 529]. Neuronal differentiation and maturation of cultured mouse ESCs occurs far more quickly than that exhibited by human stem cells [149, 161, 317, 318]. A key factor involved in this process appears to be the species-specific behaviour of neural progenitor cells. A study by Otani et al., (2016) demonstrated that human stem cell-derived NPCs underwent a longer proliferative phase and more frequent symmetric divisions, which resulted in a greater expansion of the progenitor pool than observed for non-human primate stem cell-derived NPCs [529]. Although neurogenesis started at a similar time for human and non-human primates, the onset of upper-layer neuron generation was delayed in the human cortical cultures. Furthermore, the development of action potential firing occurred later in the human stem-cell derived neurons, in comparison to those generated from non-human primates. Interestingly, the species-specific timing of cortical neurogenesis was comparable for 2D and 3D cultures and was conserved by NPCs that were cultured with NPCs from another species [529]. Such an “intrinsic clock” of stem-cell derived neuronal differentiation and maturation is further exhibited through transplantation studies. Grafting of dopaminergic NPCs into the midbrain of 6-OHDA lesioned rats, a commonly used rodent model of Parkinson’s disease, demonstrated an improvement of motor function in just a few weeks using cells derived from mouse ESCs [530-532]. Comparatively, a significant behavioural recovery was not observed in rats

grafted with human ESC-derived cells until 4-5 months post-transplantation [533, 534]. Similar experiments using foetal tissue-derived grafts have also demonstrated slow behavioural recovery times for rats transplanted with human cells, which were shorter when using cells isolated from pigs, and quicker still for mouse-derived grafts [535]. These data indicate that species-specific aspects of differentiation are not unique to stem-cell derived cells.

The grafting of stem-cell derived cells into rodents offers a method to grow cells in a far more physiological environment than that currently generated by 2D or 3D cell culture protocols. Interestingly, a study assessing the functional properties of human ESC-derived neurons that had been grafted into mouse cortex bore a strong resemblance to mature adult neurons [161]. However, these properties were reported for only a small number of neurons and were assessed after 9 months post-transplantation [161]. During the post-transplantation period, the human ESC-derived neurons also exhibited a striking morphological maturation over time and showed *MAPT* transcript expression similar to that observed in the adult human brain [161, 184]. Studies that have performed transplantation of human stem-cell derived neurons have demonstrated the synaptic integration of grafted cells into host circuitry [158, 161, 536, 537], and perhaps more remarkably, their ability to induce behavioural improvements in disease models, as described above. These studies support the *in vitro* observations of cell-autonomous developmental timing, but perhaps suggest that the *in vivo* environment may provide greater support for mature neurons. This approach could provide a platform to investigate synaptic plasticity at human synapses, which would firstly require the degree of connectivity between human grafted cells to be established. Recently, brain organoids have been transplanted into rodents and exhibited neuronal activity and vascularisation by the host [538]. This strategy is likely to provide a greater probability of intra-graft connectivity, although the effect of host-cell signals would be diminished. However, the complexity and time required for such experiments is likely to prohibit their routine use. Transplantation of human ESC-derived neurons into rodent slice cultures has been tested, and may provide a simpler

alternative, but is limited by the short viability of the host tissue [539, 540]. Nevertheless, the successful growth of mature functional neurons in rodent primary cultures suggest that the *in vitro* environment can provide sufficient support for mature neurons.

The protracted time-scale of directed human neuronal differentiation is likely to sway researchers towards the further use and development of transcription-factor based differentiation protocols. Whilst neuronal differentiation with neurogenin-2 is a simple method that can generate active neuronal networks, the functional results obtained from the prolonged culture of human iPSC-derived neurons expressing neurogenin-2 may suggest that this approach has a limited maturation potential [158, 270]. The derivation of the BAM-factor neuronal conversion protocol in mouse ESCs clearly demonstrated the synergistic action of multiple transcription factors in the generation of functional neuronal properties [152]. Neurogenin-2 is a pro-neural transcription factor, which can initiate neuronal differentiation, but is downregulated during maturation and is not expressed by adult mature neurons [371, 486]. Perhaps the additional expression of other, possibly unidentified, transcription factors that are expressed later in neuronal differentiation, may be able to further advance neuronal maturation in a 2D culture setting. A transcriptomic analysis of developing rodent cultures at different maturational stages may provide further insights into transcription factors that are involved in neuronal differentiation and maturation. A similar comparison of iPSC-derived neuronal transcriptomes with mature human neurons may also highlight subsets of genes that are absent or poorly expressed, which could be candidates for future transcription-factor based iPSC-neuronal differentiation approaches.

8.3.5. How well can diseases of aging be modelled using iPSC-derived neurons?

The species-specific timeline of development is likely to pose an additional challenge for modelling diseases of aging, such as AD. During development the process of maturation is considered to be the gradual acquisition of functional properties, whilst aging marks a period of deteriorating

functional capacity [541]. Although iPSCs can be generated from aged donors, the process of reprogramming has been reported to erase age-dependent differences in cellular phenotypes and transcriptional profiles [542, 543]. To address this, researchers have begun to develop strategies to generate age-related phenotypes in iPSC-derived cells. To this end, Miller et al., (2013) explored the use of progerin in a human iPSC-derived model of Parkinson's disease [543]. Progerin is a pathological protein that accumulates in the nuclear membrane of cells in patients with Hutchinson-Gilford progeria syndrome, which causes premature aging [544]. The overexpression of progerin in iPSC-derived dopaminergic neurons was found to restore a number of age-related markers that are lost during the reprogramming of the donor fibroblasts [543]. The expression of progerin in familial Parkinson's disease (PD) patient iPSC-derived dopaminergic neurons resulted in the exhibition of several disease-associated phenotypes, which were not evident otherwise. These phenotypes were consistent with the age-related pathology observed in PD patients, such as increased cell death, an enlargement of mitochondria, and greater loss of cells positive for the dopaminergic neuronal marker TH that had been grafted into a mouse model of PD [543]. Meanwhile, others have used cellular stressors to uncover disease-associated phenotypes in iPSC-derived neurons, which were not exhibited under control conditions, and to demonstrate enhanced vulnerability of patient-derived cells [545]. An alternative approach which prevents cellular rejuvenation has been to avoid reprogramming cells into iPSCs altogether. Instead, the direct conversion of fibroblasts into neurons has been found to retain cellular markers of age and age-related transcriptional profiles. The neuronal conversion efficiency is low with this approach, although was reported to be unaffected by the donor age, which ranged from 0-89 years of age [542]. Similarly, there was no apparent effect of donor age upon neuronal function, supporting the idea that aging and maturation are not equivalent processes. This implies that aging is likely to present a further challenge, operating beyond neuronal maturation, for the demonstration of synaptic phenotypes and other disease-related changes in iPSC-derived models of AD. The

strategies summarised above provide several options that could be applied to iPSC-derived models of AD and may be beneficial in promoting the expression of disease-related phenotypes.

8.4. Concluding remarks

In this thesis I have generated human iPSC-derived cortical neurons from healthy control individuals and fAD patients. These neurons were able to exhibit a disease associated biochemical phenotype, but displayed immature functional properties. Firstly, I explored and refined methods to promote the functional maturation of human iPSC-derived cortical neurons. Secondly, I performed the first characterization of excitatory monosynaptic connections in human iPSC-derived cortical cultures. The properties of excitatory monosynaptic connections were found to be similar to those described in rodent cortex and exhibited robust expression of functional synaptic AMPA and NMDA receptors. Using dual-patch clamp electrophysiology, I found that the probability of detecting a monosynaptic connection was low. However, I demonstrated that the expression of ChR2 in a subset of neurons could enable the generation of light-evoked monosynaptic responses, which were detected more frequently. Lastly, I explored synaptic plasticity in human iPSC-derived cortical cultures, which could not be induced at monosynaptic connections. Similarly, miniature excitatory synaptic transmission was unaffected by a cLTP protocol. However, using ChR2, I show that prolonged activation of pre-synaptic neurons during culturing induces a potentiation of miniature excitatory current amplitude, which was primarily driven by a mature subset of post-synaptic neurons. This study provides direct evidence for an activity-dependent change in synaptic efficacy in human iPSC-derived cortical neurons, whilst indicating that neuronal maturity continues to limit the investigation of synaptic transmission in these cultures. This work has extended the range of experimental assays that can be applied to human iPSC-derived cortical neurons for the study of excitatory synaptic transmission, and provides a foundation for future investigations into synaptic plasticity.

References

1. Lepeta, K., et al., *Synaptopathies: synaptic dysfunction in neurological disorders – A review from students to students.* Journal of Neurochemistry, 2016. **138**(6): p. 785-805.
2. Prince, M.J., et al., *World Alzheimer Report 2015 - The Global Impact of Dementia*. An analysis of prevalence, incidence, cost and trends. 2015: Alzheimer's Disease International.
3. Burns, A. and S. Iliffe, *Alzheimer's disease.* BMJ, 2009. **338**.
4. Hoyert, D.L. and H.M. Rosenberg, *Alzheimer's disease as a cause of death in the United States.* Public Health Rep, 1997. **112**(6): p. 497-505.
5. Cavanaugh, S.E., J.J. Pippin, and N.D. Barnard, *Animal models of Alzheimer disease: historical pitfalls and a path forward.* Altex, 2014. **31**(3): p. 279-302.
6. Yiannopoulou, K.G. and S.G. Papageorgiou, *Current and future treatments for Alzheimer's disease.* Therapeutic Advances in Neurological Disorders, 2013. **6**(1): p. 19-33.
7. Cummings, J.L., T. Morstorf, and K. Zhong, *Alzheimer's disease drug-development pipeline: few candidates, frequent failures.* Alzheimers Res Ther, 2014. **6**(4): p. 37.
8. Selkoe, D.J. and J. Hardy, *The amyloid hypothesis of Alzheimer's disease at 25 years.* EMBO Molecular Medicine, 2016. **8**(6): p. 595-608.
9. Shipton, O.A., et al., *Tau protein is required for amyloid {beta}-induced impairment of hippocampal long-term potentiation.* J Neurosci, 2011. **31**(5): p. 1688-92.
10. Rapoport, M., et al., *Tau is essential to β-amyloid-induced neurotoxicity.* Proceedings of the National Academy of Sciences, 2002. **99**(9): p. 6364-6369.
11. Roberson, E.D., et al., *Reducing Endogenous Tau Ameliorates Amyloid ß-Induced Deficits in an Alzheimer's Disease Mouse Model.* Science, 2007. **316**(5825): p. 750-754.
12. Ballatore, C., V.M.Y. Lee, and J.Q. Trojanowski, *Tau-mediated neurodegeneration in Alzheimer's disease and related disorders.* Nature Reviews Neuroscience, 2007. **8**: p. 663.
13. Ittner, L.M. and J. Götz, *Amyloid-β and tau — a toxic pas de deux in Alzheimer's disease.* Nature Reviews Neuroscience, 2010. **12**: p. 67.
14. Ittner, L.M., et al., *Dendritic Function of Tau Mediates Amyloid-β Toxicity in Alzheimer's Disease Mouse Models.* Cell, 2010. **142**(3): p. 387-397.
15. Ronicke, R., et al., *Early neuronal dysfunction by amyloid beta oligomers depends on activation of NR2B-containing NMDA receptors.* Neurobiol Aging, 2011. **32**(12): p. 2219-28.
16. Zhang, Y., et al., *Dysfunction of NMDA receptors in Alzheimer's disease.* Neurological Sciences, 2016. **37**(7): p. 1039-1047.
17. Snyder, E.M., et al., *Regulation of NMDA receptor trafficking by amyloid-beta.* Nat Neurosci, 2005. **8**(8): p. 1051-8.
18. Braak, H. and E. Braak, *Evolution of the neuropathology of Alzheimer's disease.* Acta Neurologica Scandinavica, 1996. **94**(S165): p. 3-12.
19. Braak, H. and E. Braak, *Neuropathological stageing of Alzheimer-related changes.* Acta Neuropathol, 1991. **82**(4): p. 239-59.
20. Nelson, P.T., et al., *Correlation of Alzheimer Disease Neuropathologic Changes With Cognitive Status: A Review of the Literature.* Journal of neuropathology and experimental neurology, 2012. **71**(5): p. 362-381.
21. Price, J.L., et al., *Neuropathology of nondemented aging: Presumptive evidence for preclinical Alzheimer disease.* Neurobiology of Aging, 2009. **30**(7): p. 1026-1036.
22. Shankar, G.M., et al., *Amyloid β-Protein Dimers Isolated Directly from Alzheimer Brains Impair Synaptic Plasticity and Memory.* Nature medicine, 2008. **14**(8): p. 837-842.
23. Esparza, T.J., et al., *Amyloid-beta oligomerization in Alzheimer dementia versus high-pathology controls.* Ann Neurol, 2013. **73**(1): p. 104-19.
24. Hebert, L.E., et al., *Alzheimer disease in the United States (2010-2050) estimated using the 2010 census.* Neurology, 2013. **80**(19): p. 1778-83.

25. Bekris, L.M., et al., *Genetics of Alzheimer Disease.* Journal of geriatric psychiatry and neurology, 2010. **23**(4): p. 213-227.
26. Cruts, M., J. Theuns, and C. Van Broeckhoven, *Locus-specific mutation databases for neurodegenerative brain diseases.* Human Mutation, 2012. **33**(9): p. 1340-1344.
27. Zhang, Y.-w., et al., *APP processing in Alzheimer's disease.* Molecular Brain, 2011. **4**: p. 3-3.
28. Xu, X., *γ-Secretase Catalyzes Sequential Cleavages of the AβPP Transmembrane Domain.* Journal of Alzheimer's disease : JAD, 2009. **16**(2): p. 211-224.
29. Burdick, D., et al., *Assembly and aggregation properties of synthetic Alzheimer's A4/beta amyloid peptide analogs.* J Biol Chem, 1992. **267**(1): p. 546-54.
30. Weggen, S. and D. Beher, *Molecular consequences of amyloid precursor protein and presenilin mutations causing autosomal-dominant Alzheimer's disease.* Alzheimer's Research & Therapy, 2012. **4**(2): p. 9-9.
31. Head, E., et al., *Alzheimer's Disease in Down Syndrome.* European journal of neurodegenerative disease, 2012. **1**(3): p. 353-364.
32. Shen, J. and R.J. Kelleher, 3rd, *The presenilin hypothesis of Alzheimer's disease: evidence for a loss-of-function pathogenic mechanism.* Proc Natl Acad Sci U S A, 2007. **104**(2): p. 403-9.
33. Murayama, O., et al., *Enhancement of amyloid β 42 secretion by 28 different presenilin 1 mutations of familial Alzheimer's disease.* Neuroscience Letters, 1999. **265**(1): p. 61-63.
34. Ghetti, B., et al., *Invited review: Frontotemporal dementia caused by microtubule-associated protein tau gene (MAPT) mutations: a chameleon for neuropathology and neuroimaging.* Neuropathology and Applied Neurobiology, 2015. **41**(1): p. 24-46.
35. *Mutations Database, Alzforum.* http://www.alzforum.org/mutations. 2016, Accessed 19/9/2018.
36. Holmes, C. and S. Lovestone, *The clinical phenotype of familial and sporadic late onset Alzheimer's disease.* Int J Geriatr Psychiatry, 2002. **17**(2): p. 146-9.
37. Tosto, G. and C. Reitz, *Genome-wide Association Studies in Alzheimer's Disease: A Review.* Current Neurology and Neuroscience Reports, 2013. **13**(10): p. 381.
38. Corder, E., et al., *Gene dose of apolipoprotein E type 4 allele and the risk of Alzheimer's disease in late onset families.* Science, 1993. **261**(5123): p. 921-923.
39. Corder, E.H., et al., *Protective effect of apolipoprotein E type 2 allele for late onset Alzheimer disease.* Nat Genet, 1994. **7**(2): p. 180-184.
40. Osenkowski, P., et al., *Direct and potent regulation of gamma-secretase by its lipid microenvironment.* J Biol Chem, 2008. **283**(33): p. 22529-40.
41. Jiang, Q., et al., *ApoE promotes the proteolytic degradation of Abeta.* Neuron, 2008. **58**(5): p. 681-93.
42. Deane, R., et al., *apoE isoform-specific disruption of amyloid beta peptide clearance from mouse brain.* J Clin Invest, 2008. **118**(12): p. 4002-13.
43. Van Cauwenberghe, C., C. Van Broeckhoven, and K. Sleegers, *The genetic landscape of Alzheimer disease: clinical implications and perspectives.* Genet Med, 2016. **18**(5): p. 421-430.
44. Gotz, J. and L.M. Ittner, *Animal models of Alzheimer's disease and frontotemporal dementia.* Nat Rev Neurosci, 2008. **9**(7): p. 532-544.
45. Sturchler-Pierrat, C., et al., *Two amyloid precursor protein transgenic mouse models with Alzheimer disease-like pathology.* Proc Natl Acad Sci U S A, 1997. **94**(24): p. 13287-92.
46. Sadowski, M., et al., *Amyloid-beta deposition is associated with decreased hippocampal glucose metabolism and spatial memory impairment in APP/PS1 mice.* J Neuropathol Exp Neurol, 2004. **63**(5): p. 418-28.
47. Duff, K., et al., *Increased amyloid-beta42(43) in brains of mice expressing mutant presenilin 1.* Nature, 1996. **383**(6602): p. 710-3.
48. Borchelt, D.R., et al., *Familial Alzheimer's disease-linked presenilin 1 variants elevate Abeta1-42/1-40 ratio in vitro and in vivo.* Neuron, 1996. **17**(5): p. 1005-13.

49. Oakley, H., et al., *Intraneuronal beta-amyloid aggregates, neurodegeneration, and neuron loss in transgenic mice with five familial Alzheimer's disease mutations: potential factors in amyloid plaque formation.* J Neurosci, 2006. **26**(40): p. 10129-40.
50. Schindowski, K., et al., *Alzheimer's Disease-Like Tau Neuropathology Leads to Memory Deficits and Loss of Functional Synapses in a Novel Mutated Tau Transgenic Mouse without Any Motor Deficits.* The American Journal of Pathology, 2006. **169**(2): p. 599-616.
51. Oddo, S., et al., *Triple-Transgenic Model of Alzheimer's Disease with Plaques and Tangles: Intracellular Aβ and Synaptic Dysfunction.* Neuron, 2003. **39**(3): p. 409-421.
52. Drummond, E. and T. Wisniewski, *Alzheimer's disease: experimental models and reality.* Acta neuropathologica, 2017. **133**(2): p. 155-175.
53. Kuo, Y.-M., et al., *Comparative Analysis of Amyloid-β Chemical Structure and Amyloid Plaque Morphology of Transgenic Mouse and Alzheimer's Disease Brains.* Journal of Biological Chemistry, 2001. **276**(16): p. 12991-12998.
54. Goedert, M., et al., *Cloning and sequencing of the cDNA encoding an isoform of microtubule-associated protein tau containing four tandem repeats: differential expression of tau protein mRNAs in human brain.* The EMBO journal, 1989. **8**(2): p. 393-399.
55. McMillan, P., et al., *Tau isoform regulation is region- and cell-specific in mouse brain.* The Journal of comparative neurology, 2008. **511**(6): p. 788-803.
56. Andorfer, C., et al., *Hyperphosphorylation and aggregation of tau in mice expressing normal human tau isoforms.* Journal of Neurochemistry, 2003. **86**(3): p. 582-590.
57. Hanes, J., et al., *Rat tau proteome consists of six tau isoforms: implication for animal models of human tauopathies.* J Neurochem, 2009. **108**(5): p. 1167-76.
58. Cohen, R.M., et al., *A Transgenic Alzheimer Rat with Plaques, Tau Pathology, Behavioral Impairment, Oligomeric Aβ, and Frank Neuronal Loss.* The Journal of Neuroscience, 2013. **33**(15): p. 6245-6256.
59. Inestrosa, N.C., et al., *Human-like rodent amyloid-β-peptide determines Alzheimer pathology in aged wild-type Octodon degu.* Neurobiology of Aging, 2005. **26**(7): p. 1023-1028.
60. Steffen, J., et al., *Revisiting rodent models: Octodon degus as Alzheimer's disease model?* Acta Neuropathologica Communications, 2016. **4**(1): p. 91.
61. van Groen, T., et al., *Age-related brain pathology in Octodon degu: Blood vessel, white matter and Alzheimer-like pathology.* Neurobiology of Aging, 2011. **32**(9): p. 1651-1661.
62. Trommer, B.L., et al., *ApoE isoform affects LTP in human targeted replacement mice.* Neuroreport, 2004. **15**(17): p. 2655-8.
63. Bales, K.R., et al., *Lack of apolipoprotein E dramatically reduces amyloid [beta]-peptide deposition.* Nat Genet, 1997. **17**(3): p. 263-264.
64. Dodart, J.-C., et al., *Gene delivery of human apolipoprotein E alters brain Aβ burden in a mouse model of Alzheimer's disease.* Proceedings of the National Academy of Sciences of the United States of America, 2005. **102**(4): p. 1211-1216.
65. Sparks, D.L., et al., *Induction of Alzheimer-like β-Amyloid Immunoreactivity in the Brains of Rabbits with Dietary Cholesterol.* Experimental Neurology, 1994. **126**(1): p. 88-94.
66. Sarasa, M. and P. Pesini, *Natural Non-Trasgenic Animal Models for Research in Alzheimer's Disease.* Current Alzheimer Research, 2009. **6**(2): p. 171-178.
67. Terry, R.D., et al., *Physical basis of cognitive alterations in Alzheimer's disease: synapse loss is the major correlate of cognitive impairment.* Ann Neurol, 1991. **30**(4): p. 572-80.
68. Davies, C.A., et al., *A quantitative morphometric analysis of the neuronal and synaptic content of the frontal and temporal cortex in patients with Alzheimer's disease.* J Neurol Sci, 1987. **78**(2): p. 151-64.
69. Masliah, E., et al., *Altered expression of synaptic proteins occurs early during progression of Alzheimer's disease.* Neurology, 2001. **56**(1): p. 127-129.

70. Naslund, J., et al., *Correlation between elevated levels of amyloid beta-peptide in the brain and cognitive decline.* Jama, 2000. **283**(12): p. 1571-7.
71. Mucke, L., et al., *High-Level Neuronal Expression of Aβ1–42 in Wild-Type Human Amyloid Protein Precursor Transgenic Mice: Synaptotoxicity without Plaque Formation.* The Journal of Neuroscience, 2000. **20**(11): p. 4050-4058.
72. Chapman, P.F., et al., *Impaired synaptic plasticity and learning in aged amyloid precursor protein transgenic mice.* Nat Neurosci, 1999. **2**(3): p. 271-276.
73. Chen, Q.-S., et al., *Impairment of hippocampal long-term potentiation by Alzheimer amyloid β-peptides.* Journal of Neuroscience Research, 2000. **60**(1): p. 65-72.
74. Wang, Q., et al., *Block of Long-Term Potentiation by Naturally Secreted and Synthetic Amyloid β-Peptide in Hippocampal Slices Is Mediated via Activation of the Kinases c-Jun N-Terminal Kinase, Cyclin-Dependent Kinase 5, and p38 Mitogen-Activated Protein Kinase as well as Metabotropic Glutamate Receptor Type 5.* The Journal of Neuroscience, 2004. **24**(13): p. 3370-3378.
75. Moechars, D., et al., *Early Phenotypic Changes in Transgenic Mice That Overexpress Different Mutants of Amyloid Precursor Protein in Brain.* Journal of Biological Chemistry, 1999. **274**(10): p. 6483-6492.
76. Dewachter, I., et al., *Neuronal deficiency of presenilin 1 inhibits amyloid plaque formation and corrects hippocampal long-term potentiation but not a cognitive defect of amyloid precursor protein [V717I] transgenic mice.* J Neurosci, 2002. **22**(9): p. 3445-53.
77. Bliss, T.V. and G.L. Collingridge, *A synaptic model of memory: long-term potentiation in the hippocampus.* Nature, 1993. **361**(6407): p. 31-9.
78. Larson, J., et al., *Alterations in synaptic transmission and long-term potentiation in hippocampal slices from young and aged PDAPP mice.* Brain Research, 1999. **840**(1): p. 23-35.
79. Hsia, A.Y., et al., *Plaque-independent disruption of neural circuits in Alzheimer's disease mouse models.* Proceedings of the National Academy of Sciences, 1999. **96**(6): p. 3228-3233.
80. Battaglia, F., et al., *Cortical plasticity in Alzheimer's disease in humans and rodents.* Biol Psychiatry, 2007. **62**(12): p. 1405-12.
81. Crouzin, N., et al., *Area-Specific Alterations of Synaptic Plasticity in the 5XFAD Mouse Model of Alzheimer's Disease: Dissociation between Somatosensory Cortex and Hippocampus.* PLOS ONE, 2013. **8**(9): p. e74667.
82. Zaman, S.H., et al., *Enhanced Synaptic Potentiation in Transgenic Mice Expressing presenilin 1 Familial Alzheimer's Disease Mutation Is Normalized with a Benzodiazepine.* Neurobiology of Disease, 2000. **7**(1): p. 54-63.
83. Schneider, I., et al., *Mutant Presenilins Disturb Neuronal Calcium Homeostasis in the Brain of Transgenic Mice, Decreasing the Threshold for Excitotoxicity and Facilitating Long-term Potentiation.* Journal of Biological Chemistry, 2001. **276**(15): p. 11539-11544.
84. Parent, A., et al., *Synaptic Transmission and Hippocampal Long-Term Potentiation in Transgenic Mice Expressing FAD-Linked Presenilin 1.* Neurobiology of Disease, 1999. **6**(1): p. 56-62.
85. Begley, J.G., et al., *Altered Calcium Homeostasis and Mitochondrial Dysfunction in Cortical Synaptic Compartments of Presenilin-1 Mutant Mice.* Journal of Neurochemistry, 1999. **72**(3): p. 1030-1039.
86. Seabrook, G.R., et al., *Mechanisms contributing to the deficits in hippocampal synaptic plasticity in mice lacking amyloid precursor protein.* Neuropharmacology, 1999. **38**(3): p. 349-359.
87. Wong, P.C., et al., *Presenilin 1 is required for Notch 1 and Dll1 expression in the paraxial mesoderm.* Nature, 1997. **387**: p. 288.

88. Saura, C.A., et al., *Loss of Presenilin Function Causes Impairments of Memory and Synaptic Plasticity Followed by Age-Dependent Neurodegeneration.* Neuron, 2004. **42**(1): p. 23-36.
89. Zhang, C., et al., *Presenilins are essential for regulating neurotransmitter release.* Nature, 2009. **460**(7255): p. 632-6.
90. Stéphan, A., S. Laroche, and S. Davis, *Generation of Aggregated β-Amyloid in the Rat Hippocampus Impairs Synaptic Transmission and Plasticity and Causes Memory Deficits.* The Journal of Neuroscience, 2001. **21**(15): p. 5703-5714.
91. Cullen, W.K., et al., *Block of LTP in rat hippocampus in vivo by beta-amyloid precursor protein fragments.* Neuroreport, 1997. **8**(15): p. 3213-7.
92. Freir, D.B., C. Holscher, and C.E. Herron, *Blockade of Long-Term Potentiation by β-Amyloid Peptides in the CA1 Region of the Rat Hippocampus In Vivo.* Journal of Neurophysiology, 2001. **85**(2): p. 708-713.
93. Ryan, D.A., et al., *An Improved Method for Generating Consistent Soluble Amyloid-beta Oligomer Preparations for In Vitro Neurotoxicity Studies.* Journal of neuroscience methods, 2010. **190**(2): p. 171-179.
94. Roychaudhuri, R., et al., *Amyloid beta-protein assembly and Alzheimer disease.* J Biol Chem, 2009. **284**(8): p. 4749-53.
95. Podlisny, M.B., et al., *Aggregation of secreted amyloid beta-protein into sodium dodecyl sulfate-stable oligomers in cell culture.* J Biol Chem, 1995. **270**(16): p. 9564-70.
96. Walsh, D.M., et al., *Naturally secreted oligomers of amyloid beta protein potently inhibit hippocampal long-term potentiation in vivo.* Nature, 2002. **416**(6880): p. 535-9.
97. Bayés, À., et al., *Comparative Study of Human and Mouse Postsynaptic Proteomes Finds High Compositional Conservation and Abundance Differences for Key Synaptic Proteins.* PLOS ONE, 2012. **7**(10): p. e46683.
98. Di Lorenzo, F., et al., *P271 Impaired spike timing dependent cortico-cortical plasticity in Alzheimer's disease patients.* Clinical Neurophysiology, 2017. **128**(3): p. e143.
99. Koch, G., et al., *Impaired LTP- but not LTD-like cortical plasticity in Alzheimer's disease patients.* J Alzheimers Dis, 2012. **31**(3): p. 593-9.
100. Di Lorenzo, F., et al., *Long-term potentiation-like cortical plasticity is disrupted in Alzheimer's disease patients independently from age of onset.* Ann Neurol, 2016. **80**(2): p. 202-10.
101. Negoro, T., H. Okura, and A. Matsuyama, *Induced Pluripotent Stem Cells: Global Research Trends.* BioResearch Open Access, 2017. **6**(1): p. 63-73.
102. Eiges, R., et al., *Developmental study of fragile X syndrome using human embryonic stem cells derived from preimplantation genetically diagnosed embryos.* Cell Stem Cell, 2007. **1**(5): p. 568-77.
103. Mateizel, I., et al., *Derivation of human embryonic stem cell lines from embryos obtained after IVF and after PGD for monogenic disorders.* Hum Reprod, 2006. **21**(2): p. 503-11.
104. Biancotti, J.C., et al., *Human embryonic stem cells as models for aneuploid chromosomal syndromes.* Stem Cells, 2010. **28**(9): p. 1530-40.
105. Ding, Q., et al., *A TALEN Genome-Editing System for Generating Human Stem Cell-Based Disease Models.* Cell Stem Cell, 2013. **12**(2): p. 238-251.
106. Verfaillie, C., *Pluripotent stem cells.* Transfusion Clinique et Biologique, 2009. **16**(2): p. 65-69.
107. Evans, M.J. and M.H. Kaufman, *Establishment in culture of pluripotential cells from mouse embryos.* Nature, 1981. **292**(5819): p. 154-156.
108. Thomson, J.A., et al., *Embryonic Stem Cell Lines Derived from Human Blastocysts.* Science, 1998. **282**(5391): p. 1145-1147.
109. Takahashi, K. and S. Yamanaka, *Induction of Pluripotent Stem Cells from Mouse Embryonic and Adult Fibroblast Cultures by Defined Factors.* Cell, 2006. **126**(4): p. 663-676.

110. Takahashi, K., et al., *Induction of Pluripotent Stem Cells from Adult Human Fibroblasts by Defined Factors.* Cell, 2007. **131**(5): p. 861-872.
111. Zhang, X.-B., *Cellular Reprogramming of Human Peripheral Blood Cells.* Genomics, Proteomics & Bioinformatics, 2013. **11**(5): p. 264-274.
112. Beltrao-Braga, P.C., et al., *Feeder-free derivation of induced pluripotent stem cells from human immature dental pulp stem cells.* Cell Transplant, 2011. **20**(11-12): p. 1707-19.
113. Galat, V., et al., *Transgene Reactivation in Induced Pluripotent Stem Cell Derivatives and Reversion to Pluripotency of Induced Pluripotent Stem Cell-Derived Mesenchymal Stem Cells.* Stem Cells and Development, 2016. **25**(14): p. 1060-1072.
114. Fusaki, N., et al., *Efficient induction of transgene-free human pluripotent stem cells using a vector based on Sendai virus, an RNA virus that does not integrate into the host genome.* Proc Jpn Acad Ser B Phys Biol Sci, 2009. **85**(8): p. 348-62.
115. Lister, R., et al., *Hotspots of aberrant epigenomic reprogramming in human induced pluripotent stem cells.* Nature, 2011. **471**(7336): p. 68-73.
116. Hu, S., et al., *Effects of cellular origin on differentiation of human induced pluripotent stem cell–derived endothelial cells.* JCI Insight, 2016. **1**(8): p. e85558.
117. Polo, J.M., et al., *Cell type of origin influences the molecular and functional properties of mouse induced pluripotent stem cells.* Nat Biotechnol, 2010. **28**(8): p. 848-55.
118. Hu, B.-Y., et al., *Neural differentiation of human induced pluripotent stem cells follows developmental principles but with variable potency.* Proceedings of the National Academy of Sciences, 2010. **107**(9): p. 4335-4340.
119. Feng, Q., et al., *Hemangioblastic derivatives from human induced pluripotent stem cells exhibit limited expansion and early senescence.* Stem Cells, 2010. **28**(4): p. 704-12.
120. Narsinh, K.H., et al., *Single cell transcriptional profiling reveals heterogeneity of human induced pluripotent stem cells.* The Journal of Clinical Investigation, 2011. **121**(3): p. 1217-1221.
121. Kim, K., et al., *Epigenetic memory in induced pluripotent stem cells.* Nature, 2010. **467**: p. 285.
122. Rouhani, F., et al., *Genetic Background Drives Transcriptional Variation in Human Induced Pluripotent Stem Cells.* PLOS Genetics, 2014. **10**(6): p. e1004432.
123. Soldner, F., et al., *Generation of Isogenic Pluripotent Stem Cells Differing Exclusively at Two Early Onset Parkinson Point Mutations.* Cell, 2011. **146**(2): p. 318-331.
124. Morgan, P., et al., *Can the flow of medicines be improved? Fundamental pharmacokinetic and pharmacological principles toward improving Phase II survival.* Drug Discovery Today, 2012. **17**(9): p. 419-424.
125. Vargas-Caballero, M., et al., *The use of human neurons for novel drug discovery in dementia research.* Expert Opin Drug Discov, 2016. **11**(4): p. 355-67.
126. McNeish, J., et al., *From Dish to Bedside: Lessons Learned While Translating Findings from a Stem Cell Model of Disease to a Clinical Trial.* Cell Stem Cell, 2015. **17**(1): p. 8-10.
127. Wainger, Brian J., et al., *Intrinsic Membrane Hyperexcitability of Amyotrophic Lateral Sclerosis Patient-Derived Motor Neurons.* Cell Reports, 2014. **7**(1): p. 1-11.
128. Trounson, A. and N.D. DeWitt, *Pluripotent stem cells progressing to the clinic.* Nature Reviews Molecular Cell Biology, 2016. **17**: p. 194.
129. Wertheim, J.A. and J.R. Leventhal, *Induced pluripotent stem cell therapy in transplantation—A potential role for immunologic tolerance.* American journal of transplantation : official journal of the American Society of Transplantation and the American Society of Transplant Surgeons, 2015. **15**(4): p. 887-890.
130. Mandai, M., et al., *Autologous Induced Stem-Cell–Derived Retinal Cells for Macular Degeneration.* New England Journal of Medicine, 2017. **376**(11): p. 1038-1046.

131. Mann, D.M.A., et al., *THE PROGRESSION OF THE PATHOLOGICAL CHANGES OF ALZHEIMER'S DISEASE IN FRONTAL AND TEMPORAL NEOCORTEX EXAMINED BOTH AT BIOPSY AND AT AUTOPSY.* Neuropathology and Applied Neurobiology, 1988. **14**(3): p. 177-195.
132. Hemmati-Brivanlou, A. and D. Melton, *VERTEBRATE NEURAL INDUCTION.* Annual Review of Neuroscience, 1997. **20**(1): p. 43-60.
133. Colas, J.-F. and G.C. Schoenwolf, *Towards a cellular and molecular understanding of neurulation.* Developmental Dynamics, 2001. **221**(2): p. 117-145.
134. Stiles, J. and T.L. Jernigan, *The Basics of Brain Development.* Neuropsychology Review, 2010. **20**(4): p. 327-348.
135. Bystron, I., C. Blakemore, and P. Rakic, *Development of the human cerebral cortex: Boulder Committee revisited.* Nat Rev Neurosci, 2008. **9**(2): p. 110-122.
136. Jiang, X. and J. Nardelli, *Cellular and molecular introduction to brain development.* Neurobiology of Disease, 2016. **92**: p. 3-17.
137. Wonders, C.P. and S.A. Anderson, *The origin and specification of cortical interneurons.* Nat Rev Neurosci, 2006. **7**(9): p. 687-96.
138. Letinic, K., R. Zoncu, and P. Rakic, *Origin of GABAergic neurons in the human neocortex.* Nature, 2002. **417**(6889): p. 645-9.
139. Zhang, S.-C., et al., *In vitro differentiation of transplantable neural precursors from human embryonic stem cells.* Nat Biotech, 2001. **19**(12): p. 1129-1133.
140. Watanabe, K., et al., *Directed differentiation of telencephalic precursors from embryonic stem cells.* Nat Neurosci, 2005. **8**(3): p. 288-296.
141. Watanabe, K., et al., *A ROCK inhibitor permits survival of dissociated human embryonic stem cells.* Nat Biotechnol, 2007. **25**(6): p. 681-6.
142. Eiraku, M., et al., *Self-organized formation of polarized cortical tissues from ESCs and its active manipulation by extrinsic signals.* Cell Stem Cell, 2008. **3**(5): p. 519-32.
143. Kadoshima, T., et al., *Self-organization of axial polarity, inside-out layer pattern, and species-specific progenitor dynamics in human ES cell–derived neocortex.* Proceedings of the National Academy of Sciences, 2013. **110**(50): p. 20284-20289.
144. Mariani, J., et al., *Modeling human cortical development in vitro using induced pluripotent stem cells.* Proceedings of the National Academy of Sciences of the United States of America, 2012. **109**(31): p. 12770-12775.
145. Lancaster, M.A., et al., *Cerebral organoids model human brain development and microcephaly.* Nature, 2013. **501**(7467): p. 10.1038/nature12517.
146. James, D., et al., *TGFbeta/activin/nodal signaling is necessary for the maintenance of pluripotency in human embryonic stem cells.* Development, 2005. **132**(6): p. 1273-82.
147. Schier, A.F., *Nodal signaling in vertebrate development.* Annu Rev Cell Dev Biol, 2003. **19**: p. 589-621.
148. Chambers, S.M., et al., *Highly efficient neural conversion of human ES and iPS cells by dual inhibition of SMAD signaling.* Nature biotechnology, 2009. **27**(3): p. 275-280.
149. Shi, Y., P. Kirwan, and F.J. Livesey, *Directed differentiation of human pluripotent stem cells to cerebral cortex neurons and neural networks.* Nat Protoc, 2012. **7**(10): p. 1836-46.
150. Shi, Y., et al., *Human cerebral cortex development from pluripotent stem cells to functional excitatory synapses.* Nat Neurosci, 2012. **15**(3): p. 477-86, S1.
151. Pasca, A.M., et al., *Functional cortical neurons and astrocytes from human pluripotent stem cells in 3D culture.* Nat Meth, 2015. **12**(7): p. 671-678.
152. Vierbuchen, T., et al., *Direct conversion of fibroblasts to functional neurons by defined factors.* Nature, 2010. **463**(7284): p. 1035-1041.
153. Ladewig, J., et al., *Small molecules enable highly efficient neuronal conversion of human fibroblasts.* Nat Meth, 2012. **9**(6): p. 575-578.
154. Pang, Z.P., et al., *Induction of human neuronal cells by defined transcription factors.* Nature, 2011. **476**(7359): p. 220-223.

155. Yoo, A.S., et al., *MicroRNA-mediated conversion of human fibroblasts to neurons.* Nature, 2011. **476**(7359): p. 228-31.
156. Ring, Karen L., et al., *Direct Reprogramming of Mouse and Human Fibroblasts into Multipotent Neural Stem Cells with a Single Factor.* Cell Stem Cell, 2012. **11**(1): p. 100-109.
157. Thier, M., et al., *Direct conversion of fibroblasts into stably expandable neural stem cells.* Cell Stem Cell, 2012. **10**(4): p. 473-9.
158. Zhang, Y., et al., *Rapid single-step induction of functional neurons from human pluripotent stem cells.* Neuron, 2013. **78**(5): p. 785-98.
159. Paşca, S.P., et al., *Using iPSC-derived neurons to uncover cellular phenotypes associated with Timothy syndrome.* Nature Medicine, 2011. **17**: p. 1657.
160. Israel, M.A., et al., *Probing sporadic and familial Alzheimer's disease using induced pluripotent stem cells.* Nature, 2012. **482**(7384): p. 216-20.
161. Espuny-Camacho, I., et al., *Pyramidal neurons derived from human pluripotent stem cells integrate efficiently into mouse brain circuits in vivo.* Neuron, 2013. **77**(3): p. 440-56.
162. Shcheglovitov, A., et al., *SHANK3 and IGF1 restore synaptic deficits in neurons from 22q13 deletion syndrome patients.* Nature, 2013. **503**(7475): p. 267-71.
163. Brennand, K., et al., *Modeling schizophrenia using hiPSC neurons.* Nature, 2011. **473**(7346): p. 221-225.
164. Kondo, T., et al., *Modeling Alzheimer's disease with iPSCs reveals stress phenotypes associated with intracellular Abeta and differential drug responsiveness.* Cell Stem Cell, 2013. **12**(4): p. 487-96.
165. Moore, S., et al., *APP metabolism regulates tau proteostasis in human cerebral cortex neurons.* Cell Rep, 2015. **11**(5): p. 689-96.
166. Muratore, C.R., et al., *The familial Alzheimer's disease APPV717I mutation alters APP processing and Tau expression in iPSC-derived neurons.* Hum Mol Genet, 2014. **23**(13): p. 3523-36.
167. Shi, Y., et al., *A human stem cell model of early Alzheimer's disease pathology in Down syndrome.* Sci Transl Med, 2012. **4**(124): p. 124ra29.
168. Sproul, A.A., et al., *Characterization and Molecular Profiling of PSEN1 Familial Alzheimer's Disease iPSC-Derived Neural Progenitors.* PLoS ONE, 2014. **9**(1): p. e84547.
169. Yagi, T., et al., *Modeling familial Alzheimer's disease with induced pluripotent stem cells.* Hum Mol Genet, 2011. **20**(23): p. 4530-9.
170. Armijo, E., et al., *Increased susceptibility to Abeta toxicity in neuronal cultures derived from familial Alzheimer's disease (PSEN1-A246E) induced pluripotent stem cells.* Neurosci Lett, 2017. **639**: p. 74-81.
171. Mahairaki, V., et al., *Induced Pluripotent Stem Cells from Familial Alzheimer's Disease Patients Differentiate into Mature Neurons with Amyloidogenic Properties.* Stem Cells and Development, 2014. **23**(24): p. 2996-3010.
172. Chang, C.-Y., et al., *N-butylidenephthalide Attenuates Alzheimer's Disease-Like Cytopathy in Down Syndrome Induced Pluripotent Stem Cell-Derived Neurons.* Scientific Reports, 2015. **5**: p. 8744.
173. Duan, L., et al., *Stem cell derived basal forebrain cholinergic neurons from Alzheimer's disease patients are more susceptible to cell death.* Molecular Neurodegeneration, 2014. **9**: p. 3-3.
174. Hossini, A.M., et al., *Induced pluripotent stem cell-derived neuronal cells from a sporadic Alzheimer's disease donor as a model for investigating AD-associated gene regulatory networks.* BMC Genomics, 2015. **16**(1): p. 84.
175. Woodruff, G., et al., *The Presenilin-1 ΔE9 Mutation Results in Reduced γ-Secretase Activity, but Not Total Loss of PS1 Function, in Isogenic Human Stem Cells.* Cell Reports, 2013. **5**(4): p. 974-985.

176. Honda, M., et al., *The modeling of Alzheimer's disease by the overexpression of mutant Presenilin 1 in human embryonic stem cells.* Biochemical and Biophysical Research Communications, 2016. **469**(3): p. 587-592.
177. Nieweg, K., et al., *Alzheimer's disease-related amyloid-β induces synaptotoxicity in human iPS cell-derived neurons.* Cell Death & Disease, 2015. **6**(4): p. e1709.
178. Vazin, T., et al., *Efficient derivation of cortical glutamatergic neurons from human pluripotent stem cells: a model system to study neurotoxicity in Alzheimer's disease.* Neurobiol Dis, 2014. **62**: p. 62-72.
179. Yang, J., et al., *Early pathogenic event of Alzheimer's disease documented in iPSCs from patients with PSEN1 mutations.* Oncotarget, 2017. **8**(5): p. 7900-7913.
180. Raja, W.K., et al., *Self-Organizing 3D Human Neural Tissue Derived from Induced Pluripotent Stem Cells Recapitulate Alzheimer's Disease Phenotypes.* PLOS ONE, 2016. **11**(9): p. e0161969.
181. Choi, S.H., et al., *A three-dimensional human neural cell culture model of Alzheimer's disease.* Nature, 2014. **515**(7526): p. 274-8.
182. Chow, V.W., et al., *An Overview of APP Processing Enzymes and Products.* Neuromolecular medicine, 2010. **12**(1): p. 1-12.
183. Cataldo, A., et al., *Endocytic disturbances distinguish among subtypes of Alzheimer's disease and related disorders.* Ann Neurol, 2001. **50**(5): p. 661-5.
184. Espuny-Camacho, I., et al., *Hallmarks of Alzheimer's Disease in Stem-Cell-Derived Human Neurons Transplanted into Mouse Brain.* Neuron, 2017. **93**(5): p. 1066-1081.e8.
185. Hebb, D.O., *The organization of behavior; a neuropsychological theory*. The organization of behavior; a neuropsychological theory. 1949, Oxford, England: Wiley. xix, 335-xix, 335.
186. Bliss, T.V.P. and T. Lømo, *Long-lasting potentiation of synaptic transmission in the dentate area of the anaesthetized rabbit following stimulation of the perforant path.* The Journal of Physiology, 1973. **232**(2): p. 331-356.
187. Bliss, T.V.P. and A.R. Gardner-Medwin, *Long-lasting potentiation of synaptic transmission in the dentate area of the unanaesthetized rabbit following stimulation of the perforant path.* The Journal of Physiology, 1973. **232**(2): p. 357-374.
188. Schwartzkroin, P.A. and K. Wester, *Long-lasting facilitation of a synaptic potential following tetanization in thein vitro hippocampal slice.* Brain Research, 1975. **89**(1): p. 107-119.
189. Iriki, A., et al., *Long-term potentiation in the motor cortex.* Science, 1989. **245**(4924): p. 1385-7.
190. Kauer, J.A., R.C. Malenka, and R.A. Nicoll, *A persistent postsynaptic modification mediates long-term potentiation in the hippocampus.* Neuron, 1988. **1**(10): p. 911-917.
191. Jorntell, H. and C. Hansel, *Synaptic memories upside down: bidirectional plasticity at cerebellar parallel fiber-Purkinje cell synapses.* Neuron, 2006. **52**(2): p. 227-38.
192. Boyden, E.S., et al., *Millisecond-timescale, genetically targeted optical control of neural activity.* Nature Neuroscience, 2005. **8**: p. 1263.
193. Xiong, W. and X. Jin, *Optogenetic field potential recording in cortical slices.* Journal of neuroscience methods, 2012. **210**(2): p. 119-124.
194. Pascoli, V., M. Turiault, and C. Lüscher, *Reversal of cocaine-evoked synaptic potentiation resets drug-induced adaptive behaviour.* Nature, 2011. **481**: p. 71.
195. Fleming, J.J. and P.M. England, *AMPA receptors and synaptic plasticity: a chemist's perspective.* Nature Chemical Biology, 2010. **6**: p. 89.
196. Goodman, L.S., et al., *Goodman & Gilman's the pharmacological basis of therapeutics.* 12th ed, ed. L.L. Brunton. 2011, US: McGraw-Hill New York.
197. Nicoll, R.A., *A Brief History of Long-Term Potentiation.* Neuron, 2017. **93**(2): p. 281-290.
198. Davies, C.H., et al., *GABAB autoreceptors regulate the induction of LTP.* Nature, 1991. **349**: p. 609.

199. Gustafsson, B., et al., *Long-term potentiation in the hippocampus using depolarizing current pulses as the conditioning stimulus to single volley synaptic potentials.* The Journal of Neuroscience, 1987. **7**(3): p. 774-780.
200. Zhang, Y.P., N. Holbro, and T.G. Oertner, *Optical induction of plasticity at single synapses reveals input-specific accumulation of alphaCaMKII.* Proc Natl Acad Sci U S A, 2008. **105**(33): p. 12039-44.
201. Zhang, Y.-P. and T.G. Oertner, *Optical induction of synaptic plasticity using a light-sensitive channel.* Nat Meth, 2007. **4**(2): p. 139-141.
202. Lisman, J., R. Yasuda, and S. Raghavachari, *Mechanisms of CaMKII action in long-term potentiation.* Nature Reviews Neuroscience, 2012. **13**: p. 169.
203. Benke, T.A., et al., *Modulation of AMPA receptor unitary conductance by synaptic activity.* Nature, 1998. **393**(6687): p. 793-7.
204. Malinow, R. and R.C. Malenka, *AMPA Receptor Trafficking and Synaptic Plasticity.* Annual Review of Neuroscience, 2002. **25**(1): p. 103-126.
205. Granger, A.J. and R.A. Nicoll, *Expression mechanisms underlying long-term potentiation: a postsynaptic view, 10 years on.* Philosophical Transactions of the Royal Society B: Biological Sciences, 2014. **369**(1633): p. 20130136.
206. Padamsey, Z. and N. Emptage, *Two sides to long-term potentiation: a view towards reconciliation.* Philosophical Transactions of the Royal Society B: Biological Sciences, 2014. **369**(1633): p. 20130154.
207. Bekkers, J.M. and C.F. Stevens, *Presynaptic mechanism for long-term potentiation in the hippocampus.* Nature, 1990. **346**: p. 724.
208. Malinow, R. and R.W. Tsien, *Presynaptic enhancement shown by whole-cell recordings of long-term potentiation in hippocampal slices.* Nature, 1990. **346**: p. 177.
209. Malinow, R., *Transmission between pairs of hippocampal slice neurons: quantal levels, oscillations, and LTP.* Science, 1991. **252**(5006): p. 722-724.
210. Ryan, T.A., N.E. Ziv, and S.J. Smith, *Potentiation of evoked vesicle turnover at individually resolved synaptic boutons.* Neuron, 1996. **17**(1): p. 125-34.
211. Zakharenko, S.S., L. Zablow, and S.A. Siegelbaum, *Visualization of changes in presynaptic function during long-term synaptic plasticity.* Nat Neurosci, 2001. **4**(7): p. 711-7.
212. Stanton, P.K., et al., *Imaging LTP of presynaptic release of FM1-43 from the rapidly recycling vesicle pool of Schaffer collateral-CA1 synapses in rat hippocampal slices.* Eur J Neurosci, 2005. **22**(10): p. 2451-61.
213. Bayazitov, I.T., et al., *Slow presynaptic and fast postsynaptic components of compound long-term potentiation.* J Neurosci, 2007. **27**(43): p. 11510-21.
214. Emptage, N., T.V.P. Bliss, and A. Fine, *Single Synaptic Events Evoke NMDA Receptor–Mediated Release of Calcium from Internal Stores in Hippocampal Dendritic Spines.* Neuron, 1999. **22**(1): p. 115-124.
215. Enoki, R., et al., *Expression of Long-Term Plasticity at Individual Synapses in Hippocampus Is Graded, Bidirectional, and Mainly Presynaptic: Optical Quantal Analysis.* Neuron, 2009. **62**(2): p. 242-253.
216. Isaac, J.T.R., R.A. Nicoll, and R.C. Malenka, *Evidence for silent synapses: Implications for the expression of LTP.* Neuron, 1995. **15**(2): p. 427-434.
217. Liao, D., N.A. Hessler, and R. Malinow, *Activation of postsynaptically silent synapses during pairing-induced LTP in CA1 region of hippocampal slice.* Nature, 1995. **375**: p. 400.
218. Matsuzaki, M., et al., *Structural basis of long-term potentiation in single dendritic spines.* Nature, 2004. **429**(6993): p. 761-766.
219. Montgomery, J.M., P. Pavlidis, and D.V. Madison, *Pair Recordings Reveal All-Silent Synaptic Connections and the Postsynaptic Expression of Long-Term Potentiation.* Neuron, 2001. **29**(3): p. 691-701.

220. Durand, G.M., Y. Kovalchuk, and A. Konnerth, *Long-term potentiation and functional synapse induction in developing hippocampus.* Nature, 1996. **381**(6577): p. 71-75.
221. Watt, A.J., et al., *A proportional but slower NMDA potentiation follows AMPA potentiation in LTP.* Nat Neurosci, 2004. **7**(5): p. 518-24.
222. Muller, D. and G. Lynch, *Long-term potentiation differentially affects two components of synaptic responses in hippocampus.* Proceedings of the National Academy of Sciences, 1988. **85**(23): p. 9346-9350.
223. Nicoll, R.A. and R.C. Malenka, *Contrasting properties of two forms of long-term potentiation in the hippocampus.* Nature, 1995. **377**: p. 115.
224. Castillo, P.E., *Presynaptic LTP and LTD of Excitatory and Inhibitory Synapses.* Cold Spring Harbor Perspectives in Biology, 2012. **4**(2): p. a005728.
225. Yang, Y. and N. Calakos, *Presynaptic long-term plasticity.* Frontiers in Synaptic Neuroscience, 2013. **5**: p. 8.
226. Bliss, T.V.P. and G.L. Collingridge, *Expression of NMDA receptor-dependent LTP in the hippocampus: bridging the divide.* Molecular Brain, 2013. **6**: p. 5-5.
227. Ngezahayo, A., M. Schachner, and A. Artola, *Synaptic Activity Modulates the Induction of Bidirectional Synaptic Changes in Adult Mouse Hippocampus.* The Journal of Neuroscience, 2000. **20**(7): p. 2451-2458.
228. Mulkey, R.M. and R.C. Malenka, *Mechanisms underlying induction of homosynaptic long-term depression in area CA1 of the hippocampus.* Neuron, 1992. **9**(5): p. 967-975.
229. Dudek, S.M. and M.F. Bear, *Homosynaptic long-term depression in area CA1 of hippocampus and effects of N-methyl-D-aspartate receptor blockade.* Proc Natl Acad Sci U S A, 1992. **89**(10): p. 4363-7.
230. Malenka, R.C., *Synaptic plasticity in the hippocampus: LTP and LTD.* Cell, 1994. **78**(4): p. 535-538.
231. Hansel, C., A. Artola, and W. Singer, *Different threshold levels of postsynaptic [Ca2+]i have to be reached to induce LTP and LTD in neocortical pyramidal cells.* Journal of Physiology-Paris, 1996. **90**(5): p. 317-319.
232. Lisman, J., *A mechanism for the Hebb and the anti-Hebb processes underlying learning and memory.* Proc Natl Acad Sci U S A, 1989. **86**(23): p. 9574-8.
233. Lee, H.-K., et al., *Regulation of distinct AMPA receptor phosphorylation sites during bidirectional synaptic plasticity.* Nature, 2000. **405**: p. 955.
234. Larson, J., D. Wong, and G. Lynch, *Patterned stimulation at the theta frequency is optimal for the induction of hippocampal long-term potentiation.* Brain Research, 1986. **368**(2): p. 347-350.
235. Staubli, U. and G. Lynch, *Stable hippocampal long-term potentiation elicited by 'theta' pattern stimulation.* Brain Research, 1987. **435**(1): p. 227-234.
236. Bi, G.-q. and M.-m. Poo, *Synaptic Modifications in Cultured Hippocampal Neurons: Dependence on Spike Timing, Synaptic Strength, and Postsynaptic Cell Type.* The Journal of Neuroscience, 1998. **18**(24): p. 10464-10472.
237. Feldman, Daniel E., *The Spike-Timing Dependence of Plasticity.* Neuron, 2012. **75**(4): p. 556-571.
238. Nevian, T. and B. Sakmann, *Single spine Ca2+ signals evoked by coincident EPSPs and backpropagating action potentials in spiny stellate cells of layer 4 in the juvenile rat somatosensory barrel cortex.* J Neurosci, 2004. **24**(7): p. 1689-99.
239. Watanabe, S., et al., *Dendritic K+ channels contribute to spike-timing dependent long-term potentiation in hippocampal pyramidal neurons.* Proc Natl Acad Sci U S A, 2002. **99**(12): p. 8366-71.
240. Stuart, G.J. and M. Häusser, *Dendritic coincidence detection of EPSPs and action potentials.* Nature Neuroscience, 2001. **4**: p. 63.

241. Magee, J.C. and D. Johnston, *A Synaptically Controlled, Associative Signal for Hebbian Plasticity in Hippocampal Neurons.* Science, 1997. **275**(5297): p. 209-213.
242. Koester, H.J. and B. Sakmann, *Calcium dynamics in single spines during coincident pre- and postsynaptic activity depend on relative timing of back-propagating action potentials and subthreshold excitatory postsynaptic potentials.* Proceedings of the National Academy of Sciences, 1998. **95**(16): p. 9596-9601.
243. Hess, G., C.D. Aizenman, and J.P. Donoghue, *Conditions for the induction of long-term potentiation in layer II/III horizontal connections of the rat motor cortex.* Journal of Neurophysiology, 1996. **75**(5): p. 1765-1778.
244. Hirsch, J.C., G. Barrionuevo, and F. Crepel, *Homo- and heterosynaptic changes in efficacy are expressed in prefrontal neurons: An in vitro study in the rat.* Synapse, 1992. **12**(1): p. 82-85.
245. Artola, A. and W. Singer, *Long-term potentiation and NMDA receptors in rat visual cortex.* Nature, 1987. **330**: p. 649.
246. Froemke, R.C., et al., *Contribution of Individual Spikes in Burst-Induced Long-Term Synaptic Modification.* Journal of Neurophysiology, 2006. **95**(3): p. 1620-1629.
247. Markram, H., et al., *Regulation of Synaptic Efficacy by Coincidence of Postsynaptic APs and EPSPs.* Science, 1997. **275**(5297): p. 213-215.
248. Sjöström, P.J., G.G. Turrigiano, and S.B. Nelson, *Rate, Timing, and Cooperativity Jointly Determine Cortical Synaptic Plasticity.* Neuron, 2001. **32**(6): p. 1149-1164.
249. Sjöström, P.J. and M. Häusser, *A Cooperative Switch Determines the Sign of Synaptic Plasticity in Distal Dendrites of Neocortical Pyramidal Neurons.* Neuron, 2006. **51**(2): p. 227-238.
250. Feldman, D.E., *Timing-based LTP and LTD at vertical inputs to layer II/III pyramidal cells in rat barrel cortex.* Neuron, 2000. **27**(1): p. 45-56.
251. Sjöström, P.J., G.G. Turrigiano, and S.B. Nelson, *Neocortical LTD via Coincident Activation of Presynaptic NMDA and Cannabinoid Receptors.* Neuron, 2003. **39**(4): p. 641-654.
252. Rodríguez-Moreno, A. and O. Paulsen, *Spike timing–dependent long-term depression requires presynaptic NMDA receptors.* Nature Neuroscience, 2008. **11**: p. 744.
253. Nakamura, T., et al., *Synergistic Release of Ca2+ from IP3-Sensitive Stores Evoked by Synaptic Activation of mGluRs Paired with Backpropagating Action Potentials.* Neuron, 1999. **24**(3): p. 727-737.
254. Buonomano, D.V., *Distinct Functional Types of Associative Long-Term Potentiation in Neocortical and Hippocampal Pyramidal Neurons.* The Journal of Neuroscience, 1999. **19**(16): p. 6748-6754.
255. Castro-Alamancos, M.A. and B.W. Connors, *Distinct forms of short-term plasticity at excitatory synapses of hippocampus and neocortex.* Proceedings of the National Academy of Sciences, 1997. **94**(8): p. 4161-4166.
256. Teyler, T.J., et al., *Long-term potentiation of human visual evoked responses.* Eur J Neurosci, 2005. **21**(7): p. 2045-50.
257. Clapp, W.C., et al., *Induction of LTP in the human auditory cortex by sensory stimulation.* Eur J Neurosci, 2005. **22**(5): p. 1135-40.
258. Huang, Y.Z., et al., *Theta burst stimulation of the human motor cortex.* Neuron, 2005. **45**(2): p. 201-6.
259. Koch, G., et al., *Hebbian and Anti-Hebbian Spike-Timing-Dependent Plasticity of Human Cortico-Cortical Connections.* The Journal of Neuroscience, 2013. **33**(23): p. 9725-9733.
260. Wankerl, K., et al., *L-type voltage-gated Ca2+ channels: a single molecular switch for long-term potentiation/long-term depression-like plasticity and activity-dependent metaplasticity in humans.* J Neurosci, 2010. **30**(18): p. 6197-204.
261. Stefan, K., et al., *Induction of plasticity in the human motor cortex by paired associative stimulation.* Brain, 2000. **123**(3): p. 572-584.

262. Beck, H., et al., *Synaptic plasticity in the human dentate gyrus.* J Neurosci, 2000. **20**(18): p. 7080-6.
263. Chen, W.R., et al., *Long-term modifications of synaptic efficacy in the human inferior and middle temporal cortex.* Proceedings of the National Academy of Sciences of the United States of America, 1996. **93**(15): p. 8011-8015.
264. Testa-Silva, G., et al., *Human Synapses Show a Wide Temporal Window for Spike-Timing-Dependent Plasticity.* Frontiers in Synaptic Neuroscience, 2010. **2**: p. 12.
265. Verhoog, M.B., et al., *Mechanisms Underlying the Rules for Associative Plasticity at Adult Human Neocortical Synapses.* The Journal of Neuroscience, 2013. **33**(43): p. 17197-17208.
266. Odawara, A., et al., *Induction of long-term potentiation and depression phenomena in human induced pluripotent stem cell-derived cortical neurons.* Biochem Biophys Res Commun, 2016. **469**(4): p. 856-62.
267. Fink, J.J., et al., *Disrupted neuronal maturation in Angelman syndrome-derived induced pluripotent stem cells.* Nature Communications, 2017. **8**: p. 15038.
268. Fink, J.J., et al., *Hyperexcitable phenotypes in iPSC-derived neurons from patients with 15q11-q13 duplication syndrome, a genetic form of autism.* bioRxiv, 2018.
269. Kirwan, P., et al., *Development and function of human cerebral cortex neural networks from pluripotent stem cells in vitro.* Development, 2015. **142**(18): p. 3178-3187.
270. Lam, R.S., et al., *Functional Maturation of Human Stem Cell-Derived Neurons in Long-Term Cultures.* PLOS ONE, 2017. **12**(1): p. e0169506.
271. Gupta, K., G.E. Hardingham, and S. Chandran, *NMDA receptor-dependent glutamate excitotoxicity in human embryonic stem cell-derived neurons.* Neuroscience Letters, 2013. **543**(0): p. 95-100.
272. Lieberman, R., et al., *Pilot Study of iPS-derived Neural Cells to Examine Biological Effects of Alcohol on Human Neurons in vitro.* Alcoholism, clinical and experimental research, 2012. **36**(10): p. 1678-1687.
273. Neagoe, I., et al., *The GluN2B subunit represents a major functional determinant of NMDA receptors in human induced pluripotent stem cell-derived cortical neurons.* Stem Cell Research, 2018. **28**: p. 105-114.
274. Zhang, W.-B., et al., *Fyn Kinase regulates GluN2B subunit-dominant NMDA receptors in human induced pluripotent stem cell-derived neurons.* Scientific Reports, 2016. **6**: p. 23837.
275. Nehme, R., et al., *Combining NGN2 Programming with Developmental Patterning Generates Human Excitatory Neurons with NMDAR-Mediated Synaptic Transmission.* Cell Reports, 2018. **23**(8): p. 2509-2523.
276. Tang, X., et al., *Astroglial cells regulate the developmental timeline of human neurons differentiated from induced pluripotent stem cells.* Stem cell research, 2013. **11**(2): p. 743-757.
277. Arancio, O., E.R. Kandel, and R.D. Hawkins, *Activity-dependent long-term enhancement of transmitter release by presynaptic 3',5'-cyclic GMP in cultured hippocampal neurons.* Nature, 1995. **376**: p. 74.
278. Musleh, W., et al., *Glycine-induced long-term potentiation is associated with structural and functional modifications of α-amino-3-hydroxyl-5-methyl-4-isoxazolepropionic acid receptors.* Proceedings of the National Academy of Sciences, 1997. **94**(17): p. 9451-9456.
279. Malgaroli, A. and R.W. Tsien, *Glutamate-induced long-term potentiation of the frequency of miniature synaptic currents in cultured hippocampal neurons.* Nature, 1992. **357**(6374): p. 134-139.
280. Deisseroth, K., H. Bito, and R.W. Tsien, *Signaling from Synapse to Nucleus: Postsynaptic CREB Phosphorylation during Multiple Forms of Hippocampal Synaptic Plasticity.* Neuron, 1996. **16**(1): p. 89-101.

281. Ninan, I., et al., *Early presynaptic changes during plasticity in cultured hippocampal neurons.* The EMBO Journal, 2006. **25**(18): p. 4361-4371.
282. Fitzjohn, S.M., et al., *An electrophysiological characterisation of long-term potentiation in cultured dissociated hippocampal neurones.* Neuropharmacology, 2001. **41**(6): p. 693-699.
283. Lu, W.-Y., et al., *Activation of Synaptic NMDA Receptors Induces Membrane Insertion of New AMPA Receptors and LTP in Cultured Hippocampal Neurons.* Neuron, 2001. **29**(1): p. 243-254.
284. Goda, Y. and C.F. Stevens, *Long-Term Depression Properties in a Simple System.* Neuron, 1996. **16**(1): p. 103-111.
285. Shahi, K. and M. Baudry, *Glycine-induced changes in synaptic efficacy in hippocampal slices involve changes in AMPA receptors.* Brain Research, 1993. **627**(2): p. 261-266.
286. Otmakhov, N., et al., *Forskolin-Induced LTP in the CA1 Hippocampal Region Is NMDA Receptor Dependent*. Vol. 91. 2004. 1955-1962.
287. Chevy, Q., et al., *KCC2 Gates Activity-Driven AMPA Receptor Traffic through Cofilin Phosphorylation.* The Journal of Neuroscience, 2015. **35**(48): p. 15772-15786.
288. Kopec, C.D., et al., *Glutamate Receptor Exocytosis and Spine Enlargement during Chemically Induced Long-Term Potentiation.* The Journal of Neuroscience, 2006. **26**(7): p. 2000-2009.
289. Hartfield, E.M., et al., *Physiological Characterisation of Human iPS-Derived Dopaminergic Neurons.* PLOS ONE, 2014. **9**(2): p. e87388.
290. Young, L., et al., *Detection of Mycoplasma in cell cultures.* Nat. Protocols, 2010. **5**(5): p. 929-934.
291. Bardy, C., et al., *Neuronal medium that supports basic synaptic functions and activity of human neurons in vitro.* Proceedings of the National Academy of Sciences, 2015. **112**(20): p. E2725-E2734.
292. Maherali, N., et al., *A high-efficiency system for the generation and study of human induced pluripotent stem cells.* Cell Stem Cell, 2008. **3**(3): p. 340-5.
293. Zhang, F., et al., *Multimodal fast optical interrogation of neural circuitry.* Nature, 2007. **446**(7136): p. 633-9.
294. Cathala, L., C. Misra, and S. Cull-Candy, *Developmental Profile of the Changing Properties of NMDA Receptors at Cerebellar Mossy Fiber–Granule Cell Synapses.* The Journal of Neuroscience, 2000. **20**(16): p. 5899-5905.
295. Jacobsen, J.S., et al., *Early-onset behavioral and synaptic deficits in a mouse model of Alzheimer's disease.* Proceedings of the National Academy of Sciences of the United States of America, 2006. **103**(13): p. 5161-5166.
296. Licht, E.A., et al., *Cognitive Differences between Early- and Late-Onset Alzheimer's Disease.* American Journal of Alzheimer's Disease & Other Dementias®, 2007. **22**(3): p. 218-222.
297. Koedam, E.L., et al., *Early-versus late-onset Alzheimer's disease: more than age alone.* J Alzheimers Dis, 2010. **19**(4): p. 1401-8.
298. Lippa, C.F., et al., *Familial and sporadic Alzheimer's disease.* Neuropathology cannot exclude a final common pathway, 1996. **46**(2): p. 406-412.
299. Cánovas, J., et al., *The Specification of Cortical Subcerebral Projection Neurons Depends on the Direct Repression of TBR1 by CTIP1/BCL11a.* The Journal of Neuroscience, 2015. **35**(19): p. 7552-7564.
300. Rakic, P., *Neurons in Rhesus Monkey Visual Cortex: Systematic Relation between Time of Origin and Eventual Disposition.* Science, 1974. **183**(4123): p. 425-427.
301. Hansen, D.V., et al., *Non-epithelial stem cells and cortical interneuron production in the human ganglionic eminences.* Nature Neuroscience, 2013. **16**: p. 1576.
302. Ma, T., et al., *Subcortical origins of human and monkey neocortical interneurons.* Nature Neuroscience, 2013. **16**: p. 1588.
303. Testa-Silva, G., et al., *High Bandwidth Synaptic Communication and Frequency Tracking in Human Neocortex.* PLoS Biology, 2014. **12**(11): p. e1002007.

304. Zhang, Z.-w., *Maturation of Layer V Pyramidal Neurons in the Rat Prefrontal Cortex: Intrinsic Properties and Synaptic Function.* Journal of Neurophysiology, 2004. **91**(3): p. 1171-1182.
305. Ziv, N.E. and S.J. Smith, *Evidence for a role of dendritic filopodia in synaptogenesis and spine formation.* Neuron, 1996. **17**(1): p. 91-102.
306. Cao, S.-Y., et al., *Enhanced derivation of human pluripotent stem cell-derived cortical glutamatergic neurons by a small molecule.* Scientific Reports, 2017. **7**(1): p. 3282.
307. Bahrey, H.L.P. and W.J. Moody, *Early Development of Voltage-Gated Ion Currents and Firing Properties in Neurons of the Mouse Cerebral Cortex.* Journal of Neurophysiology, 2003. **89**(4): p. 1761-1773.
308. Picken Bahrey, H.L. and W.J. Moody, *Early development of voltage-gated ion currents and firing properties in neurons of the mouse cerebral cortex.* J Neurophysiol, 2003. **89**(4): p. 1761-73.
309. Watari, H., A.J. Tose, and M.M. Bosma, *Hyperpolarization of resting membrane potential causes retraction of spontaneous Ca(i)²⁺ transients during mouse embryonic circuit development.* The Journal of physiology, 2013. **591**(4): p. 973-983.
310. Ramoa, A.S. and D.A. McCormick, *Developmental changes in electrophysiological properties of LGNd neurons during reorganization of retinogeniculate connections.* J Neurosci, 1994. **14**(4): p. 2089-97.
311. Pirchio, M., et al., *Postnatal Development of Membrane Properties and δ Oscillations in Thalamocortical Neurons of the Cat Dorsal Lateral Geniculate Nucleus*. Vol. 17. 1997. 5428-44.
312. Yan-Chiang, L., et al., *Development of excitatory synapses in cultured neurons dissociated from the cortices of rat embryos and rat pups at birth.* Journal of Neuroscience Research, 2002. **67**(4): p. 484-493.
313. Schmidt-Hieber, C., P. Jonas, and J. Bischofberger, *Enhanced synaptic plasticity in newly generated granule cells of the adult hippocampus.* Nature, 2004. **429**(6988): p. 184-187.
314. Mongiat, L.A., et al., *Reliable activation of immature neurons in the adult hippocampus.* PloS one, 2009. **4**(4): p. e5320-e5320.
315. Li, L., et al., *Silent synapses generate sparse and orthogonal action potential firing in adult-born hippocampal granule cells.* eLife, 2017. **6**: p. e23612.
316. Handel, A.E., et al., *Assessing similarity to primary tissue and cortical layer identity in induced pluripotent stem cell-derived cortical neurons through single-cell transcriptomics.* Human Molecular Genetics, 2016. **25**(5): p. 989-1000.
317. Bibel, M., et al., *Differentiation of mouse embryonic stem cells into a defined neuronal lineage.* Nature Neuroscience, 2004. **7**: p. 1003.
318. Barth, L., et al., *Functional differentiation of stem cell-derived neurons from different murine backgrounds.* Front Cell Neurosci, 2014. **8**: p. 49.
319. Bayer, S.A., et al., *Timetables of neurogenesis in the human brain based on experimentally determined patterns in the rat.* Neurotoxicology, 1993. **14**(1): p. 83-144.
320. Sposito, T., et al., *Developmental regulation of tau splicing is disrupted in stem cell derived neurons from frontotemporal dementia patients with the 10+16 splice-site mutation in MAPT.* Human Molecular Genetics, 2015.
321. Iovino, M., et al., *Early maturation and distinct tau pathology in induced pluripotent stem cell-derived neurons from patients with MAPT mutations.* Brain : a journal of neurology, 2015. **138**(Pt 11): p. 3345-3359.
322. Brown, J.T., et al., *Altered intrinsic neuronal excitability and reduced Na+ currents in a mouse model of Alzheimer's disease.* Neurobiology of Aging, 2011. **32**(11): p. 2109.e1-2109.e14.
323. Kerrigan, T.L., J.T. Brown, and A.D. Randall, *Characterization of altered intrinsic excitability in hippocampal CA1 pyramidal cells of the Abeta-overproducing PDAPP mouse.* Neuropharmacology, 2014. **79**(100): p. 515-24.

324. Minkeviciene, R., et al., *Amyloid β-Induced Neuronal Hyperexcitability Triggers Progressive Epilepsy.* The Journal of Neuroscience, 2009. **29**(11): p. 3453-3462.
325. Rocher, A.B., M.S. Kinson, and J.I. Luebke, *Significant structural but not physiological changes in cortical neurons of 12-month-old Tg2576 mice.* Neurobiology of disease, 2008. **32**(2): p. 309-318.
326. Nimmrich, V., et al., *Amyloid beta oligomers (A beta(1-42) globulomer) suppress spontaneous synaptic activity by inhibition of P/Q-type calcium currents.* J Neurosci, 2008. **28**(4): p. 788-97.
327. Moore, B.D., et al., *Overlapping profiles of Aβ peptides in the Alzheimer's disease and pathological aging brains.* Alzheimer's research & therapy, 2012. **4**(3): p. 18-18.
328. Roher, A.E., et al., *Amyloid beta peptides in human plasma and tissues and their significance for Alzheimer's disease.* Alzheimer's & Dementia, 2009. **5**(1): p. 18-29.
329. McLean, C.A., et al., *Soluble pool of Aβ amyloid as a determinant of severity of neurodegeneration in Alzheimer's disease.* Annals of Neurology, 1999. **46**(6): p. 860-866.
330. Murphy, M.P. and H. LeVine, 3rd, *Alzheimer's disease and the amyloid-beta peptide.* Journal of Alzheimer's disease : JAD, 2010. **19**(1): p. 311-323.
331. Duering, M., et al., *Mean age of onset in familial Alzheimer's disease is determined by amyloid beta 42.* Neurobiology of Aging, 2005. **26**(6): p. 785-788.
332. Kuperstein, I., et al., *Neurotoxicity of Alzheimer's disease Abeta peptides is induced by small changes in the Abeta42 to Abeta40 ratio.* EMBO J, 2010. **29**(19): p. 3408-20.
333. Hu, N.-W., et al., *Extracellular Forms of Aβ and Tau from iPSC Models of Alzheimer's Disease Disrupt Synaptic Plasticity.* Cell Reports, 2018. **23**(7): p. 1932-1938.
334. Correa-Gillieron, E.M. and L.A. Cavalcante, *Synaptogenesis in Retino-Receptive Layers of the Superior Colliculus of the Opossum Didelphis marsupialis.* Brain, Behavior and Evolution, 1999. **54**(2): p. 71-84.
335. Yamada, K., et al., *Dynamic transformation of Bergmann glial fibers proceeds in correlation with dendritic outgrowth and synapse formation of cerebellar Purkinje cells.* J Comp Neurol, 2000. **418**(1): p. 106-20.
336. Pfrieger, F.W. and B.A. Barres, *Synaptic Efficacy Enhanced by Glial Cells in Vitro.* Science, 1997. **277**(5332): p. 1684-1687.
337. McKellar, C.E. and C.J. Shatz, *Synaptogenesis in Purified Cortical Subplate Neurons.* Cerebral Cortex, 2009. **19**(8): p. 1723-1737.
338. Ullian, E.M., et al., *Control of Synapse Number by Glia.* Science, 2001. **291**(5504): p. 657-661.
339. Tsai, H.-H., et al., *Regional Astrocyte Allocation Regulates CNS Synaptogenesis and Repair.* Science, 2012. **337**(6092): p. 358-362.
340. Bouwman, J., et al., *Quantification of synapse formation and maintenance in vivo in the absence of synaptic release.* Neuroscience, 2004. **126**(1): p. 115-126.
341. Kwon, H.-B. and B.L. Sabatini, *Glutamate induces de novo growth of functional spines in developing cortex.* Nature, 2011. **474**: p. 100.
342. Young, S.H. and M.-m. Poo, *Spontaneous release of transmitter from growth cones of embryonic neurones.* Nature, 1983. **305**: p. 634.
343. Soto, F., et al., *Spontaneous Activity Promotes Synapse Formation in a Cell-Type-Dependent Manner in the Developing Retina.* The Journal of Neuroscience, 2012. **32**(16): p. 5426-5439.
344. Sugiura, H. and T. Yamauchi, *Developmental changes in the levels of Ca2+/calmodulin-dependent protein kinase II α and β proteins in soluble and particulate fractions of the rat brain.* Brain Research, 1992. **593**(1): p. 97-104.
345. Frese, C.K., et al., *Quantitative Map of Proteome Dynamics during Neuronal Differentiation.* Cell Rep, 2017. **18**(6): p. 1527-1542.

346. Jones, E.G., G.W. Huntley, and D.L. Benson, *Alpha calcium/calmodulin-dependent protein kinase II selectively expressed in a subpopulation of excitatory neurons in monkey sensory-motor cortex: comparison with GAD-67 expression.* J Neurosci, 1994. **14**(2): p. 611-29.
347. Vicario-Abejón, C., et al., *Neurotrophins Induce Formation of Functional Excitatory and Inhibitory Synapses between Cultured Hippocampal Neurons.* The Journal of Neuroscience, 1998. **18**(18): p. 7256-7271.
348. Ohgoh, M., et al., *Apoptotic Cell Death of Cultured Cerebral Cortical Neurons Induced by Withdrawal of Astroglial Trophic Support.* Experimental Neurology, 1998. **149**(1): p. 51-63.
349. Lepski, G., et al., *cAMP promotes the differentiation of neural progenitor cells in vitro via modulation of voltage-gated calcium channels.* Frontiers in Cellular Neuroscience, 2013. **7**: p. 155.
350. Shin, D.-M., et al., *Ascorbic acid responsive genes during neuronal differentiation of embryonic stem cells.* NeuroReport, 2004. **15**(12): p. 1959-1963.
351. Kratzing, C., J. Kelly, and J. Kratzing, *Ascorbic Acid in Fetal Rat Brain.* Journal of Neurochemistry, 1985. **44**(5): p. 1623-1624.
352. Björklund, U., et al., *Primary Cultures From Cerebral Cortex and Hippocampus Enriched in Glutamatergic and GABAergic Neurons.* Neurochemical Research, 2010. **35**(11): p. 1733-1742.
353. Ben-Ari, Y., et al., *GABAA, NMDA and AMPA receptors: a developmentally regulated `ménage à trois'.* Trends in Neurosciences, 1997. **20**(11): p. 523-529.
354. Odawara, A., et al., *Long-term electrophysiological activity and pharmacological response of a human induced pluripotent stem cell-derived neuron and astrocyte co-culture.* Biochem Biophys Res Commun, 2014. **443**(4): p. 1176-81.
355. Schutte, R.J., et al., *Astrocyte-enriched feeder layers from cryopreserved cells support differentiation of spontaneously active networks of human iPSC-derived neurons.* Journal of Neuroscience Methods, 2018. **294**: p. 91-101.
356. Oni, E.N., et al., *Increased nicotine response in iPSC-derived human neurons carrying the CHRNA5 N398 allele.* Scientific Reports, 2016. **6**: p. 34341.
357. Azevedo, F.A.C., et al., *Equal numbers of neuronal and nonneuronal cells make the human brain an isometrically scaled-up primate brain.* The Journal of Comparative Neurology, 2009. **513**(5): p. 532-541.
358. Allen, N.J., *Astrocyte Regulation of Synaptic Behavior.* Annual Review of Cell and Developmental Biology, 2014. **30**(1): p. 439-463.
359. Wei, C., et al., *Inducible ablation of astrocytes shows that these cells are required for neuronal survival in the adult brain.* Glia, 2001. **34**(4): p. 272-282.
360. Wagner, B., et al., *Neuronal survival depends on EGFR signaling in cortical but not midbrain astrocytes.* The EMBO Journal, 2006. **25**(4): p. 752-762.
361. Bardy, C., et al., *Predicting the functional states of human iPSC-derived neurons with single-cell RNA-seq and electrophysiology.* Molecular Psychiatry, 2016. **21**: p. 1573.
362. Ivenshitz, M. and M. Segal, *Neuronal Density Determines Network Connectivity and Spontaneous Activity in Cultured Hippocampus*. Vol. 104. 2010. 1052-1060.
363. Toyomoto, M., et al., *Production of NGF, BDNF and GDNF in mouse astrocyte cultures is strongly enhanced by a cerebral vasodilator, ifenprodil.* Neuroscience Letters, 2005. **379**(3): p. 185-189.
364. Trupp, M., et al., *Ret-dependent and -independent Mechanisms of Glial Cell Line-derived Neurotrophic Factor Signaling in Neuronal Cells.* Journal of Biological Chemistry, 1999. **274**(30): p. 20885-20894.
365. Wilson, J.X., et al., *Glutamate stimulates ascorbate transport by astrocytes.* Brain Research, 2000. **858**(1): p. 61-66.
366. Su, C.T.E., et al., *An Optogenetic Approach for Assessing Formation of Neuronal Connections in a Co-culture System.* Journal of Visualized Experiments : JoVE, 2015(96): p. 52408.

367. Weick, J.P., Y. Liu, and S.-C. Zhang, *Human embryonic stem cell-derived neurons adopt and regulate the activity of an established neural network.* Proceedings of the National Academy of Sciences of the United States of America, 2011. **108**(50): p. 20189-20194.
368. Heng, J. and F. Guillemot, *Proneural Proteins and the Development of the Cerebral Cortex*, in *Cortical Development: Neural Diversity and Neocortical Organization*, R. Kageyama and T. Yamamori, Editors. 2013, Springer Japan: Tokyo. p. 19-41.
369. Scardigli, R., et al., *Direct and concentration-dependent regulation of the proneural gene Neurogenin2 by Pax6.* Development, 2003. **130**(14): p. 3269-3281.
370. Schuurmans, C., et al., *Sequential phases of cortical specification involve Neurogenin-dependent and -independent pathways.* The EMBO Journal, 2004. **23**(14): p. 2892-2902.
371. Hand, R., et al., *Phosphorylation of Neurogenin2 Specifies the Migration Properties and the Dendritic Morphology of Pyramidal Neurons in the Neocortex.* Neuron, 2005. **48**(1): p. 45-62.
372. Heng, J., et al., *Neurogenin 2 controls cortical neuron migration through regulation of Rnd2*. Vol. 455. 2008. 114-8.
373. Johnson, M.A., et al., *Functional Neural Development from Human Embryonic Stem Cells: Accelerated Synaptic Activity via Astrocyte Coculture.* The Journal of Neuroscience, 2007. **27**(12): p. 3069-3077.
374. Wu, H., et al., *Integrative genomic and functional analyses reveal neuronal subtype differentiation bias in human embryonic stem cell lines.* Proc Natl Acad Sci U S A, 2007. **104**(34): p. 13821-6.
375. Ho, S.M., et al., *Rapid Ngn2-induction of excitatory neurons from hiPSC-derived neural progenitor cells.* Methods, 2016. **101**: p. 113-24.
376. Lund, R.J., E. Närvä, and R. Lahesmaa, *Genetic and epigenetic stability of human pluripotent stem cells.* Nature Reviews Genetics, 2012. **13**: p. 732.
377. Gossen, M., et al., *Transcriptional activation by tetracyclines in mammalian cells.* Science, 1995. **268**(5218): p. 1766-1769.
378. Szymczak, A.L., et al., *Correction of multi-gene deficiency in vivo using a single self-cleaving 2A peptide–based retroviral vector.* Nature Biotechnology, 2004. **22**: p. 589.
379. Kovach, C., et al., *Neurog2 Simultaneously Activates and Represses Alternative Gene Expression Programs in the Developing Neocortex.* Cerebral Cortex, 2013. **23**(8): p. 1884-1900.
380. Frega, M., et al., *Rapid Neuronal Differentiation of Induced Pluripotent Stem Cells for Measuring Network Activity on Micro-electrode Arrays.* 2017(119): p. e54900.
381. Wang, C., et al., *Scalable Production of iPSC-Derived Human Neurons to Identify Tau-Lowering Compounds by High-Content Screening.* Stem Cell Reports, 2017. **9**(4): p. 1221-1233.
382. Roybon, L., et al., *GABAergic Differentiation Induced by Mash1 Is Compromised by the bHLH Proteins Neurogenin2, NeuroD1, and NeuroD2.* Cerebral Cortex, 2010. **20**(5): p. 1234-1244.
383. Feldmeyer, D., et al., *Reliable synaptic connections between pairs of excitatory layer 4 neurones within a single 'barrel' of developing rat somatosensory cortex.* The Journal of Physiology, 1999. **521**(Pt 1): p. 169-190.
384. Feldmeyer, D., et al., *Synaptic connections between layer 4 spiny neurone- layer 2/3 pyramidal cell pairs in juvenile rat barrel cortex: physiology and anatomy of interlaminar signalling within a cortical column.* The Journal of Physiology, 2002. **538**(Pt 3): p. 803-822.
385. Markram, H., et al., *Physiology and anatomy of synaptic connections between thick tufted pyramidal neurones in the developing rat neocortex.* The Journal of Physiology, 1997. **500**(Pt 2): p. 409-440.
386. Nevian, T. and B. Sakmann, *Spine Ca2+ signaling in spike-timing-dependent plasticity.* J Neurosci, 2006. **26**(43): p. 11001-13.

387. Zeng, H. and L. Madisen, *Mouse transgenic approaches in optogenetics.* Progress in brain research, 2012. **196**: p. 193-213.
388. Petreanu, L., et al., *Channelrhodopsin-2–assisted circuit mapping of long-range callosal projections.* Nature Neuroscience, 2007. **10**: p. 663.
389. Petreanu, L., et al., *The subcellular organization of neocortical excitatory connections.* Nature, 2009. **457**: p. 1142.
390. Arenkiel, B.R., et al., *In vivo light-induced activation of neural circuitry in transgenic mice expressing channelrhodopsin-2.* Neuron, 2007. **54**(2): p. 205-18.
391. Wang, H., et al., *High-speed mapping of synaptic connectivity using photostimulation in Channelrhodopsin-2 transgenic mice.* Proc Natl Acad Sci U S A, 2007. **104**(19): p. 8143-8.
392. M Thomson, A. and J. Deuchars, *Synaptic interactions in neocortical local circuits: Dual intracellular recordings in vitro*. Vol. 7. 1997. 510-22.
393. Yoshimura, Y., J.L.M. Dantzker, and E.M. Callaway, *Excitatory cortical neurons form fine-scale functional networks.* Nature, 2005. **433**: p. 868.
394. Mason, A., A. Nicoll, and K. Stratford, *Synaptic transmission between individual pyramidal neurons of the rat visual cortex in vitro.* J Neurosci, 1991. **11**(1): p. 72-84.
395. Lefort, S., et al., *The Excitatory Neuronal Network of the C2 Barrel Column in Mouse Primary Somatosensory Cortex.* Neuron, 2009. **61**(2): p. 301-316.
396. Tarusawa, E., et al., *Establishment of high reciprocal connectivity between clonal cortical neurons is regulated by the Dnmt3b DNA methyltransferase and clustered protocadherins.* BMC Biology, 2016. **14**: p. 103.
397. Song, S., et al., *Highly Nonrandom Features of Synaptic Connectivity in Local Cortical Circuits.* PLOS Biology, 2005. **3**(3): p. e68.
398. Perin, R., T.K. Berger, and H. Markram, *A synaptic organizing principle for cortical neuronal groups.* Proceedings of the National Academy of Sciences of the United States of America, 2011. **108**(13): p. 5419-5424.
399. Takahashi, N., et al., *Circuit topology for synchronizing neurons in spontaneously active networks.* Proceedings of the National Academy of Sciences, 2010. **107**(22): p. 10244-10249.
400. Chen, W. and D.V. Buonomano, *Developmental Shift of Short-term Synaptic Plasticity in Cortical Organotypic Slices.* Neuroscience, 2012. **213**: p. 38-46.
401. Miles, R. and R.K. Wong, *Excitatory synaptic interactions between CA3 neurones in the guinea-pig hippocampus.* The Journal of Physiology, 1986. **373**: p. 397-418.
402. Smith, K.L., et al., *Diverse neuronal populations mediate local circuit excitation in area CA3 of developing hippocampus.* Journal of Neurophysiology, 1995. **74**(2): p. 650-672.
403. Pavlidis, P. and D.V. Madison, *Synaptic Transmission in Pair Recordings From CA3 Pyramidal Cells in Organotypic Culture.* Journal of Neurophysiology, 1999. **81**(6): p. 2787-2797.
404. Debanne, D., et al., *Physiology and pharmacology of unitary synaptic connections between pairs of cells in areas CA3 and CA1 of rat hippocampal slice cultures.* Journal of Neurophysiology, 1995. **73**(3): p. 1282-1294.
405. Nakayama, K., K. Kiyosue, and T. Taguchi, *Diminished Neuronal Activity Increases Neuron-Neuron Connectivity Underlying Silent Synapse Formation and the Rapid Conversion of Silent to Functional Synapses.* The Journal of Neuroscience, 2005. **25**(16): p. 4040-4051.
406. Wilcox, K.S., J. Buchhalter, and M.A. Dichter, *Properties of inhibitory and excitatory synapses between hippocampal neurons in very low density cultures.* Synapse, 1994. **18**(2): p. 128-151.
407. Schuz, A. and G. Palm, *Density of neurons and synapses in the cerebral cortex of the mouse.* J Comp Neurol, 1989. **286**(4): p. 442-55.
408. Szegedi, V., et al., *Plasticity in Single Axon Glutamatergic Connection to GABAergic Interneurons Regulates Complex Events in the Human Neocortex.* PLOS Biology, 2016. **14**(11): p. e2000237.

409. Molnár, G., et al., *Complex Events Initiated by Individual Spikes in the Human Cerebral Cortex.* PLoS Biology, 2008. **6**(9): p. e222.
410. Regehr, W.G., *Short-Term Presynaptic Plasticity.* Cold Spring Harbor Perspectives in Biology, 2012. **4**(7).
411. Graziane, N. and Y. Dong, *Measuring Presynaptic Release Probability*, in *Electrophysiological Analysis of Synaptic Transmission*, N. Graziane and Y. Dong, Editors. 2016, Springer New York: New York, NY. p. 133-143.
412. Nowak, L., et al., *Magnesium gates glutamate-activated channels in mouse central neurones.* Nature, 1984. **307**: p. 462.
413. Liu, X.-B., K.D. Murray, and E.G. Jones, *Switching of NMDA Receptor 2A and 2B Subunits at Thalamic and Cortical Synapses during Early Postnatal Development.* The Journal of Neuroscience, 2004. **24**(40): p. 8885-8895.
414. Sans, N., et al., *A Developmental Change in NMDA Receptor-Associated Proteins at Hippocampal Synapses.* The Journal of Neuroscience, 2000. **20**(3): p. 1260-1271.
415. Vicini, S., et al., *Functional and Pharmacological Differences Between RecombinantN-Methyl-d-Aspartate Receptors.* Journal of Neurophysiology, 1998. **79**(2): p. 555-566.
416. Huttenlocher, P.R., *Morphometric study of human cerebral cortex development.* Neuropsychologia, 1990. **28**(6): p. 517-527.
417. Levitt, P., *Structural and functional maturation of the developing primate brain.* The Journal of Pediatrics, 2003. **143**(4, Supplement): p. 35-45.
418. Williams, M.E., et al., *Cadherin-9 Regulates Synapse-Specific Differentiation in the Developing Hippocampus.* Neuron, 2011. **71**(4): p. 640-655.
419. Reyes, A. and B. Sakmann, *Developmental Switch in the Short-Term Modification of Unitary EPSPs Evoked in Layer 2/3 and Layer 5 Pyramidal Neurons of Rat Neocortex.* The Journal of Neuroscience, 1999. **19**(10): p. 3827-3835.
420. Zhang, S. and L.O. Trussell, *Voltage clamp analysis of excitatory synaptic transmission in the avian nucleus magnocellularis.* J Physiol, 1994. **480 (Pt 1)**: p. 123-36.
421. Weick, J.P., et al., *Functional control of transplantable human ESC-derived neurons via optogenetic targeting.* Stem Cells, 2010. **28**(11): p. 2008-16.
422. Sun, Alfred X., et al., *Direct Induction and Functional Maturation of Forebrain GABAergic Neurons from Human Pluripotent Stem Cells.* Cell Reports, 2016. **16**(7): p. 1942-1953.
423. Jackman, S.L., et al., *Achieving High-Frequency Optical Control of Synaptic Transmission.* The Journal of Neuroscience, 2014. **34**(22): p. 7704-7714.
424. Cruikshank, S.J., et al., *Pathway-specific feedforward circuits between thalamus and neocortex revealed by selective optical stimulation of axons.* Neuron, 2010. **65**(2): p. 230-245.
425. Lin, J.Y., et al., *Characterization of Engineered Channelrhodopsin Variants with Improved Properties and Kinetics.* Biophysical Journal, 2009. **96**(5): p. 1803-1814.
426. LoTurco, J.J., et al., *GABA and glutamate depolarize cortical progenitor cells and inhibit DNA synthesis.* Neuron, 1995. **15**(6): p. 1287-1298.
427. Maric, D., et al., *Functional ionotropic glutamate receptors emerge during terminal cell division and early neuronal differentiation of rat neuroepithelial cells.* Journal of Neuroscience Research, 2000. **61**(6): p. 652-662.
428. Washbourne, P., J.E. Bennett, and A.K. McAllister, *Rapid recruitment of NMDA receptor transport packets to nascent synapses.* Nature Neuroscience, 2002. **5**: p. 751.
429. Cottrell, J.R., et al., *Distribution, Density, and Clustering of Functional Glutamate Receptors Before and After Synaptogenesis in Hippocampal Neurons.* Journal of Neurophysiology, 2000. **84**(3): p. 1573-1587.
430. Gonzalez-Burgos, G., et al., *Functional Maturation of Excitatory Synapses in Layer 3 Pyramidal Neurons during Postnatal Development of the Primate Prefrontal Cortex.* Cerebral Cortex, 2008. **18**(3): p. 626-637.

431. Wu, G.-Y., R. Malinow, and H.T. Cline, *Maturation of a Central Glutamatergic Synapse.* Science, 1996. **274**(5289): p. 972-976.
432. Zhang, W. and D.J. Linden, *The other side of the engram: experience-driven changes in neuronal intrinsic excitability.* Nature Reviews Neuroscience, 2003. **4**: p. 885.
433. Bolshakov, V. and S. Siegelbaum, *Regulation of hippocampal transmitter release during development and long-term potentiation.* Science, 1995. **269**(5231): p. 1730-1734.
434. Liao, D. and R. Malinow, *Deficiency in induction but not expression of LTP in hippocampal slices from young rats.* Learning & Memory, 1996. **3**(2-3): p. 138-149.
435. Harris, K.M. and T.J. Teyler, *Developmental onset of long-term potentiation in area CA1 of the rat hippocampus.* The Journal of Physiology, 1984. **346**: p. 27-48.
436. Yasuda, H., et al., *A developmental switch in the signaling cascades for LTP induction.* Nature Neuroscience, 2002. **6**: p. 15.
437. Meredith, R.M., A.M. Floyer-Lea, and O. Paulsen, *Maturation of Long-Term Potentiation Induction Rules in Rodent Hippocampus: Role of GABAergic Inhibition.* The Journal of Neuroscience, 2003. **23**(35): p. 11142-11146.
438. Ishibashi, H., A.J. Moorhouse, and J. Nabekura, *Perforated Whole-Cell Patch-Clamp Technique: A User's Guide*, in *Patch Clamp Techniques: From Beginning to Advanced Protocols*, Y. Okada, Editor. 2012, Springer Japan: Tokyo. p. 71-83.
439. Tyzio, R., et al., *The Establishment of GABAergic and Glutamatergic Synapses on CA1 Pyramidal Neurons is Sequential and Correlates with the Development of the Apical Dendrite.* The Journal of Neuroscience, 1999. **19**(23): p. 10372-10382.
440. Groen, M.R., et al., *Development of dendritic tonic GABAergic inhibition regulates excitability and plasticity in CA1 pyramidal neurons.* Journal of Neurophysiology, 2014. **112**(2): p. 287-299.
441. Stuart, G., et al., *Action potential initiation and backpropagation in neurons of the mammalian CNS.* Trends in Neurosciences, 1997. **20**(3): p. 125-131.
442. Spruston, N., et al., *Activity-dependent action potential invasion and calcium influx into hippocampal CA1 dendrites.* Science, 1995. **268**(5208): p. 297-300.
443. Isomura, Y. and N. Kato, *Action potential-induced dendritic calcium dynamics correlated with synaptic plasticity in developing hippocampal pyramidal cells.* J Neurophysiol, 1999. **82**(4): p. 1993-9.
444. Malenka, R.C., et al., *The impact of postsynaptic calcium on synaptic transmission — its role in long-term potentiation.* Trends in Neurosciences, 1989. **12**(11): p. 444-450.
445. Feldmeyer, D. and G. Radnikow, *Developmental alterations in the functional properties of excitatory neocortical synapses.* The Journal of Physiology, 2009. **587**(Pt 9): p. 1889-1896.
446. Valtcheva, S., et al., *Developmental control of spike-timing-dependent plasticity by tonic GABAergic signaling in striatum.* Neuropharmacology, 2017. **121**: p. 261-277.
447. Ben-Ari, Y., *Excitatory actions of gaba during development: the nature of the nurture.* Nat Rev Neurosci, 2002. **3**(9): p. 728-739.
448. Livesey, M.R., et al., *Maturation of AMPAR composition and the GABAAR reversal potential in hPSC-derived cortical neurons.* J Neurosci, 2014. **34**(11): p. 4070-5.
449. Malenka, R.C. and R.A. Nicoll, *NMDA-receptor-dependent synaptic plasticity: multiple forms and mechanisms.* Trends in Neurosciences, 1993. **16**(12): p. 521-527.
450. Bayés, À., et al., *Characterization of the proteome, diseases and evolution of the human postsynaptic density.* Nature Neuroscience, 2010. **14**: p. 19.
451. Zoghbi, H.Y. and M.F. Bear, *Synaptic dysfunction in neurodevelopmental disorders associated with autism and intellectual disabilities.* Cold Spring Harbor perspectives in biology. **4**(3): p. a009886.
452. Lim, S., et al., *Characterization of the Shank Family of Synaptic Proteins: MULTIPLE GENES, ALTERNATIVE SPLICING, AND DIFFERENTIAL EXPRESSION IN BRAIN AND DEVELOPMENT.* Journal of Biological Chemistry, 1999. **274**(41): p. 29510-29518.

453. Sala, C., et al., *Regulation of Dendritic Spine Morphology and Synaptic Function by Shank and Homer.* Neuron, 2001. **31**(1): p. 115-130.
454. Bozdagi, O., et al., *Haploinsufficiency of the autism-associated Shank3 gene leads to deficits in synaptic function, social interaction, and social communication.* Molecular autism, 2010. **1**(1): p. 15-15.
455. Amir, R.E., et al., *Rett syndrome is caused by mutations in X-linked MECP2, encoding methyl-CpG-binding protein 2.* Nature Genetics, 1999. **23**: p. 185.
456. Chao, H.-T., H.Y. Zoghbi, and C. Rosenmund, *MeCP2 Controls Excitatory Synaptic Strength by Regulating Glutamatergic Synapse Number.* Neuron, 2007. **56**(1): p. 58-65.
457. Nelson, E.D., E.T. Kavalali, and L.M. Monteggia, *MeCP2-Dependent Transcriptional Repression Regulates Excitatory Neurotransmission.* Current Biology, 2006. **16**(7): p. 710-716.
458. Dani, V.S. and S.B. Nelson, *Intact Long-Term Potentiation but Reduced Connectivity between Neocortical Layer 5 Pyramidal Neurons in a Mouse Model of Rett Syndrome.* The Journal of Neuroscience, 2009. **29**(36): p. 11263-11270.
459. Catts, V.S., et al., *Postsynaptic density levels of the NMDA receptor NR1 subunit and PSD-95 protein in prefrontal cortex from people with schizophrenia.* Npj Schizophrenia, 2015. **1**: p. 15037.
460. Mohn, A.R., et al., *Mice with reduced NMDA receptor expression display behaviors related to schizophrenia.* Cell, 1999. **98**(4): p. 427-36.
461. Glausier, J.R. and D.A. Lewis, *Dendritic spine pathology in schizophrenia.* Neuroscience, 2013. **251**: p. 90-107.
462. Selemon, L.D. and N. Zecevic, *Schizophrenia: a tale of two critical periods for prefrontal cortical development.* Translational Psychiatry, 2015. **5**: p. e623.
463. Schizophrenia Working Group of the Psychiatric Genomics, C., et al., *Biological insights from 108 schizophrenia-associated genetic loci.* Nature, 2014. **511**: p. 421.
464. Sullivan, P.F., K.S. Kendler, and M.C. Neale, *Schizophrenia as a complex trait: Evidence from a meta-analysis of twin studies.* Archives of General Psychiatry, 2003. **60**(12): p. 1187-1192.
465. Marchetto, M.C.N., et al., *A model for neural development and treatment of Rett Syndrome using human induced pluripotent stem cells.* Cell, 2010. **143**(4): p. 527-539.
466. Farra, N., et al., *Rett syndrome induced pluripotent stem cell-derived neurons reveal novel neurophysiological alterations.* Molecular Psychiatry, 2012. **17**(12): p. 1261-1271.
467. Wen, Z., et al., *Synaptic dysregulation in a human iPS cell model of mental disorders.* Nature, 2014. **515**: p. 414.
468. Schoenenberger, P., et al., *Optimizing the spatial resolution of Channelrhodopsin-2 activation.* Brain Cell Biol, 2008. **36**(1-4): p. 119-27.
469. Rickgauer, J.P. and D.W. Tank, *Two-photon excitation of channelrhodopsin-2 at saturation.* Proceedings of the National Academy of Sciences, 2009. **106**(35): p. 15025-15030.
470. Nikolenko, V., K.E. Poskanzer, and R. Yuste, *Two-photon photostimulation and imaging of neural circuits.* Nat Methods, 2007. **4**(11): p. 943-50.
471. Baker, C.A., et al., *Cellular resolution circuit mapping with temporal-focused excitation of soma-targeted channelrhodopsin.* eLife, 2016. **5**: p. e14193.
472. Dunwiddie, T.V. and G. Lynch, *The relationship between extracellular calcium concentrations and the induction of hippocampal long-term potentiation.* Brain Research, 1979. **169**(1): p. 103-110.
473. Huang, Y.Y., H. Wigström, and B. Gustafsson, *Facilitated induction of hippocampal long-term potentiation in slices perfused with low concentrations of magnesium.* Neuroscience, 1987. **22**(1): p. 9-16.
474. Hsu, K.-S., et al., *Transient Removal of Extracellular Mg2+ Elicits Persistent Suppression of LTP at Hippocampal CA1 Synapses Via PKC Activation.* Journal of Neurophysiology, 2000. **84**(3): p. 1279-1288.

475. Busetto, G., M.J. Higley, and B.L. Sabatini, *Developmental presence and disappearance of postsynaptically silent synapses on dendritic spines of rat layer 2/3 pyramidal neurons.* The Journal of Physiology, 2008. **586**(Pt 6): p. 1519-1527.
476. Liao, D., et al., *Regulation of morphological postsynaptic silent synapses in developing hippocampal neurons.* Nat Neurosci, 1999. **2**(1): p. 37-43.
477. Liao, D., R.H. Scannevin, and R. Huganir, *Activation of Silent Synapses by Rapid Activity-Dependent Synaptic Recruitment of AMPA Receptors.* The Journal of Neuroscience, 2001. **21**(16): p. 6008-6017.
478. Kügler, S., E. Kilic, and M. Bähr, *Human synapsin 1 gene promoter confers highly neuron-specific long-term transgene expression from an adenoviral vector in the adult rat brain depending on the transduced area.* Gene Therapy, 2003. **10**: p. 337.
479. Holmgren, C., et al., *Pyramidal cell communication within local networks in layer 2/3 of rat neocortex.* The Journal of Physiology, 2003. **551**(Pt 1): p. 139-153.
480. Packer, A.M. and R. Yuste, *Dense, unspecific connectivity of neocortical parvalbumin-positive interneurons: a canonical microcircuit for inhibition?* The Journal of neuroscience : the official journal of the Society for Neuroscience, 2011. **31**(37): p. 13260-13271.
481. Nissen, W., et al., *Cell type-specific long-term plasticity at glutamatergic synapses onto hippocampal interneurons expressing either parvalbumin or CB1 cannabinoid receptor.* The Journal of neuroscience : the official journal of the Society for Neuroscience, 2010. **30**(4): p. 1337-1347.
482. Lu, J.-t., et al., *Spike-Timing-Dependent Plasticity of Neocortical Excitatory Synapses on Inhibitory Interneurons Depends on Target Cell Type.* The Journal of Neuroscience, 2007. **27**(36): p. 9711-9720.
483. Li, R., et al., *Recapitulating cortical development with organoid culture in vitro and modeling abnormal spindle-like (ASPM related primary) microcephaly disease.* Protein & Cell, 2017. **8**(11): p. 823-833.
484. Qi, Y., et al., *Combined small-molecule inhibition accelerates the derivation of functional cortical neurons from human pluripotent stem cells.* Nat Biotechnol, 2017. **35**(2): p. 154-163.
485. Zielske, S.P., et al., *Limited Lentiviral Transgene Expression with Increasing Copy Number in an MGMT Selection Model: Lack of Copy Number Selection by Drug Treatment.* Molecular Therapy, 2004. **9**(6): p. 923-931.
486. Galichet, C., F. Guillemot, and C.M. Parras, *Neurogenin 2 has an essential role in development of the dentate gyrus.* Development, 2008. **135**(11): p. 2031-2041.
487. Krencik, R., et al., *Specification of transplantable astroglial subtypes from human pluripotent stem cells.* Nature Biotechnology, 2011. **29**: p. 528.
488. Serio, A., et al., *Astrocyte pathology and the absence of non-cell autonomy in an induced pluripotent stem cell model of TDP-43 proteinopathy.* Proceedings of the National Academy of Sciences of the United States of America, 2013. **110**(12): p. 4697-4702.
489. Krencik, R., et al., *Systematic Three-Dimensional Coculture Rapidly Recapitulates Interactions between Human Neurons and Astrocytes.* Stem Cell Reports, 2017. **9**(6): p. 1745-1753.
490. Shaltouki, A., et al., *Efficient Generation of Astrocytes from Human Pluripotent Stem Cells in Defined Conditions.* STEM CELLS, 2013. **31**(5): p. 941-952.
491. Han, X., et al., *Forebrain Engraftment by Human Glial Progenitor Cells Enhances Synaptic Plasticity and Learning in Adult Mice.* Cell Stem Cell, 2013. **12**(3): p. 342-353.
492. Oberheim, N.A., et al., *Uniquely hominid features of adult human astrocytes.* The Journal of neuroscience : the official journal of the Society for Neuroscience, 2009. **29**(10): p. 3276.
493. Di Giorgio, F.P., et al., *Non-cell autonomous effect of glia on motor neurons in an embryonic stem cell-based ALS model.* Nat Neurosci, 2007. **10**(5): p. 608-14.

494. Frost, G.R. and Y.M. Li, *The role of astrocytes in amyloid production and Alzheimer's disease.* Open Biol, 2017. **7**(12).
495. Wyss-Coray, T., et al., *Adult mouse astrocytes degrade amyloid-beta in vitro and in situ.* Nat Med, 2003. **9**(4): p. 453-7.
496. Abramov, A.Y., L. Canevari, and M.R. Duchen, *Changes in intracellular calcium and glutathione in astrocytes as the primary mechanism of amyloid neurotoxicity.* J Neurosci, 2003. **23**(12): p. 5088-95.
497. Zhao, J., T. O'Connor, and R. Vassar, *The contribution of activated astrocytes to Abeta production: implications for Alzheimer's disease pathogenesis.* J Neuroinflammation, 2011. **8**: p. 150.
498. Garwood, C.J., et al., *Astrocytes are important mediators of Abeta-induced neurotoxicity and tau phosphorylation in primary culture.* Cell Death Dis, 2011. **2**: p. e167.
499. Oksanen, M., et al., *PSEN1 Mutant iPSC-Derived Model Reveals Severe Astrocyte Pathology in Alzheimer's Disease.* Stem Cell Reports, 2017. **9**(6): p. 1885-1897.
500. Lin, Y.-T., et al., *APOE4 Causes Widespread Molecular and Cellular Alterations Associated with Alzheimer's Disease Phenotypes in Human iPSC-Derived Brain Cell Types.* Neuron, 2018. **98**(6): p. 1141-1154.e7.
501. Huang, Y.-W.A., et al., *ApoE2, ApoE3 and ApoE4 Differentially Stimulate APP Transcription and Aβ Secretion.* Cell, 2017. **168**(3): p. 427-441.e21.
502. Sahara, S., et al., *The fraction of cortical GABAergic neurons is constant from near the start of cortical neurogenesis to adulthood.* The Journal of Neuroscience, 2012. **32**(14): p. 4755-4761.
503. Tremblay, R., S. Lee, and B. Rudy, *GABAergic Interneurons in the Neocortex: From Cellular Properties to Circuits.* Neuron, 2016. **91**(2): p. 260-292.
504. Owens, D.F., et al., *Excitatory GABA responses in embryonic and neonatal cortical slices demonstrated by gramicidin perforated-patch recordings and calcium imaging.* J Neurosci, 1996. **16**(20): p. 6414-23.
505. Khazipov, R., et al., *Early development of neuronal activity in the primate hippocampus in utero.* J Neurosci, 2001. **21**(24): p. 9770-81.
506. Akerman, C.J. and H.T. Cline, *Depolarizing GABAergic conductances regulate the balance of excitation to inhibition in the developing retinotectal circuit in vivo.* J Neurosci, 2006. **26**(19): p. 5117-30.
507. Wang, D.D. and A.R. Kriegstein, *GABA Regulates Excitatory Synapse Formation in the Neocortex via NMDA Receptor Activation.* The Journal of Neuroscience, 2008. **28**(21): p. 5547-5558.
508. Maroof, A.M., et al., *Directed differentiation and functional maturation of cortical interneurons from human embryonic stem cells.* Cell stem cell, 2013. **12**(5): p. 559-572.
509. Nicholas, Cory R., et al., *Functional Maturation of hPSC-Derived Forebrain Interneurons Requires an Extended Timeline and Mimics Human Neural Development.* Cell Stem Cell, 2013. **12**(5): p. 573-586.
510. Liu, Y., et al., *Directed differentiation of forebrain GABA interneurons from human pluripotent stem cells.* Nature protocols, 2013. **8**(9): p. 1670-1679.
511. Kim, T.-G., et al., *Efficient specification of interneurons from human Pluripotent stem cells by dorsoventral and rostrocaudal modulation.* Stem cells (Dayton, Ohio), 2014. **32**(7): p. 1789-1804.
512. Xu, J.-C., et al., *Cultured networks of excitatory projection neurons and inhibitory interneurons for studying human cortical neurotoxicity.* Science Translational Medicine, 2016. **8**(333): p. 333ra48-333ra48.
513. Birey, F., et al., *Assembly of Functional Forebrain Spheroids from Human Pluripotent Cells.* Nature, 2017. **545**(7652): p. 54-59.

514. Kang, S., et al., *Characteristic analyses of a neural differentiation model from iPSC-derived neuron according to morphology, physiology, and global gene expression pattern.* Scientific Reports, 2017. **7**: p. 12233.
515. Prinz, M. and J. Priller, *Microglia and brain macrophages in the molecular age: from origin to neuropsychiatric disease.* Nature Reviews Neuroscience, 2014. **15**: p. 300.
516. Guerreiro, R., et al., *TREM2 variants in Alzheimer's disease.* N Engl J Med, 2013. **368**(2): p. 117-27.
517. Harold, D., et al., *Genome-wide association study identifies variants at CLU and PICALM associated with Alzheimer's disease.* Nat Genet, 2009. **41**(10): p. 1088-93.
518. Karch, C.M. and A.M. Goate, *Alzheimer's Disease Risk Genes and Mechanisms of Disease Pathogenesis.* Biological Psychiatry, 2015. **77**(1): p. 43-51.
519. Wu, Y., et al., *Microglia: Dynamic Mediators of Synapse Development and Plasticity.* Trends in immunology, 2015. **36**(10): p. 605-613.
520. Lim, S.-H., et al., *Neuronal Synapse Formation Induced by Microglia and Interleukin 10.* PLoS ONE, 2013. **8**(11): p. e81218.
521. Miyamoto, A., et al., *Microglia contact induces synapse formation in developing somatosensory cortex.* Nature Communications, 2016. **7**: p. 12540.
522. Paolicelli, R.C., et al., *Synaptic Pruning by Microglia Is Necessary for Normal Brain Development.* Science, 2011. **333**(6048): p. 1456-1458.
523. Haenseler, W., et al., *A Highly Efficient Human Pluripotent Stem Cell Microglia Model Displays a Neuronal-Co-culture-Specific Expression Profile and Inflammatory Response.* Stem Cell Reports, 2017. **8**(6): p. 1727-1742.
524. Muffat, J., et al., *Efficient derivation of microglia-like cells from human pluripotent stem cells.* Nat Med, 2016. **22**(11): p. 1358-1367.
525. Takata, K., et al., *Induced-Pluripotent-Stem-Cell-Derived Primitive Macrophages Provide a Platform for Modeling Tissue-Resident Macrophage Differentiation and Function.* Immunity, 2017. **47**(1): p. 183-198.e6.
526. Abud, E.M., et al., *iPSC-Derived Human Microglia-like Cells to Study Neurological Diseases.* Neuron, 2017. **94**(2): p. 278-293.e9.
527. Pandya, H., et al., *Differentiation of human and murine induced pluripotent stem cells to microglia-like cells.* Nat Neurosci, 2017. **20**(5): p. 753-759.
528. Park, J., et al., *A 3D human triculture system modeling neurodegeneration and neuroinflammation in Alzheimer's disease.* Nature Neuroscience, 2018. **21**(7): p. 941-951.
529. Otani, T., et al., *2D and 3D Stem Cell Models of Primate Cortical Development Identify Species-Specific Differences in Progenitor Behavior Contributing to Brain Size.* Cell Stem Cell, 2016. **18**(4): p. 467-480.
530. Rodríguez-Gómez, J.A., et al., *Persistent Dopamine Functions of Neurons Derived from Embryonic Stem Cells in a Rodent Model of Parkinson Disease.* STEM CELLS, 2007. **25**(4): p. 918-928.
531. Barberi, T., et al., *Neural subtype specification of fertilization and nuclear transfer embryonic stem cells and application in parkinsonian mice.* Nature Biotechnology, 2003. **21**: p. 1200.
532. Kim, J.H., et al., *Dopamine neurons derived from embryonic stem cells function in an animal model of Parkinson's disease.* Nature, 2002. **418**(6893): p. 50-6.
533. Kriks, S., et al., *Floor plate-derived dopamine neurons from hESCs efficiently engraft in animal models of PD.* Nature, 2011. **480**(7378): p. 547-551.
534. Kirkeby, A., et al., *Generation of Regionally Specified Neural Progenitors and Functional Neurons from Human Embryonic Stem Cells under Defined Conditions.* Cell Reports, 2012. **1**(6): p. 703-714.
535. Isacson, O., O. Isacson, and T. Deacon, *Neural transplantation studies reveal the brain's capacity for continuous reconstruction.* Trends in Neurosciences, 1997. **20**(10): p. 477-482.

536. Espuny-Camacho, I., et al., *Human Pluripotent Stem-Cell-Derived Cortical Neurons Integrate Functionally into the Lesioned Adult Murine Visual Cortex in an Area-Specific Way.* Cell Reports, 2018. **23**(9): p. 2732-2743.
537. Tornero, D., et al., *Synaptic inputs from stroke-injured brain to grafted human stem cell-derived neurons activated by sensory stimuli.* Brain, 2017. **140**(3): p. 692-706.
538. Mansour, A.A., et al., *An in vivo model of functional and vascularized human brain organoids.* Nature Biotechnology, 2018. **36**: p. 432.
539. Hiragi, T., et al., *Differentiation of Human Induced Pluripotent Stem Cell (hiPSC)-Derived Neurons in Mouse Hippocampal Slice Cultures.* Frontiers in Cellular Neuroscience, 2017. **11**: p. 143.
540. Avaliani, N., et al., *Optogenetics Reveal Delayed Afferent Synaptogenesis on Grafted Human-Induced Pluripotent Stem Cell-Derived Neural Progenitors.* STEM CELLS, 2014. **32**(12): p. 3088-3098.
541. Cornacchia, D. and L. Studer, *Back and Forth in Time: Directing Age in iPSC-Derived Lineages.* Brain research, 2017. **1656**: p. 14-26.
542. Mertens, J., et al., *Directly Reprogrammed Human Neurons Retain Aging-Associated Transcriptomic Signatures and Reveal Age-Related Nucleocytoplasmic Defects.* Cell Stem Cell, 2015.
543. Miller, J.D., et al., *Human iPSC-based modeling of late-onset disease via progerin-induced aging.* Cell Stem Cell, 2013. **13**(6): p. 691-705.
544. Pollex, R.L. and R.A. Hegele, *Hutchinson-Gilford progeria syndrome.* Clin Genet, 2004. **66**(5): p. 375-81.
545. Nguyen, H.N., et al., *LRRK2 Mutant iPSC-Derived DA Neurons Demonstrate Increased Susceptibility to Oxidative Stress.* Cell stem cell, 2011. **8**(3): p. 267-280.